New Strategies

for

Nerve Regeneration

Théophile Pierre-Eugène DÉJARDIN (MSc)

Submitted in fulfilment of the requirements for the Degree of

Doctor of Philosophy

Centre for Cell Engineering

College of Medical, Veterinary and Life Sciences

Institute of Molecular, Cell and Systems Biology

University of Glasgow

October 2013

Abstract

Nerve repair is still a major challenge in surgery, regenerative medicine and tissue engineering even if progress has been made over the last 30 years. Functional recovery after severe lesions to a nerve is often incomplete and rarely totally successful.

In this thesis I present a multi-disciplinary approach to improve the regenerative potential of "nerve repair tubes" that aim to reconnect wounded nerves and refine or replace autologous nerve graft, the clinical current gold standard. The efficacy of such tubes has already been shown in the clinic especially for small gap injuries, but the outcomes are still limited, and ought to be improved by e.g. micro/nano-topography, growth factor delivery systems, supportive cells or active features such as electrical stimulation, which have individually been shown to enhance nerve regeneration. In this study organotypic cultures of dorsal root ganglions (DRG) isolated from neonatal rats were used throughout as an *in vitro* model of nerve regeneration. Here I tested different devices in combination with growth factors to contribute to the fundamental and technical knowledge necessary to improve the regenerative potential of such tubes.

I investigated the interaction between surface features and growth factors in their joined influence on regenerating DRGs. For this polydimethylsiloxane (PDMS), a polymer with adjustable elasticity was used together with photolithography to build devices of different stiffness with different surface microgrooves, on which DRG could be grown. To optimise the use of nerve growth factor (NGF) in conjunction with these devices, and to show how NGF interacts with stiffness and topography the reaction of the DRG was tested. To ease the making of three-dimensional internally microstructured tubes I have developed up a novel, timesaving, fabrication technique for polycaprolactone (PCL) "Swiss roll" nerve repair tubes. This technique improves the reproducibility of the scaffold, and using DRG its potential for nerve regeneration is being demonstrated.

The influence of time-variant, balanced, pulsed electric stimulation is a potentially useful means to influence nerve regeneration. To narrow down the parameter space the effect of various electric fields was tested in their effect on DRG regeneration using commercially available devices. In collaboration with Christopher Martin from the School of Engineering, novel custom-made devices that allowed us to quantify the directional response of the regenerating axons were developed, and the guidance effect of pulsed alternating current (AC) electrical fields on regenerating DRGs axons was investigated *in vitro*. This approach allows in principle to transfer the use of this nerve guiding strategy to potentially improve nerve repair tubes.

Table of contents

List of tables

List of figures

List of accompanying materials

Cell Patterning with a Heptagon Acoustic Tweezer – Application in Neurite Guidance

Frank Gesellchen, Anne L. Bernassau, Théophile Déjardin, David R.S. Cumming and Mathis O. Riehle

Directed Nerve Regeneration Enabled by Wirelessly Powered Electrodes Printed on a Biodegradable Polymer

Christopher Martin, Théophile Dejardin, Andrew Hart, Mathis O. Riehle and David R. S. Cumming

In memory of my grandfather, Joseph Déjardin, who wanted to be a doctor.

Acknowledgments

First of all, I would like to thank the reader of this document because your interest makes the presentation of this work useful. I also thank the Stephen Forrest trust for funding this independent research work, which would have been impossible without their generosity. The first person I would like to thank is Dr. Mathis Riehle who has been an excellent thesis supervisor. During this work he has been the closest, the more pleasant, present, and available person. He gave me numerous advices and provided me with coffee, ideas, and jokes. I will miss our brainstorming meeting. The second person I would like to thank is Christopher Martin and also our common supervisors, Prof. Andrew Hart and Dr. David Cummings for their collaboration, their advices and their supervisions of the projects. I would like to thank the team of the Center For Cell Engineering (CCE), particularly Dr. Catherine Berry who first welcomed me in the CCE, Dr. Sun Tao, Dr Lewis Ross, Dr. Frank Gesellchen, and Dr. Anne Bernassau for their collaboration and also Carol-Anne Smith and Dr. Thomas Edlein for their availability, Prof. Adam Smith for his jokes and anecdotes, Jemma Roberts, Dr. Hannah Child and Diana Samuel for the good times spent in the office and for the fun I had feeding blue frogs. I would also like to thank Dr. Laura Mc Namara and Dr. Suzanne Thomson for their enthusiasm. To finish with the professional side, I would like to thanks Prof. Terenghi who welcomed me in exchange in his lab in Manchester where I studied Schwann cell and adipose derived stem cell culture. I would also like to thank my parents for their support in everything, my brothers and my sister for their fraternity and my family in general for showing me the way to Science through nature contemplation. Among all the friends I want to thank, I regret to cite only a few: Paul-Edouard Mias, who is now like a brother to me and who made me discover Glasgow, and Dr. Simon Bordage for his help with the introduction chapter. More generally I would like to thanks the Mungos'HiFi crew especially Jerome Jolly, for the fabulous night they organise and people I met through them. They allow me to relax and enjoy my PhD course even in the hardest working times.

"Et voila"!

Author Declaration

I declare that, except where explicit reference is made to the contribution of others, that this dissertation is the result of my own work and has not been submitted for any other degree at he University of Glasgow or any other institution.

Théophile Déjardin

List of Abbreviations

3Rs	Replacement, reduction, refinement
AC	Alternating Current
ALCAR	Acetyl-L-carnitine
APC	Adenomatous polyposis coli
ASC	Adipose-derived stem cell
ATF	cAMP-dependent transcription factor
BDNF	Brain-derived neurotrophic factor
cAMP	Cyclic adenosine mono-phosphate
CCE	Center for cell engineering
CCE	Centre for Cell Engineering
CE	Conformité Européenne
CGRP	Calcitonin gene related peptide
CNS	Central nervous system
CNTF	Ciliary neurotrophic factor
CREB	cAMP-response element binding protein
DC	Direct current
DRG	Dorsal root ganglion
ECM	Extracellular Matrix
EGF	Endothelial Growth Factor
ERK	Extracellular signal-regulated kinase
ES	Electrical stimulation
FBS	Foetal bovine serum
FDA	Food and drug administration
FGF	Fibroblast growth factor
GAP	Growth-activated protein
GEE	Glycin ethyl esther
GFAP	Glial fibrillary protein
GTP	Guanosine tri-phosphate
HER	Epidermal growth factor receptor
HGF	Hepatocyte growth factor
IGF	Insulin-like growth factor
IL	Interleukin
IPA	Isopropanol
JWNC	James Watt nanofabrication centre
Krox20	Early Growth Response Protein 2
LIF	Leukaemia inhibitory factor
LPA	Lysophosphatidic acid
MAP	Microtubule associated protein
MAPK	Mitogen-activated protein kinase
MD	Doctor of Medicine
mRNA	Messenger RNA
MSC	Mesenchymal stem cell
mTOR	Mammalian target of rapamycin
NAC	N-acetyl-cysteine

NGF	Nerve growth factor
NSC	Neural stem cell
NT	Neurotrophin
OEC	Olfactory ensheathing cell
PAA	Polyacrilyc Acid
PAP	Parent aniline pentamere
PCB	Printed circuit board
PCL	Polycaprolactone
PDGF	Platelet-derived growth factor
PDMS	Polydimethylsiloxane
PEB	Post exposure bake
PEMF	Pulsed electromagnetic fields
PGA	Polyglycolic-acid
PGLA	Poly(lactic-co-glycolic acid)
pH	Potential hydrogen
PHB	Poly(3-hydroxybutyrate)
PHEMA-MMA	Poly(2-hydroxyethyl methacrylate-co-methyl methacrylate)
PI-3K	Phosphoinositol-3-kinase
PLA	Polylactic acid
PLL	Poly-L-lysine
PNS	Peripheral nerve system
PPy	Polypyrrole
PT	Pleiotrophin
PTEN	Phosphatase and tensin homolog
PTFE	Polytetrafluoroethylene
RER	Rough endoplasmic reticulum
Rho	Ras homolog gene family
RNA	Ribonucleic acid
RO	Reverse osmosis
ROCK	Rho-associated kinase
SEM	Scanning electron microscopy
Sox11	Sex Determining Region Y (SRY)-Box 11 transcription factor
STAT	Signal transducer and activator of transcription 3
TEM	Transmission electron microscopy
TGF	Transforming growth factor
UK	United Kingdom
US	United States
UV	Ultra-violet
VEGF	Vascular endothelial growth factor
WTA	Water surface angle

1 General Introduction

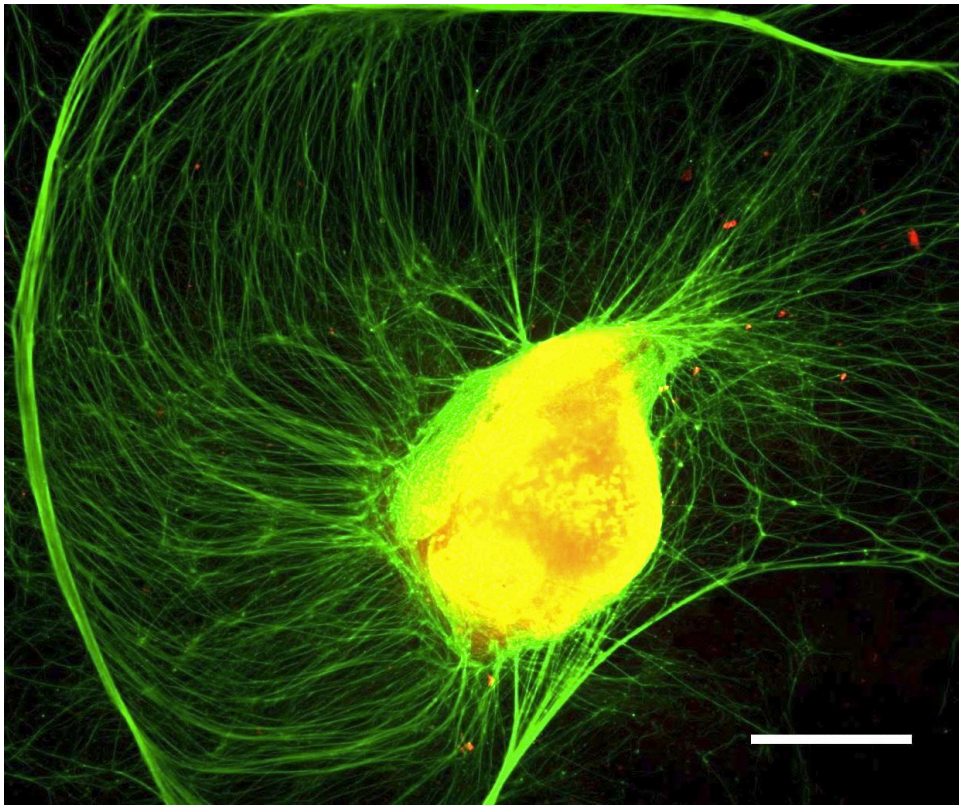

An organotypic DRG culture after ten days growth on glass. Scale : 500 µm

1.1 Generalities

1.1.1 Peripheral nerve histology and electrophysiology

The most basic cellular structural unit of the nervous system in general is the neuron. Neurons of the peripheral nervous system have a large cell body which has inclusions called Nissl bodies which are numerous cisternae of rough endoplasmic reticulum, dendrites receiving afferent nerve input from upstream neurons, and an axon conveying the nervous signal downstream to other neurons or effector organs by action potential propagation (Figure 1, Hanley, 1992, Hakim, 1999).

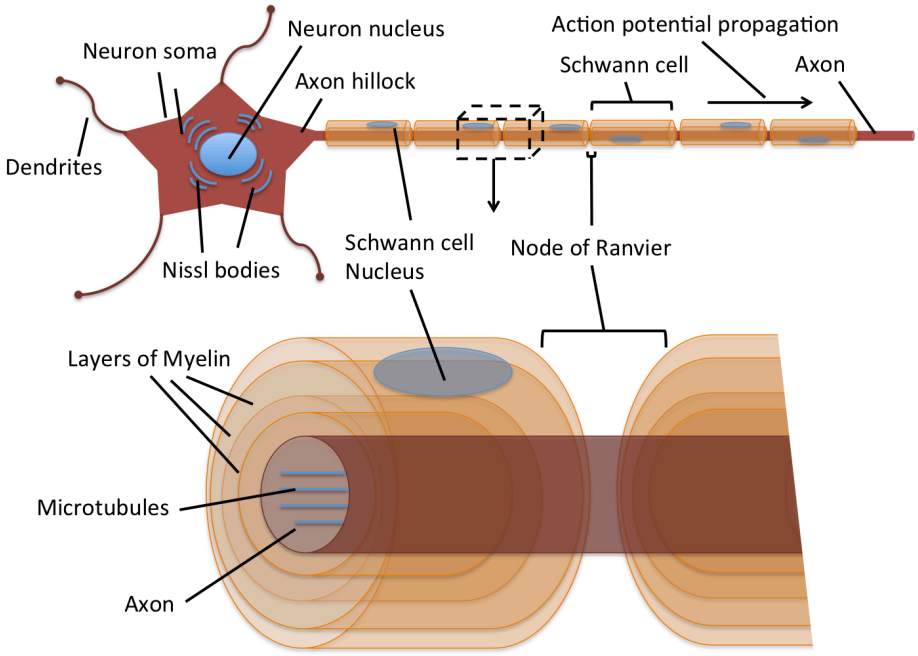

Figure 1: The neuron, the structural unit of the nervous system. They have a large cell body, dendrites receiving afferent nerve signals from upstream neurons, and an axon conveying the signal downstream by action potentials. In the PNS thin, fast conducting axons are generally wrapped in layers of myelin created by individual Schwann cells. These leave only small parts open in between them, termed nodes of Ranvier, where the saltatory axon potential propagation takes place. Schwann cells can also engulf more than one axon when they have a non-myelinating phenotype. In these unmyelinated axons, nervous signal propagation will be slower due to the absence of saltatory conduction of axon potentials.

The soma of motor neurons sits in the spinal cord, those of sensory nerves in the dorsal root, or other sensory ganglia (Hanley, 1992). Their axons are

long, thin extensions specialised to efficiently conduct electrical impulses from or to the neuron's cell body or soma. All the information streaming in the peripheral nervous system (PNS) is transmitted along axons by electrochemical signals called action potentials. The axons are supported by Schwann cells, which can wrap them in a myelin sheath (Figure 1 and Figure 2) to facilitate action potential transmission. Groupings of these two cell types ("fascicles" in Figure 2), form the basis of the peripheral nerve.

The action potential is propagated along the axon by a membrane depolarisation due to passive sodium influx across the axon membrane through voltage-gated ion channels. The action potential is characterized by an alteration of the membrane potential from a resting potential of -70 mV to +30 mV (Hodgkin and Huxley, 1939).

In myelinated axons (Figure 1) Schwann cells synthesise insulating myelin to form a tightly wound stack of membranes around the axon that creates an insulated zone, but they can also sheath more than one unmyelinated axon. The distance over which an individual Schwann cell isolates an axon is between 0.2 and 2 mm long. The electrochemical action potential propagation is comparatively slow without myelination (ca.1m/s). The action potential in myelinated axons only takes place at the nodes of Ranvier, which are the gaps between two successive Schwann cells (Figure 1), resulting in saltatory conduction at velocities of up to 70 m/s. This phenomenon is called saltatory conduction (Huxley and Stampfli, 1949). In the central nervous system (CNS) (spinal cord and brain) a different cell type, called "oligodendrocytes", myelinate axons (Hanley, 1992).

Anatomically, peripheral nerves are hierarchically structured. Each axon and its associated Schwann cells are surrounded by an extracellular matrix (ECM) called the endoneurium. This ECM consists of a mix of collagen, heparansulfate, laminins, fibronectin and proteoglycans, which have mostly been secreted by fibroblasts. The endoneurium gives robustness to the biomechanical properties of the peripheral nerve, and also includes seams of

loose connective tissue providing pathways for small arterioles and venules. Axons are thereby grouped into bundles, or “fascicles”, bound by a thin connective cellular layer called the perineurium. A number of these fascicles along with vasculature and an outer collagen sheath, termed epineurium, form the hierarchical structure of a nerve (Figure 2).

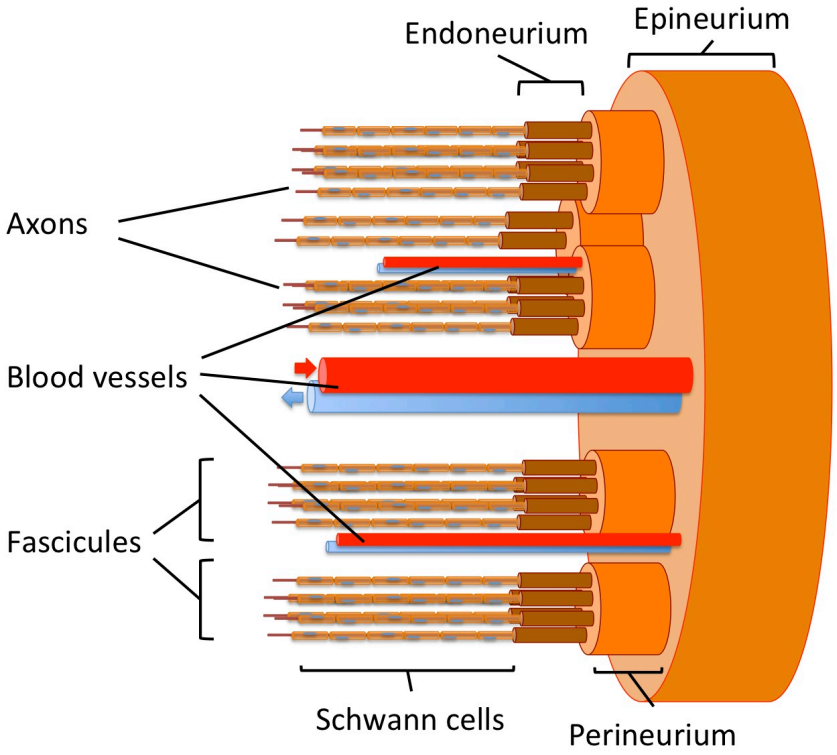

Figure 2: Histology of a peripheral nerve. A nerve is a complex tissue. It is a collection of axons with their Schwann cells surrounded by a connective tissue matrix and blood vessels. Axons are grouped into fascicles, and bound by a connective cellular layer called the perineurium. Fascicles along with vasculature and an outer collagen sheath, termed epineurium, form the nerve.

The classification of nerve fibres is based on axonal conduction velocity, myelination, and fibre diameter (Whitwam, 1976). Individual axons have a diameter of few microns, but can be up to about a meter in length (e.g. those of the sciatic nerve, parts of which runs from the base of the spine to the big toe of each foot). At their terminal extremity peripheral axons make contact with other cells, such as sensory organelles, muscle or gland cells, at junctions called synapses. There, either neurotransmitters transmit chemical signals across the gap between the cells, or they are directly coupled via electrochemical synapses.

1.1.2 Experimental model: Dorsal root ganglia (DRG)

The experimental model used in this work is an organotypic culture of DRG, each of which contain approximately 10,000 pseudo-unipolar sensory afferent neurons, together with their associated Schwann and satellite cells (Nascimento *et al.*, 2008), as well as fibroblasts maintaining the connective tissue, tissue resident macrophages, and endothelia (Zareen and Greene, 2009). DRGs contain three subpopulations of sensory neurons when simplistically classified by functionality: prioprioceptive, mechanoreceptive and nociceptive neurons. The former predominantly innervate muscle spindles or Golgi tendon organs, and subserve awareness of changes in muscles length and muscle tension. Mechanoreceptors relay pressure, touch, and vibratory stimuli. Nociceptive neurons relay information about noxious, or potentially injurious, stimuli (Figure 3, Marmigere and Ernfors, 2007). Other common structural cells within DRGs include satellite cells, fibroblasts, and endothelia (Figure 3).

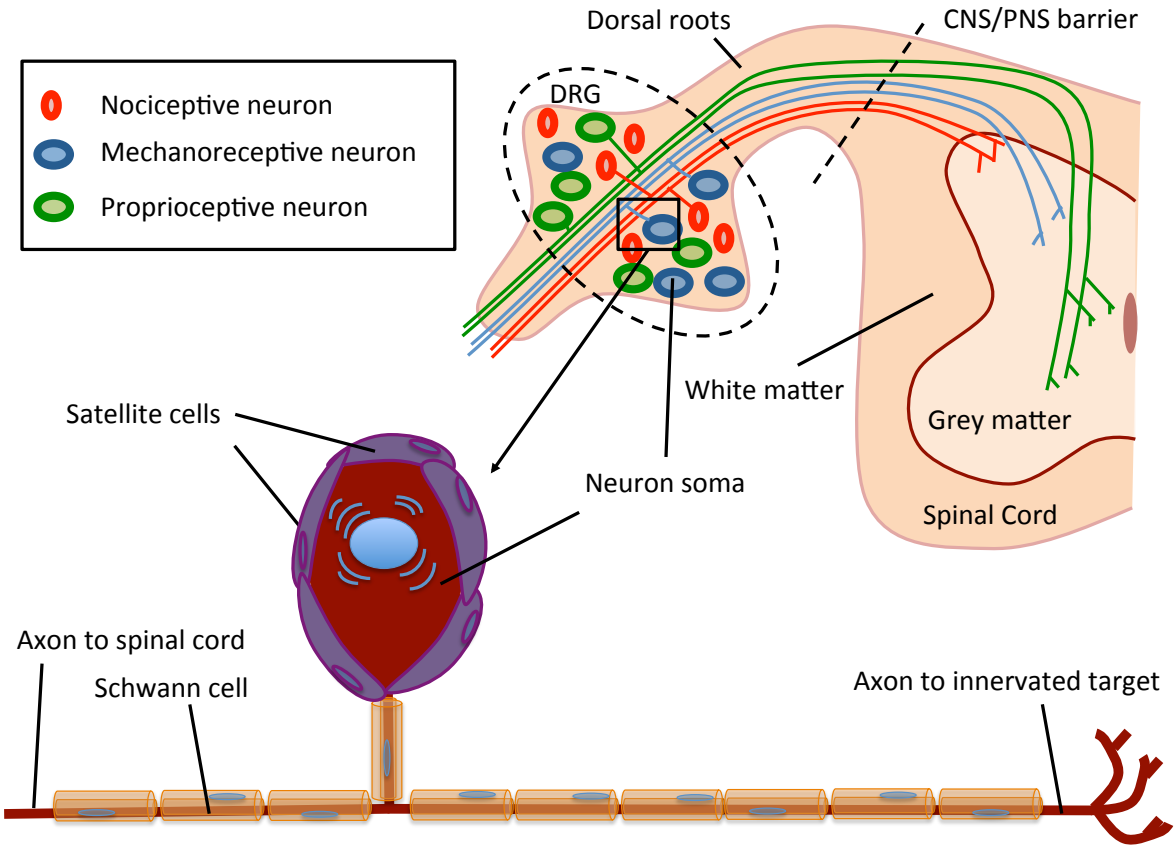

Figure 3: Dorsal root ganglion (DRG) neuronal subpopulation. DRGs neurons are classified by functionality: Proprioceptive neurons (green) ended by muscle spindle or Golgi tendon organ, provide information about changes in muscles length and muscle tension. Mechanoreceptive neurons (blue) relay pressure, touch, sound stimuli and change in posture. Nociceptive neurons (red) relay information about noxious stimuli. Satellite cells (purple cells) are closely engulfing the neuron and are believed to provide metabolic support to the neuron. Schwann cells (orange cells) provide insulation and quicker nervous signal propagation by producing a myelin sheath wrapped around the axon. Adapted from Marmigere and Ernfors (2007).

Post-mortem DRG extraction (n~20/animal) involves bilateral transection of the dorsal roots, mimicking an acute DRG avulsion in combination with a peripheral nerve injury. During axonal outgrowth from the DRG in culture, fibroblasts and glial cells grow out from the DGR and provide a more complex and translationally relevant in vitro model than most common neuronal co-culture models (Corey *et al.*, 2007, Ribeiro-Resende *et al.*, 2009, Zareen and Greene, 2009, Nicolini *et al.*, 2011). The model also reduces animal use and pain as well as cost of *in vivo* models.

1.2 Peripheral nerve injuries

1.2.1 Peripheral nerve Injury classification

In 1943 Seddon classified peripheral nerve injuries into three main categories (Table 1), and this remains the main clinical means to stratify these injuries even if Sunderland added more histomorphologically accurate sub-classes of axonotmesis (Seddon, 1943, Sunderland, 1951, Sunderland, 1990).

Table 1: Classification of nerve injuries

Seddon	Observations	Sunderland
Neurapraxia	Epineurium, perineurium and endoneurium intact Localised conduction block No Wallerian degeneration Segmental demyelination Distal motor or sensory failure Full recovery without surgery	First degree
Axonotmesis	Disruption of axons Endoneurial connective tissue elements remain intact Conduction failure Wallerian degeneration Distal motor and sensory deficit Spontaneous recovery without surgery occurs by axonal regeneration	Second degree
Axonotmesis	Same as second degree but endoneurium is also disrupted Incomplete spontaneous recovery, by incomplete / misdirected axonal regeneration	Third degree
Axonotmesis	Same as third degree but perineurium is also disrupted Little recovery without surgery	Fourth degree
Neurotmesis	Total disruption of the nerve Wallerian degeneration Severe distal motor sensory deficit No recovery without surgery	Fifth degree

1.2.2 Pathophysiolgical, cellular and biomolecular aspects of nerve Regeneration

After a peripheral nerve is injured (Sunderland Grades III-V) the transected vasculature within the nerve haemorrhages and a blood clot forms. The disrupted fascicles (Sunderland Grade IV) or proximal nerve stump (Sunderland Grade V) retracts due to the intrinsic elasticity of peripheral nerve. Axonal injury initiates an active somatofugal retraction of the injured axons (to the next node of Ranvier in myelinated axons), and a number of changes occur in the cell body of the injured neurons (see details below in the paragraph "neuronal changes"). These represent a switch from a normal to an injury phenotype, as the cell either enters an active cell death pathway, or begins to regenerate (Hart *et al.*, 2008). Neuronal death is very extensive after proximal nerve injury. Within days of peripheral injury the loss of target-derived neurotrophic support, and other more acute factors, initiates the death of around 30-70 % of the sensory neurons (Ygge, 1989, Hart *et al.*, 2004), and, after proximal injury only, of 30-80 % of motorneurons (Hart *et al.*, 2008).

A process termed "Wallerian degeneration" (Figure 4) takes place, starting within minutes to hours after injury in the distal nerve stump, which contains the axons that have been separated from their somata (Johnson *et al.*, 2005). The distal axons swell, and calcium influx from extracellular environment activates ubiquitin- and calpain-proteases.

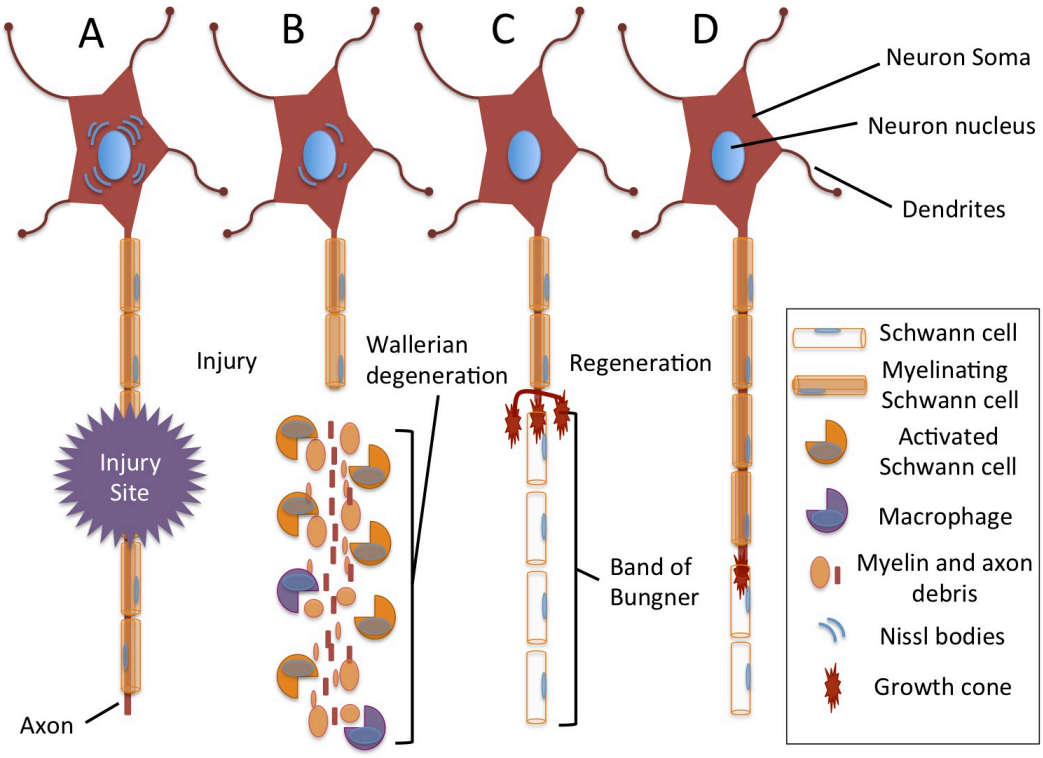

Figure 4: Mechanisms of nerve regeneration. After nerve injury (A), Wallerian degeneration (B) starts: Schwann cells surrounding the axons at the transected area stop making myelin in the distal part of the nerve, severed from its somata. Distally to the injury axons are without nutritive support from their cell body, they detach from their myelin sheath and are phagocytosed by macrophages and activated Schwann cells. Distal Schwann cells migrate to the site of injury, proliferate, and bridge any defect in nerve continuity by forming a solid column, consisting of a series of nucleated cellular cords called band of Büngner. These form conduits for axonal regeneration (C). Within 3 to 24 hours axons begin to regenerate, stimulated by contact and chemotactic guidance provided by Schwann cells, creating multiple new small-diameter axons or axonal sprouts which try to bridge the lesion at a rate of 0.25 to 1.0 mm per day. The leading edges of the axons are termed growth cones. Freshly regenerated axons are initially unmyelinated but induce adjacent Schwann cells to proliferate and initiate myelin formation around the axon as it regenerates (D). Only one single axon of the growth cone will be regenerating down the endoneurial tube in the distal stump. Axonal sprouts continue to regrow and aim to reinnervate the tissue that was deinnervated by injury-induced axonal degeneration. Adpadted from Allodi et al. (2012)

The consequences of protease activation are the degradation of: the endoplasmic reticulum, mitochondria, cytoskeletal elements of the axon, and neurofilaments (Allodi *et al.*, 2012). Because Schwann cells detach off their dying axons they stop making myelin and become activated: they start to recruit macrophages and T-cells by the secretion of interleukins (IL): IL-1ß, IL-6, IL-10 and leukaemia inhibitory factor (LIF). The orchestrated release of the ILs, LIF, and the attraction of macrophages results in phagocytosis of the axonal debris and myelin sheaths residues (Maruda, 2012). This clearance occurs during the later inflammatory stages and marks the beginning of the

repair phase. In the PNS this process takes weeks, whereas in the CNS, it is a matter of months due to the blood/brain barrier, which slows the migration of macrophages down.

Both a living neuronal cell body and an intact endoneurial sheath, beyond the region of injury, are essential for axonal regeneration. The process of nerve regeneration begins early after injury by a well-established sequence of events that are set and maintained by the orchestrated interaction of many cell types, as reviewed by Allodi *et al*. (2012).

1.2.2.1 Injured neurons biology

If they survive axotomy, which occurs in the first three month post-injury, neurons switch back to the growth state they were in during embryonic development. Significant changes occur in the cell body: first a rise in cytoplasmic RNA that is associated in parts with the increased synthesis of lysosomal acid phosphatase, and then a dispersion of Nissl bodies. Nissl bodies are mainly enlarged rough endoplasmic reticulum (RER), required for the high degree of protein synthesis that a neuron needs to maintain its normal function (Figure 1, Torvik, 1976, Aldskogius and Arvidsson, 1978, Fawcett and Keynes, 1990). This loss of Nissl bodies is also called chromatolysis.

One of the first events after axotomy is a burst of action potentials due to calcium and sodium influx in the severed axon (Mandolesi *et al*., 2004). This rise in calcium concentration induces a quick increase in cyclic adenosine mono-phosphate (cAMP) in the soma, which is essential to trigger regeneration via the cAMP-response element binding protein (CREB) pathway (Figure 5). The interruption of retrograde transport along the axon, e.g. nerve growth factor (NGF) that is transported from the innervated organ to the soma (Stoeckel *et al*., 1975) also triggers the switches in the neurons to a regenerating phenotype (Raivich *et al*., 1991). The NGF concentration in DRG neurons decreases dramatically 6 h after the injury due to interruption of its retrograde transport, but it recovers to a normal level within two days

thereafter (Lee *et al.*, 1998) as NGF expression increases in the injured neurons (Brown *et al.*, 2007). Another consequence of this signalling pathway is that an application of high NGF concentration impairs and delays nerve regeneration by delaying the switch to a regenerative state in axotomised sensory neurons *in vivo* (Gold, 1997, Allodi *et al.*, 2012).

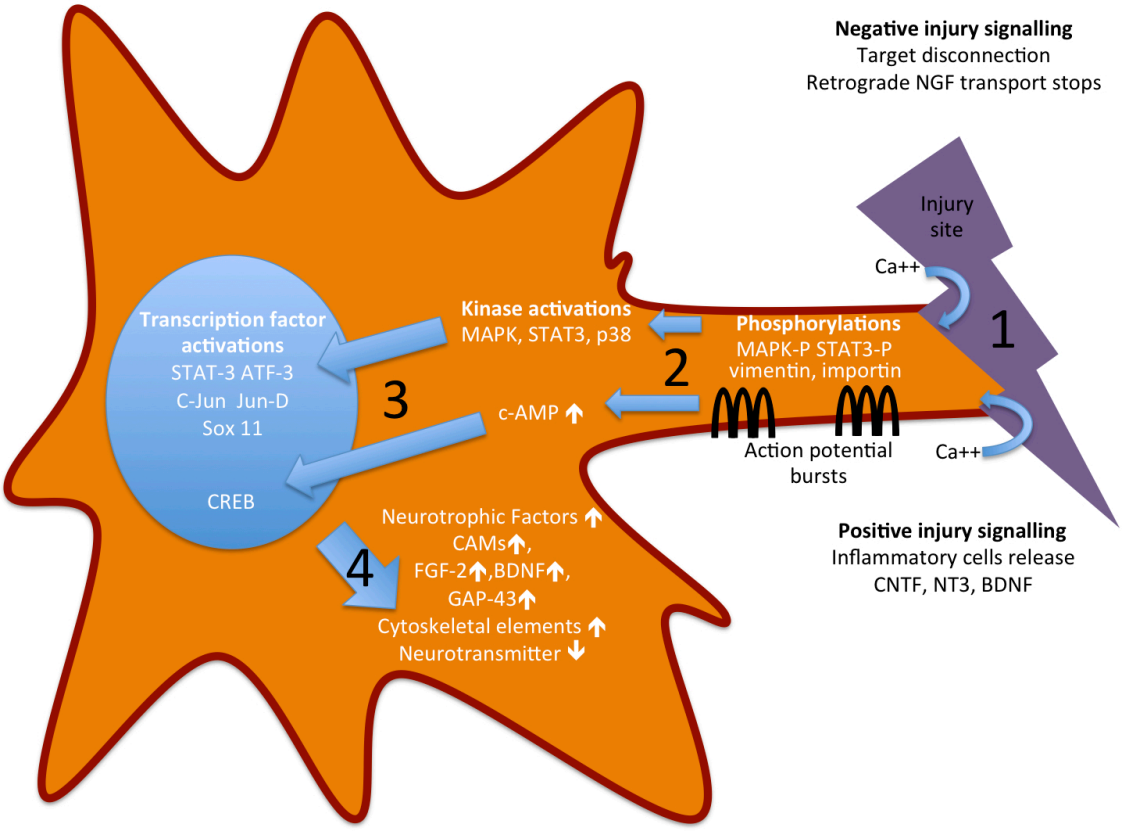

Figure 5: Early signalling in peripheral nerve injury. Calcium influx at the injury site triggers a burst of action potentials in the severed axon. The interruption of retrograde transport of trophic molecule, such as NGF from the previously innervated organ, and phosphorylation of proteins (MAPK, STAT, …) at the injury site followed by their active migration by importin and vimentin to the soma, switch the phenotype of the neuron into a regenerating mode. These positive injury signals activate transcription factors regulating the expression of regeneration-associated proteins such as GAP43 and BDNF. Adapted from Allodi et al. (2012).

Neuronal phenotype is affected mainly through the expression of transcription factors, which regulate expression of genes involved in nerve regeneration (Leah *et al.*, 1991, Herdegen *et al.*, 1993, Schwaiger *et al.*, 2000, Seijffers *et al.*, 2007). As an early response triggering these changes, local protein carrier like importins and vimentins are locally synthesised at the site of the injury, and by interacting with dynein allow retrograde

transport of phosphorylated mitogen activated protein kinase (MAPK) and of signal transducer and activator of transcription 3 (STAT3) (Hanz *et al.*, 2003). Thus in animal models, extracellular signal-regulated kinases (ERK) (Agthong *et al.*, 2006), cAMP-dependent transcription factor 3 (ATF3), Sex Determining Region Y (SRY)-Box 11 (Sox11) transcription factor, c-Fos, c-Jun, Jun-D (Herdegen *et al.*, 1997, Sheu *et al.*, 2000, Donnerer *et al.*, 2005, Jankowski *et al.*, 2009) are phosphorylated, co-localize in the nucleus, trigger the change of phenotype and regulate the expression of trophic factors in injured neurons. This jointly constitutes the so called “positive injury signalling” (Figure 5, Obata *et al.*, 2003, Lindwall and Kanje, 2005, Agthong *et al.*, 2009). Exposure of neurons to trophic factors, such as ciliary neurotrophic factor (CNTF), neurotrophin-3 (NT3), and brain derived neurotrophic factor (BDNF) which are secreted by inflammatory cells, activated Schwann cells, and fibroblasts at the injury site, are also triggers for the switch to the regenerative phenotype. For instance CNTF has been shown to induce the STAT3 signalling pathway during peripheral nerve injury in mice (Kirsch *et al.*, 2003, Allodi *et al.*, 2012).

As a consequence of the changed transcription factor profile after injury and during regeneration, neuroregulins are expressed differentially compared to the normal phenotype. Motor neurons show an increase in calcitonin gene related peptide (CGRP) expression, whereas in sensory neurons CGRP is down regulated together with substance P (Inaishi *et al.*, 1992, Kalous and Keast, 2010) when the retrograde transport of NGF to the soma is interrupted (Eriksson *et al.*, 1997, Shadiack and Zigmond, 1998, Shadiack *et al.*, 2001). BDNF (Kobayashi *et al.*, 1996, Kashiba and Senba, 1999) and fibroblast growth factor FGF-2 (Klimaschewski *et al.*, 1999) are over-expressed after injury in both sensory and motor axons. Neuropeptides like Galanin, neuropeptide Y and vasoactive intestinal polypeptides are also up-regulated after axotomy and might be involved in regenerative and survival process post injury (Villar *et al.*, 1989, Villar *et al.*, 1991, Zhang *et al.*, 1993). This switch to a regenerative phenotype also leads to an increase in the expression of actin, growth specific tubulin isotypes, growth-activated protein 43 (GAP-43) genes,

and a decrease in the expression of neurofilament, ion channels, and transmitter-related genes (Hoffman and Cleveland, 1988, Costigan *et al.*, 2002, Allodi *et al.*, 2012).

Additionally mammalian target of rapamycin (mTOR) over-expression, which also increases GAP43 levels after nerve injury until 3 to 4 days post injury, might be a regulator of the STAT pathway involved in axon regeneration. If mTOR is chronically over-expressed regenerating axons are misdirected (Rossi *et al.*, 2007, Park *et al.*, 2008, Abe *et al.*, 2010). Inhibition of phosphatase and tensin homolog (PTEN), a negative regulator of the phosphoinositol-3-kinase (PI3K) pathway, and an upstream inhibitor of the mTOR pathway, seems to increase the regenerative potential of axons independent of the state of mTOR activation (Christie *et al.*, 2009). Interestingly the PTEN and PI3K pathways also seem to be deeply involved in the mechanism by which endogenous electric fields can guide tissue regeneration in general (Zhao *et al.*, 2006).

1.2.2.2 Schwann cells phenotypic changes

Schwann cells have a crucial role in early and late peripheral nerve regeneration. They can have a myelinating or non-myelinating phenotype depending on the axon fibre they are supporting. When mature, differentiated Schwann cells are passively or actively detached from axonal fragments they easily switch back to a proliferative/progenitor phenotype.

As mentioned earlier one of the roles of Schwann cells in Wallerian degeneration is to secrete ILs and recruit inflammatory cells (Maruda, 2012). Originally between one to five days after injury distal Schwann cells migrate to the site of injury, proliferate for a few weeks, and bridge defects in nerve continuity, forming a solid column along the previous axonal pathways. These series of nucleated cellular cords are called bands of Büngner (Figure 4, Fawcett and Keynes, 1990). The expression of the transcription factor Krox20 is lost after injury (Ghislain *et al.*, 2002). This might be responsible for de-differentiation and proliferation through the activation of c-Jun expression

which seems to be a master switch activating the regenerative phenotype (Parkinson *et al.*, 2004, Arthur-Farraj *et al.*, 2012) Another mechanism leading to proliferative and regenerative state of Schwann cells is the over expression of human epidermal growth factor receptor 2 and 4 (HER-2 and HER-4), also a receptor of glial growth factor (GGF), in response to macrophage IL-1 (Li *et al.*, 1997, Hall, 2001, Allodi *et al.*, 2012).

Directional collective migration of Schwann cells out of the nerve stumps guiding regrowing axons across the wound has recently been shown to result from ephrin-B/EphB2 signalling between fibroblasts and Schwann cells (Parrinello *et al.*, 2010). Each band of Büngner acts like an interconnected cellular tube, and is a natural conduit for axonal regeneration. The tissue may stay in this activated state for months, even in absence of nerve regeneration but will then progressively atrophy and lose responsiveness to axonal ingrowth (Terenghi *et al.*, 1998, Johnson *et al.*, 2005).

The phenotype of denervated Schwann cells switches to a proliferative and ontogenic state in the distal stump, and is characterised by an up-regulation of NGF, glial derived neurotrophic growth factor (GDNF), BDNF, LIF, GAP-43 (Curtis, 1993), GGF receptor messenger ribonucleic acid (mRNA), CNTF, pleiotrophin (PT) neurotrophin-4 (NT4), and even vascular endothelial growth factor (VEGF) in case of nerve compression (Gillen *et al.*, 1997, Hammarberg *et al.*, 1996, Li *et al.*, 1997, Hoke *et al.*, 2006). The synthesis of these factors depends on the type of axons (motor or sensory) they were supporting. They also synthesize ECM proteins such as laminin, fibronectin, tenascin, and collagen (Carey *et al.*, 1983) until connected by the regenerating axons (Allodi *et al.*, 2012).

Thus Schwann cells are essential for the guidance and support of regenerating axons, and that interaction is principally regulated and controlled by GGF since it has been shown to be the most effective growth factors influencing Schwann cell proliferation and glial-neuronal cell interaction (Terenghi, 1999).

1.2.2.3 The regenerating growth cones and axonal elongation

Within 72 hours after injury axons begin to regenerate, and are stimulated by contact with, and chemotactic guidance provided by Schwann cells (Wang *et al.*, 2012). Multiple new small-diameter axons or axonal sprouts are created, which try to grow across the lesion at a rate of 0.25 to 1.0 mm per day. Those advancing cellular edges of the regenerating axons are termed the "growth cone" and are highly dynamic structures. These leading edges of axons sense the surrounding environment and their role is critical in reaching the distal end of the endoneurial tube of the nerve. A parent axon sprouts an average of 3 to over 10 daughter axons, which will atrophy and disappear if they cannot reinnervate any organ. A greater amount of neural death generally leads to greater sprouting, since there is less competition for access to the target (Allodi *et al.*, 2012). If the growth cones fail to find their way to the distal nerve stump because the gap is too large, or if the collagenous scar blocks them, they will form a neuroma (Figure 7, Peterson and Gordon, 2004).

There are three steps in growth cone movement: protrusion, engorgement, and consolidation (Mortimer 2008). Bouquet and Nothias divided the growth cone structure in three parts: the central domain that ends the axon is rich in microtubules (C-domain), and is separated from the peripheral domain (P-domain) along the edge of the growth cone that is rich in actin by a myosin rich transition zone (T-zone) (Figure 6). The most motile zone of the growth cone, the P-zone, shows filipodia that lead to an overall hand-shape form of this pushing and pulling structure (Figure 6, Heidemann *et al.*, 1990, Betz *et al.*, 2011, Koch *et al.*, 2012). In this P-domain, actin polymerization is the main motor of protrusion of the growth cone. By moving forward and by linking to the substrate it allows the extension of microtubules in the C-domain. Meanwhile myosin in the T-Zone contracts the actin network in a semi–circular shape. Thus the C-domain moves forward, strengthens the advance, and consolidates the direction of regeneration.

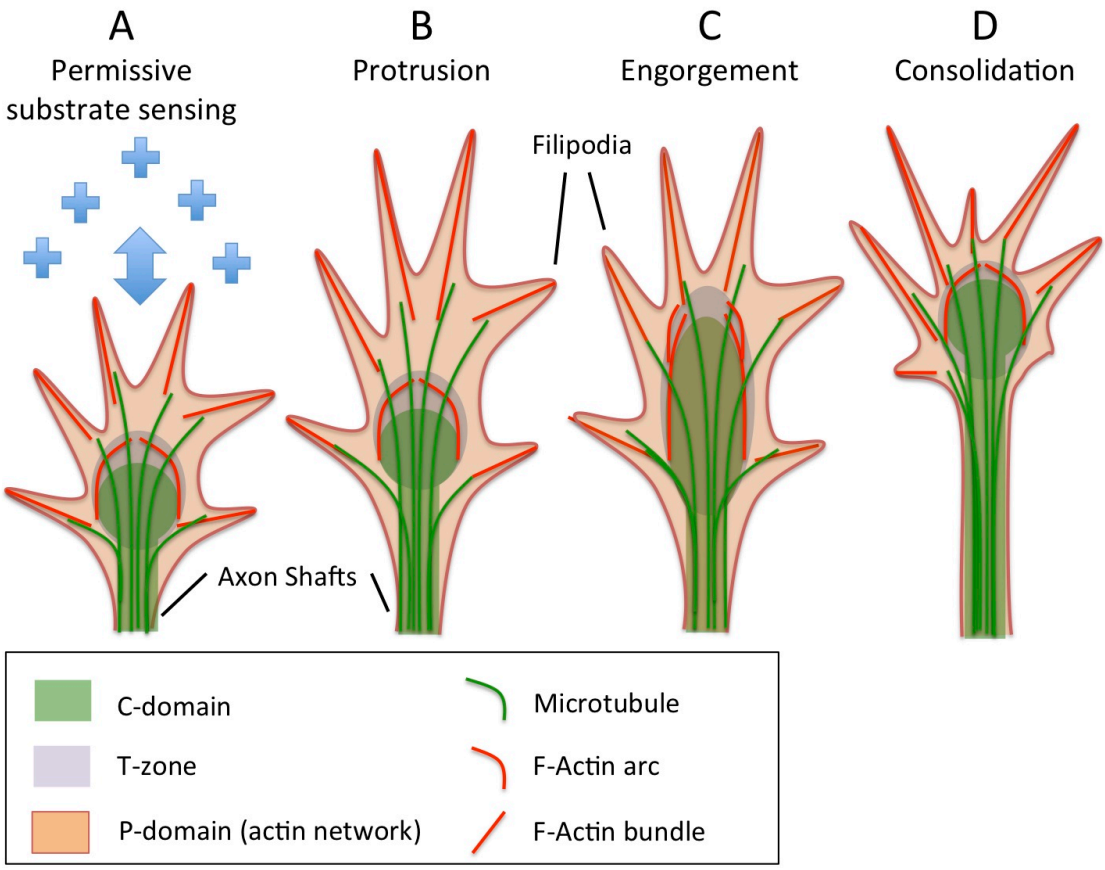

Figure 6: Growth cone elongation mechanisms.Growth cone receptors bind to substrate and link the substrate to the actin cytoskeleton (A). The protrusion step is the result of F-actin polymerization in the peripheral (P-domain) to form filopodia and lamellipodia-like structures that move forward (B). During engorgement phase, microtubules (MTs) are being synthetised forward and cross the transfer zone (T-zone) following the actin arcs and central domain (C-domain) actin bundles(C). The last step is a consolidation of the C-domain while the proximal part of the growth cone tightens to be the continuity of the current axon (D). A new C-domain is created by contraction of actin arcs by Myosin II resulting in compression of MTs. During this phase there is also a retraction of filopodia of the proximal which contribute to the consolidation of the new segment of axon shaft. Figure adapted from Lowery and Van Vactor (2009)

During the switch to the regenerating phenotype the number of expressed tubulin isoforms increases, whilst the quantity of actin, peripherin, and of neurofilaments decreases. The control of microtubule assembly and their incorporation in the axon cytoskeleton might involve calcium, cyclic nucleotides, microtubule associated proteins (MAPs), and Tau protein (Gordonweeks and Mansfield, 1991). MAPs are highly phosphorylated proteins (MAP1- MAP5) and lead to phosphorylation of other enzymes. GAPs- especially GAP43 in this case - are typically associated with regenerating axon phenotype (Skene, 1989, Allodi *et al.*, 2012).

Receptor complexes at the growth cone tip can also activate GTPases and cytoskeletal proteins that are essential for the contractility of the actin-myosin network. Rho-associated kinases have been shown to have an important role in growth cone elongation by upstream signalling of small GTPases of the Rho family (Luo, 2002) and Rho-associated kinases (ROCKs), as well as activation of these pathways by neurotrophins and laminin. Lipid rafts are perceived to amplify these signals for growth cone elongation (Guirland *et al.*, 2004, Fujitani *et al.*, 2005, Allodi *et al.*, 2012).

Dorsal roots or other sensory ganglia axonal sprouts extend their filopodia that will explore and bind with integrin receptors ($\alpha_1\beta_1$, $\alpha2\beta1$, $\alpha3\beta1$, $\alpha4\beta1$, $\alpha5\beta1$, $\alpha6\beta1$, $\alpha7\beta1$) to ECM molecules such as collagens, laminins and fibronectin, which are secreted by Schwann cells and fibroblasts (Tomaselli, 1991, Vogelezang *et al.*, 2001, Ekstrom *et al.*, 2003, Gardiner *et al.*, 2005, Gardiner *et al.*, 2007). Motorneurons have a different subset of integrins ($\alpha3\beta1$, $\alpha6\beta1$, $\alpha7\beta1$) to do so (Pinkstaff *et al.*, 1998, Werner *et al.*, 2000, Hammarberg *et al.*, 2000) and preferentially form adhesions on laminin (Horstkorte and Fuss, 2012).

Once the endoneurial tube is reached, axonal sprouts continue to grow and aim to reinnervate the tissue that was de-innervated (Johnson *et al.*, 2005). After a period of competitive dieback, only a single axon will regenerate down each endoneurial tube in the distal stump towards the end-organ target. These freshly regenerated axons are initially unmyelinated but induce adjacent Schwann cells to proliferate and initiate myelin formation around the axon as it regenerates (Figure 4).

When a regenerating axon has found found its target organ, it gradually increase in thickness, driven mainly by an increase in the expression of nestin, peripherin, vimentin and other neurofilaments. The axonal diameter and thickness of the myelin sheath of the regenerated neurons usually does not reach normal/pre-injury levels, even though they increase after contact with the target organ. This is another factor contributing towards complete

functional recovery being very rare (Johnson *et al.*, 2005, Allodi *et al.*, 2012).

1.3 Nerve regeneration problems and limits

Due to the complexity of peripheral nerve, which are generally mixed (motor and sensory axons), there is an inevitable inaccuracy during the attempted return of an axon to its original target and a low rate of successful reconnections due to axotomy (Hart *et al.*, 2008). Schwann cell modalities, fibre diameter and innervations are different for motor and sensory nervous pathway (Moradzadeh *et al.*, 2008, Daly *et al.*, 2012) and regenerating axons are not specifically guided to their previous endoneurial tube.

The lack of specificity of regenerating axons changes the alignment of the bodily representation of the temporarily deafferented motor and sensory unit by an encroachment of neighbouring neurotomes. Due to cortical plasticity it can be overcome by reinterpretation, the reversal and re-establishment of the neurotomes when the peripheral target has been re-connected (Ebel *et al.*, 2000).

Target reinnervation (e.g muscle or sensory organ) is a slow process, and relates directly to the distance from the site of injury to the target organ. Without being able to stimulate a target organ, or receive primary sensory input, neural cell bodies will atrophy and eventually die (Rich *et al.*, 1987, Hart *et al.*, 2008). Neurotrophic stimulation is necessary to retain dennervated target sites viable and to prevent their atrophy (Johnson *et al.*, 2005). In absence of quick reinnervation muscle atrophy start after few weeks and becomes irreversible after 12 to 18 month (Campbell, 2008). That is why Mackinnon (1989) demonstrated better clinical outcome after immediate nerve repair.

After loosing contact with a peripheral nerve, skin, sweat glands as well as sensory organs atrophy. In an animal model of PNS injury Merkel's discs

(sensing touch) disappeared after one month, Meissner's corpuscles (sensing light touch) degenerated after 6 months, and Pacinian corpuscles (sensing pressure) ten months after denervation (Burgess *et al.*, 1974, Zelena, 1982, Hart, 2011). In case of unsuccessful reinnervation a permanent loss of intra-epidermal fibres (sensing temperature, pain, pressure) is also observed.

Another mechanism due to the response of the fibroblasts contained within the endoneurium to the inflammatory molecules released after nerve transection injuries impair peripheral nerve regeneration. These fibroblasts migrate to the injury site, proliferate and produce a collagenous scar that acts as a barrier and misdirect or block axonal regeneration and which size depends on the length of injury gap. Such deviated axons are either cleaved or grow into a disorganised mass called a neuroma (Figure 7, Sinis *et al.*, 2007).

The endogenous static electric fields due to Potassium and Sodium ion gradients across wounded tissues, which guide nerve sprouting (Song *et al.*, 2004), can also have an adverse effect by misdirecting the severed axons, This aspect of nerve regeneration problem is more detailed below in section 1.7.

In the distal stump if denervation is chronic, Schwann cells that are not in contact with an axon or a neuron slowly shrink in diameter. Without receiving a regenerating axon, Schwann cells lose their capability to support regenerating axons. They become unresponsive to GGF by down-regulation of its receptor after two to six month, and are progressively surrounded and replaced by fibrous tissue, a phenomenon termed endoneurial fibrosis (Sulaiman and Gordon, 2000, Mirsky *et al.*, 2002).

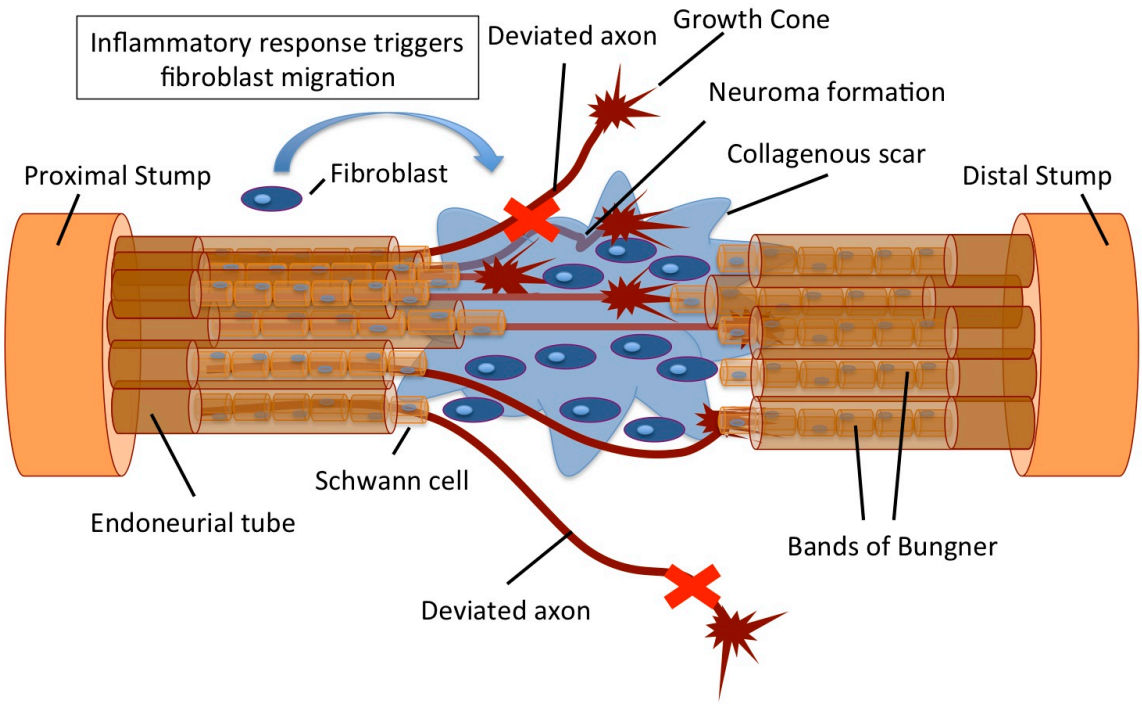

Figure 7: Scar formation during nerve regeneration. Fibroblasts proliferate and produce a collagenous scar around the nerve trunk during the repair and remodelling phases. This collagenous scar acts like a barrier and deviates or blocks axonal regeneration by misdirecting sprouting axons that cannot find their target or can no longer get into contact with a Schwann cell conduit. Such axons are either cleaved or grow into a disorganized mass called a neuroma.

1.4 Clinical challenges

Nerve reconstruction remains a great challenge. The PNS is more subject to injury than the CNS because bones and cartilage do not protect it. In Europe and in the US there are more than 300 000 cases of major peripheral nerve injury are reported per year (Wiberg and Terenghi, 2003). Brachial plexus injury, congenital reconstruction, nerve tumours and palsy are also big challenges for clinicians and researchers. Different clinical options for nerve reconstruction are available depending on the type of injury, the gap length and the tension of the nerve (Siemionow and Brzezicki, 2009):

If the injury is clean and sharp and presents no nerve tissue loss, and minimal tension when the nerves stump are approximated, immediate direct

neurorraphy (also called end-to-end repair) or epineurial sleeve repair are the two surgical options. If the proximal end is unavailable (e.g. due to avulsion) end-to-side repair tubulisation or nerve transfer are the current surgical options.

In the case of a short gap injury (1-2 cm) epineurial and fascicular repair are possible for end to side suture. For long gap injuries, nerve grafts have been the gold standard so far and particularly the autologous graft. This is not an ideal treatment, because of the problem of the denervation of the tissue the donor nerve was supporting. That is why the development of nerve conduits for the treatment of peripheral nerve injury is important. Even in the best cases regeneration is still slow, on the order of 1mm per day. There is also a loss of the half of the axonal ingrowths into the distal stump if there is a delay in repairing the nerve injury (Hart, 2011).

If the patient status is too severe, if nerve contusion and tension are the cause of the nerve injury, or if the wound is infected, the nerve repair is delayed to allow spontaneous recovery and evaluation of the remaining nerve function (Siemionow and Brzezicki, 2009).

If the tension required to apposite the stumps for an end-to-end repair is too high and the gap length is longer than 3 cm, vascularised nerve transfer or a nerve autograft mostly using the sural nerve is the best surgical option. If the gap length is inferior to 3 cm vein grafts or nerve conduit tubulisation are options.

These later three would be sutured to the ends of the severed nerve to bridge the injury gap, sometimes together with the use of fibrin glue (Siemionow and Brzezicki, 2009, Schonauer, 2012).

The clinical challenge for clinician and tissue engineer is due to the limits of these clinical options. Autografts are limited to a transfer of 5 cm, generally of the sural nerve, and allografts, used for longer gap injury, require immunosuppressive treatment for up to 18 month. Both increase

healing time, because the host macrophages need first to enter and remove the existing myelin from the graft, before regenerating axons will readily enter (Daly *et al.*, 2012).

1.5 Designing nerve repair conduits

Nerve repair conduits are a good alternative for autologous nerve graft repair, which has the associated problem of an added intervention as well as damage to the donor site. Even if many nerve tubes are being marketed, it is hard to identify, choose and combine those properties needed to increase the efficiency of the currently used conduits. However it is now clear that factors, such as biomaterial properties, milli/micro/nanostructure, supporting cells, growth factors, electrical stimulation or guidance and synergistic interactions between these design parameters will improve the regenerative potential of nerve conduits. (Figure 8, Pfister *et al.*, 2007, Rosson *et al.*, 2009).

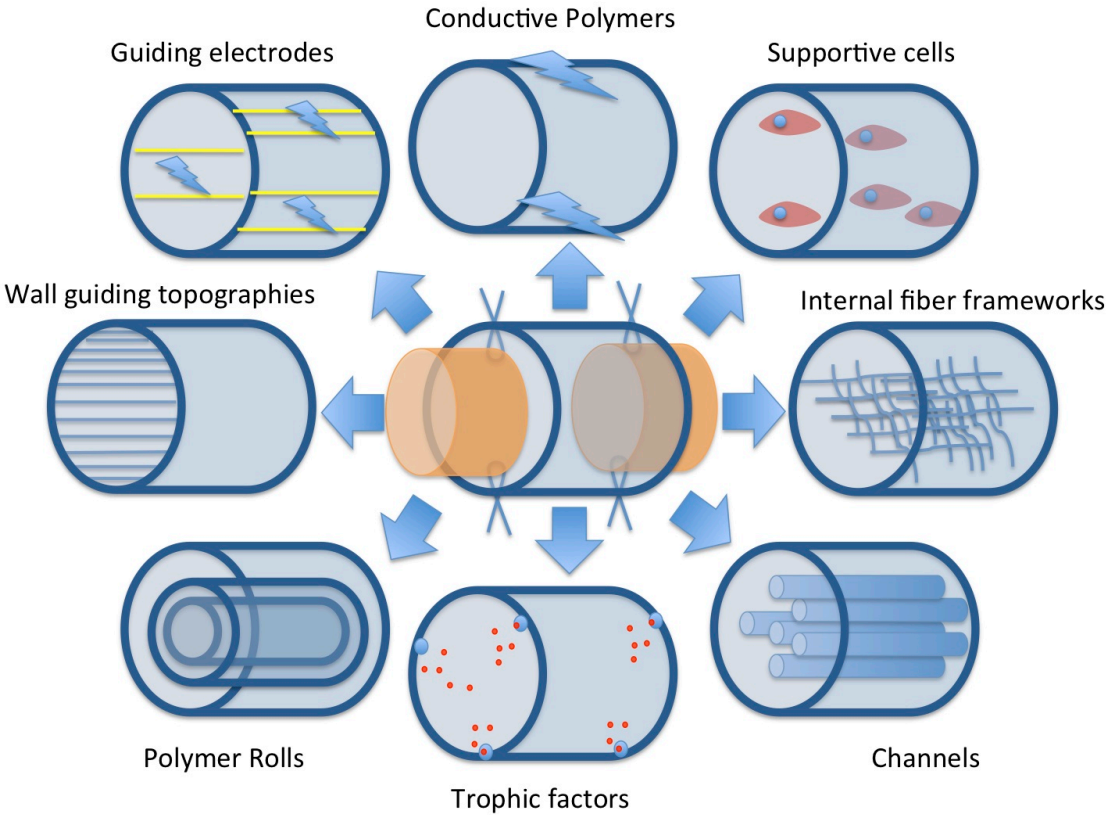

Figure 8: Different strategies to aid repair in nerve guidance tube design. Properties and modification of the common hollow nerve tube like porosity of the biomaterial, growth factors releasing systems, internal frameworks, pre-seeding with supportive cells, multichannel structure and use of conductive polymer are being investigated. Progress in this field may increase the injury gap that can be bridged.

The choice of biomaterial is generally the first step when designing a conduit because it forms the stable backbone of the construct. It is important that the chosen material is neither toxic nor triggers an immune response. It also has to be biodegradable to avoid both compression and constriction around the regenerated nerves, as well as a second intervention to remove any non-degrading conduit. The physical properties such as permeability, flexibility, and swelling are important factors that can influence regeneration area, tissue interaction, effective cell supports, and drug release.

1.5.1 Biomaterials

There is a wide range of existing polymers approved for medical use, with different physical properties. The main polymers and co-polymers investigated in the context of peripheral nerve tissue engineering are poly(3-hydroxybutyrate) (PHB) (Young *et al.*, 2002), polylactic acid (PLA) (Hurtado *et al.*, 2011) and polyglycolic acid (PGA) (Ito *et al.*, 2003) and their composites poly(lactic-co-glycolic acid) (PGLA) (Mackinnon and Dellon, 1990), polycaprolactone (PCL) (Sun *et al.*, 2010, Donoghue *et al.*, 2013), poly-lactide-co-caprolactone (PCLA)(Dendunnen *et al.*, 1993, Gartner *et al.*, 2012, Luis *et al.*, 2008) polyphosphazen (Langone *et al.*, 1995), polytetrafluoroethylene (PTFE) (Stanec and Stanec, 1998, Miloro and Macy, 2000, Vasconcelos and Gay-Escoda, 2000), bioglass (Bunting *et al.*, 2005), poly(2-hydroxyethyl methacrylate-co-methyl methacrylate)(PHEMA-MMA) hydrogels (Atzet *et al.*, 2008), gelatin and collagen (Cirillo *et al.*, 2012, Yang *et al.*, 2011, Mligiliche *et al.*, 1999, Gamez *et al.*, 2004) and, chitin (Yang *et al.*, 2009, Zhang et *al.*, 2005). Their characteristics are summarised in Table 2.

Permeability of the polymer is important because *nutrients*, cellular waste, oxygen, and growth factor must be able to diffuse across the conduit before and during vascularisation, which in a construct of 2mm thickness takes 1 to 2 weeks to arrive at the centre to then directly supports cellular survival (Singh *et al.*, 2011). The conduit ought to permit and support the migration of supportive cells and allow their survival. Different techniques are available to obtain the desired permeability for oxygen, nutrients and waste. The simplest one would be to cut holes into the walls of the tubes. Polymer spinning and rolling of meshes to form a Swiss roll is also commonly used. Sugar or salt crystal leaching after fabrication, and injection moulding or casting followed by solvent evaporation in order to obtain foams or frameworks are also efficient techniques to introduce porosity. Finally another important property of the polymer is its hydrophilicity, as it determines cell adhesion. The hydrophilicity of polymers – which are in their

natural state quite hydrophobic (water contact angle, WCA≥70°) can be improved by plasma treatment, which can be used to increases surface charge by exposure of the surface to the desired radicals (e.g. NH_x•, O•, OH•, COOH•) in the plasma reducing the WCA (≤60 °)(Garcia *et al.*, 2010).

Long gap injuries (> 2 cm) require nerve tubes that have enough flexibility to allow for movement, and stabilisation against kinking. The chosen polymer and fabrication technique must allow a good compromise between pliability, porosity of the conduit, and other design parameter such as presence of an internal framework, thickness and the diameter of the lumen. A problem that arises, and needs to be considered when designing longer tubes is that when bent (e.g. in fingers crossing joints) kinking can obliterate any free volume in the centre of the conduit.

Table 2: Most widely studied materials for nerve conduits with related properties and selected studies where they were used. Modified from Pfister et al. (2007) with permission.

Nerve Conduit Material	Characteristics	References
PDMS: polydimethylsiloxane	Highly elastomeric polymer, not biodegradable, bioinert, impermeable, hydrophobic, oxygen permeable	Lundborg *et al.* (1982a); Braga-Silva (1999)
Collagen: structural protein	Protein, enzymatically degradable, good cell interactions, can be chemically cross-linked, approved by the Food and Drug Administration (FDA)	Archibald *et al.* (1991; 1995); Li *et al.* (1992); Krarup *et al.* (2002)
PGA: polyglycolic acid	Aliphatic polyester, impermeable, biodegradable by hydrolysis, approved by FDA	Weber *et al.* (2000); Battiston *et al.* (2005)
PHB: poly(3-hydroxybutyrate)	Aliphatic polyester, biodegradable by hydrolysis, approved by FDA	Young *et al.* (2002); Mosahebi *et al.* (2003)
PLA: polylactic acid	Aliphatic polyester, very slowly biodegradable by hydrolysis	Widmer *et al.* (1998); Evans *et al.* (2000)
Chitosan: ß-(1-4)-linked D-glucosamine	Polysaccharide, enzymatically degradable, positively charged, permeable,good cell interactions	Itoh *et al.* (2003); Yamaguchi *et al.* (2003)
Polyester urethane	Elastomeric polymer, impermeable,biodegradable	Borkenhagen *et al.* (1998)
PHEMA-MMA: poly(2-hydroxyethyl methacrylate-co-methyl methacrylate)	Hydrogel-forming polymer, not biodegradable, stiffness in the range of nerve tissue	Dalton *et al.* (2002); Belkas *et al.* (2005)
PCL: Polycaprolactone	Aliphatic Polyester, biodegradable, FDA approved	Sun *et al.* (2010); Sun *et al.* (2011); Donoghue *et al.* (2013)
PPy: Polypyrolle	Conductive,impermeable, not biodegradable	Shi *et al.* (2004), Wang *et al.* (2004); Zhang *et al.* (2007); George *et al.* (2009); Zhang *et al.* (2010)
PEDOT: poly(3,4-ethylenedioxythiophene)	Conductive, impermeable, not biodegradable	Abidian *et al.* (2012)
Polyphosphazen	Conductive,impermeable, biodegradable	Langone *et al.* (1995); Zhang *et al.* (2010)

1.5.2 Polymer bioresorption

Degradation and bioresorption of the material of the conduit is important for many reasons. Biodegradable materials are mainly ones that contain molecular bonds that are hydrolysable such as esters. They swell in water-based solutions allowing access of water molecules into the material. A huge advantaged is that degradation and bioresorption of the polymeric implant will eliminate the need for a second surgery. A polymer scaffold should protect the injury area against mechanical stresses, provide a suitable surface for cell attachment and growth, degrade at a rate that avoids constriction and compression of the new tissue, and not release detrimental molecules whilst degrading. The mechanical properties should also approximate those of the tissue. The most commonly used degradable biomaterials to create nerve tubes are PLA, PGA and their composites or co-polymers PGLA, PCL, collagen, gelatine, chitin and polyphosphazen (Table 2, de Ruiter *et al.*, 2009).

Bioresorption of polymers with and aliphatic-ester in aqueous media occurs within two steps. Firstly water penetrates the bulk of the material (Das *et al.*, 2011), the chemical ester bonds are attacked and long polymer chains are broken into shorter and shorter and in the end water-soluble fragments. The second step metabolisation and erosion begins thereafter. This mechanism of material clearance is possible if the monomerisation reaction is slower than the rate of water penetration into the bulk polymer. It is important to choose a polymer, which slowly degrades and allows transfer of stress at the appropriate rate to the surrounding tissues as they heal. To do so it is necessary to balance the chemical stability of the polymer backbone, the three-dimensional geometry of the device, the surface to volume ratio, and surface treatments that might influence water penetration into the bulk polymer. There are additional factors such as the mechanical strain that the device is exposed to, the fabrication technique used to create the device, and the chemical nature of the environment in the body (redox

state and/or oxygenation state of the tissue) that influence degradation time, stress transfer and resilience of the device (Das *et al.*, 2011).

1.5.3 Conductive polymers

Electrical stimulation has a positive effect on nerve regeneration, axonal guidance and elongation, and supportive cells (Borgens *et al.*, 1990, Brushart *et al.*, 2002, Alexander *et al.*, 2006, Lu *et al.*, 2008, Huang *et al.*, 2010). Thus the ideal polymer to design a peripheral nerve conduit should either be conductive, or allow to be modified such that layers of conductive polymer can be added. At the moment conductive polypyrrole (PPy) polymer or copolymer conduits have been investigated but most of these are non-biodegradable even if they provide a good way to apply electrical stimulation (Shi *et al.*, 2004, Wang *et al.*, 2004, Zhang *et al.*, 2007, George *et al.*, 2009, Zhang *et al.*, 2010).

More recently solution-processed melanin thin films (0.341 nm roughness, $7.00 \pm 1.10 \times 10^{-5}$ S cm^{-1} conductivity) have been used as a biodegradable semiconducting biomaterial for use in tissue engineering applications. Melanin thin films enhanced Schwann cells growth and neurite extensions compared to collagen films *in vitro* and have been resorbed within 8 weeks (Bettinger *et al.*, 2009).

Additionally synthetic strategies were developed to synthesise novel electrically conductive biodegradable polyphosphazen polymers containing parent aniline pentamer (PAP) and glycine ethyl ester (GEE). The electrical conductivity of the polymer was similar to melanin at 2×10^{-5} S cm^{-1}, making this also a semiconductor. The polymer is biodegradable, allows cell adhesion, and proliferation. It also shows good solubility in common organic solvents, and good film-forming properties. This novel polymer now needs further study *in vivo* as to further develop its applicability for scaffolds for PNS regeneration (Langone *et al.*, 1995, Zhang *et al.*, 2010).

Copoplymers of conductive poly(3,4-ethylenedioxythiophene)(PEDOT) and agarose are also studied for use in peripheral nerve tissue engineering use (Abidian *et al.*, 2012).

1.5.4 Macro fabrication technique

There are plenty of methods to build a polymer conduit and its internal framework if needed. Here I will just focus on the most commonly used techniques. Some means to make nerve tubes are commonly used e.g. woven fibres in the shape of a conduit (Yoshitani *et al.*, 2007). Melt-extrusion, moulding (Widmer *et al.*, 1998), unidirectional freezing (Bozkurt *et al.*, 2007, Hu *et al.*, 2009), and electro spinning (Cirillo *et al.*, 2012) are more sophisticated fabrication techniques.

1.5.4.1 Melt processes

Biodegradable polymers are usually melt-processed by conventional techniques such as compression or injection moulding and extrusion (Chiono *et al.*, 2009). In most biodegradable polymers a thermodynamic equilibrium exists between the polymerisation reaction and the reverse reaction that results in monomer formation. This equilibrium can be shifted by temperature. Thus it is important to avoid an excessively high processing temperature that may result in monomer formation during the moulding and extrusion process. At the scale of a nerve conduit, a micro-fabricated mould designed by lithography or electron beam lithography might be necessary (Seunarine, 2008). Electro-spinning is another commonly used process (Lee *et al.*, 2011, Croisier *et al.*, 2012, Cirillo *et al.*, 2012): an electrical charge draws very fine (micro or nano scale) fibre of dissolved, or molten polymer and accumulates these on the surface of an oppositely charged metal, semiconductor sheet, or mandrill, which are used as internal scaffold forming the free space within the conduit. Thin biomaterial sheet formation by spin-coating of a polymer solution on a silicon wafer, followed by a micro/nano-structure hot-embossing and a rolling step is also a commonly used melt-

process to fabricate so-called “Swiss-rolls” conduit (Chapter3, Seunarine, 2008, Donoghue *et al.*, 2013).

1.5.4.2 Unidirectional freezing

Unidirectional freezing was used e.g. to form a chitosan/collagen scaffold with aligned organised micrometric pores. The first step is to obtain a homogenous solution of the biopolymers and to solidify it. The solution is then degassed under a vacuum and injected into a hollow, cylindrical copper mould. The mould is vertically placed in a nitrogen canister with the bottom of the mould at 20cm above the liquid nitrogen surface. The mould is then slowly dipped in the liquid nitrogen at a slow velocity ($2x10^{-5}$m/s) until the complete solution is immersed. The next step is a lyophilization of the solution in a freeze dryer for 24 h. After the removal of the mould the scaffold is cross linked with a 1 % (wt/wt) solution of genepin for 48 h and sterilized by γ-irradiation (^{60}Co) and ethanol (Bozkurt *et al.*, 2007, Hu *et al.*, 2009).

1.5.5 Natural and synthetic scaffolds

Considering tissue engineering, scaffolds are very important. To enhance regeneration and nerve guidance by the stabilization of the fibrin matrix, different shapes and sizes of scaffolds have been investigated, such as sponges, denatured muscle tissue, vessels or fibres. The aim of these scaffolds was to provide more surface area for cell attachments, orient the cells and potentially locally release growth factors. Additionally the microarchitecture modifies the physical properties of the conduit affecting permeability, and flexibility, and influences the cross-section available for nerve growth. Additionally better results have been achieved when the interior of the conduit had been coated with adhesion promoting substances or proteins be that non-specific ones such as poly-L-lysine (PLL), or specific ones such as gelatin, collagen, or laminin (Bruder *et al.*, 2007, Atzet *et al.*, 2008, Cao *et al.*, 2009, Li, 2010, Kuppan *et al.*, 2013).

1.5.6 Grooved surfaces

Grooved frameworks have been used to guide astrocyte and neurites e.g. in *in vitro* models of the CNS and PNS with success (Sorensen *et al.*, 2007, Sun *et al.*, 2010, Donoghue *et al.*, 2013), and for aligned fibroblast growth (Rajnicek *et al.*, 1997). Microgrooves provide a good shape to align neurites, and around 12.5 µm width and 5µm depth seems optimal. In legacy of Seunarine (2008) it is the microtopography selected to work with in this study as it is relatively easy to fabricate. More details about the use of this fabrication process will be given in Chapters 2, 3, and 5.

1.5.7 Fibres

Fibres (Figure 8, Figure 9), especially laminin-coated ones have been shown to be extremely potent neurite-extension promoting agents in vitro (de Ruiter *et al.*, 2009). The effect of laminin on the regeneration of axons *in vivo*, using a cord of polyester fibres coated with laminin as a guide to replace a 10-mm segment of the rat sciatic nerve was followed by transmission electron microspocy TEM after four weeks. The study showed that many regenerated axons were seen in the laminin-coated group, whereas no axons were observed in the non-coated controls (Yoshii *et al.*, 1987).

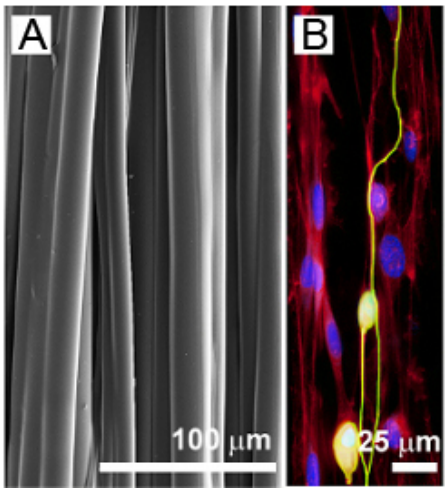

Figure 9: Example of the use of fibre structures in nerve tissue engineering.The fibrous structure of nerve tissue has inspired bio-engineer to create microtubular polymeric arrays which mimic the oriented nature of peripheral nerves (A). (B) DRG neuron (green) and Schwann cell (red) co-cultures are aligned on tubules depicted in (A); cell nucleus are coloured in blue. From (Li, 2010) with permission

Furthermore, pronounced Schwann cell alignment has been shown on ultrathin, continuous PCL filaments with longitudinal microgrooves. Precoated PCL filaments proved to be non-cytotoxic and displayed good cell attachment, and supported Schwann cell proliferation as well as guided axonal outgrowth. Polarized expression of the Schwann cells adhesion molecule L1 similar to that seen in vivo in bands of Bunger after sciatic nerve crush in adult rats has been observed in vitro on these PCL filaments. These results show that bioengineered bands of Büngner, are a good approach to initiate an efficient nerve regeneration across longer gaps (Figure 9, Ribeiro-Resende *et al.*, 2009, Li, 2010).

1.5.8 Channels

Even if grooved surfaces and filaments have been successfully fabricated and are capable of physically guiding linear outgrowth of regenerating axons, they still differ from the guiding principle of the basal lamina micro channels in nerve autografts, which are the gold standard to heal peripheral nerve injuries. Scaffolds with dimensions of the basal lamina micro channel made of a copolymer of chitosan and collagen have been investigated in a very recent study and these show really promising results which suggest that such

a micropatterned scaffold could be used as an alternative to nerve autografts for peripheral nerve regeneration (Hu *et al.*, 2009).

1.5.9 Supportive cells

1.5.9.1 Schwann cells

As mentioned earlier, Schwann cells are essential for the mechanism of peripheral nerve because they coordinate and guide the natural regenerative process (Arthur-Farraj *et al.*, 2012, Allodi *et al.*, 2012). Thus autologous Schwann cells are the gold standard as supportive cells inside a nerve repair conduit. In animal model Schwann cell have been successfully cultured and implanted using nerve repair conduit and scaffolds *in vivo* (Hadlock *et al.*, 2000, Kim *et al.*, 2007, Kalbermatten *et al.*, 2008, Georgiou *et al.*, 2013). These studies are good examples of the tissue engineering principle applied to peripheral nerve repair. They demonstrated the efficiency of preseeded Schwann cells to improve nerve regeneration across large gap model (10 to 15 mm in rat) in terms of morphological and electrophysiological outcome measures, as well as functionality scores.

Another interesting tissue engineering approach used genetically modified Schwann cells over-expressing NGF and BDNF in the spinal cord injury rat model have shown promising results to improve axonal regeneration strategies (Feng *et al.*, 2005).

1.5.9.2 Olfactory ensheathing cells (OECs)

First considered as Schwann cells of the olfactory system because of their location ensheathing axons connecting the sensory epithelium of the nose to the CNS, and their morphology, they were found to be a different cell type sharing some similarities with astrocytes of the CNS such as glial fibrillary acidic protein expression (GFAP) but also receptor to the low affinity NGF receptor specific to non-myelinating Schwann cells (for review see Higginson and Barnett (2011)). In principle OECs have a similar role to Schwann cells

but they are specialised to ensheath the axons of the olfactory receptor neuron. They have a higher proliferation rate than Schwann cells, which makes them a good candidate to support nerve regeneration. In animal models they have been implied as an alternative to Schwann cells that can be transplanted to improve outcomes in peripheral nerve injury (Verdu *et al.*, 1999, Franklin and Barnett, 2000, Fodor *et al.*, 2002, Pascual *et al.*, 2002, Li *et al.*, 2003, Radtke *et al.*, 2009, Chiono *et al.*, 2009, Guerout *et al.*, 2011) and also in CNS injury (Ramer *et al.*, 2004).

1.5.9.3 Stem cells

The following three types of stem cells have been shown to have a positive effect on nerve regeneration: neural stem cells, mesenchymal stem cells and adipose derived stem cells (Terenghi *et al.*, 2009, Walsh and Midha, 2009).

In 1992, the discovery of cells that have the potential to differentiate into neurons, astrocytes, and oligodendrocytes ended the dogma that neurogenesis stop after birth, and gave rise to the acceptance of neural stem cells (NSCs). These cells the ability to populate or repopulate a degenerated or damaged region of the nervous system (Reynolds and Weiss, 1992). Tissue engineering studies have shown that NSCs offer great regeneration potential because of their multipotency, strong plasticity, high migration ability. They can self-renew and be continuously transplanted. When they were used in chitosan conduits together with NGF to bridge 10-mm facial nerve defects in rabbit they promoted regeneration (Parker *et al.*, 2005, Zhang *et al.*, 2008). They have also been genetically modified to over express glial cell-line derived neurotrophic factor (GDNF) and BDNF to improve PNS regeneration (Heine *et al.*, 2004, Fu *et al.*, 2011).

When mesenchymal stem cells (MSCs) were placed in nerve the injury sites are induced to express morphological, molecular and functional phenotypic markers of Schwann cells. Once differentiated, MSCs can myelinate axons and act like Schwann cells. They also synthesise and secrete

neurotrophins, and they have been shown to up-regulate myelin gene and protein expression when they were co-cultured *in vitro* with neuronal cells (Tohill *et al.*, 2004, Caddick *et al.*, 2006, Mahay *et al.*, 2008, Brohlin *et al.*, 2009). A study by Oliveira *et al.* (2010) shows that they improve nerve regeneration in a polycaprolactone nerve conduit preseeded with MCSs *in vivo*.

Contrary to NSCs and MSCs, Adipose derived stem cells (ASCs) are available in large number by lipo-aspiration (e.g. 2 % ASC of cells in fat and 0.001 % of MSC in bone marrow), which could address the problem of the need for rapidly available large numbers of cells (Kingham *et al.*, 2007). In rats, ASCs proliferate at a faster rate than MSCs and can express all the markers found in Schwann cell as demonstrated by Tholpady *et al.* (2003) and Kingham *et al.* (2007). ASCs thus potentially form a plentiful source of new Schwann cells. ASC derived Schwann cells have enhanced peripheral nerve regeneration in recent studies and are one of the most promising strategies for the improvement of nerve regeneration (di Summa *et al.*, 2009, Georgiou *et al.*, 2012).

1.5.10 Neurotrophic factors and neuroprotective molecules

Growth factors are key factors in regeneration and tissue engineering. In the area of the nerve regeneration the effect of growth factors on cell functions that promote regeneration is of major interest. The factor that determines the rate of axotomy-induced cell death is the loss of distal bi-directional neurotrophic support, e.g. the retrograde transport of NGF picked up from target cells to neuron soma (Allodi *et al.*, 2012). The challenge is to improve nerve regeneration, mimicking and enhancing the effect of the natural process in which growth factors play a crucial role, by including the use of these factors in the design of the nerve repair tube.

Among the different neurotrophic factors NGF, BDNF, GDNF, NT-3, are those suggested to be the best candidates to be used in combination with

nerve conduits (Table 3, Hamburger *et al.*, 1981, Pean *et al.*, 1999, Groves *et al.*, 1999, Piantino *et al.*, 2005, Gibbons *et al.*, 2005, Vogelin *et al.*, 2006). CNTF, Insulin-like growth factor (IGF-1), FGFs, LIF and have been shown to have a greater effect on promoting regeneration than on neuroprotection (Walter *et al.*, 1993, Ho *et al.*, 1998, Grothe and Nikkhah, 2001, Fansa *et al.*, 2002, Hart *et al.*, 2003, Ohta *et al.*, 2004).

As the effect of neurotrophic factors are often dose dependant and requires constant release over extended periods of time, slow release systems such as hydrogels, absorption to fibronectin mats (Ahmed *et al.*, 1999), collagen matrices (Ho *et al.*, 1998), bovine serum albumin (BSA) or microspheres (Gu, 2012) have been used in nerve tissue engineering.

Delivery of trophic factors via natural or synthetic nerve conduit has also been widely investigated (Table 3, Pang *et al.*, 1993, Santos *et al.*, 1998, Trigg *et al.*, 1998, Smith and Browne, 1998, Ahmed *et al.*, 1999, Bryan *et al.*, 2000, Sulaiman and Gordon, 2002, Midha *et al.*, 2003, Wang *et al.*, 2003, Xu *et al.*, 2003, Gravvanis *et al.*, 2004, Li *et al.*, 2008, Dodla and Bellamkonda, 2008, Chang, 2009a, Shakhbazau *et al.*, 2012)

Table 3: Growth factors used in peripheral nerve regeneration studies, their putative targets, and selected studies where these factors were used. Adapted from Pfister et al. (2007) with permission.

Growth factor	Major target	References
NGF: nerve growth factor	Sensory neurons, small axons	Pang *et al*. (1993); Santos *et al*. (1998); Ahmed *et al*. (1999); Xu *et al*. (2003); Gravvanis *et al*. (2004); Lee *et al*. (2006); Dodla and Bellamkonda (2008); Chang (2009a)
NT-3: neurotrophin 3	Sensory neurons, small- and medium-size axons	Shakhbazau *et al*. (2012)
BDNF: brain-derived neurotrophic factor	Sensory neurons, large axons	Ho *et al*. (1998); Terris *et al*. (2001)
GDNF: glial-derived neurotrophic factor	Motor neurons	Barras *et al*. (2002)
FGF-1: fibroblast growth factor 1 (acidic fibroblast growth factor)	Vascular endothelial cells	Cordeiro *et al*. (1989); Walter *et al*.(1993); Trigg *et al*. (1998); Midha *et al*. (2003); Wang *et al*. (2003)
FGF-2: fibroblast growth factor 2 (basic fibroblast growth factor)	Vascular endothelial cells	Trigg *et al*. (1998); Ohta *et al*. (2004)
GGF: glial growth factor	Schwann cells	Bryan *et al*. (2000); Mohanna *et al*. (2005)
PDGF: platelet-derived growth factor	Schwann cells	Wells *et al*. (1997)
CNTF: ciliary neurotrophic factor	Schwann cells (injury factor)	Ho *et al*. (1998)
VEGF: vascular endothelial growth factor	Vascular endothelial cells	Hobson (2002)
IGF-I: insulin-like growth factor I	Inflammatory cells (anti-inflammatory)	Fansa *et al*. (2002)
LIF: leukemia inhibitory factor	Neurons (injury factor)	McKay Hart *et al*. (2003)
HGF: Hepatocyte growth factor	Schwann cells Neurons Vascular endothelial cells	Li *et al*. (2008)
EGF: Endothelial growth factor	Vascular endothelial cells	Smith and Browne (1998)
TGF: Transforming growth factor	Schwann cells	Sulaiman and Gordon (2002)

A possible of drawback of the widely studied NGF could be that it impairs neuron response to injury by delaying the early regeneration mechanism (Hirata *et al.*, 2002). Furthermore most neuronal sub-populations have shown cell type specific response for individual pleiotrophic neurotrophic factor. These two problems might be overcome by the use of single agent such as LIF, which stimulates expression of neuronal regenerative phenotypic markers, or GGF that and induces the secretion of a spectrum of neurotrophic factors by activated Schwann cells (Hart *et al.*, 2003).

N-acetyl-cysteine (NAC) as well as acetyl-L-carnitine (ALCAR) have been shown to be neuroprotective and act by inhibiting the mitochondria mediated apoptosis, these compounds also have a good therapeutic potential(Hart *et al.*, 2004, Wilson *et al.*, 2007, Wilson *et al.*, 2003, Hart *et al.*, 2002).

1.6 Clinical market

Current success rates using food and drug administration (FDA) and "conformité européenne" (CE) approved nerve conduit have been summarised by (Meek and Coert, 2013) for digital nerve injury and show promising results even if their use is limited to short gap injury. This study mentions that up to 4 cm gaps can be bridged by resorbable nerve conduits, with a 75 % success rate of some improved sensory outcome after 11 months. Another review by (Daly *et al.*, 2012) allows a good overview of the clinical market.

Neuroflex®, Neuromatrix® and Neuromend® commercialised by Stryker Orthopaedics® (US) are bioresorbable in four to twelve month, flexible, semi-permeable bovine collagen type I based tubular matrix. Neuragen® by Integra®(US) is also a collagen type I nerve tube with a longer resorbation time of four year. Revolnev® is a porcine collagen type I and III nerve tube, commercialised by Orthomed® (France).

Neurolac® marketed by Polyganics BV™ (Netherland) is a poly-(DL-Lactide-ε-Caprolactone) tube, and Neurotube® marketed by Synovis MCA® (US), a Poly-glycolic-Acid (PGA) tube.

All these nerve repair tube are selectively permeable and bioresorbable. Only Neuroflex® and Neurotube® are corrugated, which prevents kinking, and makes the tubes bendable and thus and allows for an earlier mobilisation of the limb.

Other tubes like Salubridge®/Hydrosheath® or Salutunnel® (Salumedica®, US) made of polyvinyl alcohol hydrogel (PVA), Surgisis Nerve Cuff/Axoguard® made of porcine small intestinal submucosa matrix (Cook Biotech®, US) or

AxonScaff/Cellscaff/StemScaff® made of PHB (Axongen,Sweden) are also available (Daly *et al.*, 2012).

However robust clinical data is scarce or lacking for all but the Neurotube®, which presents outcomes comparable to direct repair and nerve grafting on terminal or digital nerves for nerve gap around 3 cm. Additionally Neurolac® is apparently complicated to handle and has efficacy issues (Rosson *et al.*, 2009, Daly *et al.*, 2012).

Neurowrap® from Integra® is an new commercially available collagen type-1 nerve repair tube that has been used by Georgiou *et al.* (2013) in combination with a preseeded collagen scaffold in a rat model of peripheral nerve injury, and have shown promising results for its transfer to clinic.

1.7 Electric stimulation for nerve repair

1.7.1 Effect of electrical stimulation (ES) on nerve regeneration

Naturally produced electric currents entering damaged portion of a nerve are carried by Na^{+} and Ca^{++} ions and are reversed in the case of injury. The accumulation of these cations in the cytoplasm of the injured nerve cell

causes direct destruction of the architecture of the axon at this site, but at the same time triggers the cellular repair processes (Borgens *et al.*, 1980, Allodi *et al.*, 2012, Kerns *et al.*, 1987). To neutralize the damaging flow of ions equivalent to densities of 100's of μA /cm^2 significant current must be apply to the injury site (Borgens, 1988a, Borgens, 1988b, Borgens, 2003).

Another problem in nerve regeneration is poor functional recovery generally attributed to irreversible target atrophy and neuronal loss (Fu and Gordon, 1995).

In the 1980s, studies in animal suggest that low-frequencies alternating current (AC) stimulation of the crushed nerve quickened the return of reflexes and functionality in animal models (Nix and Hopf, 1983, Pockett and Gavin, 1985, Roman *et al.*, 1987).

More recently many reports show a positive effect of direct current (DC) or AC electrical fields on PNS regeneration (Al-Majed *et al.*, 2000, Brushart *et al.*, 2002, Cheng and Lin, 2004, Gordon *et al.*, 2008) for review see (Gordon *et al.*, 2009). In rats with chronic axotomy of the femoral nerve up to one year with atrophy of Schwann cells in the distal nerve stumps, an ES proximal to the site of nerve stump reunion with delivery of a suprathreshold (3–10 V) biphasic pulses at a frequency of 20 Hz for 1 hour and up to two weeks has been shown to accelerate axon outgrowth across suture sites is associated with elevated neuronal neurotrophic factor and receptors quantities (Gordon *et al.*, 2008). In humans with severe carpal tunnel syndrome, the same electrical simulation simulation but only applied for minutes during the operation promoted the full re-innervation of the thenar muscle (Gordon *et al.*, 2008). Another study showed, by quantitative histology in rats, that a 10 mm gap injury of the sciatic nerve healed better after a percutaneous ES of 15 minutes per day of the injured nerves within a silicon-rubber conduit. This was especially evident when using a DC stimulation protocol (2 Hz 1 mA): these repaired nerves had a more mature structure with a smaller cross-sectional area, more myelinated fibres, higher axon density, and higher ratio

of blood vessel to total nerve area compared to the controls (Lu *et al.*, 2008).

Cellular aspects of these results could be explained by more fundamental studies e.g. (Patel and Poo, 1982) show a preferential growth of axon toward the cathode of a DC field of 10 V/cm *in vitro* using salt bridges. (Huang *et al.*, 2010) demonstrated that electrical stimulation resulted in a four-fold increase of NGF secretion by Schwann cells *in vitro* by applying a 5 V/cm 1Hz electric field. It should be noted that that this ES effect is linked to the activity of calcium channels and that it mobilises calcium from intracellular stores. ES also increases IL-6 and IL-8 secretion from fibroblasts (Shi *et al.*, 2008) and BDNF from hippocampus neurons *in vitro* (Gartner and Staiger, 2002).

1.7.2 Problems of electrical devices in vivo

Many problems can occur, when using electrical devices *in vivo* and *in vitro* because of the complex chemical environment that includes ions, and amphiphile surfactants, proteins which are electrode poisons, electro catalysts such as glutathione or ascorbic acid, and a tissue matrix that both restricts mass transport to the electrode surface and reacts physiologically (Keohan *et al.*, 2007, Green *et al.*, 2008).

If a DC field is applied molecular hydrogen is produced in association with a rise in pH to highly alkaline condition at the cathode. At the anode, a precipitous fall in pH to highly acidic condition leads to more destructive reactions than those occurring at the cathode. Production of toxic metal salts, the generation of peroxides, and other damaging chemicals are also observed in association with these primary reactions (Veiga *et al.*, 2005). It is therefore essential that when applying any AC stimulation, the slow chemical reactions that produce these unwanted tissue changes taken into account and the field reversed every 15 minutes. This balances the pH at about neutral (~ 7.4) during the entire period of stimulation. Considering this fact AC is the

only way to impose high current (i.e. hundreds of µAs) through tissues without damaging them (Borgens *et al.*, 1999, Shapiro *et al.*, 2005).

Another problem is the usage of the electrical power within the body and with this the need to disconnect and to remove any power source easily. There are three possibilities to implement power supply: batteries, direct leads to the outside, transformer setup with a delivery coil on the outside and an internal pick-up coil. A novel fabrication of the later in the context of this work is detailed in Appendix 1.

1.8 Effect of magnetic field on nerve regeneration

Both the effects of static- and pulsed magnetic fields were investigated with regards to their respective effect on nerve repair. To study the effects of static fields on nerve repair in sheep small magnets were applied to the sides of a biodegradable glass tube, before the median nerve first cut, and then repaired. The sheep were allowed to recover and were re-examined 10 months later using morphometric measurements, and electrophysiological, as well as isometric muscle tension assessments. The authors concluded that static magnetic fields do not enhance peripheral nerve regeneration (Kelleher *et al.*, 2006).

However pulsed electromagnetic fields (PEMF) seems to be more efficient. Two studies have shown beneficial effects of PEMF on rat sciatic nerve regeneration after a crush lesion. Rats were placed between a pair of Helmholtz coils and exposed to PEMF of 2 Hz using magnetic flux densities of 0.3 mT for either 4 h, or 15min per day for 3-6 days. Either regime increased the rate of nerve regeneration. This stimulatory effect was independent of the orientation of the coils. However exposure times of 1 h/day-10 h/day were equally effective in stimulating nerve regeneration. Even a PEMF pre-treatment before crush conditioned the rat sciatic nerve in a manner similar, which means that PEMF affects the neuronal cell body (Sisken *et al.*, 1989, Kanje *et al.*, 1993).

More recently electromagnetic field have also been shown to activate tyrosine kinases known as the SRC family, which could influence cellular growth (Kristupaitis *et al.*, 1998, Dibirdik *et al.*, 1998).

1.9 Aims and goals

Reviewing the literature it is clear that the nerve repair tube of the future will not be as simple as the ones presently on the biomedical market today. The aims of this thesis were to contribute to the basis of the field of neuro tissue engineering and regenerative medicine, fundamental for the development of future nerve tubes by:

I) Investigating if scaffold parameters such as substrate stiffness, and the possible surface structuring to guide neurons – here microtopography would interact with the intended use of growth factors, either locally released or delivered.

II) Developing a simpler process for scaffold fabrication and investigate how scaffold dimensionality (thickness, number of layers) influences regeneration.

III) Studying the influence of pulsed field stimulation on the growth and orientation of regenerating axons *in vitro*.

   a. Scanning the parameter space for effective amplitudes and frequencies using a commercially available micro-electrode array (MEA)
   b. Developing a combined topography and electrode system that allows the assessment of the effectiveness of pulsed field stimulation on nerve regeneration.
   c. Assessing the effect that various parameters (electrode design and orientation, amplitude, frequency) have on axonal regeneration and orientation.

DRG isolated from neonatal rats have been chosen as a model because it allowed me to reduce the use of animals. This model is widely accepted thus background information is readily available (Balgude *et al.*, 2001, Alexander *et al.*, 2006, Plantman *et al.*, 2008, Ribeiro-Resende *et al.*, 2009).

2 Physical Substrate Factors Affect NGF Response in DRG

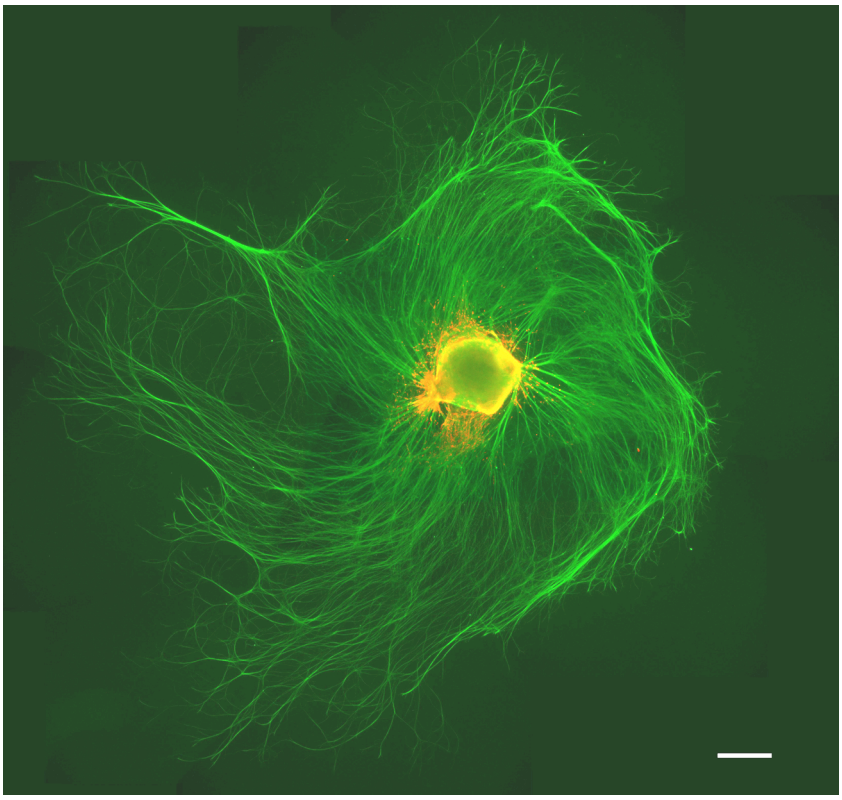

An organotypic DRG culture (green: axons, red: Schwann cells) after ten days growth on PDMS. Scale: 500 µm

2.1 Introduction

In this chapter the study aims to focus on the interaction between three major parameters considered of interest in nerve tube design:

- the physical cue provided by a microgrooved substrate of different width
- the mechanical properties (stiff-/softness) of the substrate,
- the influence of growth factor concentration.

Microgrooved substrates have already been shown to provide guidance cues to growing neurons of the PNS and the CNS (Sorensen *et al.*, 2007, Deumens *et al.*, 2006, Sun *et al.*, 2010). Modifications to the common hollow nerve tube, such as the addition of supportive cells (Kalbermatten *et al.*, 2008, Kim *et al.*, 2007), stem cells (Kemp *et al.*, 2008, di Summa *et al.*, 2009), neurotrophins (Chang, 2009a), internal frameworks (Hu *et al.*, 2009), and electronic components (Shi *et al.*, 2004, Runge *et al.*, 2010) are currently investigated in order to increase the gap length that can be bridged and to achieve better clinical outcomes. One of the neurotrophins under investigation is NGF, which was discovered in 1954, and has been shown to be a key factor for neuron survival, outgrowth and differentiation in the PNS (Cohen *et al.*, 1954). It has also been demonstrated that NGF, released by the post-synaptic targets, such as muscle, or secondary sensory cells, will be retrogradely transported, and is essential to maintain neural circuits (Korsching and Thoenen, 1983, Delcroix *et al.*, 2003, Zhou *et al.*, 2009). NGF can also modulate the expression of its own receptors (Kitzman *et al.*, 1998, Mearow and Kril, 1995). The NGF concentration usually present in human or rat serum, and in tissues is in the range of pg/mL (Fawcett *et al.*, 1999, Murase *et al.*, 1990, Martocchia *et al.*, 2002). During peripheral nerve regeneration the NGF concentration increases at the injury site. NGF is also secreted by Schwann cells in the bands of Büngner, which act as a guide for regenerating axons (Fu and Gordon, 1997, Johnson *et al.*, 2005). Tissue engineers are currently designing new delivery strategies for neurotrophic and neurotropic factor such as microencapsulation, but the effective

quantity and type of neurotrophic factor that should be delivered within a nerve conduit still remains an important open question (Xu *et al.*, 2003). As the nerve tubes are made of a wide variety of materials their mechanical properties vary, this is of interest as substrate stiffness has been shown to influence cell adhesion, spreading, neuronal outgrowth, and differentiation, and it could be important to adapt the stiffness of a substrate to the target issue, and the potential injury (Discher *et al.*, 2005, Engler *et al.*, 2006). Modulus mismatch between an implant and its surrounding tissue can also lead to inflammatory responses, which would be detrimental to tissue regeneration, thus softer materials are favoured.

In this chapter, I investigate the interaction of NGF, which is commonly used to improve axonal outgrowth *in vitro* and *in vivo* (Cohen *et al.*, 1954, Isaacson and Crutcher, 1998), with substrate stiffness, and surface topography in a concentration dependent manner. NGF levels were systematically varied between 10 and 100 ng/mL. A DRG organotypic explant culture, was used as experimental for PNS regeneration. Each DRG contains approximately 10,000 pseudo-unipolar sensory afferent neurons, together with their satellite cells, in culture the axons regenerate and form an extensive network on a suitably adhesive surface (Corey *et al.*, 2007). Other common structural cells such as fibroblasts, endothelia, and white blood cells are also present. During extraction of the DRG the dorsal roots are cut on either side mimicking an acute DRG evulsion in combination with a peripheral nerve injury. The fibroblasts as well as the glial cells, present during axonal outgrowth from the DRG, are providing a complex and more pertinent *in vitro* model than most of the common co-cultures (Corey *et al.*, 2007, Ribeiro-Resende *et al.*, 2009, Nicolini *et al.*, 2011).

Peripheral nerves have an average Young's modulus in the range of hundreds of kPa (Borschel *et al.*, 2003), and it has been surmised that the materials properties of nerve tubes should ideally be matched to that of nerve tissue to improve regeneration. As a means to test the effect of stiffness without changing polymer chemistry on axonal regeneration we used poly-l-lysine coated polydimethylsiloxane (PDMS) as its bulk mechanical properties can easily be adjusted, it faithfully replicates

microstructures, and as it has been shown to be cell culture compatible (Balaban *et al.*, 2001). Thus we varied Young's modulus of PDMS between 0.1 MPa and 4.1 MPa, in order to establish the interaction between the stiffness, microtopography, and NGF concentration.

2.2 Materials and method

2.2.1 PDMS master fabrication

Si wafers of 100 mm diameter, 500 μm thick were cleaned in acetone, methanol and isopropanol with sonication for 5 minutes each. The wafer was then dried by a flow of dried nitrogen gas. SU-8 3005 (Microchem, Japan) was spin coated at 3000rpm 25s to form layers of 5μm thickness. The wafer was then soft-baked on a hotplate at 95 °C for 5 min. The layer was then exposed on a Suss MicroTec MA6 mask aligner with exposure energy of 100 - 200 mW/cm2 using soft contact exposure mode and a photomask featuring a 12.5, and 25 μm repeat pattern of stripes on a 13x7mm area allowing exposure of the photoresist. A post-exposure bake was then performed on a hotplate for 1 min at 65 °C and 4 mins at 95 °C. The unexposed SU-8 was then developed off using Microposit EC solvent (Shipley, Massachusetts). The surface was then rinsed with isopropanol and dried with a flow of filtered air. (Figure 10)

2.2.2 Silanisation of the master

A drop of (tridecafluoro-1,1,2,2-tetrahydrocetyl) trichlorosilane (ABCR, Germany) was pipetted out next to the master in a Petri dish under nitrogen gas flow. The Petri dish was then placed onto a hotplate at 150 °C for 15 min. The silane vapor settled unto the master and formed a thin low-adhesion coating. The Petri dish was then allowed to cool for 10 – 15 min.

2.2.3 PDMS casting

The jig used in combination with the master consists of a bottom, securing plate; a flanged plate to secure the master to the bottom plate and set the 2mm height of the chamber; and a top plate with two inlet/outlet holes. The master was placed into the carefully cleaned (70 % ethanol) moulding jig. PDMS (Sylgard® 184 Silicone Elastomer, Dow Corning, UK) base was carefully mixed at a weight-to-weight ratio of 10:1 or 40:1 with curing agent for a few minutes ensuring homogeneity of the mixture. The PDMS was then de-gassed for 30min. The PDMS was then poured into a syringe with great care being taken to not introduce any bubbles, and injected into the mould. PDMS was cured at 80°C for 2 hours. After curing and cooling the sheet of PDMS was then liberated from the casting jig, and individual 11mm diameter devices cut out with a cork borer (Figure 10 and Figure 11).

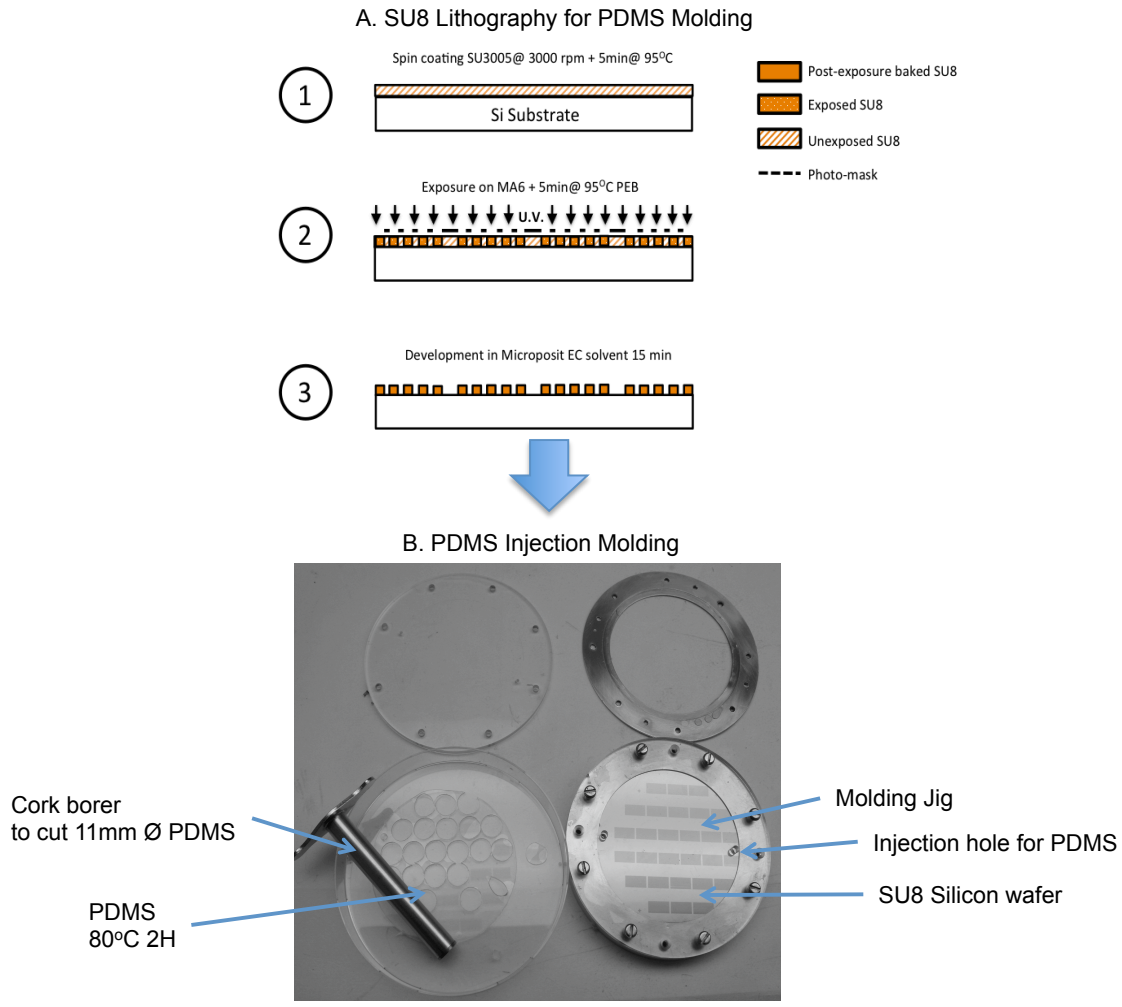

Figure 10: Scheme for the fabrication of PDMS devices. A) 1) SU-8 3005 was spin coated at 3000rpm 25s to form layers of 5μm thickness. The wafer was then soft-baked on a hotplate at 95 °C for 5 min. 2) The layer was exposed on a Suss MicroTec MA6 mask aligner with exposure energy of 100 - 200 mW/cm2 using soft contact exposure mode and a photomask featuring a 12.5, and 25 μm repeat pattern of stripes on a 13x7mm area allowing exposure of the photoresist. A post-exposure bake was then performed on a hotplate for and 5 mins at 95 °C. 3) The unexposed SU-8 was then developed off using Microposit EC solvent. (B) After silanisation the wafer was use for molding of a 1mm thick PDMS sheet in a jig. After 2h curing at 80°C the chamber was dissembled, the PDMS substrates removed and cut, the pieces placed in a plasma cleaner for a set time, sterilised in 70 % ethanol, and PLL coated before immediately being used for cell culture.

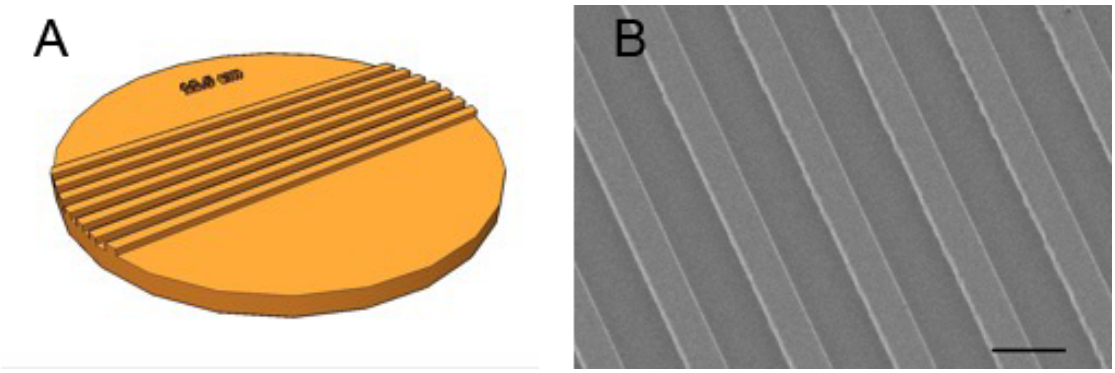

Figure 11: The microgrooves PDMS devices. 3D Schematic (A) and SEM of the microgrooved PDMS device featuring 12.5 µm wide 5 µm deep microgrooves (B). Scale : 25 µm. Image and SEM by courtesy of Lewis Ross

2.2.4 Device sterilisation

To sterilize the PDMS microgrooved devices these were immersed in 70 % ethanol for 30min. Devices were then dried with a flow of filtered (0.4µm) nitrogen gas in a laminar flow cabinet to avoid contamination.

2.2.5 Young's modulus measurement

PDMS with two different stiffnesses were used in this study. To calculate the Young's modulus of the PDMS, it was cast into a 5mL pipette and cured at 80 °C for 2 h. Deformations of PDMS cylinders of 10 cm initial length and 2.5 mm radius were then measured during stretch (<10 % initial rest length) by hanging a series of weights off it. The Young's modulus was then calculated as the slope of the stress-strain curve and were found to be 4.1 MPa for 10:1 ratio PDMS and 0.1 MPa for 40:1 ratio PDMS (Figure 12).

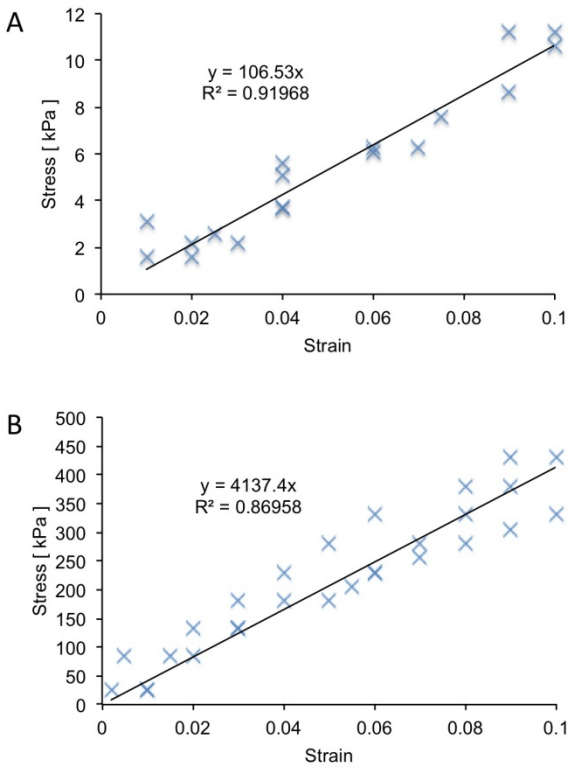

Figure 12: Stress/strain curves for (A) soft (0.1 MPa), and (B) hard (4.1 MPa) PDMS. All data points of 3 independent measurements are shown and the linear fit to these (black line). The data is fitted to y=mx+0, and the results displayed, m is the Young's modulus, R^2 is the correlation coefficient of the line fit.

2.2.6 Plasma deposition and surface contact angle measurement

The measurement of the water contact angle allowed evaluating the efficiency of the plasma cleaner to change wettability. The surface was rendered more hydrophilic thus increasing cell adhesion. The PDMS devices were treated at 29.6 W for 1 min for the 10:1 PDMS or 3min for the 40:1, using a Harrick Plasma PDC-002 Plasma Cleaner. The surface contact angle of distilled water droplets on the two types of PDMS were measured using a KSV CAM 100 goniometer (KSV Instruments, Finland) with series of thirty measurements for three different droplets for each plasma treatment time. The soft 40:1 PDMS substrates used in this study had to be treated longer because it was initially less hydrophilic (Figure 13). After plasma cleaning the devices were coated in 13 µg/mL poly-L-lysine (Sigma, UK) solution for 30min at room temperature before seeding.

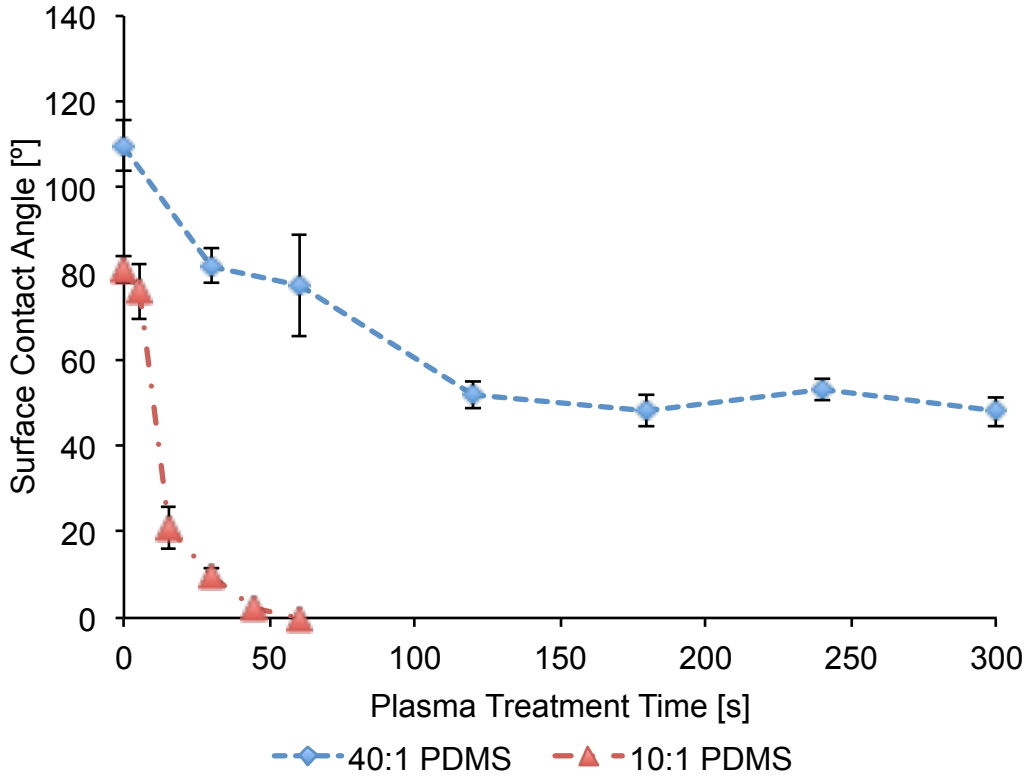

Figure 13: Water contact angle (WCA) of RO water on soft (0.1 MPa) and hard (4.1 MPa) PDMS as a function of plasma treatment time. The minimum contact angle was reached after 50s on hard PDMS and after 120 s on soft PDMS.

2.2.7 Organotypic culture of dorsal roots ganglion

During this study, 98 thoracic DRGs were isolated from 2-day-old neonatal Sprague-Dawley rat pups. Rats were euthanised by an Euthatal® injection (500 mg/Kg) in accordance with Home Office regulation, and then dissected (Figure 14). After extraction and processing to remove any nerve stump left (Figure 14 D, E, F), the DRGs were seeded in the middle of a flat PDMS disc as control, or on PDMS devices featuring 5μm deep, and either 12.5, or 25 μm wide microgrooves. DRGs were grown for 10 days at 37 °C 5 % CO_2 in 250 μL/ 15 mm diameter well L15 media (Sigma, UK) supplemented with 10 % FBS, 50 μg/mL n-acetyl-cystein (Hart *et al.*, 2004, Chao *et al.*, 2007), and 1 % antibiotic, antimycotic mixture (PAA p11-002, UK). The concentration of NGF 2.5S (Invitrogen, UK) was adjusted to: 10, 50 or 100 ng/mL. Cultures were split fed 1:1 every day.

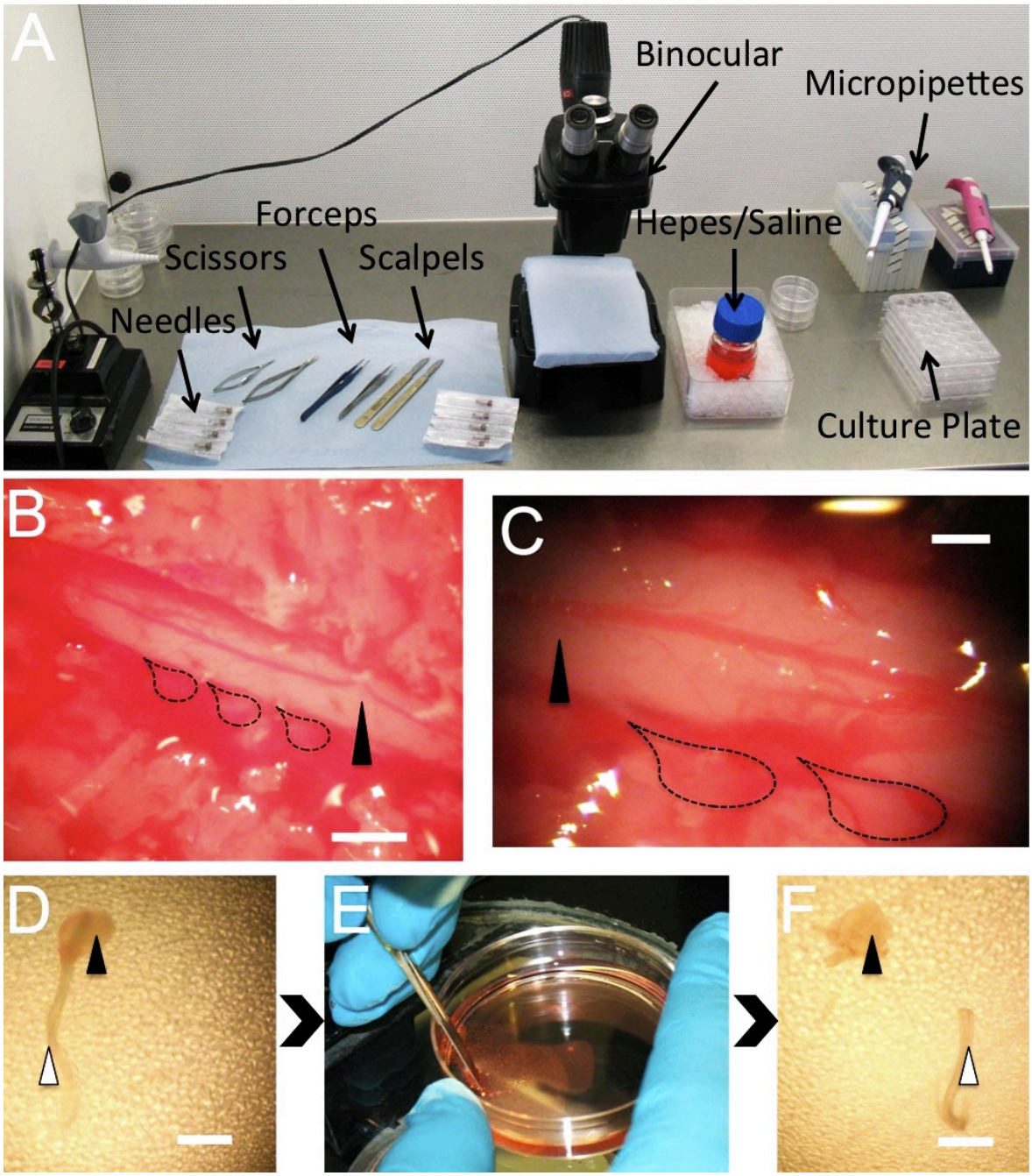

Figure 14: Procedure and set up for dissection extraction and processing of two days-old rat DRGs before seeding. The dissection was done under binocular (A), the first step is to remove carefully fat, muscle and bone tissues with the microsurgical Siccors (Fine Science Tools, US) to clear the spinal cord area (arrowhead in B and C). DRGs are found lying alongside on both side of the spinal cord (dash line in B and C). These are removed with a DuPont forceps number 5 by pulling on one of the two adjacent nerves. Once removed, the DRGs are processed with a Scalpel blade number 10, in HEPES/Saline solution to remove any nerve left attached to the DRGs (D, E, F). The DRG are then seeded on the PDMS construct.

2.2.8 Immunostaining

After 10 days growth, DRG were fixed in 4 % formaldehyde/PBS solution for 15 min at 37°C. The culture were then permeabilized in perm buffer (10.3g sucrose, 0.292 g NaCl, 0.06 g $MgCl_2$, 0.476 g HEPES 0.5 mL Triton X-100 per 100 mL PBS Sigma, UK) at 4°C for 15 min. Block solution of 1 %BSA/PBS was added at 37°C for 5min. The blocking solution was replaced by 1 % BSA/PBS solution containing anti-β3-tubulin 1:100 antibodies (mouse anti-TU-20 Santa Cruz, California) and anti-S100 antibodies 1:100 (rabbit Ab868 S100 Abcam, UK). The samples were incubated 2 h at 37 °C. The samples were then wash thrice with a PBS/Tween20 (Sigma, UK) 0.5 % solution. The sample were then incubated 1h at 37 °C in 1 % BSA/PBS solution containing 1:100 secondary Texas red anti-rabbit antobodies (Vector Laboratories, UK) and 1:100 biotinlayed anti-mouse antibodies (Vector Laboratories) and washed thrice with Tween20 0.5 /PBS. Fluorescein Streptavidin 1:100 (Vector Laboratories) in 1 % BSA/PBS was then added to the sample for 30 min at 4 °C and washed again. The samples were viewed by fluorescence microscopy (Figure 15, Figure 16, Figure 17, Figure 18, Figure 19, and Figure 20).

2.2.9 Scanning electron microscopy

SEM preparation followed the method published by Dalby *et al*. (Dalby *et al*., 2004). In short: cultures were fixed after 10 days culture with 1.5 % gluteraldehyde (Sigma, UK) buffered in 0.1 M sodium cacodylate (Agar, UK) for 1 hour at 4 °C. The cells were then post fixed in 1 % osmium tetroxide for 1 hour (Agar, UK) and 1 % tannic acid (Agar, UK) was used as a mordant. Samples were dehydrated through a series of alcohol concentrations (20 %, 30 %, 40 %, 50 %, 60 % and 70 %), stained in 0.5 % uranyl acetate, followed by further dehydratation (90 %, 96 % and 100 % alcohol). The final dehydration was done in hexamethyl-disilazane (Sigma, UK), followed by air-drying. Once dry, the samples were sputter-coated with coated with gold before

examination with a Hitachi S800 field emission SEM at an accelerating voltage of 6 kV (Figure 25).

2.2.10 Data analysis

Composite images of DRG networks were assembled in Photoshop (Adobe), and analyzed using ImageJ (Papadopulos *et al.*, 2007). The length, width and the surface area of the DRG outgrowth were measured using the "Analyse Particles" tool of ImageJ processing the picture as shown in Figure 15.

General linear models (GLM) were used to perform univariate analysis of variance (ANOVA) of the logarithmic values of the surface area and major axis of DRG axonal outgrowths under the different conditions to define the effect of the parameters NGF concentration, stiffness, topography, and their interactions, using Minitab 16 (Figure 21 and Table 4). A simple linear regression was used to determine the significance (R^2) of a relationship between NGF concentration and DRG responses.

To assess the diversion angle of individual and interacting growth cone digitations, the angle at which 30 digitations diverged from the direction of 15 axon growth cones was measured on a flat and a microgrooved 10:1 PDMS DRG cultures and a paired two tails homoscedastic Students t-test was used to test statistical significance (Figure 25 and Figure 26).

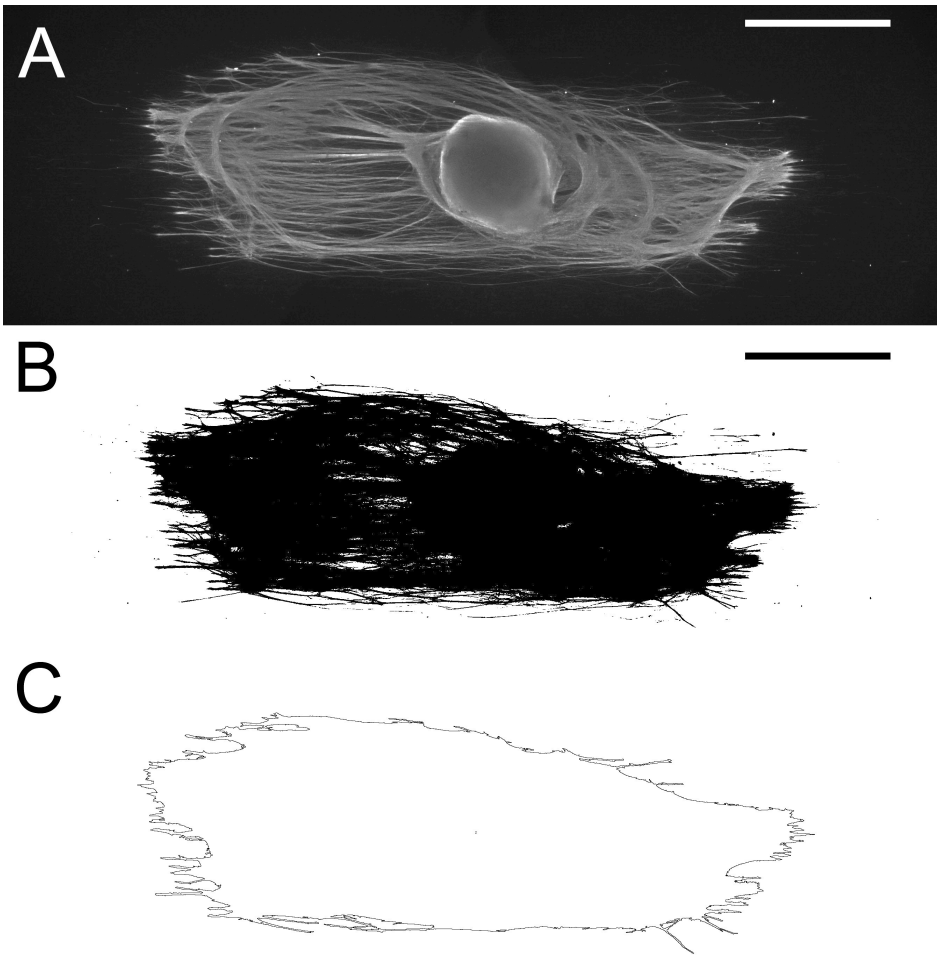

Figure 15: Image analysis with Analyse Particle tool of ImageJ software. The fluorescence image (A) is inverted and the threshold is adjusted to select the pixels of the B3 tubulin immunostaining. The software computes the length and the surface area of the shape selected (C). Scale 500 µm.

To distinguish the four fasciculation degrees (low, average, high, and extreme fasciculation) of the DRG outgrowth (Table 5, Figure 24) we used imageJ fast Fourier transform (FFT) algorithm and plot profile of grey value of axonal networks at 10, 50, and 100 ng/mL on hard PDMS (4.1 MPa) at 20x magnification. FFT algorithm transforms the pictures in an image symmetric respect to the centre with peaks corresponding to periodic components in the analysed picture. High-frequency components produce peaks close to the centre of the FFT image and low-frequency produce peaks far from the centre.

2.3 Results

The general linear models of ANOVAs of the surface area and major axis of the axonal network explain respectively 85 % and 90 % of the variance in the model. The interaction terms of the parameter of the models are in both cases validated by a p-value inferior or equal to 0.001. It means that the interaction of the NGF concentration, the stiffness of the substrate and the topography are significant factors to take into account for nerve guidance tube engineering. The interaction graphs generated by the ANOVA (Figure 22) show that the length of the DRG networks and their surface area decrease when NGF concentration increases except on the Flat topography where the trend is inverted.

The area covered by axonal networks, which extended from individual DRG on flat hard (4.1 MPa) PDMS substrates within 10 days, increased linearly (R^2=0.99) with increasing NGF concentration (Figure 21). The length of individual axons also increased with higher NGF concentrations as evident in Figure 16. On flat, soft (0.1 MPa) PDMS substrates the size of the DRG networks was not affected by an increasing NGF concentration (Figure 21). On the softer substrate the degree of fasciculation increased with NGF concentration (Table 5, Figure 24).

The network on the flat substrates had an even radial orientation of axons with any NGF concentration, and on either substrate stiffness (Figure 16, Figure 17). Axonal networks extending from DRG grown on microstructured PDMS were obviously guided by the microstructures (Figure 18, Figure 19, Figure 20, Figure 21) had a smaller overall area, were longer, had a rectangular shape, and a higher degree of fasciculation (Table 5). On either sized microgrooves (12.5 or 25 µm) the axonal extensions formed a 1mm wide aligned network as axonal outgrowth followed the grooves (Figure 18, Figure 19, Figure 20). The migration of S100 positive Schwann cells from the DRG out onto the flat or microgrooved material lagged behind the leading axons, but followed these on all substrates (Figure 20).

The longest average axonal outgrowth of 5.5 mm on either side of the DRGs was seen on stiff (4.1 MPa) PDMS with 12.5 µm wide grooves at 10 ng/mL NGF. On the soft PDMS (0.1 MPa) the maximum average length of 2.7 mm on either side of the DRGs was observed on the 25 µm wide grooves at 50 ng/mL. The DRG axons had reached the end of the 11mm diameter substrate within 10 days. When the axons reached the end of the patterned area, they immediately deviated from the linear path provided by the grooves (arrows in Figure 18 A, B). On stiff PDMS substrates the average axonal network length was slightly but significantly ($p<0.0001$) longer on the 12.5 µm wide grooves compared to the ones on 25 µm wide grooves at 50 ng/mL, suggesting that an increase of groove width decreased the efficiency of the guidance by the topography.

The effect of the high NGF concentration on the micro-patterned substrate is a decrease of the length and the surface area of the network on the more stiff PDMS (4.1 MPa) ($R^2=0.99$) with 12.5 and 25 µm wide grooves, whereas the inverse effect is observed on the flat control culture ($R^2=0.99$) (Figure 16, Figure 18, Figure 21) confirming that the modulation is the results of the combination of the topographical cue and the NGF concentration.

Outgrowing axons at lower NGF concentration (10 ng/mL) on the 4.1 MPa PDMS are guided and within ten days reached the edges of the 11mm diameter device (Figure 18A). On the softer PDMS, the axonal outgrowth was less pronounced at low NGF concentrations (10 ng/mL) and the outgrowth was very densely packed at 100 ng/mL. Stiffness had its strongest effect at 50 ng/mL, at this NGF concentration the network morphology was less packed, the axons were less grouped together in bundles or neofascicles and branched more on 0.1 MPa PDMS than on the 4.1 MPa (Figure 23).

The NGF concentration modulated the growth of the axonal network, gradually increasing the fasciculation on the stiffer, microgrooved PDMS. On the soft structured PDMS this effect shifted to a higher concentration

appearing between 50 ng/mL and 100 ng/mL NGF (Figure 18, Figure 19, Table 5).

The outgrowth on the flat PDMS was randomly oriented and lead to a final overall ovoid or round neuronal network (Figure 16, Figure 17). On the microgrooved substrate, the morphology of the axonal network changes substantially in terms of fasciculation, axonal and network length (Figure 18, Figure 19, Table 5).

The SEM images (Figure 25) show the ultrafine morphology of the axonal outgrowth and allowed to investigate the direction taken by individual growth cones at the time of fixation. A measurement of the diverging angles formed by the thin growth cones on flat versus the direction of the main fascicle/axon shortly behind the leading growth cone(s), on- or off a micropattern showed the importance of the guidance provided by the topography (Figure 25 C, D), the average angle of diversion of the growth cones was significantly lower on the 12.5 µm wide grooved substrate (Figure 26).

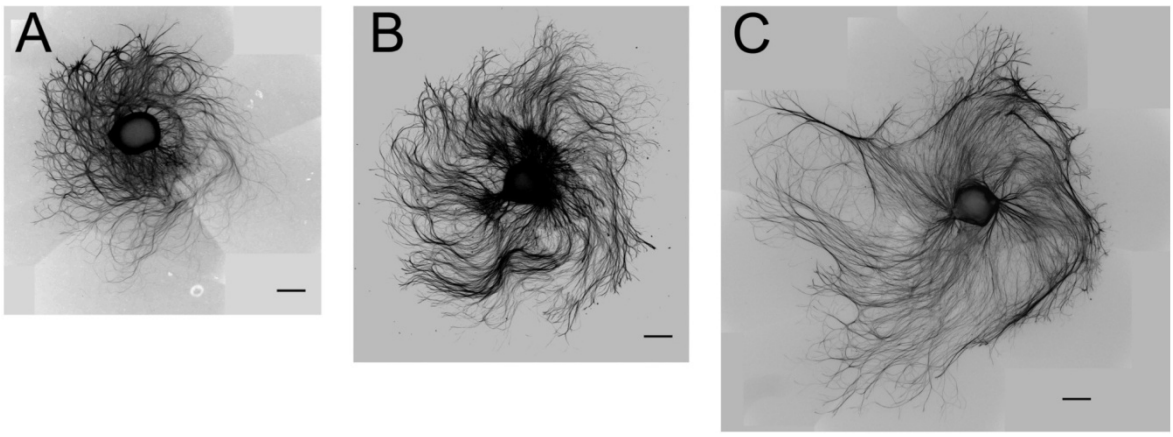

Figure 16: Immunofluorescence of the axonal (ß3-tubulin) network of DRGs on PLL coated flat and hard (4.1 MPa) PDMS. DRGs are cultured for 10 days with A) 10, B) 50, and C) 100 ng/mL NGF. The overall shape of the networks is circular to ovoid, and the axons within are oriented in large swirls with an even, radial orientation. The surface area covered by the network, and the length of individual axons increases with NGF concentration. Scale bars = 500 µm.

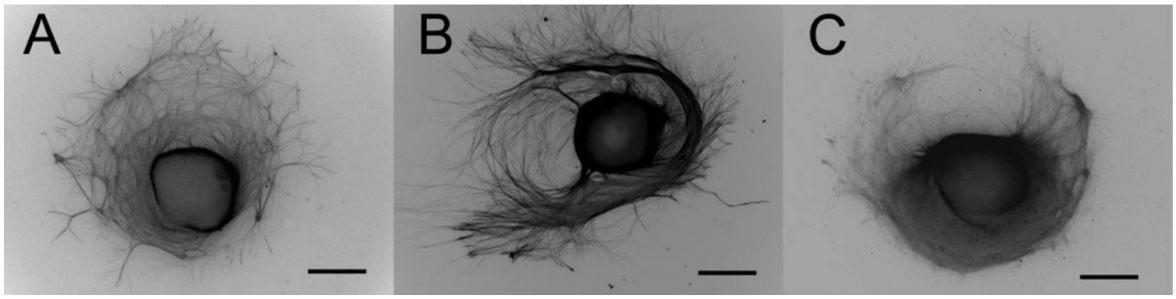

Figure 17: Immunofluorescence of the axonal (ß3-tubulin) network of DRGs on PLL coated flat and soft (0.1 MPa) PDMS. DRGs are cultured for 10 days with A) 10, B) 50, and C) 100 ng/mL NGF. The overall shape of the networks is ovoid, and the axons within are oriented in swirls with an even, radial orientation. The degree of fasciculation increases with NGF concentration, but neither surface area nor the length of individual axons are affected. Scale bars = 500 µm.

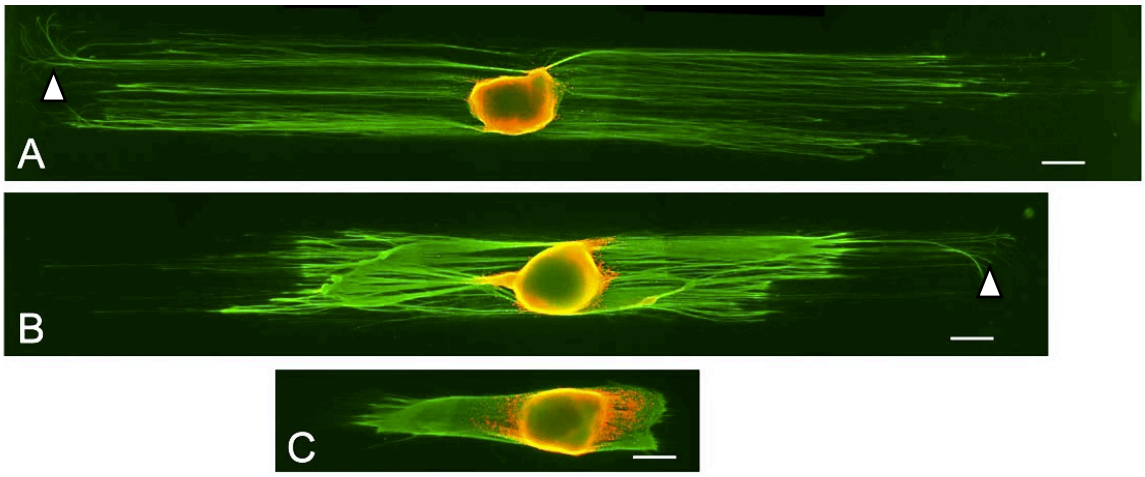

Figure 18: Immunofluorescence of the axonal network (green) and Schwann cells (red) of DRGs on PLL coated grooved (12.5 µm wide, 5 µm deep) hard (4.1 MPa) PDMS. DRGs are cultured for 10 days with A) 10, B) 50, and C) 100 ng/mL NGF. The overall shape of the networks is rectangular, and the axons within are oriented along the grooves. The surface area, and the length of individual axons decrease, and the degree of fasciculation increases with NGF concentration. The arrows in A and B indicate the edge of the grooved region of the substrate, where the axons start to loose orientation.(green: ß3-tubulin; red: S100) Scale bars = 500 µm.

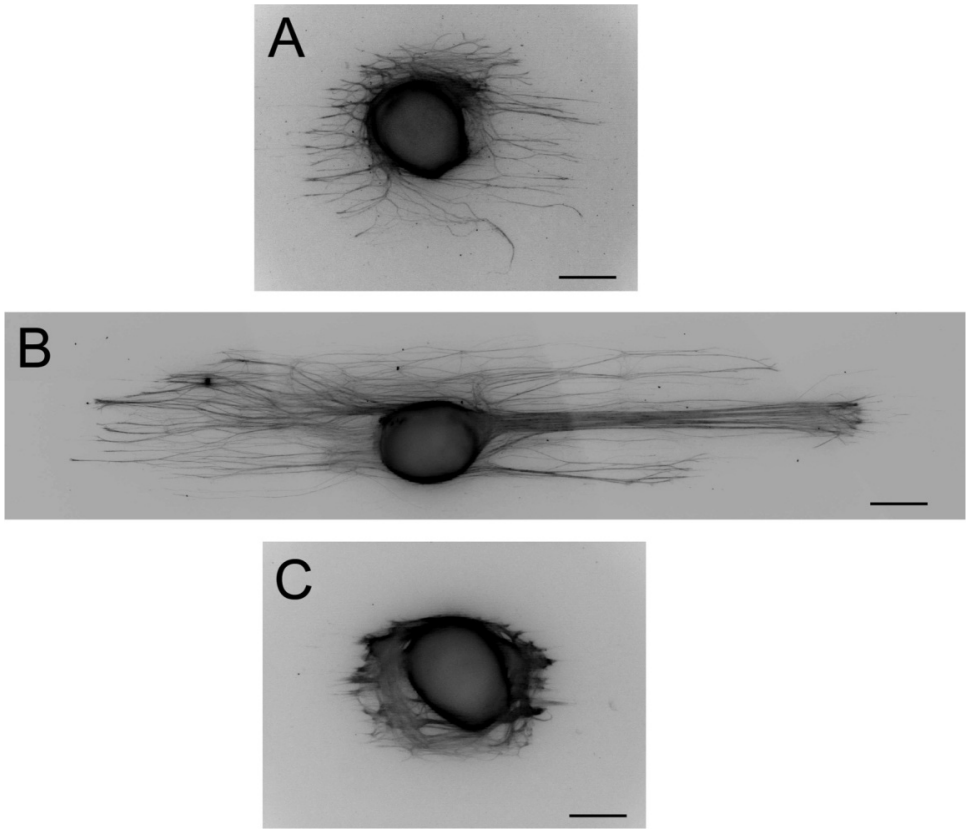

Figure 19: Immunofluorescence of the axonal (ß3-tubulin) network of DRGs cultured for 10 days on PLL coated grooved (12.5 µm wide, 5 µm deep) soft (0.1 MPa) PDMS. DRG are cultured with A) 10, B) 50, and C) 100 ng/mL NGF. The overall shape of the networks is rectangular, and the axons within are oriented along the grooves. NGF affects the surface area, and the length of individual axons, with a maximum network extension at 50 ng/mL, the degree of fasciculation increases with NGF concentration. Scale bars = 500 µm.

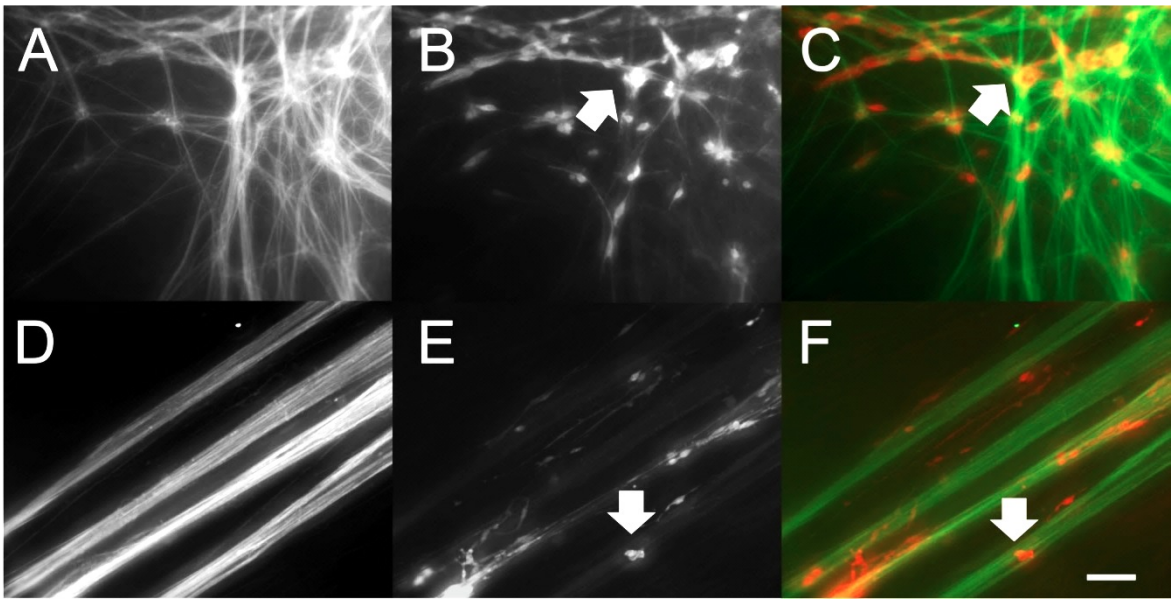

Figure 20: Part of the axonal network (green: ß3-tubulin) and of Schwann cells (red: S100) of DRGs cultured for 10 days on PLL coated PDMS.DRGs are cultured on flat (A-C), and grooved (12.5 µm wide, 5 µm deep) (D-F) hard (4.1 MPa) PDMS. A) Flat hard PDMS, axonal network illustrating the even radial distribution of axonal orientation. B) Schwann cells forming linear strings of cells that follow the axonal extensions, with some cell clusters at nodes (arrow). C) Colour overlay of A and B with an arrow indicating the same node as in B. D) Grooved hard PDMS, axonal network illustrating the linear orientation of the axons, there were no discernable nodes. The fasciculated fibre bundles initially form over ridges, but later loose this association. E) Schwann cells form linear strings of cells that follow the axonal extensions, despite the lack of nodes some S100 positive cell clusters can be seen (arrow). F) Colour overlay of D and E with an arrow indicating the same cell cluster as in E. Scale : 20 µm.

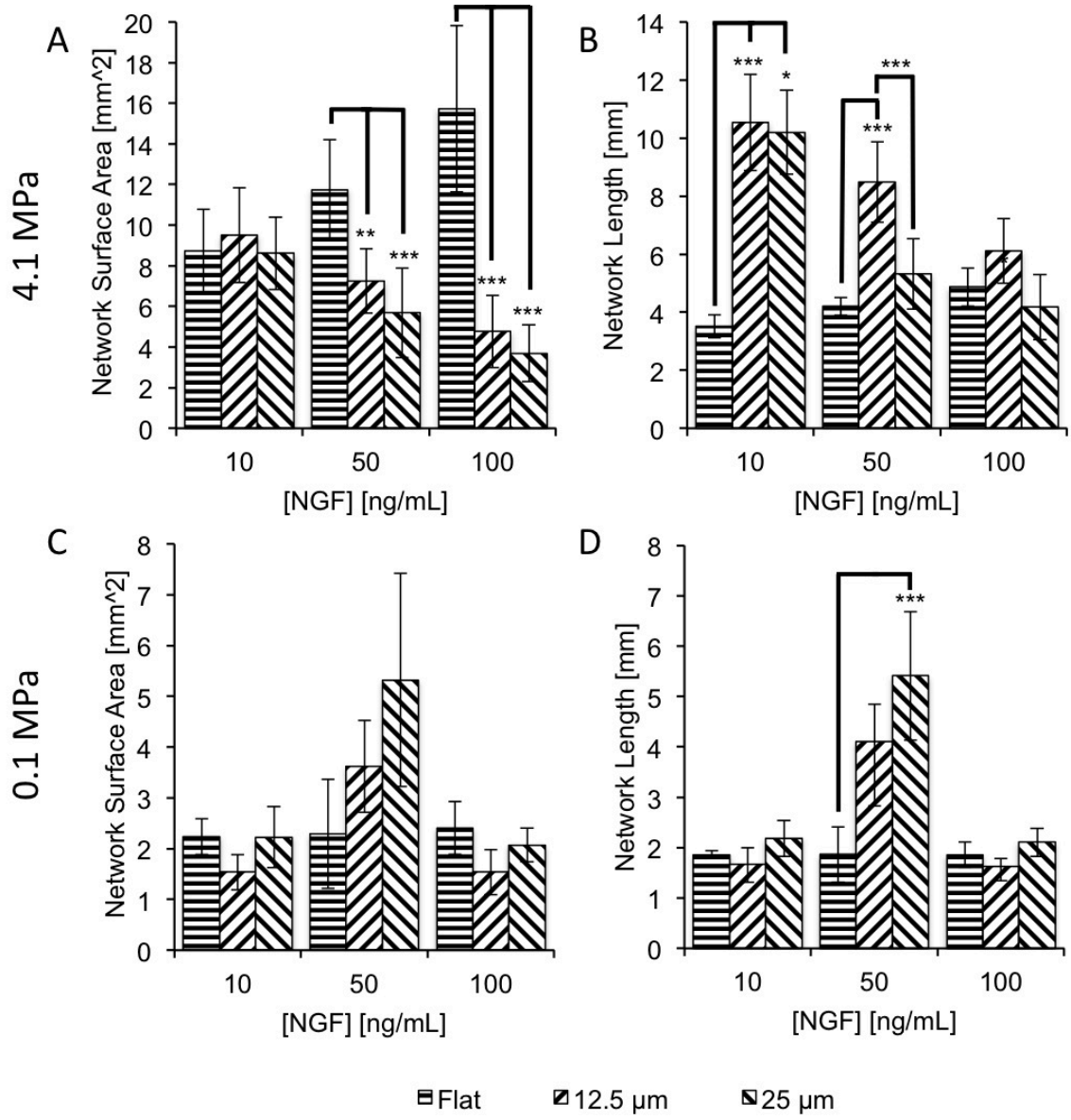

*Figure 21: Surface area and length of DRGs axonal networks after 10 days culture on hard (4.1 MPa; A, B) and soft (0.1 MPa; C, D) flat, or microgrooved (12.5 µm, and 25 µm wide 5 µm deep) PDMS. On the hard, flat PDMS (A, B) axonal networks length (A) and area (B) increased with increasing NGF concentration. Compared to flat PDMS substrate, microgrooves reduced axonal network area significantly and increase their length on hard PDMS (A). Network area and length on hard PDMS microgrooves increased proportionally to NGF concentration. On soft, flat PDMS (C, D), network length (C) and area (D) were not affected by NGF, in the range of concentrations tested. Compared to hard PDMS both area and length of the DRG networks were significantly reduced on soft substrates under all conditions (Table 4, flat/grooves; 10, 50 100 ng/mL NGF). Compared to flat substrates, 25 µm microgrooves did increase the network length significantly at 50 ng/mL(D) on soft PDMS. The error bars indicate the standard deviation and the significant difference calculated by Bonferroni post-hoc test of the ANOVA is indicated by * ($p<0.05$), ** ($p<0.01$), and *** ($p<0.005$) $n \geq 4$ independent biological repeats.*

Table 4: P-values of Bonferroni post hoc tests of ANOVA of DRG network length and surface area after 10 days culture with 10, 50, and 100 ng/mL NGF on flat as well as microgrooved (12.5 µm, 25 µm wide, 5 µm deep) 10:1 hard, and 40:1 soft (4.1, 0.1 MPa) PDMS.

	Axon Network Length				Axon Network Area		
	Sample compared		Post hoc test p-value		Sample compared		Post-hoc test p-value
4.1 MPa PDMS	flat 10ng/mL	12.5µm 10ng/mL	< 0.0001	4.1 MPa PDMS	flat 10ng/mL	flat 100ng/mL	< 0.0001
	flat 10ng/mL	12.5µm 50ng/mL	< 0.0001		flat 10ng/mL	25µm 100ng/mL	< 0.005
	flat 10ng/mL	12.5µm 100ng/mL	< 0.05		flat 50ng/mL	12.5µm 50ng/mL	< 0.05
	flat 10ng/mL	25µm 10ng/mL	< 0.05		flat 50ng/mL	12.5µm 100ng/mL	< 0.0001
	flat 50ng/mL	12.5µm 10ng/mL	< 0.0001		flat 50ng/mL	25µm 50ng/mL	< 0.001
	flat 50ng/mL	12.5µm 50ng/mL	< 0.0001		flat 50ng/mL	25µm 100ng/mL	< 0.0001
	flat 50ng/mL	25µm 10ng/mL	< 0.0001		flat 100ng/mL	12.5µm 10ng/mL	< 0.0001
	flat 100ng/mL	12.5µm 10ng/mL	< 0.0001		flat 100ng/mL	12.5µm 50ng/mL	< 0.0001
	flat 100ng/mL	12.5µm 50ng/mL	< 0.0001		flat 100ng/mL	12.5µm 100ng/mL	< 0.0001
	flat 100ng/mL	25µm 10ng/mL	< 0.0001		flat 100ng/mL	25µm 10ng/mL	< 0.0001
	12.5 µm 10ng/mL	12.5µm 50ng/mL	< 0.05		flat 100ng/mL	25µm 50ng/mL	< 0.0001
	12.5 µm 10ng/mL	12.5µm 100ng/mL	< 0.0001		flat 100ng/mL	25µm 100ng/mL	< 0.0001
	12.5 µm 10ng/mL	25µm 50ng/mL	< 0.0001		12.5µm 10ng/mL	12.5µm 100ng/mL	< 0.001
	12.5 µm 10ng/mL	25µm 100ng/mL	< 0.0001		12.5µm 10ng/mL	25µm 50ng/mL	< 0.05
	12.5 µm 50ng/mL	12.5 µm 100ng/mL	< 0.05		12.5µm 10ng/mL	25µm 100ng/mL	< 0.0001
	12.5 µm 50ng/mL	25µm 50ng/mL	< 0.0001		12.5µm 50ng/mL	25µm 100ng/mL	< 0.05
	12.5 µm 50ng/mL	25µm 100ng/mL	< 0.0001		25µm 10ng/mL	25µm 100ng/mL	< 0.005
	12.5 µm 100ng/mL	25µm 10ng/mL	< 0.0001				
	25µm 10ng/mL	25µm 50ng/mL	< 0.0001	4.1 vs 0.1 MPa PDMS	0.1 MPa flat 10ng/mL	4.1 MPa flat 10ng/mL	< 0.001
	25µm 10ng/mL	25µm 100ng/mL	< 0.0001		0.1 MPa flat 10ng/mL	4.1 MPa flat 50ng/mL	< 0.0001
					0.1 MPa flat 10ng/mL	4.1 MPa flat 100ng/mL	< 0.0001
0.1 MPa PDMS	flat 10ng/mL	25µm 50ng/mL	< 0.0005		0.1 MPa flat 10ng/mL	4.1 MPa 12.5µm 10ng/mL	< 0.0001
	flat 50ng/mL	25µm 50ng/mL	< 0.0005		0.1 MPa flat 10ng/mL	4.1 MPa 12.5µm 50ng/mL	< 0.005
	flat 100ng/mL	25µm 50ng/mL	< 0.0005		0.1 MPa flat 10ng/mL	4.1 MPa 25µm 10ng/mL	< 0.0005
	12.5µm 10ng/mL	12.5µm 50ng/mL	< 0.01		0.1 MPa flat 50ng/mL	4.1 MPa flat 10ng/mL	< 0.001
	12.5µm 10ng/mL	25µm 50ng/mL	< 0.0001		0.1 MPa flat 50ng/mL	4.1 MPa flat 50ng/mL	< 0.0001
	12.5µm 50ng/mL	12.5µm 100ng/mL	0.005		0.1 MPa flat 50ng/mL	4.1 MPa flat 100ng/mL	< 0.0001
	12.5µm 100ng/mL	25µm 50ng/mL	< 0.0001		0.1 MPa flat 50ng/mL	4.1 MPa 12.5µm 10ng/mL	< 0.0001
	25µm 10ng/mL	25µm 50ng/mL	< 0.0005		0.1 MPa flat 50ng/mL	4.1 MPa 12.5µm 50ng/mL	< 0.005
	25µm 50ng/mL	25µm 100ng/mL	< 0.0005		0.1 MPa flat 50ng/mL	4.1 MPa 25µm 10ng/mL	< 0.001
					0.1 MPa flat 100ng/mL	4.1 MPa flat 10ng/mL	< 0.0005
4.1 vs 0.1 MPa PDMS	0.1 MPa flat 10ng/mL	4.1 Mpa flat 100ng/mL	< 0.01		0.1 MPa flat 100ng/mL	4.1 MPa flat 50ng/mL	< 0.0001
	0.1 MPa flat 10ng/mL	4.1 Mpa 12.5µm 10ng/mL	< 0.0001		0.1 MPa flat 100ng/mL	4.1 MPa flat 100ng/mL	< 0.0001
	0.1 MPa flat 10ng/mL	4.1 Mpa 12.5µm 50ng/mL	< 0.0001		0.1 MPa flat 100ng/mL	4.1 MPa 12.5µm 10ng/mL	< 0.0001
	0.1 MPa flat 10ng/mL	4.1 Mpa 12.5µm 100ng/mL	< 0.0001		0.1 MPa flat 100ng/mL	4.1 MPa 12.5µm 50ng/mL	< 0.01
	0.1 MPa flat 10ng/mL	4.1 Mpa 25µm 10ng/mL	< 0.0001		0.1 MPa flat 100ng/mL	4.1 MPa 25µm 10ng/mL	< 0.0005
	0.1 MPa flat 10ng/mL	4.1 Mpa 25µm 50ng/mL	< 0.0005		0.1 MPa 12.5µm 10ng/mL	4.1 MPa flat 10ng/mL	< 0.0001
	0.1 MPa flat 10ng/mL	4.1 Mpa 25µm 100ng/mL	< 0.05		0.1 MPa 12.5µm 10ng/mL	4.1 MPa flat 50ng/mL	< 0.0001
	0.1 MPa flat 50ng/mL	4.1 Mpa flat 100ng/mL	< 0.05		0.1 MPa 12.5µm 10ng/mL	4.1 MPa flat 100ng/mL	< 0.0001
	0.1 MPa flat 50ng/mL	4.1 Mpa 12.5µm 10ng/mL	< 0.0001		0.1 MPa 12.5µm 10ng/mL	4.1 MPa 12.5µm 10ng/mL	< 0.0001
	0.1 MPa flat 50ng/mL	4.1 Mpa 12.5µm 50ng/mL	< 0.0001		0.1 MPa 12.5µm 10ng/mL	4.1 MPa 12.5µm 50ng/mL	< 0.0005
	0.1 MPa flat 50ng/mL	4.1 Mpa 12.5µm 100ng/mL	< 0.0001		0.1 MPa 12.5µm 10ng/mL	4.1 MPa 25µm 10ng/mL	< 0.0001
	0.1 MPa flat 50ng/mL	4.1 Mpa 25µm 10ng/mL	< 0.0001		0.1 MPa 12.5µm 10ng/mL	4.1 MPa 25µm 50ng/mL	< 0.05
	0.1 MPa flat 50ng/mL	4.1 Mpa 25µm 50ng/mL	< 0.001		0.1 MPa 12.5µm 50ng/mL	4.1 MPa flat 10ng/mL	< 0.005
	0.1 MPa flat 100ng/mL	4.1 Mpa flat 100ng/mL	< 0.01		0.1 MPa 12.5µm 50ng/mL	4.1 MPa flat 50ng/mL	< 0.0001
	0.1 MPa flat 100ng/mL	4.1 Mpa 12.5µm 10ng/mL	< 0.0001		0.1 MPa 12.5µm 50ng/mL	4.1 MPa flat 100ng/mL	< 0.0001
	0.1 MPa flat 100ng/mL	4.1 Mpa 12.5µm 50ng/mL	< 0.0001		0.1 MPa 12.5µm 50ng/mL	4.1 MPa 12.5µm 10ng/mL	< 0.0001
	0.1 MPa flat 100ng/mL	4.1 Mpa 12.5µm 100ng/mL	< 0.0001		0.1 MPa 12.5µm 50ng/mL	4.1 MPa 12.5µm 50ng/mL	< 0.05
	0.1 MPa flat 100ng/mL	4.1 Mpa 25µm 10ng/mL	< 0.0001		0.1 MPa 12.5µm 50ng/mL	4.1 MPa 25µm 10ng/mL	< 0.005
	0.1 MPa flat 100ng/mL	4.1 Mpa 25µm 50ng/mL	< 0.0005		0.1 MPa 12.5µm 100ng/mL	4.1 MPa flat 10ng/mL	< 0.0001
	0.1 MPa flat 100ng/mL	4.1 Mpa 25µm 100ng/mL	< 0.05		0.1 MPa 12.5µm 100ng/mL	4.1 MPa flat 50ng/mL	< 0.0001
	0.1 MPa 12.5µm 10ng/mL	4.1 Mpa flat 50ng/mL	< 0.05		0.1 MPa 12.5µm 100ng/mL	4.1 MPa flat 100ng/mL	< 0.0001
	0.1 MPa 12.5µm 10ng/mL	4.1 Mpa flat 100ng/mL	0.001		0.1 MPa 12.5µm 100ng/mL	4.1 MPa 12.5µm 10ng/mL	< 0.0001
	0.1 MPa 12.5µm 10ng/mL	4.1 Mpa 12.5µm 10ng/mL	< 0.0001		0.1 MPa 12.5µm 100ng/mL	4.1 MPa 12.5µm 50ng/mL	< 0.0005
	0.1 MPa 12.5µm 10ng/mL	4.1 Mpa 12.5µm 50ng/mL	< 0.0001		0.1 MPa 12.5µm 100ng/mL	4.1 MPa 25µm 10ng/mL	< 0.0001
	0.1 MPa 12.5µm 10ng/mL	4.1 Mpa 12.5µm 100ng/mL	< 0.0001		0.1 MPa 12.5µm 100ng/mL	4.1 MPa 25µm 50ng/mL	< 0.05
	0.1 MPa 12.5µm 10ng/mL	4.1 Mpa 25µm 10ng/mL	< 0.0001		0.1 MPa 25µm 10ng/mL	4.1 MPa flat 10ng/mL	< 0.0005
	0.1 MPa 12.5µm 10ng/mL	4.1 Mpa 25µm 50ng/mL	< 0.0001		0.1 MPa 25µm 10ng/mL	4.1 MPa flat 50ng/mL	< 0.0001
	0.1 MPa 12.5µm 10ng/mL	4.1 Mpa 25µm 100ng/mL	< 0.005		0.1 MPa 25µm 10ng/mL	4.1 MPa flat 100ng/mL	< 0.0001
	0.1 MPa 12.5µm 50ng/mL	4.1 Mpa 12.5µm 10ng/mL	< 0.0001		0.1 MPa 25µm 10ng/mL	4.1 MPa 12.5µm 10ng/mL	< 0.0001
	0.1 MPa 12.5µm 50ng/mL	4.1 Mpa 12.5µm 50ng/mL	< 0.0001		0.1 MPa 25µm 10ng/mL	4.1 MPa 12.5µm 50ng/mL	< 0.005
	0.1 MPa 12.5µm 50ng/mL	4.1 Mpa 25µm 100ng/mL	< 0.0001		0.1 MPa 25µm 10ng/mL	4.1 MPa 25µm 10ng/mL	< 0.0005
	0.1 MPa 12.5µm 100ng/mL	4.1 Mpa flat 50ng/mL	< 0.05		0.1 MPa 25µm 50ng/mL	4.1 MPa flat 50ng/mL	< 0.0001
	0.1 MPa 12.5µm 100ng/mL	4.1 Mpa flat 100ng/mL	< 0.001		0.1 MPa 25µm 50ng/mL	4.1 MPa flat 100ng/mL	< 0.0001
	0.1 MPa 12.5µm 100ng/mL	4.1 Mpa 12.5µm 10ng/mL	< 0.0001		0.1 MPa 25µm 50ng/mL	4.1 MPa 12.5µm 10ng/mL	< 0.005
	0.1 MPa 12.5µm 100ng/mL	4.1 Mpa 12.5µm 50ng/mL	< 0.0001		0.1 MPa 25µm 100ng/mL	4.1 MPa flat 10ng/mL	< 0.0001
	0.1 MPa 12.5µm 100ng/mL	4.1 Mpa 12.5µm 100ng/mL	< 0.0001		0.1 MPa 25µm 100ng/mL	4.1 MPa flat 50ng/mL	< 0.0001
	0.1 MPa 12.5µm 100ng/mL	4.1 Mpa 25µm 10ng/mL	< 0.0001		0.1 MPa 25µm 100ng/mL	4.1 MPa flat 100ng/mL	< 0.0001
	0.1 MPa 12.5µm 100ng/mL	4.1 Mpa 25µm 50ng/mL	< 0.0001		0.1 MPa 25µm 100ng/mL	4.1 MPa 12.5µm 10ng/mL	< 0.0001
	0.1 MPa 12.5µm 100ng/mL	4.1 Mpa 25µm 100ng/mL	< 0.005		0.1 MPa 25µm 100ng/mL	4.1 MPa 12.5µm 50ng/mL	< 0.001
	0.1 MPa 25µm 10ng/mL	4.1 Mpa flat 100ng/mL	< 0.05		0.1 MPa 25µm 100ng/mL	4.1 MPa 25µm 10ng/mL	< 0.0001
	0.1 MPa 25µm 10ng/mL	4.1 Mpa 12.5µm 10ng/mL	< 0.0001				
	0.1 MPa 25µm 10ng/mL	4.1 Mpa 12.5µm 50ng/mL	< 0.0001				
	0.1 MPa 25µm 10ng/mL	4.1 Mpa 12.5µm 100ng/mL	< 0.0001				
	0.1 MPa 25µm 10ng/mL	4.1 Mpa 25µm 10ng/mL	< 0.0001				
	0.1 MPa 25µm 10ng/mL	4.1 Mpa 25µm 50ng/mL	< 0.005				
	0.1 MPa 25µm 50ng/mL	4.1 Mpa 12.5µm 10ng/mL	< 0.0001				
	0.1 MPa 25µm 50ng/mL	4.1 Mpa 25µm 50ng/mL	< 0.0005				
	0.1 MPa 25µm 50ng/mL	4.1 Mpa 25µm 10ng/mL	< 0.0001				
	0.1 MPa 25µm 100ng/mL	4.1 Mpa flat 100ng/mL	< 0.05				
	0.1 MPa 25µm 100ng/mL	4.1 Mpa 12.5µm 10ng/mL	< 0.0001				
	0.1 MPa 25µm 100ng/mL	4.1 Mpa 12.5µm 50ng/mL	< 0.0001				
	0.1 MPa 25µm 100ng/mL	4.1 Mpa 12.5µm 100ng/mL	< 0.0001				
	0.1 MPa 25µm 100ng/mL	4.1 Mpa 25µm 10ng/mL	< 0.0001				
	0.1 MPa 25µm 100ng/mL	4.1 Mpa 25µm 50ng/mL	< 0.0005				

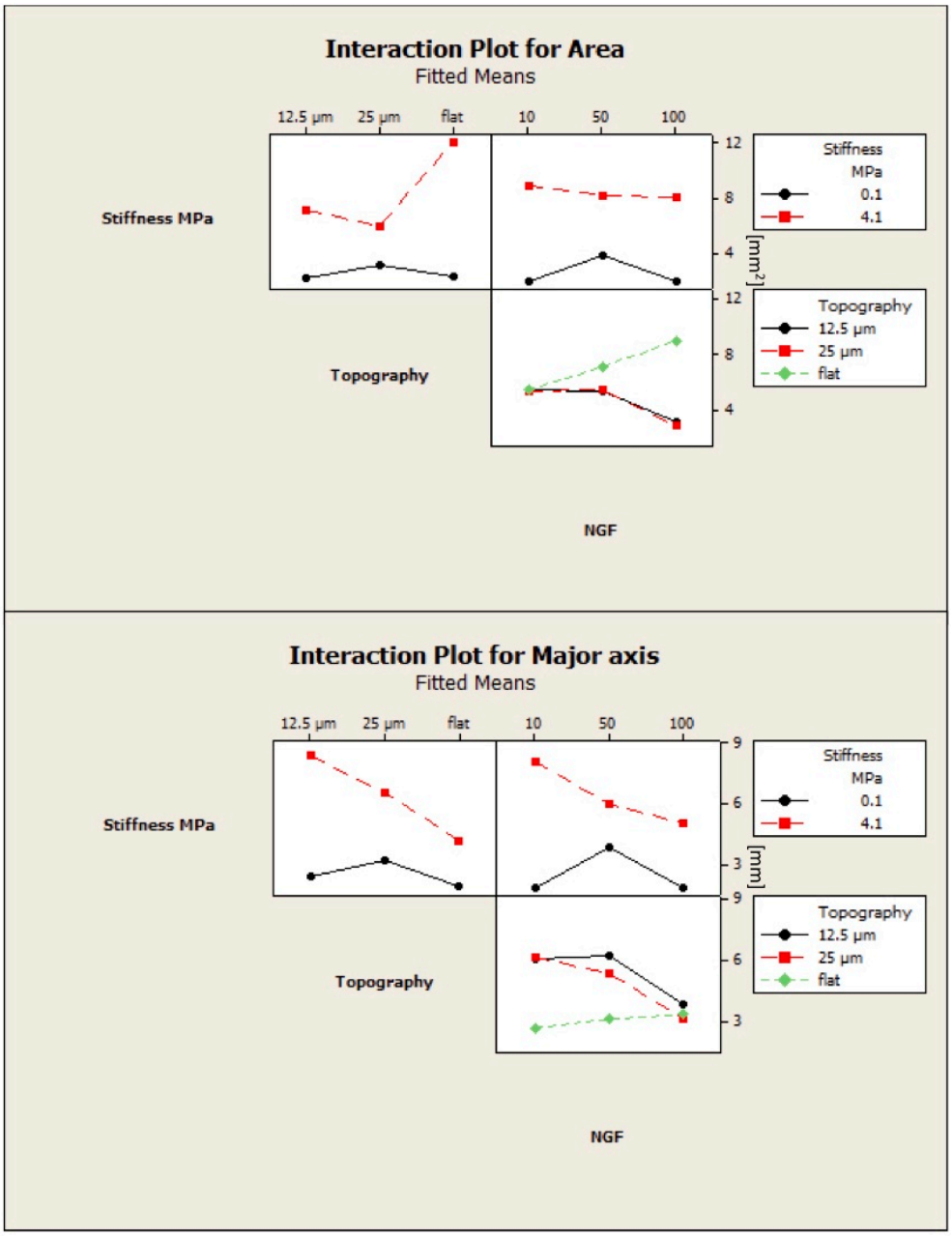

Figure 22: Interaction Plots generated by analysis of variance (ANOVA) of the surface area (A) and major axis (B) of DRG outgrowths after 10 days culture with 10, 50, and 100 ng/mL NGF on flat as well as microgrooved (12.5 µm, 25 µm wide, 5 µm deep) 10:1 hard, and 40:1 soft (4.1, 0.1 MPa) PDMS using Minitab 16.

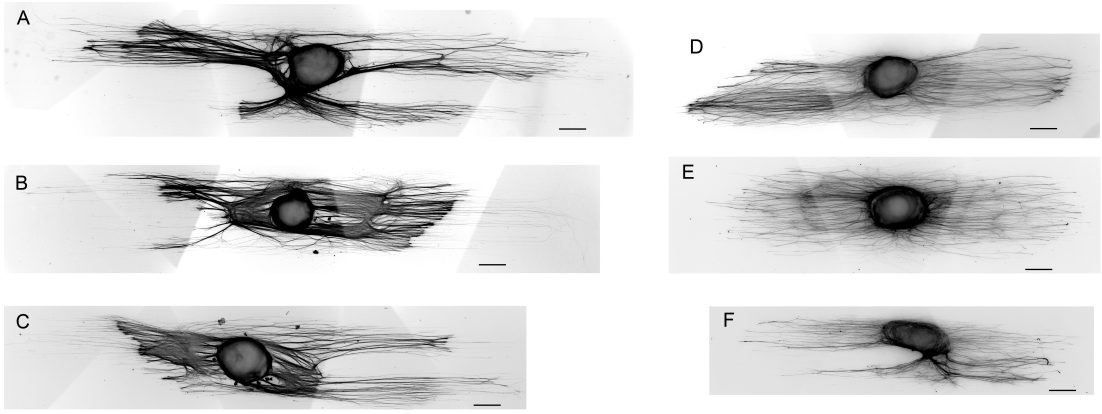

Figure 23: Immunofluorescence of the axonal (ß3-tubulin) network of DRGs cultured for 10 days with 50 ng/mL NGF on PLL coated microgrooved (12.5 µm wide, 5 µm deep) hard (4.1 MPa) (A-C) and soft (0.1 MPa) (D-F) PDMS. The overall shape of the networks on either material was rectangular, and the axons within were oriented along the grooves. The networks on the hard PDMS (A-C) were denser and showed fasciculation, whereas on the soft PDMS they were more branched and less fasciculated. Scale bars 500 µm.

Table 5: The degree of fasciculation of the axonal network as a function of PDMS stiffness and NGF concentration. (+) low fasciculation (++) average fasciculation (+++) high fasciculation (++++) extreme fasciculation (see Figure 24). The degree of fasciculation increases with NGF concentration on hard (4.1 MPa) microgrooved PDMS, and on both hard, and soft (0.1 MPa) flat PDMS. On soft microgrooved PDMS fasciculation is prominent only with 100 ng/mL NGF.

Degree of fasciculation		NGF concentration [ng/mL]		
Stiffness	Groove width [μm]	10	50	100
4.1 MPa	12.5	++	+++	++++
	25	++	+++	++++
	flat	+	+	++
0.1 MPa	12.5	+	+	++++
	25	+	+	++++
	flat	++	+++	++++

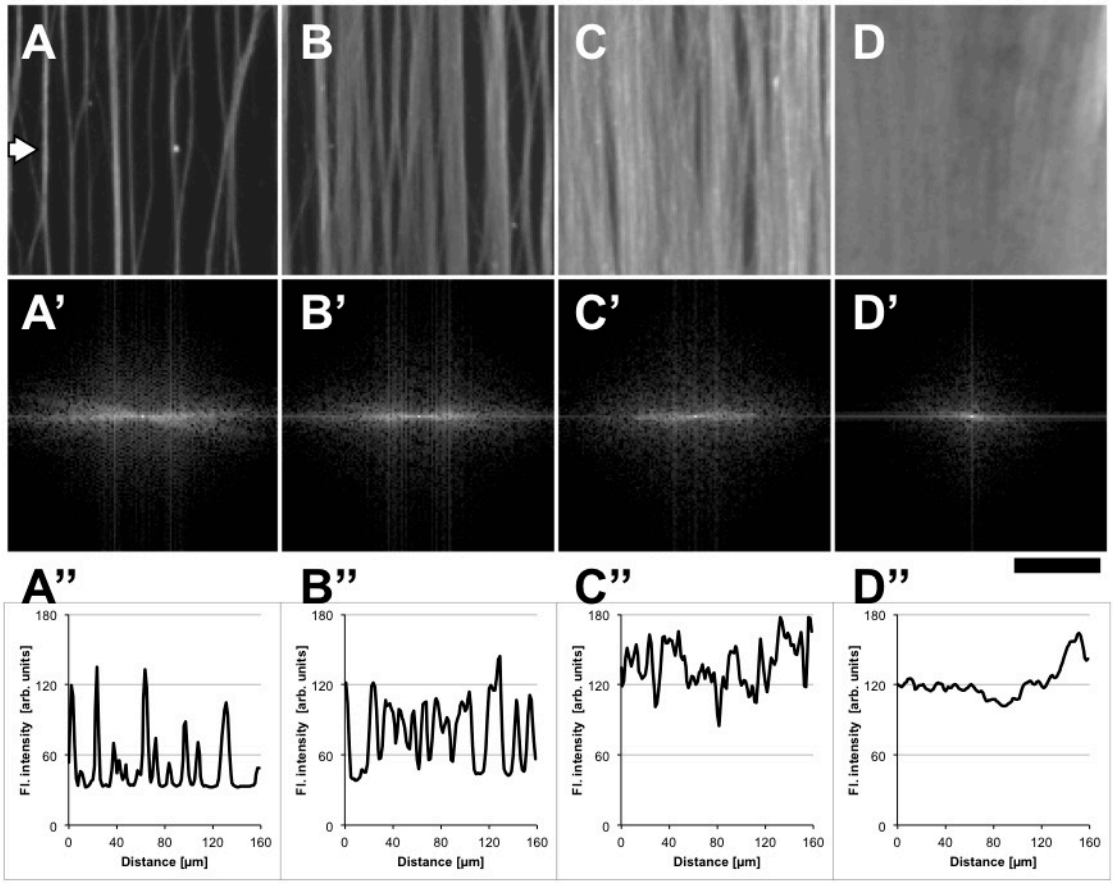

Figure 24: FFT and plot profile analysis of immunofluorescence images of the axonal (ß3-tubulin) network. DRGs are cultured for 10 days with A, B) 10, C) 50 and D) 100 ng/mL NGF on hard PDMS (4.1 MPa). These images illustrate the classification used to generate Table 5 (A, A', A") low fasciculation: many individual axons visible, little to no fasciculation, (B, B', B") average fasciculation some individual axons visible, some fasciculation, (C, C', C") high fasciculation almost no individual axons visible, individual fascicles discernible, some gaps between fascicles, (D, D', D") extreme fasciculation: no individual axons visible, almost no gaps in the fascicle, individual fascicles not obvious. The scale bar applies to A-D and is 50 μm.

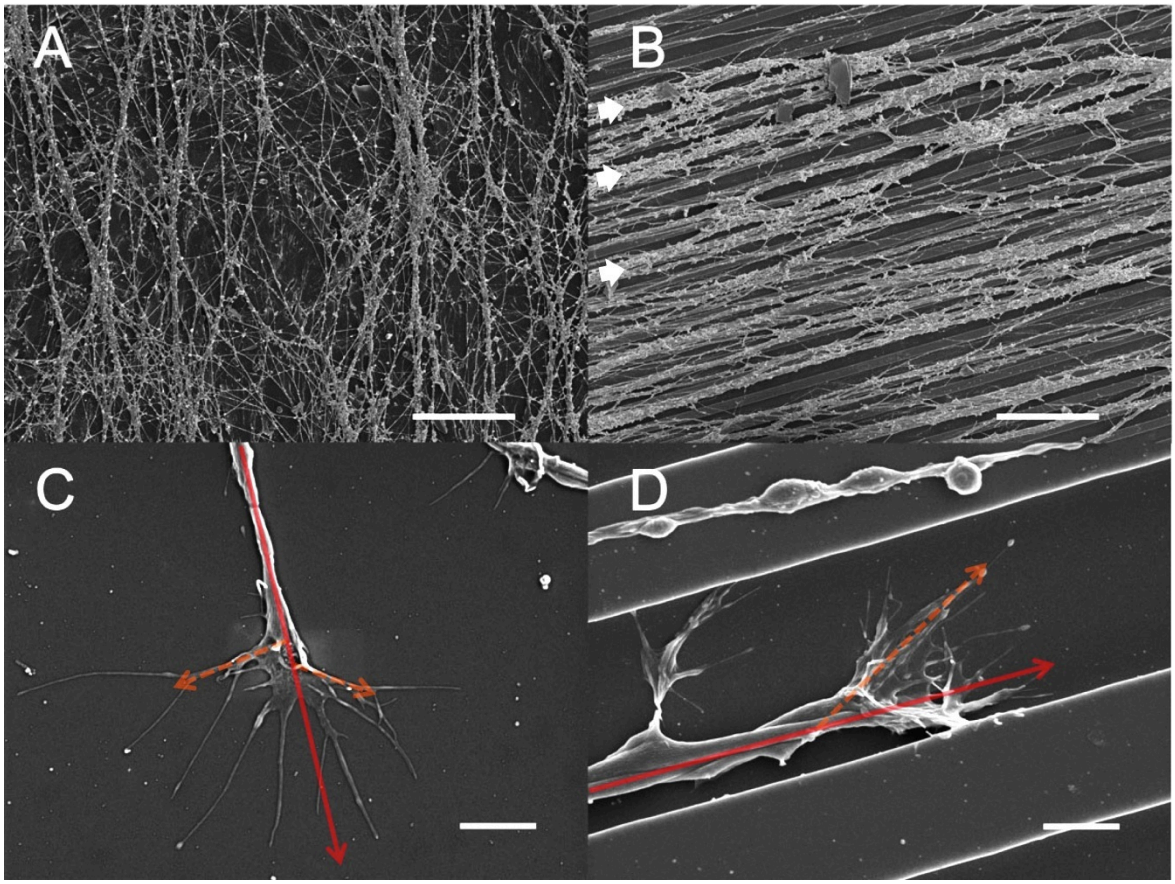

Figure 25: SEM of network extending from DRGs after 10 days culture on stiff PDMS (A, C) flat PDMS under standard culture conditions, and (B, D) 12.5 μm wide 5 μm deep microgrooves. A) On flat PDMS the network was not oriented with multiple layers of extensions many of which ran in different directions. B) On microgrooved PDMS the DRG network was unidirectional, the increased incidence and thickness of fasciculated fibre bundles was also evident (e.g. arrows). SEM of growth cones of axons on flat (C) and microgrooved (D) PDMS. It is evident from C and D that the growth cones deviated by a wider angle from the orientation of the axon/axon bundle on the flat © than the microgrooved (D) PDMS. The angle of dispersion of the growth cones was determined by measuring the degree of deviation of the orientation of a growth cone digitation (dotted arrow) from the direction of the axon/axon bundle (arrow) as indicated in C and D. Scale: A, B 100 μm; C, D 5 μm.

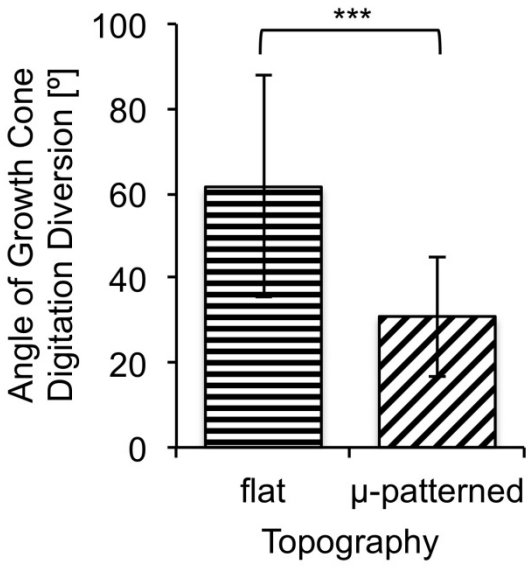

Figure 26: Average angle of deviation (±SD) of 30 growth cones digitation from the orientation of the main axon(s) on both flat and microgrooved (12.5 µm wide, 5 µm deep) hard (4.1 MPa) PDMS. These measurement were made using SEM images (e.g. Figure 25). The diversion angles were significantly different, p<0.001, 2-tailed Student T-test.

2.4 Discussion

In tissue engineering mechanotransduction and attractive or repulsive ligand/receptors interaction are usually used to study and explain the control of cell growth, morphology and even differentiation on substrates featuring different topography, stiffness or surface chemistry (Dalby *et al.*, 2007).

In the field of nerve regeneration, many studies have shown positive effects of engineered substrates using different strategies such as biomimetic scaffolds made off basal lamina derived from nerve tissue, and Schwann cell cultures (Kalbermatten *et al.*, 2008), electro-spun micro and nanofibres (Liu *et al.*), and surfaces mimicking the nerve environment (Bruder *et al.*, 2007). Guidance of both CNS and PNS neurons by microgrooved substrates has already been shown to be efficient in assisting directed outgrowth (Sorensen *et al.*, 2007, Sun *et al.*, 2010).

However, how axonal outgrowth is modulated by growth factor concentration, or the stiffness of the substrates is something rarely studied in the literature. Foley *et al*. (2005) reports on the interaction between groove size and two NGF concentrations on PC12 cells, which are immature CNS neurons. This work suggests that sub-optimal concentrations of NGF in combination with feature size and stiffness can be used to modulate length, surface area and fasciculation degree of neuritogenesis. Our findings presented here show for the first time that this modulation is also observable with a large amount of differentiated PNS neurons using an organotypic DRG culture, a model much closer to the *in vivo* situation with a healthy axonal outgrowth of ten thousand neurons, in which structural cells such as Schwann cells, and fibroblasts as well as other supportive cells are also present.

The influence of the stiffness on axonal outgrowth, particularly on growth cone morphology and the traction force these produce was investigated by Koch *et al*. (2012) in a study showing differential adaptation of cytoskeletal dynamics to substrate stiffness by CNS and PNS neuron growth cones. Briefly the stiffer a substrate is, the more traction force and actin polymerization will be observed at the leading edge of the growth cone. In 3D, neurite extensions have been shown to be correlated inversely to the stiffness of agarose gel, and to grow better down than up a stiffness gradient in a genepin crosslinked collagen system (Balgude *et al*., 2001, Sundararaghavan *et al*., 2009). The work accomplished in this chapter show how axonal outgrowth, axonal branching and fasciculation was affected by substrate stiffness, with a grooved, stiff substrate probably leading to more directional traction force and thus allowing less lateral spreading of the axonal outgrowth. It should be noted though that the sensing mechanism might be different, as the forces do not directly act on the nerve somata, as these are contained within the DRG. Furthermore the densification of the network induced by NGF is less obvious on the flat, stiff PDMS suggesting that the microgrooved topographic cue and the stiffness of the substrate are acting together to modulate axonal network morphology (Figure 18 and Figure 19). The assumption is that axon-axon interaction can occur on the topography, as

the sprouting axons are growing closer together even intertwining with each other (Figure 25 A, C) when they are guided by the pattern, whereas they are free to spread on the all area on the flat, stiff PDMS. (Figure 25 A, C). On the soft flat PDMS this effect is less evident. We interpret this, taking Koch *et al*. (2010) into account, such that the lower traction force generated by the growth cones on the soft surface reduces the extent to which these grow, and this also increases lateral interactions in which outgrowing axons are intertwined together into a big fascicule like structure.

Here the response to NGF is much reduced by a softer substrate and the effect on the surface area covered by the network reversed on a substrate that leads to an aligned outgrowth. The effect of neurotrophic NGF is a well-studied phenomenon (Cohen *et al.*, 1954, Sofroniew *et al.*, 2001). It has recently been shown that after binding to its tyrosine kinase receptor (trkA) mainly localized at the edge of the growth cone, NGF acts through a spatially regulated PI3K-GSK-3β pathway controlling axon growth via regulation of a microtubule plus end binding protein, adenomatous polyposis coli (APC) (Zhou *et al.*, 2004). NGF signal transduction is also known to be mediated by a retrograde endosomal transport after binding to trkA receptor, and uptake (Delcroix *et al.*, 2003). These *observations* lead us to the hypothesis that NGF level in the media have an effect on axon extension and morphology as shown *in vivo* (Gold, 1997). The interaction between substrate cue and cell response to growth factors has been highlighted by Grinnell and Ho (2013) who show that the response of fibroblasts to substrate stiffness was modulated by different FGF, LPA, or PDGF concentrations: cell spreading was seen to be independent of matrix rigidity if PDGF was present, in contrast the response to FGF or FBS, growth factors that increase contractility, was dependent on matrix stiffness. The effect of substrate topography on the adsorption and structure of adsorbed extracellular proteins as a potential source for these changes can be largely excluded as the substrate used are molecularly flat, in contrast to earlier observations where substrate curvature affected fibronectin structure and the display of cell binding sites (Mukhatyar *et al.*, 2011), here the incidence of areas of high curvature is low

(1 to 2 per 25mm) and the growth cones did not seem to interact specifically with edges (see e.g. Figure 25 B, D). This modulation of the response of axonal outgrowth to NGF by topography and substrate stiffness gives us important clues to apply to the design of nerve tubes in general where growth factor delivery is envisaged e.g. by microencapsulation (Xu *et al.*, 2003).

2.5 Conclusion

The results of the work presented in this chapter show that substrate stiffness, topography, and NGF concentration act through interacting pathways. Axonal outgrowth was guided by the microgrooved topography on stiff substrates (4.1 MPa) on both 12.5 µm and 25 µm wide grooves with 10ng/mL NGF in the culture media, whereas a packed and disorganized outgrowth was observed at 100 ng/mL, the highest NGF concentration tested. The morphology of the outgrowth on stiff PDMS at low NGF concentration also shows axons grouped in a neofascicular shape and supportive cells can be observed aligned with the nerve fibers. On the soft substrates (0.1 MPa) outgrowth was comparatively poor at low NGF concentrations (10 ng/mL). The main effect of the stiffness was observable at 50 ng/mL. At this NGF concentration the network morphology was less packed, the axons were less grouped together in bundles, and more branched on the soft (0.1 MPa) compared to the stiff (4.1 MPa) substrate.

These observations and the ANOVA prove that substrate cues interact with growth factor activity to modulate axonal outgrowth. The investigation of these parameters will help to refine parameters for nerve repair tube design in general. The study also allowed developing an *in vitro* system reducing the use of animal to test the axonal guidance potential of newly designed tube and neuronal remodelling system. Up to 30 dorsal root ganglions are available per animal, providing fast-growing and robust axonal network, which are easy to analyse. The system studied can mimic the case of a nerve injury wherein growing axons are cut. Nerve alignment and

guidance effect of bio-molecules, drugs, cellular therapies and use of other physical cues could be tested and developed with this *in vitro* system allowing the comparison with a guiding microgrooved topography in the same culture well.

These findings also need more investigation at a proteomic and a molecular level to specify which mechanical, trophic and tropic pathways are responsible for this combinational modulation of the axonal outgrowth.

3 Evaluation of a Polycaprolactone System for Peripheral Nerve Regeneration *In Vitro*

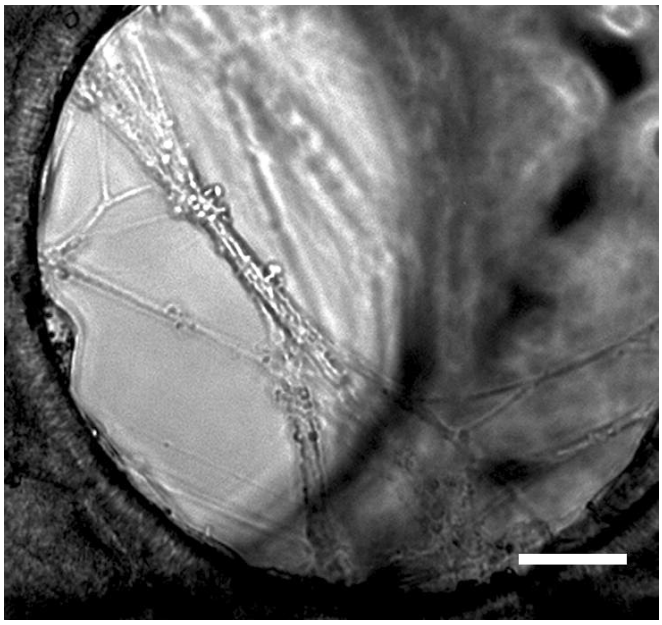

DRG axonal growth in minichamber PCL construct. Scale: 50 µm

3.1 Introduction

In this chapter the study focus on the potential of PCL as a biomaterial for nerve guidance tube. The main aims are:

- The investigation of the regenerative potential of the "Swiss roll" tube by DRG cultures on single and multi-layered PCL constructs featuring microgrooves, pores, and pillars to down scale this guidance tube environment.
- To explain the new protocol simplifying the fabrication of the Swiss roll and its reproducibility

There are ever more nerve tubes available on the clinical market (Daly *et al.*, 2012, Meek and Coert, 2013) to replace nerve graft, the gold standard for peripheral nerve repair. In addition new strategies are being developed to investigate and improve the regenerative potential of such tubes (de Ruiter *et al.*, 2009, Rosson *et al.*, 2009, Daly *et al.*, 2012). The main problem of nerve regeneration is the guidance of regenerating axons across the gap left behind by the injury. The misdirection of regenerating axons and scar formation in the boundary between the ends of the proximal and distal nerve stump lead to the death of 30-70 % of the sensory neurons, and 30-80 % of motorneurons (Ygge, 1989, Koliatsos *et al.*, 1994, Martin *et al.*, 1999, Hart *et al.*, 2008, de Ruiter *et al.*, 2008). Recent studies suggest that the ability to engineer and fabricate micro-patterned grooved and nano-patterned substrates could have potential for tissue engineering in general and for nerve regeneration particular (Lin *et al.*, 2008).

In this chapter, I used an organotypic model of neonatal DRG grown on a bioresorbable (Sun *et al.*, 2006), biocompatible and FDA approved biopolymer, PCL, to investigate and test the regenerative potential of a so-called Swiss roll design. PCL has been use in other nerve tube studies (Chiono *et al.*, 2009, Chang, 2009a, Ribeiro-Resende *et al.*, 2009, Sun *et al.*, 2010). This convenient biomaterial has a low melting temperature of about 60 °C.

That is one reason for its widely adaptation as a material for tissue engineering scaffolds in general (Ahvaz *et al.*, 2013, Kuppan *et al.*, 2013). The investigation of the Swiss roll tube already used in previous study for neuro tissue engineering (Sun *et al.*, 2010, Donoghue *et al.*, 2013) first started by evaluating the growth of axons on its simplest 12.5 µm wide microgrooved feature in a culture well. It was continued with a simplified 3D system based on stacked PCL layers termed a minichamber. This system allowed me to get systematically closer to the 3D tubular design without incurring all the associated complexities, and to evaluate the viability of the organotypic DRG culture to address the potential problem of diffusion limited survival and axonal escape through pores (Sun *et al.*, 2011).

As a final step the microfabrication technique was improved to make the fabrication of the Swiss roll a two steps process. This shortened process could replace the complex procedure designed by Seunarine (2008) described in Sun *et al.* (2011) and Donoghue *et al.* (2013). In the previous protocol, a spin-coating of a porous PCL layer on a microfabricated SU-8/silicon wafer featuring micropillars is followed by a micro-patterning by hot embossing with a PDMS stamp. The PCL sheet is then rolled to form the tube. This fabrication method makes the pores and microgroove alignment hard to control. The novel procedure allows better fabrication outcomes with a simple spin-coating step and a rolling step. I used UV photolithography technique to create the SU-8/silicon master featuring all the features (pores, pillars, microgrooves) in the same time. DRG culture was then tested in the Swiss roll construct.

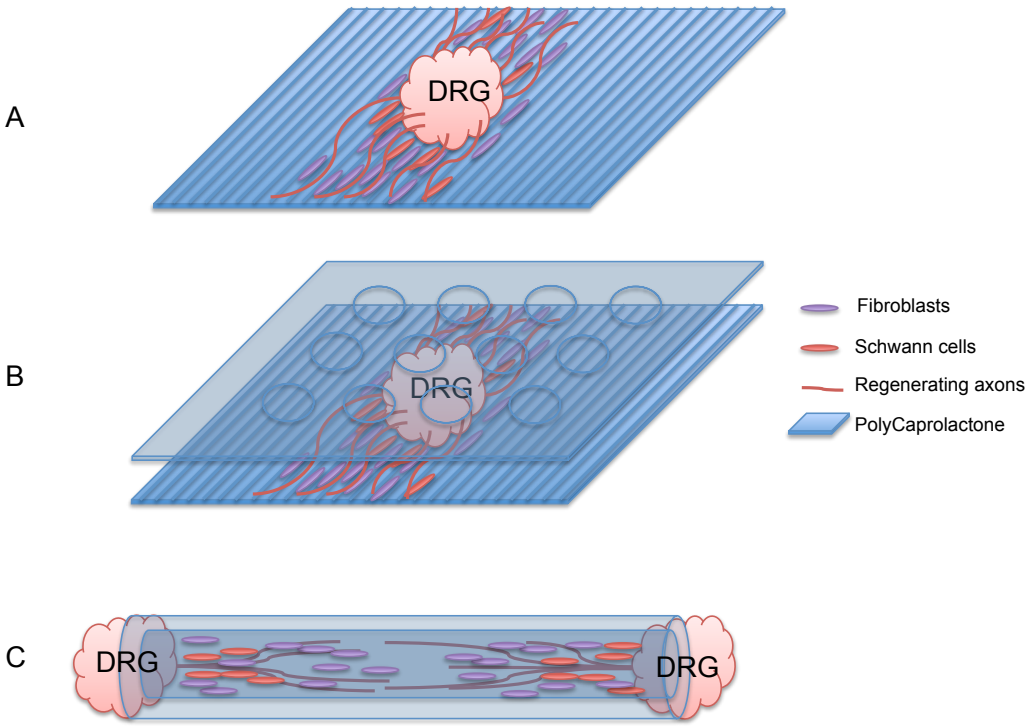

Figure 27: Scheme of the experimental approach for the development and the in vitro tests of the Swiss roll nerve guide. The DRG explants were first grown on single embossed PCL sheet (A). A second sheet of porous PCL was then added on the top of the first embossed sheet to create a first 3D in vitro model of the regenerating axon (B). The Swiss roll nerve tube design fabrication was optimised in a two step process, and two DRG were seeded at the extremities to evaluate the guidance and regenerative potential it provides to the DRG regenerating axons (C).

3.2 Materials and method

3.2.1 Fabrication of the master for PCL spin-coating

The silicon/SU-8 master for PCL spin-coating was designed and made to simplify the fabrication of "Swiss roll" nerve tubes. As the final PCL sheet used to create the Swiss roll should carry posts to separate the layers in the wound up tube, grooves to align the cells and pores to allow for diffusion across the sheet, the master needed three layers, each aimed at creating one of these features.

3.2.1.1 Design of the PCL master

To create the PCL master we used a photolithography technique (briefly described in Chapter 2). The principle of this technique is to spin-coat a photoresist (e.g SU-8) on a silicon wafer (Figure 29 and Figure 34) to form a layer which thickness is controlled by the parameters (e.g. photoresist viscosity, rotation per minute (rpm)). The photoresist layer is then cross-linked with UV in specific areas defined through a photomask to create permanent and hard micro or nanostructures (Figure 29). The unwanted photoresist (non-UV-exposed thus non-cross-linked) is then washed off the silicon wafer by development with the appropriate chemical solution leaving only the UV-exposed photoresist. To design the three different types of features with different heights (pores, pillars and microgrooves) we had to use three layers of SU-8 with three different photomasks (one for each type of features).

The three photomasks for the fabrication of the PCL master were designed using CleWin (Phoenix Software, Netherlands). The first photomask was used to create the negative surface feature needed to create pillars during casting, which are pits in the master SU-8 photoresist substrate (Figure 28 and Figure 29). As SU-8 is a positive photoresist (cross-linked with UV) the mask had to be such, that all the surface was exposed apart for the

pores, which are dissolved away during development (Figure 29). Thus they have to form the first layer during the master fabrication. The design of the pillars was modified from the initial design started by Seunarine (2008) to be round, and 200 µm in diameter, spaced 600 µm centre to centre on a rectangular grid with row to row distance of 700 µm centre to centre allowing space for the pores of the same dimension in between them, and maximise the surface available for grooves. As the pillars are needed to keep the layers apart, and the cells from being squashed as well as allowing the cells to be supported with nutrients these were designed to be 50 µm in height leaving some room for sheet flattening between pillars and room for extracellular space for nutrient and waste diffusion.

The second photomask was designed to cast 12.5 µm grooves and ridges with the intermediate second 5 µm SU8 layer on the master as it seems to give the best guidance according to the result in Chapter 2. The grooves were placed in the 500 µm wide stripe area not covered by pillars/pores. Due to the nature of SU-8 laid out above the areas exposed were thus the parts of the surface to become ridges.

The third photomask was designed to create pores of 200 µm diameter in the film during spin-casting. This diameter was chosen to minimize pore occlusion (Sun *et al.*, 2011). The pores were placed at 600 µm centre to centre and 700 µm row to row to allow a good diffusion and placement in between the pillars. Two rows of pillar/pores were placed offset by 600 µm to give a lozenge shape of pillars and pore patterns to make the diffusion of nutrients and gases more even. Again as SU-8 is a positive photoresist the mask had to be such, that only the area of surface was exposed that would later form the pillars on the master all else would later be dissolved away during development.

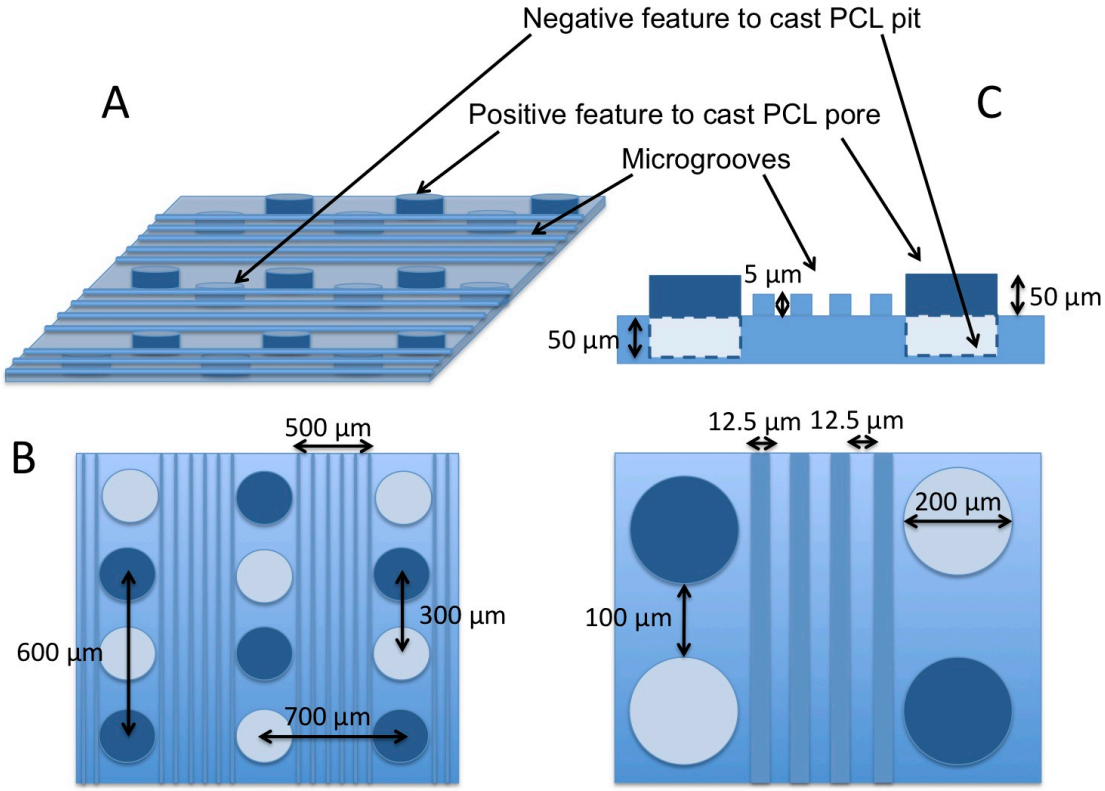

Figure 28: Scheme of the master for PCL spin-coating. Once spin-coated on the master, the PCL membrane obtained will feature pores, microgrooves and spacing pits together and will be then rolled in order to create a porous Swiss roll construct. The PCL features are pores and pillars of 200µm in diameter, spaced 600 µm centre to centre on a rectangular grid with row to row distance of 500µm center to center allowing space for the pores of the same dimension in between them in a lozenge pattern. The pillars are needed to keep the layers apart, and the cells from being squashed as well as allowing the cells to be supported with nutrients these were designed to be 50 µm in height leaving some room for sheet flattening between pillars and room for extracellular space for nutrient and waste diffusion. In between the rows of pits and pillars there is 20 grooves and ridges 12.5 µm wide and 5 µm deep to guide the regenerating axons.

3.2.2 Fabrication of the SU-8 layers on PCL the master substrate

3.2.2.1 1st layer

Si wafers of 100 mm diameter 500 µm thickness were cleaned in acetone, methanol, and isopropanol with sonication for 5 minutes each. The wafer was then dried with nitrogen gas. SU-8 3050 was spin coated at 3000 rpm 25 s to form a 50 µm thick layer. To coat the wafer ~2 mL of resist per square-inch were sufficient. The wafer was then soft-baked on a hotplate at 65 °C for 1 min, at 95 °C for 8 min, and then at 65°C for 1min (Figure 29.1). The layer was then exposed for 35 s on a Suss MicroTec MA6 mask aligner with exposure

energy of 100 - 200 mW/cm^2 using soft contact exposure mode with a photomask featuring 200μm dots allowing exposure of the photoresist in specific areas. A post-exposure bake was then performed on a hotplate for 1min, at 95 °C for 8 min then at 65°C for 1 min.

3.2.2.2 2nd Layer

SU-8 3005 was spin coated at 3000 rpm 25 s to form layers of 5 μm thick. The wafer was then soft-baked on a hotplate at 95 °C for 3 min he layer was then exposed for 12 s on a Suss MicroTec MA6 mask aligner with exposure energy of 100 - 200 mW/cm2 using a soft contact exposure mode and a photomask featuring 12.5 stripes holes allowing exposure of the photoresist in specific areas. A post-exposure bake was then performed on a hotplate for 1 min at 65 °C, 3 min at 95 °C and then 1 min at 65 °C (Figure 29.2).

3.2.2.3 3rd Layer

SU-8 3050 was spin coated at 3000 rpm 25 s to form layers of 50 μm thick.The wafer was then soft-baked on a hotplate at 65 °C for 1 min, at 95 °C for 8 min then at 65 °C for 1 min. The layer was then exposed for 35 s on a Suss MicroTec MA6 mask aligner with exposure energy of 100 - 200 mW/cm2 using soft contact exposure mode with a photomask featuring 200μm dots holes allowing exposure of the photoresist in specific areas. A post-exposure bake was then performed on a hotplate for 1min, at 95 °C for 8 min then at 65 °C for 1 min (Figure 29.4). The unexposed SU-8 was then developed off using Microposit-MF®319 developer (Shipley, UK) to get rid of the non UV-exposed SU-8. The surface was then rinsed with IPA and dried before silanisation (Figure 29.4).

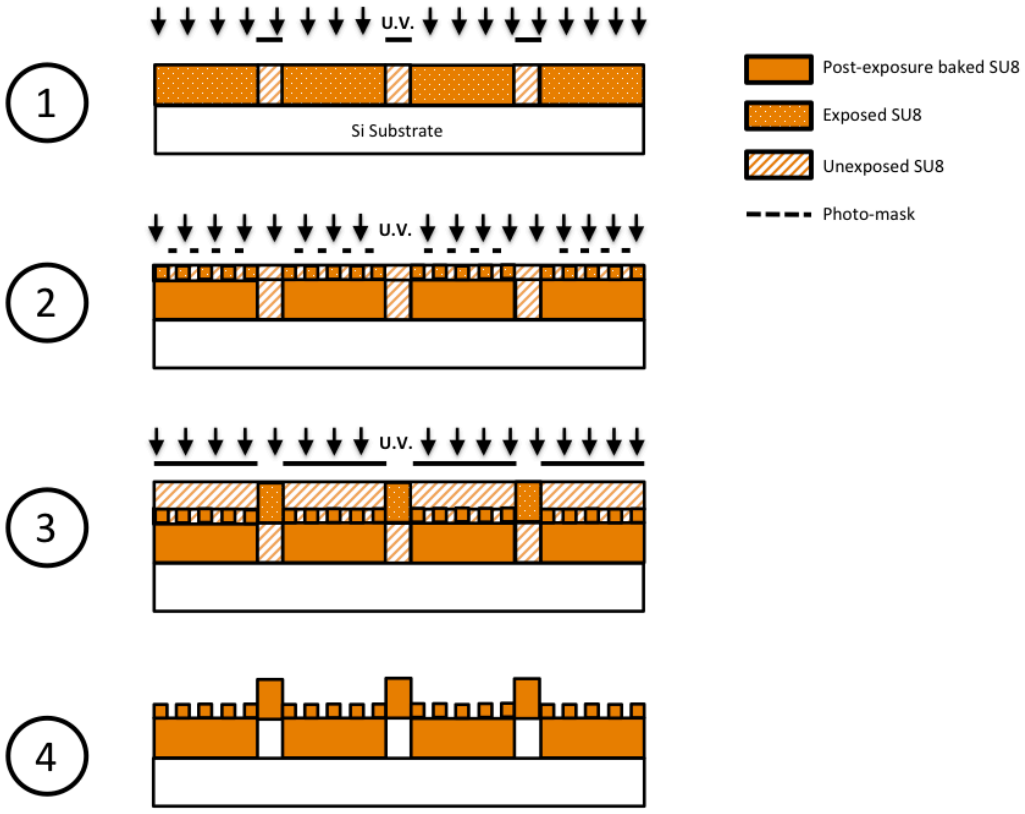

Figure 29: Fabrication step of the Silicon SU8 master for PCL spin coating. 1) Spin coated SU-8 3050 at 3000rpm 25s form a 50µm thick layer soft-baked on a hotplate at 65 °C for 1min, at 95 °C for 8 mins then at 65°C for 1min. It was then exposed for 35s on a Suss MicroTec MA6 mask aligner with exposure energy of 100 - 200 mW/cm2 using soft contact exposure mode with a photomask featuring 200µm dots. A post-exposure bake was then performed on a hotplate for 1min at 65°C, at 95 °C for 8 mins then at 65°C for 1min. 2) Spin coated SU-8 3005 at 3000rpm 25s form a 5µm thick layer soft-baked on a hotplate at 65 °C for 1min, at 95 °C for 8 mins then at 65°C for 1min. It was then exposed for on a Suss MicroTec MA6 mask aligner with exposure energy of 100 - 200 mW/cm2 using soft contact exposure mode with a using a soft contact exposure mode and a photomask featuring 12.5 stripes holes allowing exposure of the photoresist in specific areas. A post-exposure bake was then performed on a hotplate for 1min AT 65°C, at 95 °C for 4 mins then at 65°C for 1min. 3) The third step was similar to the first step except that the photomask was the inverse one. 4) The whole wafer was then developed in EC solvent and silanised.

3.2.3 Swiss roll fabrication

PCL (Mw 65 000 Da, CAS 24980-41-4, Aldrich, Poole, UK) was dissolved in chloroform at 25 % weight to weight (wt/wt) to form a solution that has the right composition for spin casting. The PCL solution is then spin coated on the SU8 master at 2000 rpm (200 rpm/s), for 30s and dried for 20 min before peeling it off the master (Figure 35). After plasma treatment with a Harrick

Plasma Cleaner (Harrick Plasma, USA) at high settings (740V DC, 40 mA DC, 29.6 W) for 5 min squares of 1 cm^2 are cut of the PCL sheet and rolled around a 1mm diameter needle to form a Swiss roll construct with the microgrooves parallel to the longitudinal axis of the needle (Figure 35). The Swiss roll is then sealed along the edge using a microscope slide heated to 100 °C, and prepared for cell culture as described for the constructs below.

3.2.4 PCL constructs

3.2.4.1 Embossed PCL in culture well

To create the simple microgrooved PCL pattern in a well, 4 mL of 25 % (wt/wt) PCL (Mw 65 000 Da, CAS 24980-41-4, Aldrich, Poole, UK) in chloroform solution was spin coated at 1500 rpm for 30s on a smooth silanised silicon wafer to create a flat PCL sheet of 10-15 µm thickness. The flat PCL membrane was cut in discs of 13 mm diameter and individual sheets were spread in a 24 well plate. The side of a 10:1 PDMS device, described in Chapter 2, featuring parallel grooves with the same width of 12.5 µm and depth of 5 µm were put on the top of the PCL discs. The well plate was then put on a hot plate at 80°C for 1min and once the PCL had melted gentle pressure was applied to the top of the PDMS device. The result was an embossing of the microstructure into the melted PCL polymer, attaching it onto the plastic of the well plate in the same time.

3.2.4.2 3D PCL minichamber fabrication

Porous PCL membrane fabrication: 4 mL of 25 % (wt/wt) PCL (Mw 65 000 Da, CAS 24980-41-4, Aldrich, Poole, UK) chloroform solution was spin coated at 1500 rpm for 30 s on a silicon wafer with microfabricated SU-8 micro-pillars (Height: 30 µm, Diameter 300 µm, Distance between each pillar: 300 µm).

A 10-15 µm thick porous PCL sheet (pore diameter: 300 µm) with pillars of 50 µm height, was peeled off the silicon wafer, once the chloroform had completely evaporated after 15 min.

A flat, smooth silicon wafer was used with the same settings to fabricate flat PCL sheets. The flat PCL membrane (1.5 cm × 3 cm) was spread on the structured side of a poly-dimethylsiloxane (PDMS) stamp featuring parallel grooves with the same width of 12.5 µm and depth of 5.0 µm and parallel rows of pillars (pillar size: 50 µm wide, 400 µm long, 75 µm high, distance between pits in each row: 100 µm, row to row distance: 400 µm). A piece of Polystyrene (1.5 cm × 3 cm) was then added on the top. A smooth PDMS stamp of the same dimension completed the hot embossing sandwich and the whole stack of material was pressed on a hotplate at 80° C for 30 s (Figure 30).

The design and the dimension of this stamp used for this fabrication section were design for earlier studies about Swiss Roll design by Seunarine (2008).

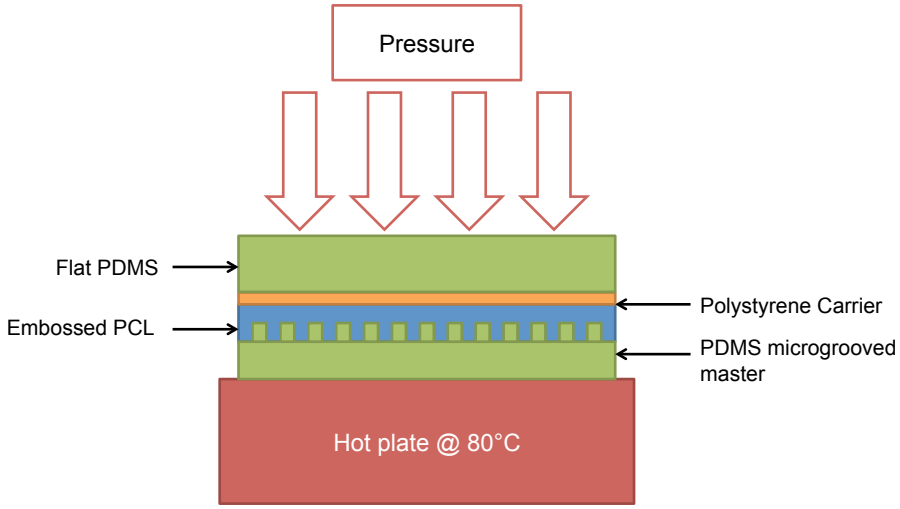

Figure 30: Scheme of PCL hot embossing. A flat PCL sheet (1.5 x 3 cm) was cut and spread on a PDMS stamp featuring 12.5 µm wide 5 µm deep microgrooves and parallel rows of pillars (pillars size: 50 µm wide, 400 µm long, 75 µm high, distance between pits in each row: 100 µm, row to row distance: 400 µm). A polystyrene carrier and flat PDMS stamp were added on the top. The stack was then put on a hotplate at 80°C for approximately 30 second. After cooling to room temperature for 3 min, the construct was peeled off the stamp and the microstructure was embossed in the PCL.

The result was an embossing of the microstructure into the molten PCL polymer, attached to the plastic carrier in the same time. The plastic carrier with the micro-structured PCL membrane was peeled off the stamp, after cooling to room temperature for 5mins, the base structure and the porous PCL membrane are then treated with a Harrick Plasma Cleaner (Harrick Plasma, USA) at high settings (740V DC, 40 mA DC, 29.6W) for 5 minutes. This was then used as is for the DRG culture (Figure 37), or used for further modification with a porous lid to form a minichamber.

Up to 8 layers of porous PCL membrane (1.5 cm× 3 cm) were sealed with two pre-heated glass slides (100 °C) pressed for 1-2 minutes on the edges of the so-called minichamber resulting in a set of layers of porous lids on top of the micro-structured base (Figure 38 and Figure 40).

3.2.5 Plasma deposition and surface contact angle measurement

The measurement of the water contact angle allowed evaluating the efficiency of the plasma cleaner to change the wettability of the PCL

surface. The surface contact angle of reverse osmosis water on flat PCL sheet was measured using a KSV CAM 100 goniometer (KSV Instruments, Finland) with series of thirty measurements for three different droplets for each plasma treatment time. The surface was rendered more hydrophilic with increasing treatment time, this coincided in the case of PLL coated PCL with increasing cell adhesion. The PCL devices were treated at 29.6 W for 5 min using a Harrick Plasma PDC-002 Plasma Cleaner. After plasma cleaning and sterilization in 70 % ethanol for 30min the devices were dried and coated in 13 µg/mL poly-L-lysine (Sigma, UK) solution for 30min at room temperature, rinsed in PBS three times before seeding.

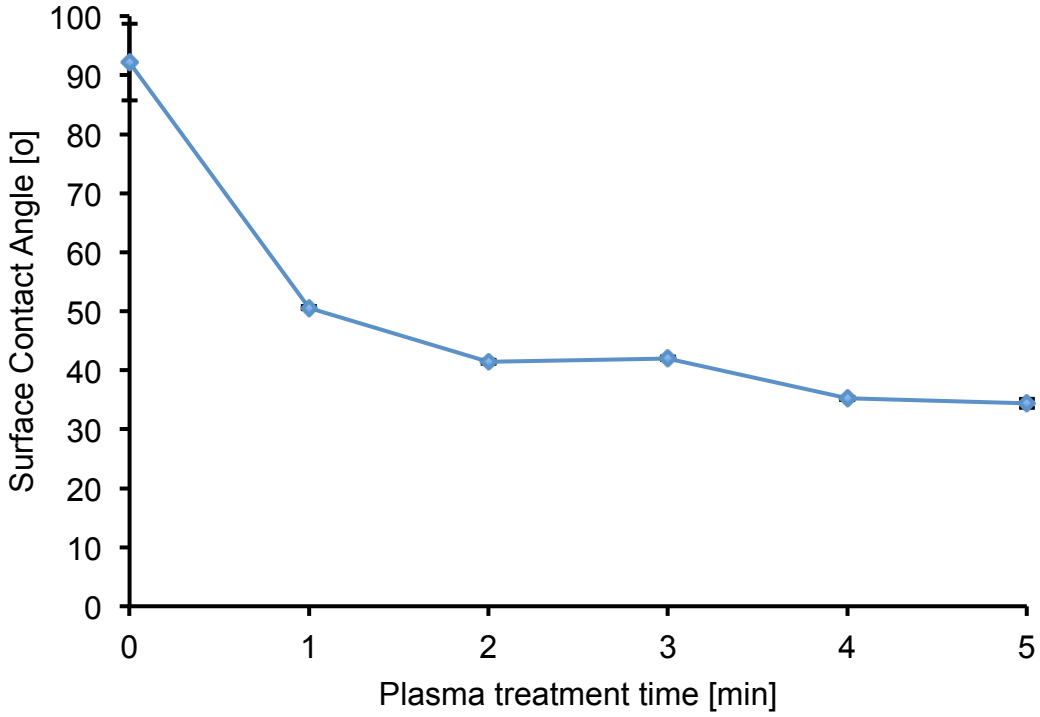

Figure 31: Surface contact angle of PCL after different Plasma treatment time.

The graph (Figure 31) shows that a 2-4 min plasma treatment is already sufficient to render the surface hydrophilic so more optimal for cell culture.

3.2.6 Explant seeding and culture

DRGs were isolated from 2 days old neonatal Sprague Dawley rats (as described in detail in Chapter 2 Figure 14), and seeded in the constructs.

DRGs were then grown for 10 days at 37 °C 5 % CO_2 in L15 media (Sigma) supplemented by 10 % FBS, 50 ng/mL NGF 2.5S (Invitrogen), 50 μg/mL n-acetyl-cystein and 1 % antibiotics antimycotic (PAA p11-002). For the embossed PCL the 200 µL of media was exchanged everyday, for the PCL minichamber and Swiss rolls, half of the media (250 µL of 500 µL) was changed every third day. After 10 days growth, cells were fixed and immunostained for β3-tubulin (ms anti-TU-20 Santa Cruz) on the 2D hot-embossed scaffold and by Coomassie blue staining in the minichambers. For the Swiss roll DRGs were cultured for 20 days and then stained with Coomassie blue. The samples were viewed by fluorescence microscopy (Figure 36) for immunostainning and bright field light microscopy for Coomassie blue staining and living culture observation (Figure 37, Figure 38, Figure 40, Figure 43, and Figure 44).

3.2.7 Data analysis

Composite images of DRG networks were assembled in Photoshop (Adobe), and the length, width, and the surface area of the DRG outgrowth measured using the Analyse Particles tool of ImageJ as described in Chapter 2 Figure 15. Due to the low number of repeat no statistical analysis was performed and the measurement were shown as a pilot study.

3.3 Results

The SU8 master for PCL Swiss roll nerve tube fabrication (Figure 32) was measured with a Dektak 6M Height Profiler (Veeco, US) (Figure 33). This measurement showed that the features designed have the wanted dimensions.

On the light micrograph of the Master (Figure 32) we can see some small cracks and residual SU8 defect, which did not impair the rest of the PCL fabrication.

The PCL spin coating on this wafer resulted in a PCL layer with 5 µm deep, 12.5 µm wide microgrooves, 200 µm diameter pores and semi-circular pillars. This deviation of the shape of the pillars from the master substrate could be an effect of the centrifuge force applied on the liquid PCL solution during the spin coating (Figure 34 and Figure 35). Overall, the fabrication technique of the internally micropatterned nerve tube has been improved and simplified compared to the previous hot embossing technique.

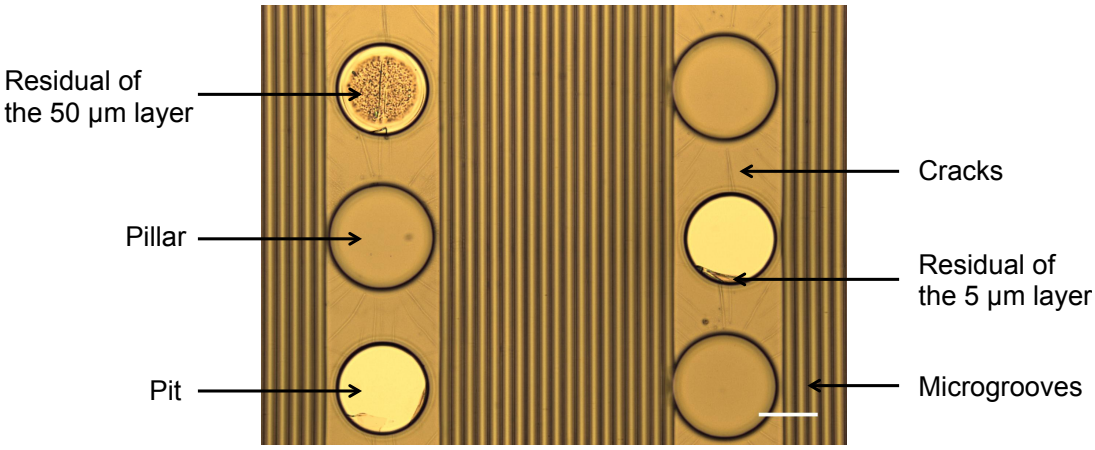

Figure 32: Micrograph of the SU8 master viewed from the top. Three layers of SU-8 photo resist were spin coated and exposed to UV through a series of photo masks with a MA -6 mask aligner, Figure 35and then post exposure baked as described. This formed 50µm deep pits, 50µm high pillars, and 5µm deep grooves (see arrows left). The whole wafer was then developed in EC solvent and silanised. The SU-8 photo resist showed some cracks as well as some residues in the negative concave features (see arrows right) meaning that the fabrication could be improved in terms of post UV exposure baking time and development time. Once spin coated the PCL membrane obtained will feature an inverse pattern of pores where the master has pillars, microgrooves, and spacing pillars where the master has pits. This microstructured membrane will be then rolled in order to create a porous Swiss roll construct (Figure 35). Scale: 100µm

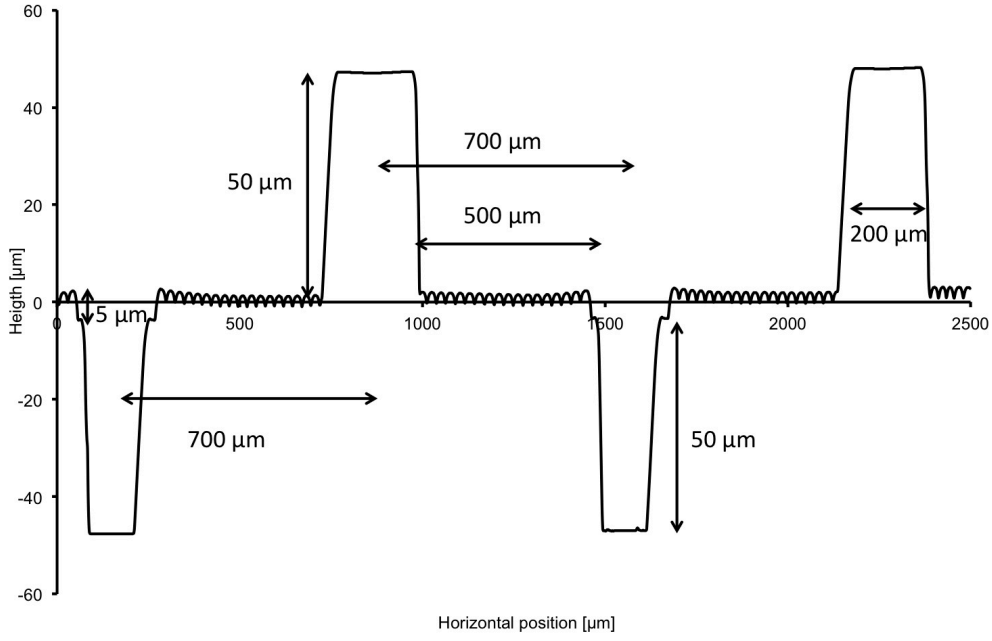

Figure 33: Graph of Veeco Dektak 6M Height Profiler measurement of the cross section of fabricated SU8/PCL Master, perpendicular to the long axis of the microgrooves. The three kinds of features designed have the right dimensions: 50µm high pits and pillars of 200 µm diameter and 12.5µm wide grooves and ridges.

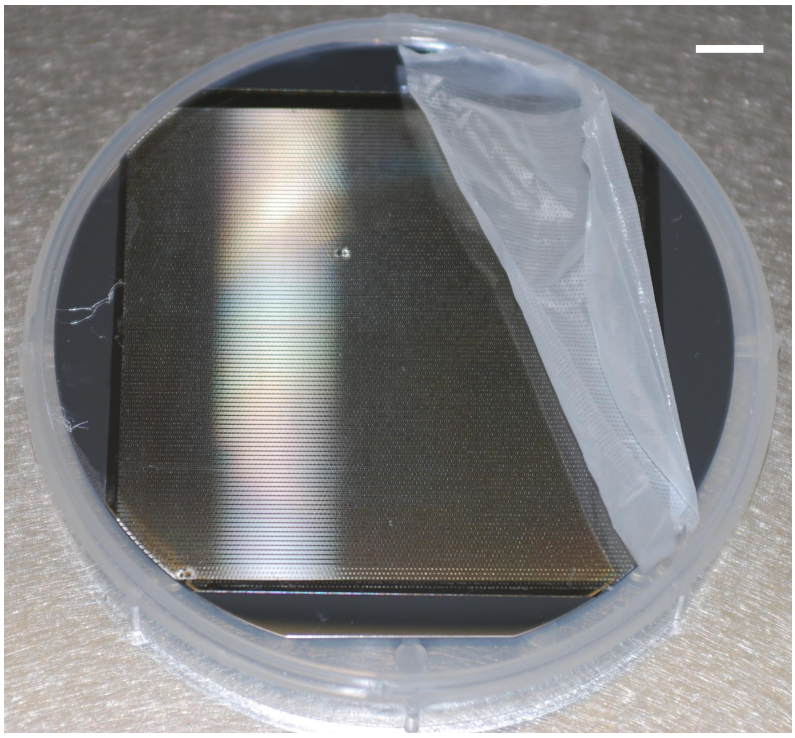

Figure 34: Silicon SU8 master for PCL spin coating. A solution of 25 % PCL in chloroform is spin coated on the SU8 master at 2000rpm 30s. The chloroform then evaporate for 15min and a PCL sheet is peeled off the master and rolled to fabricate Swiss rolls constructs.

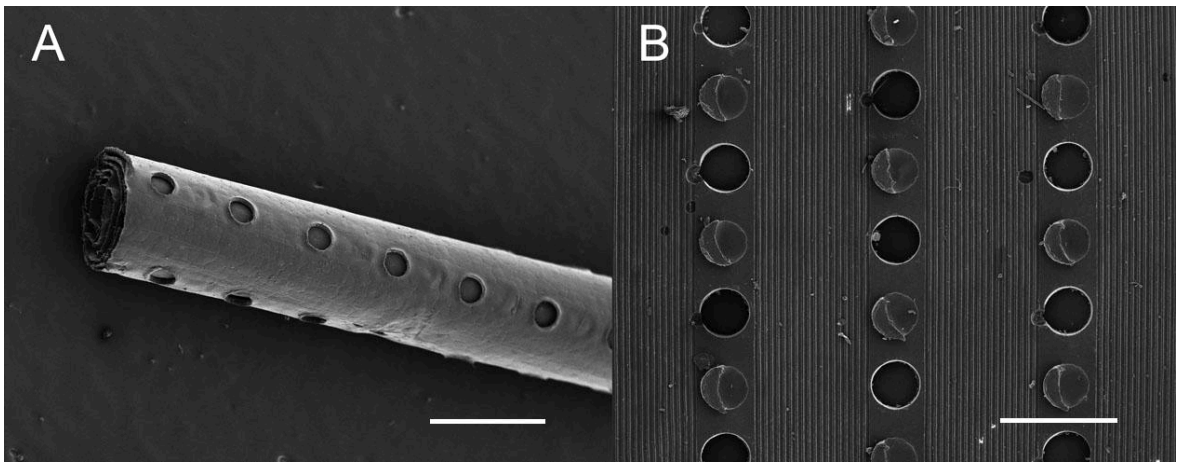

Figure 35: Scanning electron microscopy picture of a PCL Swiss roll tube for peripheral nerve repair (A).The tube is formed by rolling a spin-coated PCL sheet featuring 12.5µm wide and 5µm deep microgrooved internal pattern and, 200µm pores and pillars (B); (A) Scale bar 1 mm (B) 500 µm.

As PCL is translucent, therefore it is hard to observe DRG outgrowth in 3D within a three-dimensional construct (Figure 43, Figure 44). To avoid this problem a "2D to 3D" view was adopted. It give us the possibility to observe the effect of each features progressively starting from the microgroove, adding the pillars feature and finally adding a porous layer of PCL to form the so called minichamber.

The DRG cellular and axonal growth within the different constructs shows us that PCL provides a good environment for axonal regeneration (Figure 43, Figure 44, Figure 36, Figure 37,and Figure 38). On the embossed PCL, the guidance effect of axons and other cells from the explants seen in Figure 36 is conserved when the constructs feature the microgrooved topography, even if in some cases an escape of some axons can be observed (Figure 37, Figure 38, Figure 40,and Figure 41) especially when they are in contact with non-patterned surfaces. On Figure 36 we can observe that the thickest outgrowth occurs on the pillar, which seem to offer anchorage on the top of the guidance effect provided by the microgrooves.

The width of these regenerating axonal DRG networks changes when switching from 2D to the 3D multilayered minichambers (Figure 40). The lid being not patterned, the growing axons and cells are not guided on this surface resulting in a partly non-oriented network (Figure 40). This randomly oriented growth shows the importance of the micropattern and could be explained by the cellular and axonal escape through the pores (Figure 40, Figure 41, and Figure 42). The DRG axonal outgrowth was limited in the minichamber constructs with 8 lids (Figure 40C), which mean that the number of lids seems to be a problem for the diffusion of nutrients, waste and gases.

As Figure 40B shows, one side of the network is less developed than the other one, where the two patterns of pores in the lids are less aligned. This culture suggest, as indicated in Figure 42 that if the lid is made up of multiple layers the response to the topography is influenced by pore alignment, which influence media, nutrient, and oxygen diffusion. This culture also shows that the DRG could be sustained for prolonged periods under immersed conditions, whereas they are normally difficult to handle *in vitro*. Due to their high fat content, they normally float, if the level of media is higher than the DRG. This is the reason to only use small amounts of media used when these are cultured on glass or PDMS, and in the first 2D embossed system.

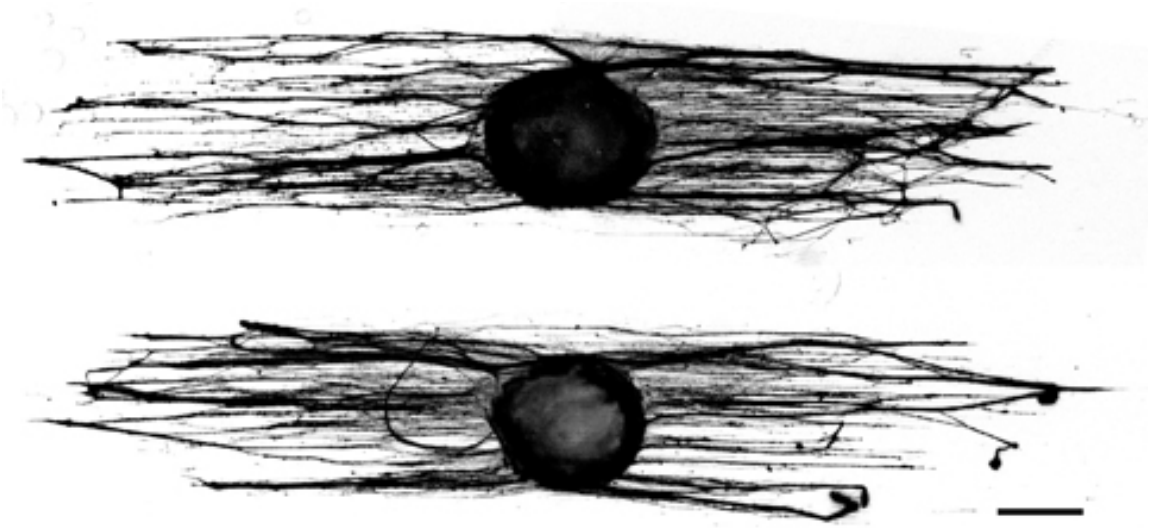

Figure 36: DRGs after 10 days culture in L15 on 12.5 µm width 5 µm depth microgrooved hot-embossed on PCL. DRGs stained for β3-tubulin. Guidance and directionality of the axon outgrowth is obvious and in alignment with the features of the embossed microstructure. Scale 500µm.

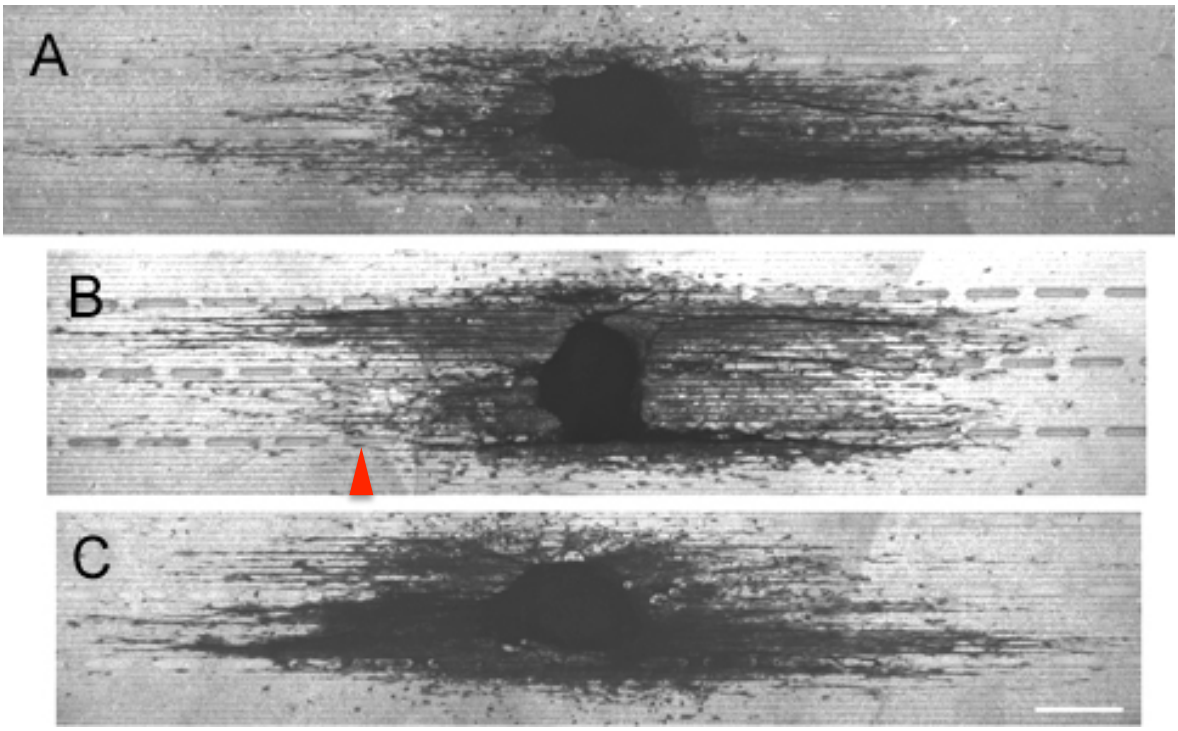

Figure 37: DRG after 10 days culture on hot embossed PCL sheet (A, B, C). The PCL sheets feature 12.5 µm wide, 5 µm deep microgrooved and parallel rows of pillars (pillars size: 50 µm wide, 400 µm long, 75 µm high, distance between pits in each row: 100 µm, row to row distance: 400 µm); coomassie blue staining. The axonal outgrowth is guided by the hot embossed microstructures. The axons interact also strongly with the pillars, using these for guidance as well, with some of these growing across these 50 µm high features (red arrowhead); scale 500µm.

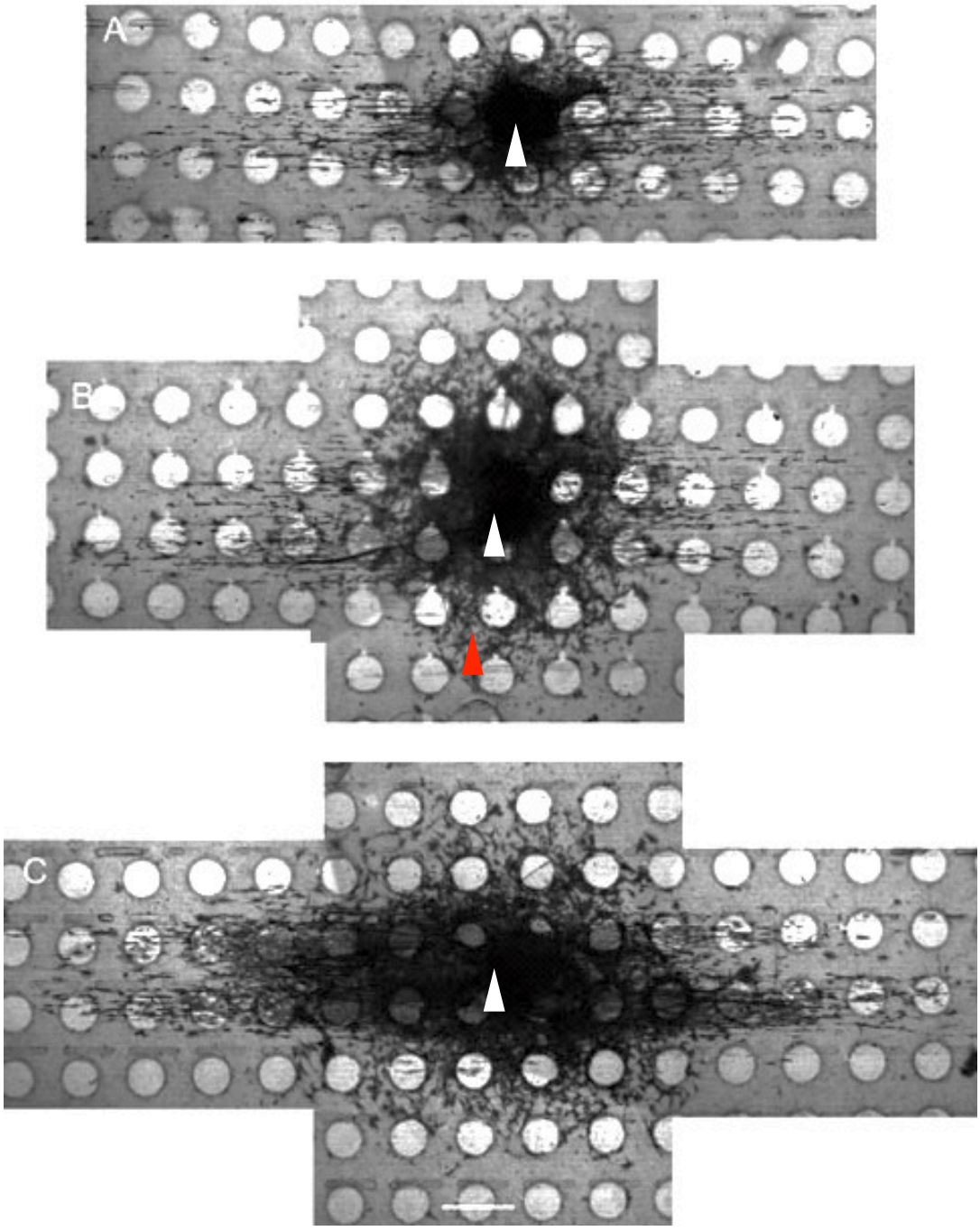

Figure 38: DRGs (arrowhead) after 10 days culture in minichamber constructs (A, B, C). DRGs are cultured between 12.5μm width 5μm depth microgrooved PCL base featuring pillars (pillar size: 50 μm wide, 400 μm long, 75 μm high, distance between pits in each row: 100 μm, row to row distance: 400 μm) and PCL lids featuring 300μm pores; Coomassie blue staining; The axons are guided by the topography on the micro-structured bases and that the networks can have various sizes due to the absence of guidance on the PCL lid (red arrowhead) and the axonal escape through the pores. Scale 500μm.

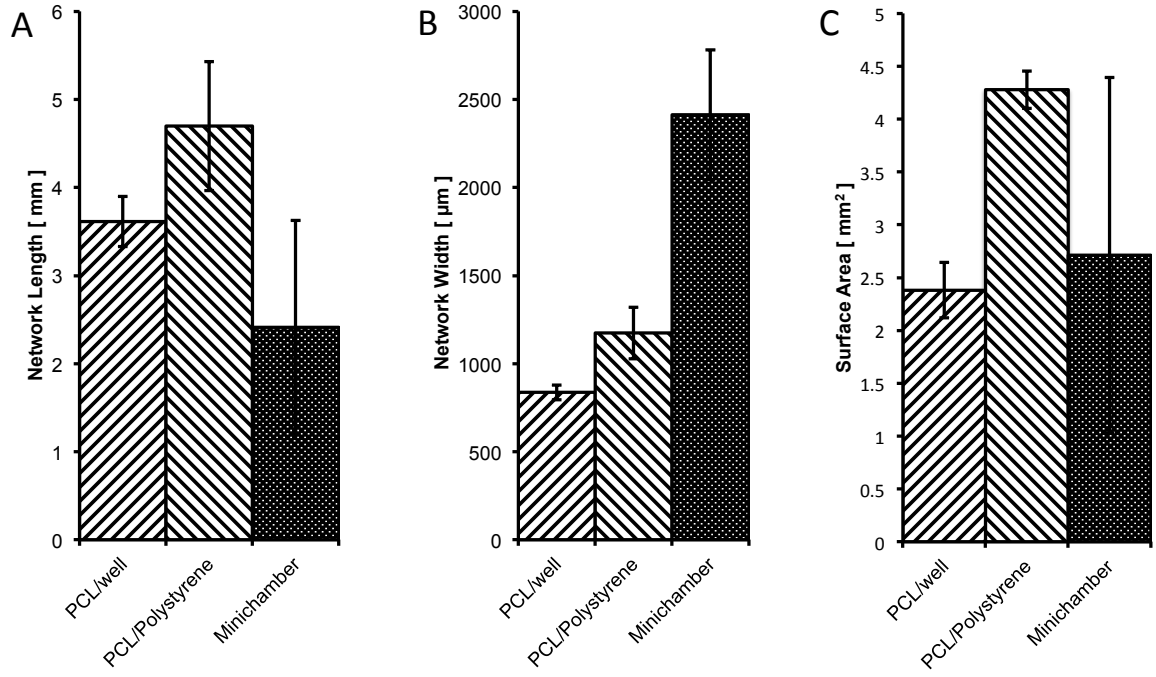

Figure 39: Analysis of the DRG network on the different constructs. The different construct are: PCL embossed on the well (Figure 36), the PCL embossed on the polystyrene (Figure 37) and in the minichamber with one porous PCL lid (Figure 38). after 10 days in culture A) network length; B) network width ; C) network area C) after 10 days growth A) The DRG network length is maximal on the PCL microstructure embossed on the polystyrene, a bit shorter in the PCL directly embossed on the well and shorter in the minichamber. B) The width of the network increase with the porous lid of the construct which provide no guidance and no directionality for the cell and the axons growing on it (n=3 repeats). Due to the low number of repeat no statistical analysis was performed.

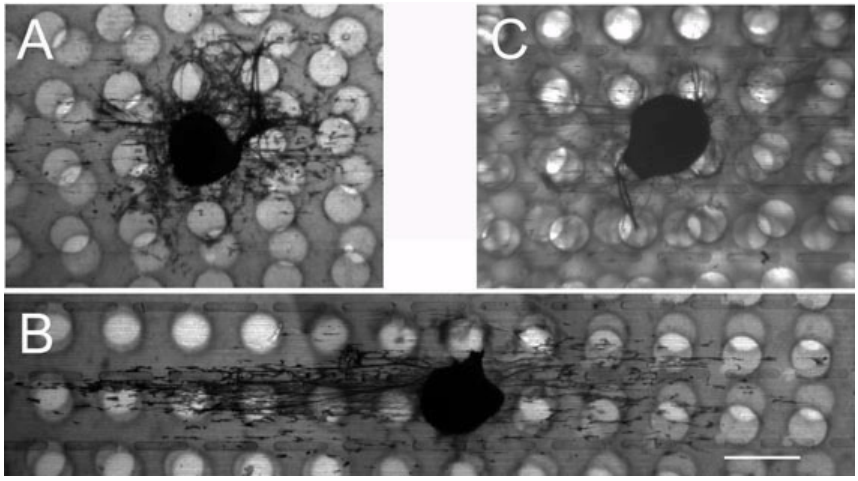

Figure 40: DRGs after 10 days culture in minichambers with microporous PCL lids. The DRGs were seeded between 12.5 µm wide, 5 µm deep microgrooved PCL base featuring pillars (pillar size: 50 µm wide, 400 µm long, 75 µm high, distance between pits in each row: 100 µm, row to row distance: 400 µm) and (B) two or (C) eight PCL lids featuring 300 µm pores and. (A) DRG seeded accidentally between the two porous lids ; Coomassie blue staining. The axons are guided by the microgrooved topography when the DRG is seeded on the base, and that the overall network grows out directional (B).In the PCL minichamber with eight lids (C), the DRG outgrowth is possible but poor, probably because of a lower diffusion of gases, and nutrients. The axonal network is not guided in the culture of the DRG seeded between the two PCL lids and its network has a ovoid shape as observed on the control on flat PDMS (Chapter 2) (A). One side of the network is less developed than the other one where the two porous PCL lids are less aligned (arrowhead in B). ; Scale: 500 µm

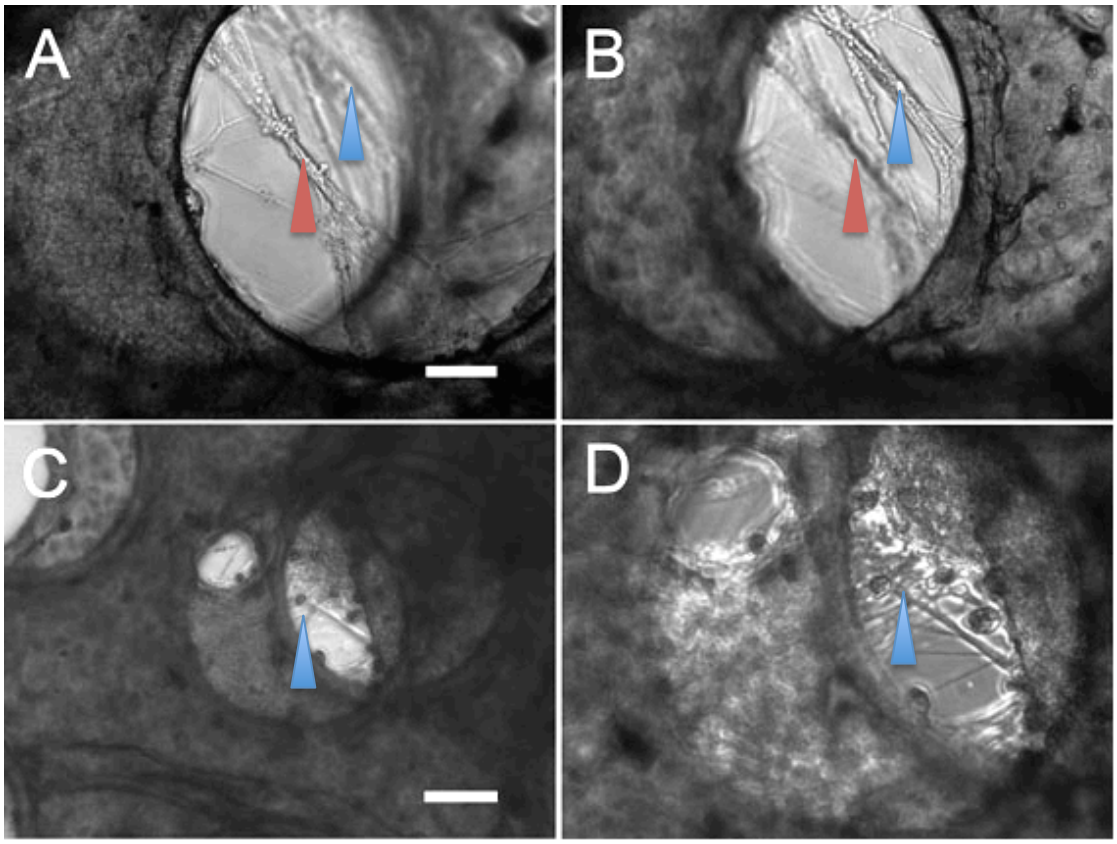

Figure 41: DRG axonal outgrowth culture in a PCL minichamber viewed by light microscopy. The pictures are taken through the pores of the two PCL lids of the minichamber. We can see some axon bundles at different focal positions (arrowheads in A and B) meaning that the outgrowth is in 3D and the network grows through the layers. A healthy axonal outgrowth from the DRG and some cells have grown on the hot embossed microgrooved PCL substrate, the base of the minichamber, (arrowhead in D and C) and is observable through the pores of the porous lids. Scale: 100 µm in C, 50 µm in A, B, D.

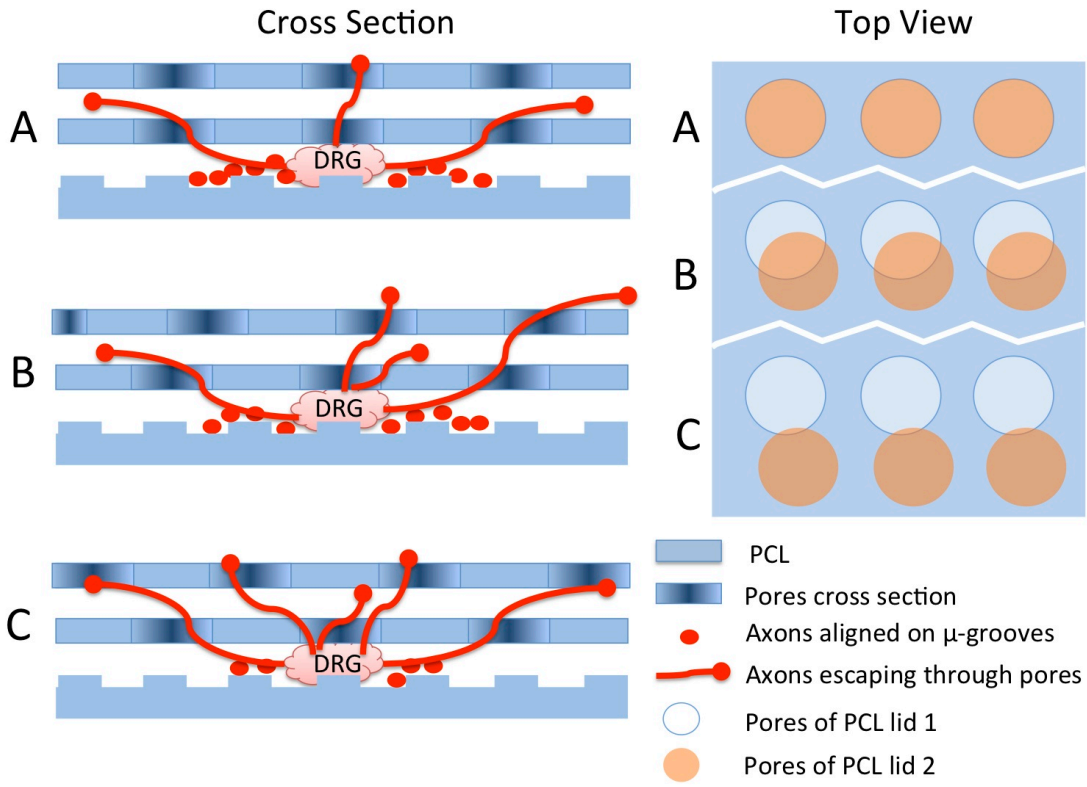

Figure 42: Scheme of the DRG outgrowths in PCL minichamber constructs with different pores alignment. The three kinds of alignment can be found in the same construct. When the pores are aligned (A) nutrient and gas diffusion is maximal in the construct. This condition changes with the degree of overlap (50 % in B, 0 % in C) and could affect the morphology and the sustainability of the axonal growth. For example, more axons would be following the pattern and there would be less axonal escape.

Within the Swiss roll oriented axon like structures, and cell colonies can be observed, which indicates that the microgroove pattern provides good guidance and support. From a macroscopic point of view the intense Coomassie staining at the ends of each of the tubes show that approximately 2 mm growth emanated from each DRG explants at the end of the tube after 20 days *in vitro* (Figure 43, Figure 44).

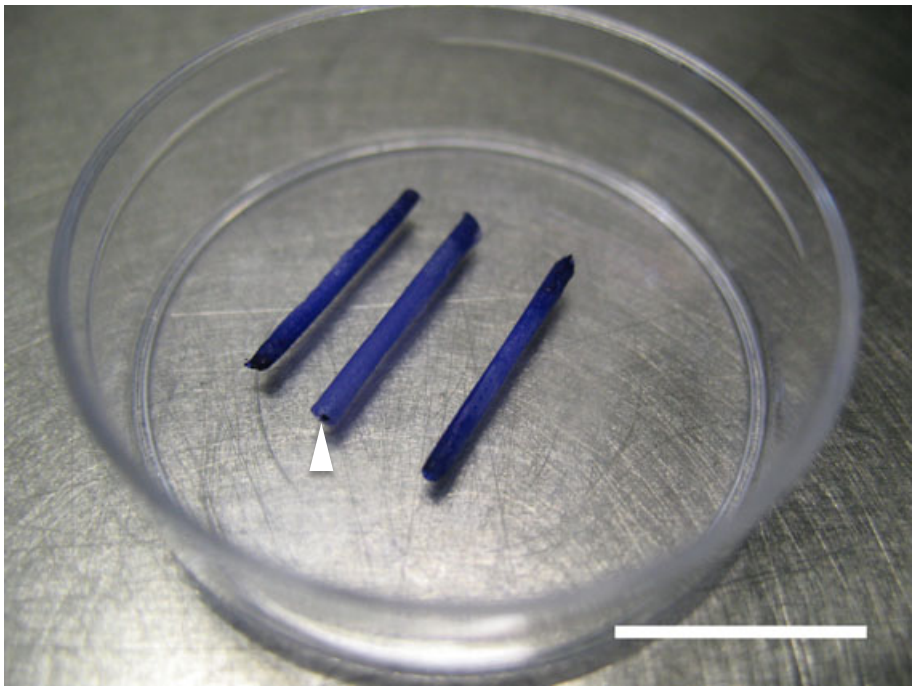

Figure 43: Coomassie blue staining of the 1 cm long Swiss rolls tube. In Swiss roll shown in Figure 35, two DRG were seeded and grown for 20 day at either ends. Cells colonised approximately 2mm of the whole tube: the staining color is more dark at the ends of conduits with DRGs seeded compare to the control cell-free end without a DRG seeded (arrowhead); Scale: 1cm.

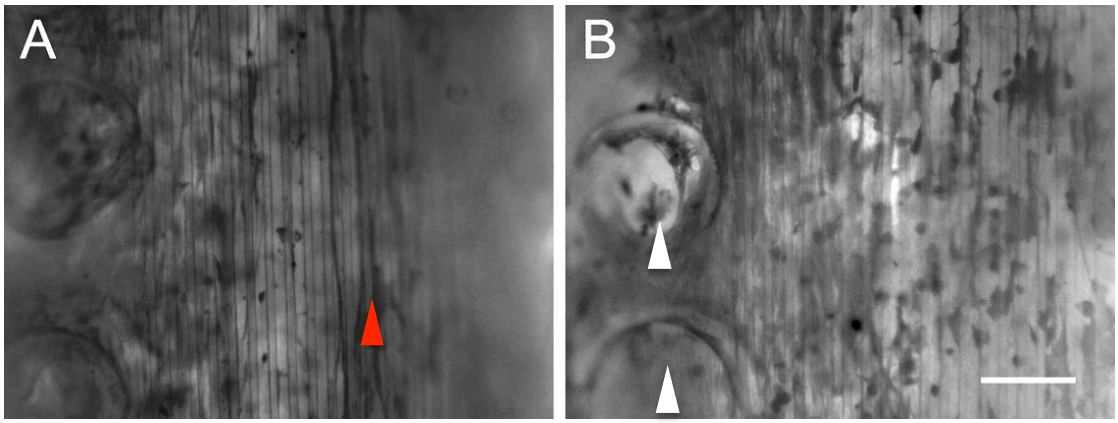

Figure 44: Coomassie blue staining of the axonal outgrowth and cells from a DRG grown in the Swiss roll tube (Figure 35) after 20 days culture. From the picture the 12.5 µm wide 5 µm deep microgrooves in PCL and the 200 µm wide pores and pits (arrowhead) are evident. We can see axon like structure (red arrowhead) guided by the microgrooves and other cells like fibroblast and Schwann cells expanding on the substrates; Scale: 100 µm.

3.4 Discussion

From previous study, microgrooved PCL have been shown to be a good candidate for neuro tissue engineering (Sun *et al.*, 2010, Donoghue *et al.*,

2013). The previous protocol for the PCL Swiss roll fabrication has been simplified and allows a better reproducibility (Figure 34 and Figure 35).

The results obtained using DRG explant cultures show that comparable growth was possible on flat 2D-, multilayered-, and the full 3D tubular-constructs . The pre-seeding of the tube with Schwann cells could complete this work, alternatively other supporting cell could be pre-seeded as shown in previous studies (di Summa *et al.*, 2009, Sun *et al.*, 2010). In comparison to other studies, where PCL was used as a material for nerve guide tube or tissue engineering (Seunarine, 2008, Chang, 2009a), the use of the pores allow a better diffusion of nutrient, gases and migration of supportive cell into the depth of the construct.

The axonal outgrowth is guided by the microtopography as we can observe clearly by scaling down the Swiss roll environment with the minichambers and other PCL constructs (Figure 37, Figure 38, Figure 40,and Figure 44). The axonal escape shown in these porous PCL environments leads us to the conclusion (Figure 40, Figure 41, and Figure 42) that both side of the rolled PCL sheet should be patterned to give the optimal guidance potential to the tube. This problem could also be overcome by the use of a second layer of guiding biomaterial, fibres (Schnell *et al.*, 2007, Corey *et al.*, 2007, Valmikinathan *et al.*, 2009, Madduri *et al.*, 2010, Hurtado *et al.*, 2011) or hydrogels (Midha *et al.*, 2003, Atzet *et al.*, 2008, McGrath *et al.*, 2010, Georgiou *et al.*, 2012, Georgiou *et al.*, 2013, Lampe *et al.*, 2013). These materials and the scaffold/membrane structure allow nutrient, oxygen diffusion, and angiogenesis at the same time that nerve regeneration occurs.

We can also make the assumption that in presence of Schwann cell colonies, aligned with the microgroove topography, these axon deviations would be attenuated.

The outgrowth in the Swiss roll shows the limit of the DRG model. In a way it makes it easy to see the early response to the neural culture in the topography and the pores and pillars feature, but it does not show the

capacity of regeneration of a whole organism with a blood system and an immune system. This is why this tube ought to be tested *in vivo,* e.g. in a large gap nerve injury model (10-15 mm) in rat, to better evaluate its regenerative potential.

Because PCL is translucent, and does not allow to take good quality immunohistochemistry pictures, and its elasticity make it difficult to cut e.g. for histology or TEM, otherwise reliable and accepted techniques used to analyse the growth in the Swiss roll tube need to be develop. A micro computed tomography (micro-CT) analysis is planed for future work.

4 Assessing the Parameter Space to Guide DRG Outgrowth with Electric AC Fields

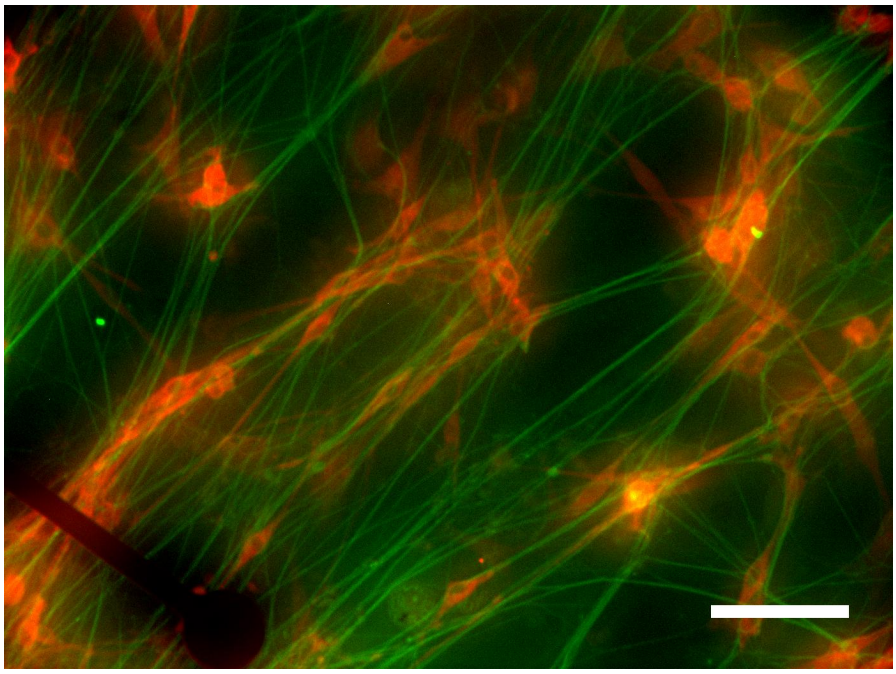

DRG axons (green) and Schwann cells (red) on MEA. Scale: 50 µm

4.1 Introduction

This chapter focus on a try to use the regenerative potential of AC fields and define their efficient parameter space by culturing DRGs on commercially available microelectrode arrays with different electric parameter (i.e. frequency, voltage ..)

As mentioned in the general introduction many studies report the beneficial use of AC stimulation on nerve regeneration *in vivo* (Al-Majed *et al.*, 2000, Brushart *et al.*, 2002, Brushart *et al.*, 2005, Gordon *et al.*, 2009, Lu *et al.*, 2008). Our goal was to observe if there would be beneficial effects *in vitro* of AC electric fields using automated time-lapse microscopy imaging, to explore the potential therapeutic uses, better understand any effects, and improve nerve regeneration protocols in general.

The demonstration of astrocyte alignment using a direct electric field of 500 mV/mm, and the guidance of dissociated DRG neuron *in vitro* by Alexander *et al.* (2006) and the famous study by Patel and Poo (1982) demonstrated the preferential growth of neurites toward the cathode. Both these studies involved salt bridges to avoid the creation of toxic species in the media at the electrode site as explained in section 1.7.2 (Veiga *et al.*, 2005). This shows the advantage to use alternating electric field as there is no ionic flow and as there is no hydrolysis at the electrodes due to the balanced and short-switched nature of the pulses and with the change of the polarity of the electrodes.

To establish which field strength would allow regenerating axons to be maintained, and not act as an electric fence, as a first step, commercially available microelectrode arrays (MEA; Multichannelsystems, Reutlingen, Germany) were used. The MEA used here feature a square grid system of round microelectrodes of titanium nitride of 30 µm diameter, spaced 500 µm centre to centre, which are commonly used to stimulate and receive stimuli

from dissociated neuronal preparation (Wagenaar *et al.*, 2006) or brain slices *in vitro* (Heuschkel *et al.*, 2002, Stett *et al.*, 2003).

Our first thought was to use these systems to generate electric fields that the regenerating DRG axons would sense, and react to, by changing their direction of growth as demonstrated *in vivo* for DC fields by Song *et al.* and Zhao *et al.* (2004, 2006). This preliminary observation on MEA should have helped us to narrow down the parameter space for the stimulation (frequency, voltage, field strength, timing …) using our own, custom made electrode systems as detailed in Chapter 5.

Two sets of two electrodes were activated and biphasic pulsed electric current applied to create a time variant electric field in the area where axons were regenerating and forming a network and so an *in vitro* model of PNS regeneration (Corey *et al.*, 2007, Nicolini *et al.*, 2011). The difficulty was to differentiate between the effect of the electric field, and normal growth over the electrode array, as there were no clear-cut differences.

The data was hard to analyse. They were mostly time lapse recording of the DRG culture under stimulation. Fluorescence staining allowed us to identify the main sub-cellular population. The work in this chapter was jointly undertaken together with Christopher Martin, who created the hard and software interface to the MEA to allow the electrical stimulation to be set up.

4.2 Materials and method

4.2.1 Organotypic DRG culture on MEA

DRGs were isolated from 2 days old neonates Sprague-Dawley rats exactly as described in Chapter 2 Figure 14, and seeded in the middle of the electrode arrays of Multi Electrode Arrays (MEA 60MEA500/30iR-Ti-gr, Multichannel Systems, Germany, Figure 1). DRG were then grown at 37°C, 5 % CO_2 in L15 media (Sigma) supplemented by 10 % FBS, 50ng/mL NGF 2.5S (Invitrogen), 50 μg/mL n-acetyl-cysteine and 1 % antibiotics antimycotic mixture (PAA p11-002). Half of the media (150 μl) was changed every day. The outgrowth of the DRG was recorded by time-lapse light microscopy during the electrical stimulation at one frame every two minutes and some were further analysed by fluorescence microscopy after immunostaining.

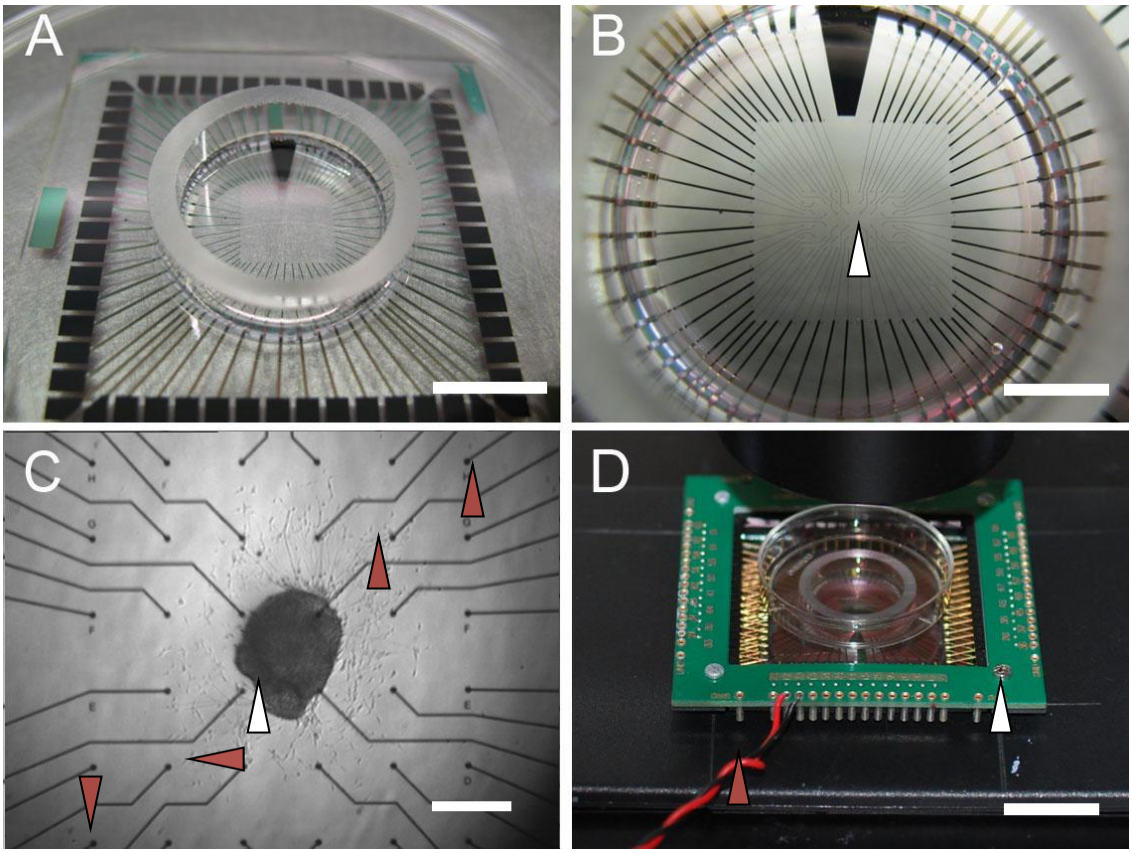

Figure 45: MEA used for to test the effect of electrical stimulation on regenerating axons of DRGs(A). The DRGs (white arrowhead in C) were seeded in the centre of the MEA culture well (arrow head in B) in the middle of the electrode array with 30µm diameter titanium nitride round electrodes and electrode spacing of 500 µm. A special MEA socket (arrowhead in D) was used to connect the MEA to the stimulation system with wires to create a local electrical field with two sets of two electrodes (see Figure 53)(red arrowheads in C) on each side of the DRG(C, D). Scale: A 1cm ; B 5 mm ; C 500 µm ; D 2cm.

4.2.2 Electrical stimulation system set up

The stimulation system (Figure 45 and Figure 46) was designed using National Instruments Labview software allowing the following functions to be included in the system:

- Control of 32 independent output channels used to stimulate neurons.
- Control of 2 firewire cameras for time lapse recording.
- Acquisition of 32 analog channels, useful in ensuring signal integrity and measuring system variables.
- Graphical user interface to allow ease of control for non-specialists.

The software controls analog acquisition and output cards. These cards are connected to a printed circuit board (PCB) used as the interface between the cards and the MEAs under test. Several MEAs can be tested in this manner in parallel, increasing the rate of experimental data that can be obtained. For each of these experiments, a rat DRG was used.

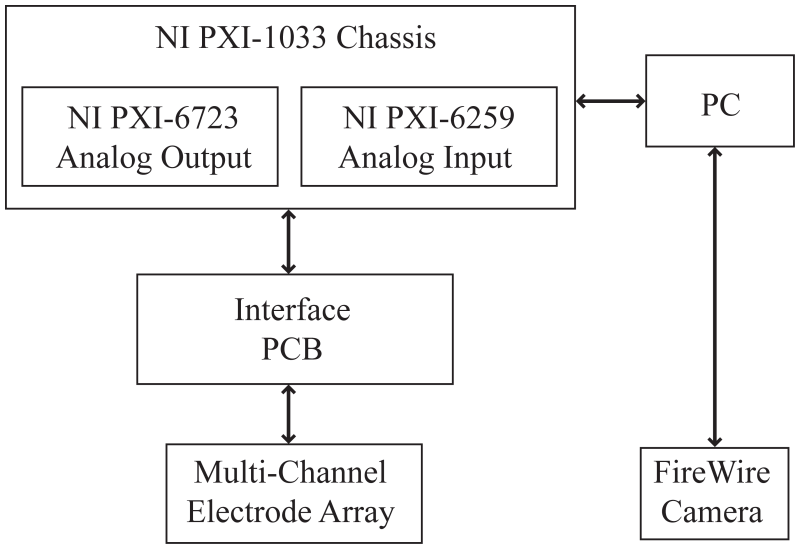

Figure 46: Scheme of the stimulation set up. A National Instrument Chassis with analog output and input was connected to a printed circuit board (PCB) interface wired to a Multi Channel electrode arrays for MEA or the Hybrid stimulation system. They were controlled by computer with the National Instruments Labview software running in a same time a time lapse recording of the DRG culture (Figure 52, Figure 54, Figure 55, and Figure 56).

The stimulation protocols used a biphasic AC with a square waveform or a sinusoidal waveform. Based on the literature we started using a frequency of 20 Hz. This low frequency was used by Al-Majed *et al.* (2000), Brushart *et al.*, (2002) and corresponds to the normal frequency of discharge of hind limb motor neurons (Loeb *et al.*, 1987). We also tested 1 Hz, 5 Hz, and 100 Hz frequencies to scan the parameter space and taking to account Cho *et al.*, (2002), Lu *et al.* (2008) and Huang *et al.* (2010) who have shown the effect of this frequency range on nerve regeneration, and calcium cellular flux. We judged the effectiveness by closely monitoring of the DRG outgrowth. Amplitudes of 100 mV corresponding to an average field intensity of 0.2 V/cm were used at the beginning. Later higher potential differences, from 300 mV (0.6 V/cm) to 10 V (2 V/cm) (Table 6) were tested because no effect was observed with the initial field used.

Table 6: Summary of the electrical stimulations of DRGs with MEA. Directionality to the electric field: (+) Parallel to the field; (0) No alignment; (-) Perpendicular to the field; (~) Movement of the DRG parallel to the field.

Test n°	Voltage [mV]	Frequency [Hz]	Signal Waveform	Time [d]	Directionality to the electric field	Culture time before stim.[d]	Observations
1	100	20	Square	6	0	15	Outgrowth not aligned
2	100	20	Square	16	+	1	Partially aligned outgrowth on the electric field (Figure 53)
3a	100	100	Square	8	0	1	Outgrowth not aligned
3b	100	20	Square	8	0	1	Outgrowth not aligned
4a	500	20	Sinusoidal	4	0	1	Outgrowth not aligned
4b	1000	20	Sinusoidal	4	0	1	Outgrowth not aligned
5	300	20	Square	6	0	1	Outgrowth not aligned
6a	100	1	Square	25	~	1	Movement of DRG parallel to the field from day 7 (Figure 54)
6b	100	5	Square	25	-	1	Alignment of axons and cell colonies opposite to the field direction (Figure 56)
7	100	5	Sinusoidal	38	0	6	Outgrowth not aligned
8a	100	5	Square	16	0	1	Outgrowth not aligned
8b	100	1	Square	16	~	1	Partially aligned outgrowth on the electric field
9a	100	1	Square	37	+	1	Partially aligned outgrowth on the electric field (figure 50, 51, 52)
9b	100	5	Square	37	0	1	Outgrowth not aligned
10a	100	1	Square	40	0	1	Outgrowth not aligned (Figure 56)
10b	100	1	Square	40	0	1	Outgrowth not aligned (Figure 55)
10c	100	1	Square	40	0	1	Outgrowth not aligned
10d	100	1	Square	40	0	1	Outgrowth not aligned
11a	100	1	Square	12	0	1	Outgrowth not aligned
11b	100	1	Square	12	0	1	Outgrowth not aligned

Test n°	Voltage [mV]	Frequency [Hz]	Signal Waveform	Time [d]	Directionality to the electric field	Culture time before stim.[d]	Observations
11c	100	1	Square	12	0	1	Outgrowth not aligned
11d	100	1	Square	12	0	1	Outgrowth not aligned
12a	500-800-1000-1200	1	Square	23	0	12	Outgrowth not aligned
12b	500-800-1000-1200	1	Square	23	0	12	Outgrowth not aligned
12c	500-800-1000-1200	1	Square	23	0	12	Outgrowth not aligned
12d	500-800-1000-1200	1	Square	23	0	12	Outgrowth not aligned
13a	1500-3000-8000-10000	1	Square	15	0	6	Outgrowth not aligned (Figure 49)
13b	1500-3000-8000-10000	1	Square	15	0	6	Outgrowth not aligned
13c	1500-3000-8000-10000	1	Square	15	0	6	Outgrowth not aligned
13d	1500-3000-8000-10000	1	Square	15	0	6	Outgrowth not aligned
Control Cultures							
1				15	0		Outgrowth not aligned
2(x5)				12	0		Outgrowth not aligned
3a				35	0		Outgrowth not aligned
3b				35	~		Outgrowth partially orientated (Figure 47)
3c				35	0		Outgrowth not aligned
4a				21	0		Outgrowth not aligned
4b				21	0		Outgrowth not aligned (Figure 46)
4(x4)				21	0		Outgrowth not aligned

4.2.3 Immunostaining

Cells were immunostained for β3-tubulin (mouse anti-TU-20 Santa Cruz) as described in detail in Chapter 2 Figure 14; in short: After the experiment was complete, DRG were fixed in 4 % formaldehyde/PBS solution for 15 minutes at 37 °C. They were then permeabilised in perm buffer (10.3 g sucrose, 0.292 g NaCl, 0.06 g MgCl2, 0.476 g HEPES 0.5mL Triton X-100 per 100 mL PBS Sigma, UK) at 4 °C for 15 min. A blocking solution of 1 % BSA/PBS was added at 37°C for 5 minutes. The blocking solution was replaced by 1 % BSA/PBS solution containing anti-b3-tubulin antibodies (1:100; mouse anti-TU-20 Santa Cruz, California) and anti-S100 antibodies (1:100; rabbit Ab868 S100 Abcam, UK). The samples were incubated at 37 °C for two hours then washed three times with a PBS/Tween20 (Sigma, UK) 0.5 % solution. They were then incubated for 1 hour at 37 °C in 1 % BSA/PBS solution containing 1:100 secondary Texas-red anti-rabbit antibodies (Vector Laboratories, UK) and 1:100 biotinylated anti-mouse antibodies (Vector Laboratories) and washed three times with Tween 20 0.5 %/PBS. Fluorescein Streptavidin 1:100 (Vector Laboratories) in 1 % BSA/PBS was then added to the sample for 30 minutes at 4 °C, before washing them again. The samples were viewed by fluorescence microscopy, and imaged using a Zeiss Axiovert 200m, with a QImaging camera, running on ImagePro+ (Media Cybernetics, UK) (Figure 47, Figure 49, Figure 50, Figure 51, and Figure 53).

4.3 Results

The application of electric fields did not result in systematic observable alignment of axons with (Figure 51, Figure 52,and Figure 53), against, or perpendicular (Figure 57) to the direction of the applied field (Table 6). Cultures were kept for as long as possible, depending on their continued growth, and successful time-lapse imaging. The stimulated cultures with interesting morphologies have been detailed below (Figure 51, Figure 52, and Figure 53) together with stimulated cultures with the same morphology

(Figure 49, Figure 50, Figure 54, Figure 55, and Figure 56) as most of the control cultures (Figure 47).

All the cultures presented a layer of cells and axonal outgrowth interacting with Shwann cell colonies that had been identified by immune staining (Figure 47, Figure 49, Figure 50, Figure 51, and Figure 53). The DRG moved from their initial seeding area with or without stimulation, sometimes ending up far from their initial position (Figure 47 and Figure 56). This must be the result of traction force form the outgrowth altogether with the surface tension generated by the meniscus on the edge of the culture well

The few cultures showing directionality and alignment parallel or against the electric field (Figure 51, Figure 52, Figure 53,and Figure 57) could have been the result of the natural alignment of nerve fibre altogether with Schwann cells and fibroblasts as this directional outgrowth is observable in one of the control culture (Table 6 control 3b, Figure 48).

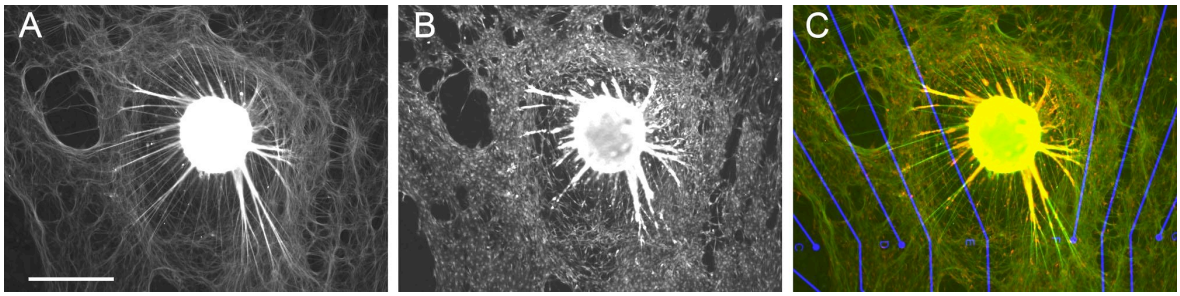

Figure 47: DRG axonal outgrowth on MEA after 21 days control culture (control 4a). Axons (A) labelled for β3-tubulin are green in C, B red in C are Schwann cells labelled for S100. We can observe a non-oriented radial and ovoid axonal and cellular network with neofascicular formation involving the gathering of Schwann cells around the axon bundles close of the DRG; Scale: 500 µm.

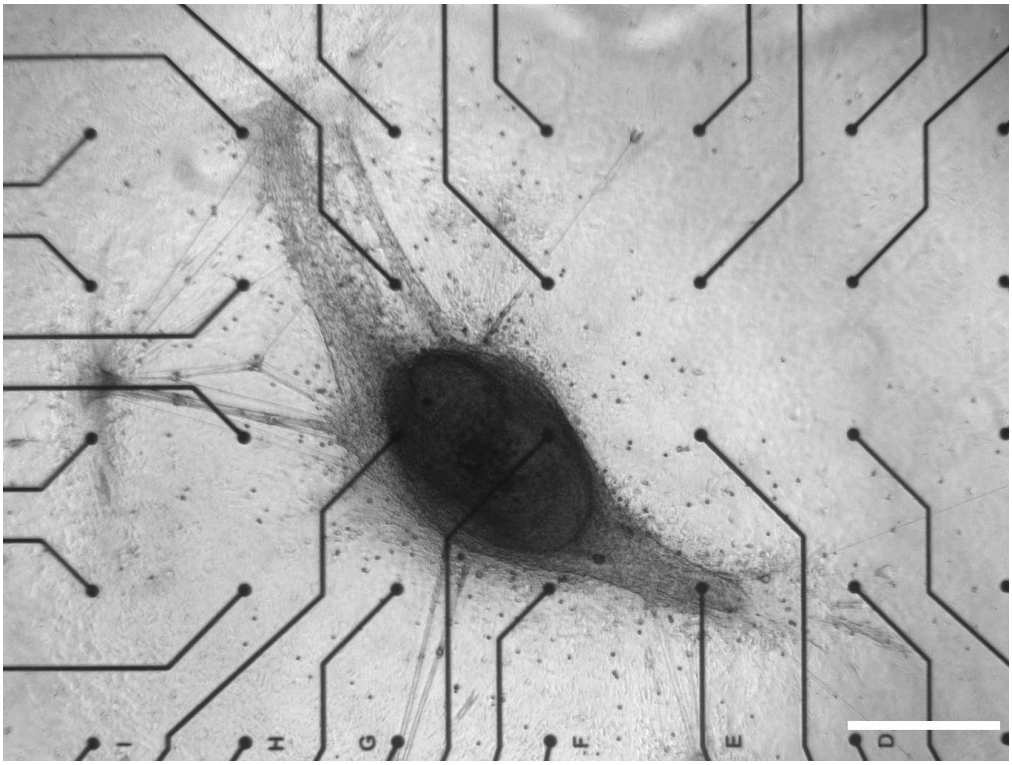

Figure 48: DRG axonal outgrowth on MEA after 35 days control culture (Table 6 control 3b). An oriented and axonal and cellular network with neofascicular formation involving the gathering of cells around the axon bundles close to the DRG; Scale: 500 µm.

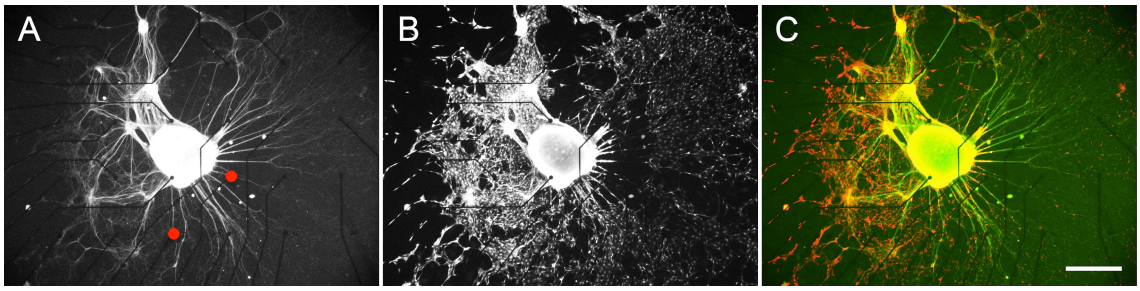

Figure 49: DRG axonal outgrowth on MEA (Table 6 test 10b). After one-day growth, the MEA were connected, and a biphasic square wave electric stimulation of 1 Hz and 100 mV amplitude (±50 mV) was provided using a set of two electrodes (red dots in (A), they are placed as in Figure 45, two electrodes are not visible on the picture) on either side of the explants for 40 days. A, green in C are axons labelled for β3-tubulin, B red in C are Schwann cells labelled for S100. We can observe a non-oriented radial axonal and cellular network as observed on the control culture as well as neofascicular formations involving the gathering of Schwann cells around the axon bundles close of the DRG; Scale: 500 µm.

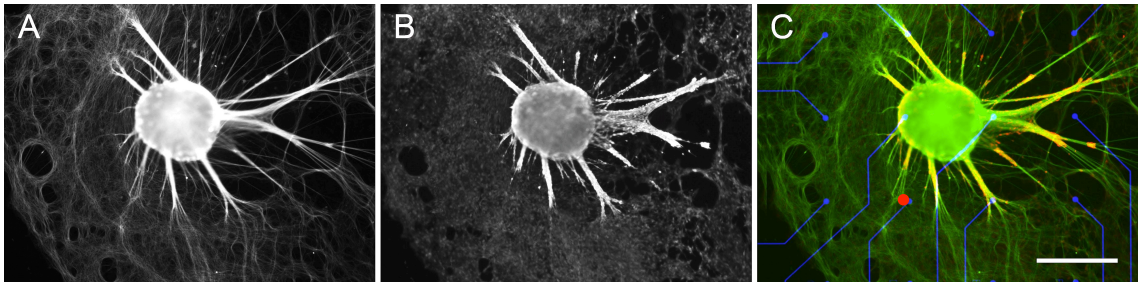

Figure 50: DRG axonal outgrowth on MEA (Table 6 test 13a). After six-day growth, the MEA were connected, and a biphasic square wave electric stimulation of 1 Hz and a ramp in amplitude from 1.5 V to 10 V was provided using a set of two electrodes (red dots in (A), placed as in figure 1, three electrodes are not visible on the picture) on either side of the explants for 15 days. A, green in C are axons labelled for β3-tubulin, B red in C are Schwann cells labelled for S100. We can observe a non-oriented radial and ovoid axonal and cellular network, as observed on the control culture as well as neofascicular formation involving the gathering of Schwann cells around the axon bundles close of the DRG; Scale: 500 µm.

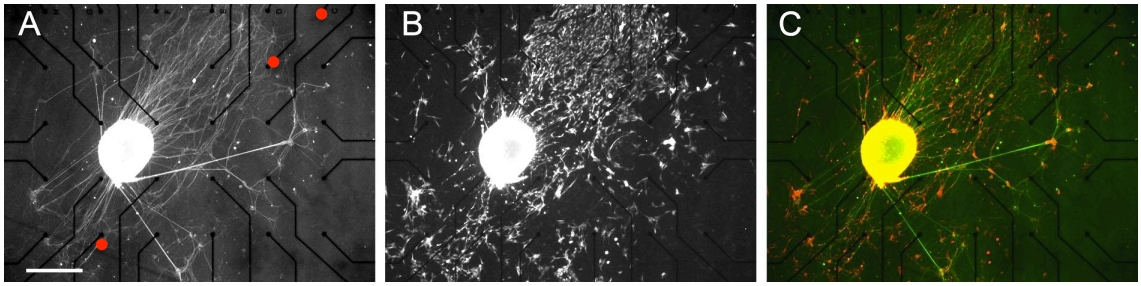

Figure 51: DRG axonal outgrowth on MEA (Table 6 test 9a). After one-day growth, the MEA were connected, and a biphasic square wave electric stimulation of 1 Hz and 100 mV amplitude (±50 mV) was provided using a set of two electrodes (red dots in (A), one electrode is not visible on the picture) on either side of the explants for 37 days. A, green in C are axons labelled for β3-tubulin, B red in C are Schwann cells labelled for S100. We can see a partially alignment of the axons altogether with Schwann cells on the electric field detailed in Figure 53; Scale: 500 µm.

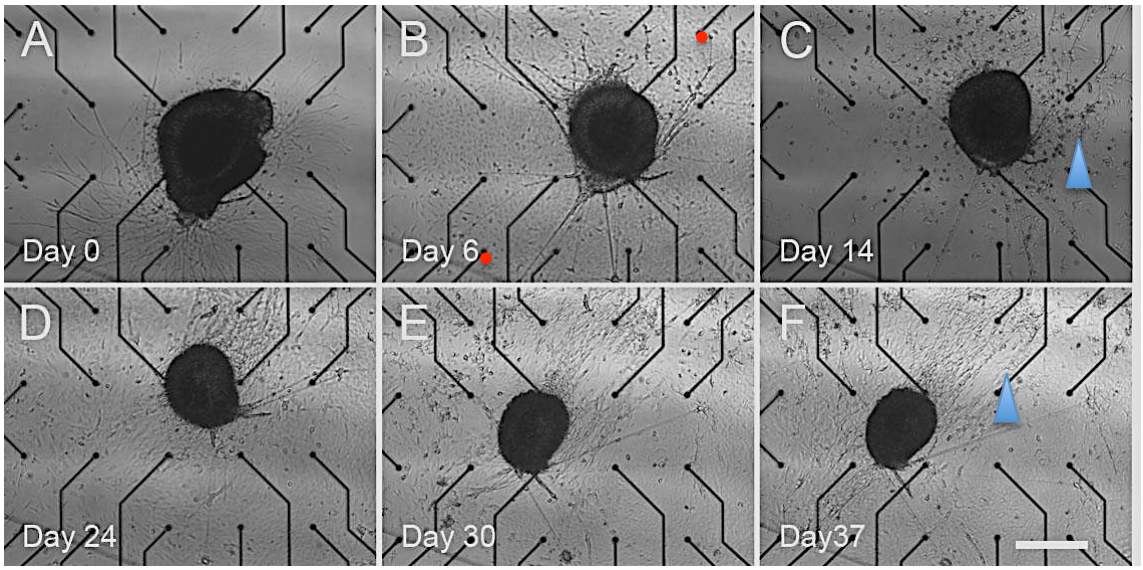

Figure 52: Time-lapse pictures of DRG axonal outgrowth on MEA (Table 6 test 9a). After one-day growth, the MEA were connected, and a biphasic square wave electric stimulation of 1 Hz and 100 mV amplitude (±50 mV) was provided using a set of two electrodes (red dots in (B), two electrodes are not visible in the pictures) on either side of the explants for 37 days. (A) At day 0 the outgrowth is radial and starts from the two stumps of the DRG. (B) At day 6 The DRG mass start moving up right, cell monolayer develops around the DRG and some axon form fascicule like structures. (C) At day 14 the DRG has moved to the right a bit more and the cell around seems to divide at a higher rate than before as more round shape ones are observable as black dots (arrowhead). (D, E, F) From day 24 to 37, the DRG starts to move back down left and the cell monolayer is more important. Some cells colonies identified in figure 3 as Schwann cells start to align on the axonal outgrowth parallel (arrowhead) to the field shown Figure 53; light microscopy; Scale: 500 µm.

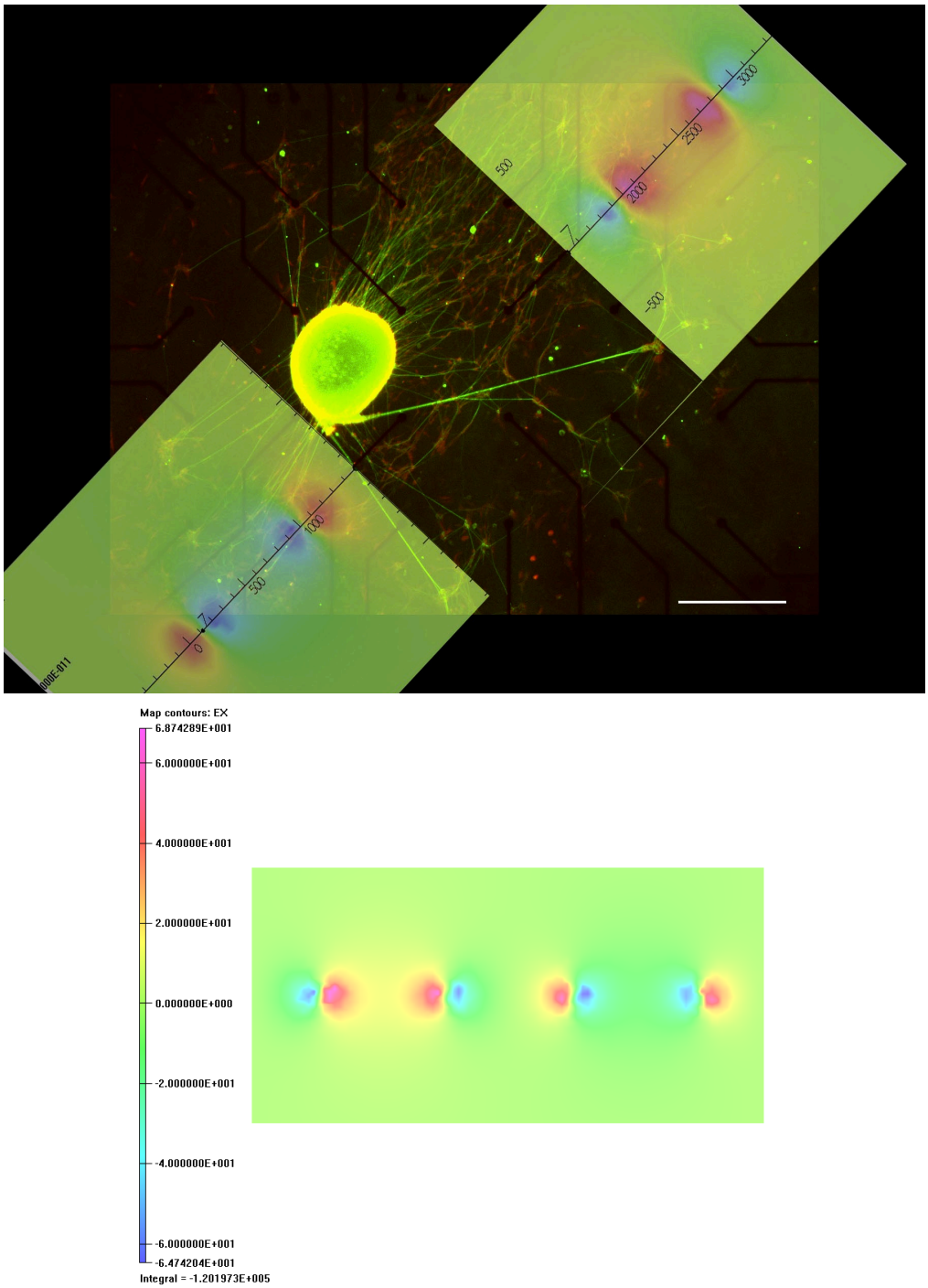

Figure 53: Overlay of electric field simulation from Opera (Cobham, UK) and DRG axonal outgrowth on MEA (Table 6 test 9a). After one-day growth, the MEA were connected, and a biphasic square wave electric stimulation of 1 Hz and 100 mV amplitude was provided using a set of two electrodes on either side of the explants for 37 days. Axons are immunostained for B3-tubulin (green), Schwann cells are immunostain by s100 (red). We can observe an obvious alignment of the axons (thin digitations) and cell network with the electric field (colour diagram); Scale: 500 µm. The simulation underneath the fluorescence picture is the field density in [V/m], the simulation overlaid shows the field density in the axis direction. Each electrode has a blue and red area corresponding to current exiting (in A/µm^2 ; blue peak ~ -3^{-11} A/µm^2 and red ~3^{-11} A/µm^2).

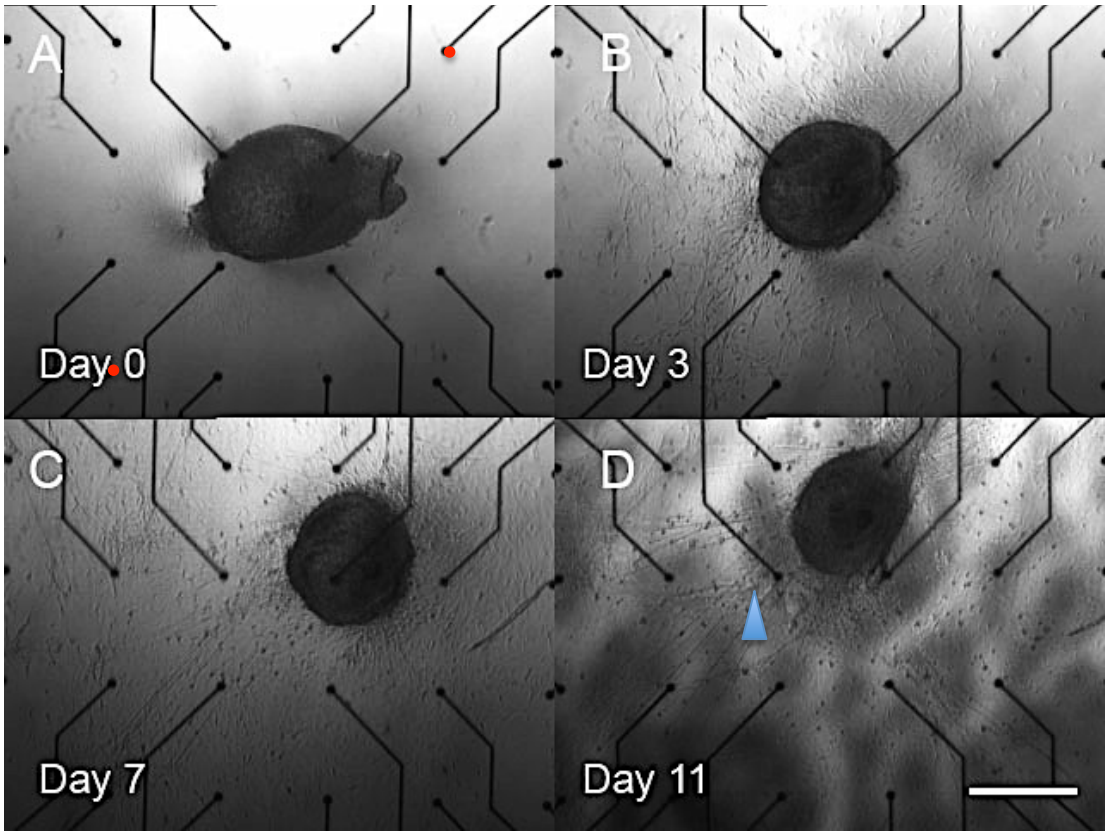

Figure 54: Time-lapse pictures of DRG axonal outgrowth on MEA (Table 6 test 2). After one-day growth, the MEA were connected, and a biphasic square wave electric stimulation of 20 Hz and 100 mV amplitude (±50 mV) was provided using a set of two electrodes (red dots in (A), two electrodes are not visible on the pictures) on either side of the explants for 16 days. (A) At day 0, the outgrowth is quite small and starts from both stumps of the DRG. (B) At day 3, the DRG size is reduced, the outgrowth is radial and a cell monolayer develops around the DRG. (C) At day 7, the DRG is moving up right, and aligned parallel axonal outgrowth (arrowhead) is visible. (D) At day 11, the DRG has moved up and seems to be stretch in the direction parallel to the field on Figure 53 as well as most of the axonal outgrowth. Light microscopy; Scale: 500 µm

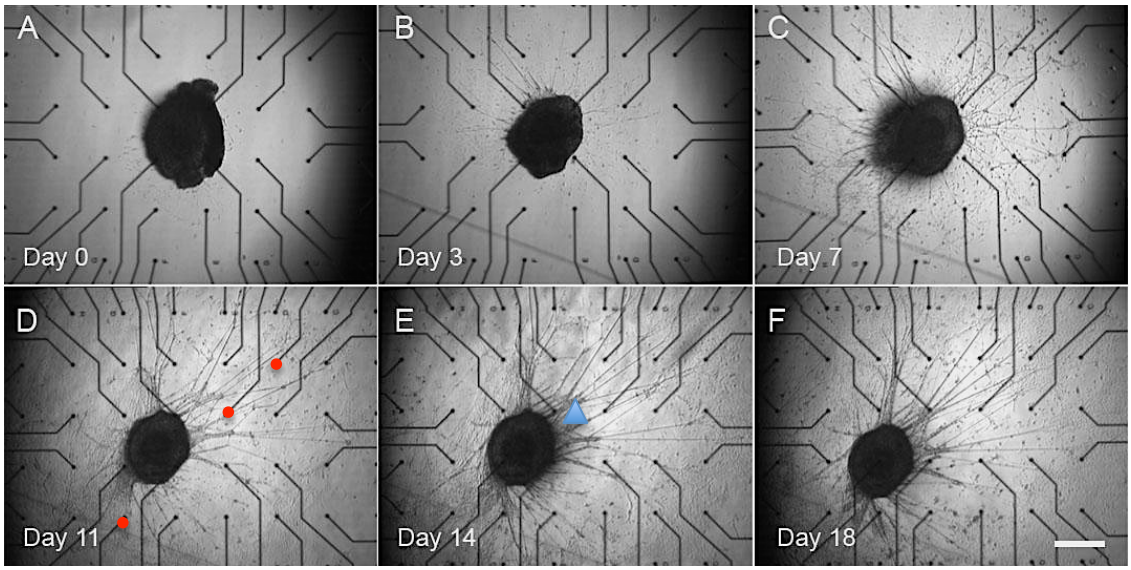

Figure 55: Time-lapse pictures of DRG axonal outgrowth on MEA (Table 6 test 6a).After one-day growth, the MEA were connected, and a biphasic square wave electric stimulation of 1 Hz and 100 mV amplitude (±50mV) was provided using a set of two electrodes (red dots in (D), one electrode is not visible on the picture) on either side of the explants for 25 days. (A, B ,C) From day 0 to day 7 the DRG do not move and a radial axonal network develops in the same time of a fibroblast layer. (D, E, F) From day 11 to day 18 the DRG mass moves down left and fascicule like structures (arrowhead) stayed anchored at their tip on the cell monolayer. Light microscopy; Scale: 500 µm.

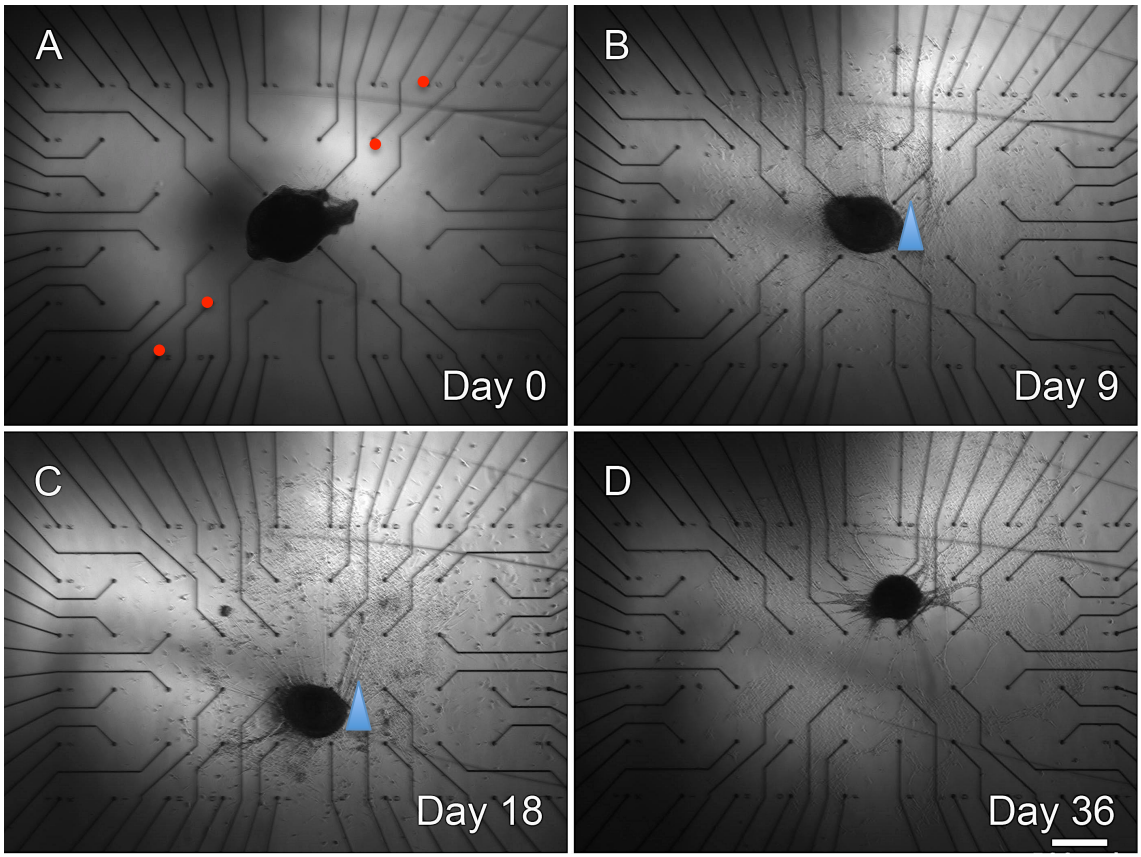

Figure 56: Time-lapse pictures of DRG axonal outgrowth on MEA (Table 6 test 10a). After one-day growth, the MEA were connected, and a biphasic square wave electric stimulation of 1 Hz and 100 mV amplitude (±50 mV) was provided using a set of two electrodes (red dots in (A)) on either side of the explants for 37 days. (A) At day 0 the outgrowth is radial and starts from the two stumps of the DRG. (B) At day 9 The DRG mass is reduced, a cell monolayer develops around the DRG and some axon form fascicule like structures (arrowhead). (C) At day 18 the DRG has moved down and some axons look stretched (arrowhead). (D) At day 36, the DRG has moved up right; Scale: 500 µm.

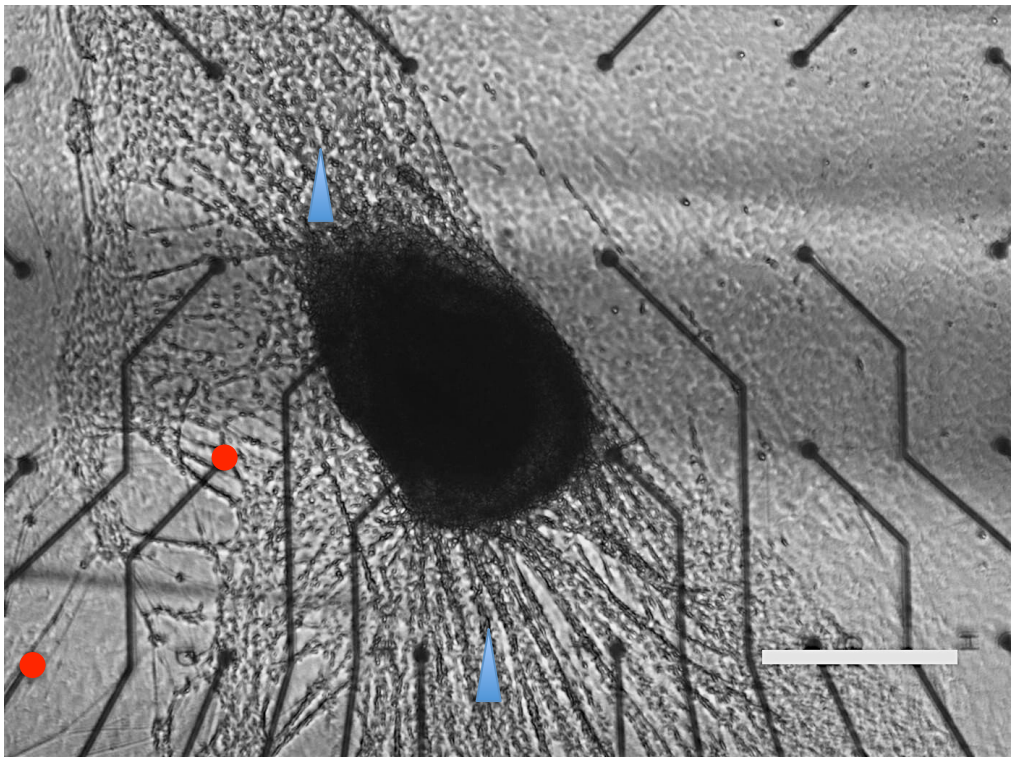

Figure 57: DRG axonal outgrowth on MEA (Table 6 test 6b). After one-day growth, the MEA were connected, and a biphasic square wave electric stimulation of 5 Hz and 100 mV amplitude (±50mV) was provided using a set of two electrodes (red dots), on either side of the explants for 25 days. We can see the DRG outgrowth is a highly aligned cell colony forming fascicule like structures (arrowheads), perpendicular to the field direction in Figure 53. Light microscopy; Scale: 500 µm.

The time-lapse recording monitored and documented the progress of DRG outgrowth *in vitro*. Around the outgrowing DRG a cell monolayer develops and most of the time the axonal outgrowth is radial on the control cultures (Figure 52, Figure 55,and Figure 56). The ramp in amplitude seems to have no effect even when applying the maximum electrical amplitude used of 10 V. No differences were observed by changing from the square waveform to a sinusoidal signal. The staining allowed us to see the structure of the outgrowth better but did not help us to discern any effect of the electric field.

4.4 Discussion

Investigating the effect of electric stimulation on the outgrowth of DRG using a MEA system with 30µm round electrodes did not allow to come to firm conclusions. The device electrodes were spaced on a square grid of 500 µm

centre-to-centre spacing, a pair of two electrodes were stimulated using a variety of fields (strength V/cm, frequency Hz). The DRG response followed by using time-lapse videography and immunocytochemistry has been such that it seemed that pulsed field electromagnectic fields did not reliably affect the outgrowth of neurites in this system (Table 6). Repeating the alignment proved difficult and the long experimental times caused a great delay in problem solving. However interesting cultures, showing alignment on the fields or movement parallel to it were observed at 1 Hz and frequency and 100 mV (Table 6 test 6a, 8b, and 9a)

The directionality of the outgrowth observed on some control and stimulated cultures may have been the consequence of an intrinsic behaviour of cells that had grown out, or differences in the subpopulation that had grown out. Especially Schwann cells and fibroblasts emanating from the DRG stump interact together to keep their fascicular organisation in which they are oriented and aligned together.

The data, although inconclusive, proved valuable for troubleshooting early problems with further electric stimulation and highlighted the need for finding a means to “organise” the encounter of the axons and cells with the electrodes, such that clear conclusions could be drawn.

During this phase of experimentation it became clear that in order to have measurable changes in neuron growth; it would be better to align them first before applying an electric field. In this way a successful electric field pattern would be one in which the pre-aligned neurons would be guided (into, away, structured…) with respect to the initiated growth pattern and could be controlled, restrained or aligned. This approach was aimed at with the development and application of the hybrid stimulation test modules developed in the next chapter.

A simulation of the magnetic fields generated by the AC electric signals used in the study shows that these are on the order of a tenth of nT in the MEAs and in the constructs used in Chapter 5. These extremely low magnetic

fields are weaker than the magnetic fields generated by the laboratory electrical system. We decided not to discuss any potential effects of these very weak magnetic fields in this work (Chapter 4 and Chapter 5) and to consider the effects observed as consequences of the “electric” fields. Thus the term “electric” field was preferred to the term “electromagnetic” field.

5 Optimisation of Systems to apply Electric Fields *In Vitro* for Peripheral Nerve Regeneration

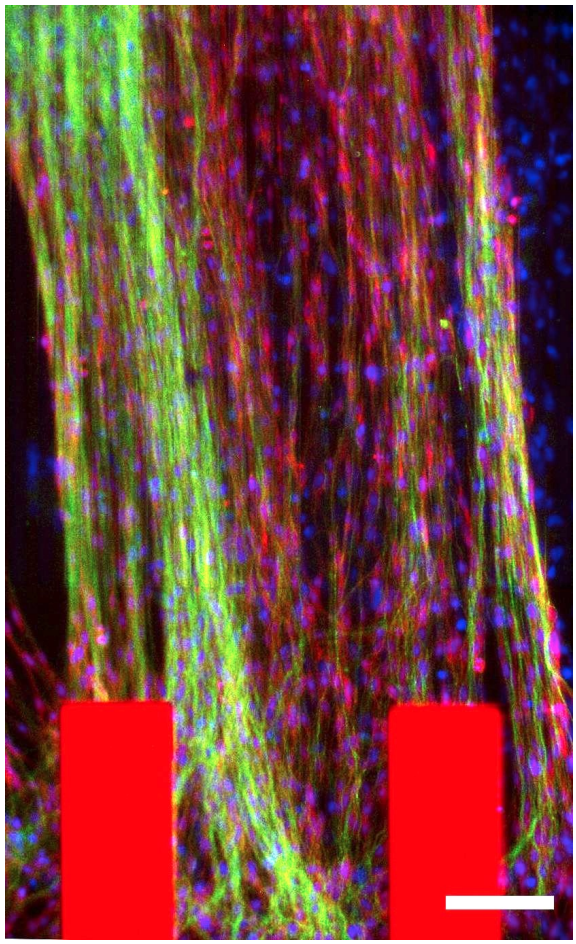

Axons (green) and Schwann cells (red) and their nuclei (blue) on a hybrid stimulation test module (electrodes in bright red). Scale: 30 µm

5.1 Introduction

This final experimental chapter aims at the use of custom-made devices featuring microelectrodes generating an AC electric fields to direct DRG axonal outgrowth to show the nerve guiding potential of such features in the context of a nerve guidance conduit.

When a wound in the skin or in a tissue is created, a static, endogenous electrical field (Song *et al.*, 2004) develops, and guides the healing process of the regenerating tissues; especially regenerating axons follow the direction of the field. These fields are created by ion gradients, and establish especially efficiently across epithelia, where the constant ionic disequilibrium results in the outside being on a negative potential with respect to the inner of the body (Zhao *et al.*, 2006). This natural regeneration process inspired scientists to enhance tissue regeneration with electric fields.

Applying the most effective principle of DC fields (Alexander *et al.*, 2006, Patel and Poo, 1982) to guide the growth cones was out of the question as within a confined system, without the use of salt bridges, the material released at the electrodes (H_2, Cl^-, $[\text{metal ions}]^+$) corrodes the electrodes, which limits their lifetime, and poisons cells locally (Veiga *et al.*, 2005). To avoid this time-variant problem, biphasic AC fields, with a time-constant short enough to not allow electrode polarisation, have been chosen to avoid any accumulation of molecular hydrogen at the cathode, and the generation of molecular chlorine, toxic metal salts, and the generation of peroxides at the anode.

Pulsed field electrical stimulations, strong enough to illicit action potentials, have been used as means to stimulate neuronal growth by calcium induced cAMP increase, which in turn activate CREB transcription factor and MAPK (Fields *et al.*, 1997). It has also been used to increase NGF secretion in

Schwann cells *in vitro* (Huang *et al.*, 2010) and in many *in vivo* studies (Al-Majed *et al.*, 2000, Brushart *et al.*, 2002, Lu *et al.*, 2008).

Here the guiding principle was not to stimulate electrical activity but to use variant electric fields as means to contactless guide the regenerating axons. This work is driven by the aim to reduce the loss of regenerating neurons by misguidance at the interface between sutured nerve stumps (Kingham and Terenghi, 2006), and at the interfaces between nerve tubes and the central as well as the distal nerve stump.

To establish which field strength would allow regenerating axons to be maintained and guided, commercially available microelectrode arrays (MEA; Multichannel systems, Reutlingen, Germany) were used as detailed in Chapter 4. As the regenerating axons formed random networks on these devices the results obtained with these devices were not conclusive. We designed and fabricated a set of hybrid stimulation and test modules in the James Watt Nanofabrication Centre (JWNC). By confining the initial growth of the DRG network by topography, a unified starting point of growth was established, before the axons encountered the electrodes and, if these were active, the electric fields. These devices allowed an array of tests to show how these electric fields influence the growth of regenerating neurons.

The work in this chapter was jointly undertaken together with Christopher Martin in Microelectronic Device Centre, who did the microfabrication of the hybrid stimulation test modules (Figure 59 and Figure 62) and the electrical stimulation set up (Figure 63). The hybrid stimulation modules feature long gold electrodes providing the electrical field and the microgrooves to guide the axons directly to the zone where the electrical field was generated (Figure 58 and Figure 62) Thus a 2D model of neuron growth in the presence of alternating electric fields, various waveform types were tested to try to manipulate, align and constrain neuron and cellular growth.

5.2 Materials and method

5.2.1 Hybrid Stimulation test modules

After realisation that upon exiting grooves the axons would spread out radially-turning through 90 degrees within ca. 250 µm (see e.g. Figure 75 in Chapter 6) Christopher Martin and I designed new device(s) (Figure 58, Figure 59 ,Figure 60 , and Figure 62) to replace the MEAs. Here the microgrooves were used to align the outgrowth and thus allow a predictable directional interaction of the axons with the electrical field. These new devices were made by Christopher Martin in the JWNC using microfabrication techniques such as photolithography and metal deposition as detailed below.

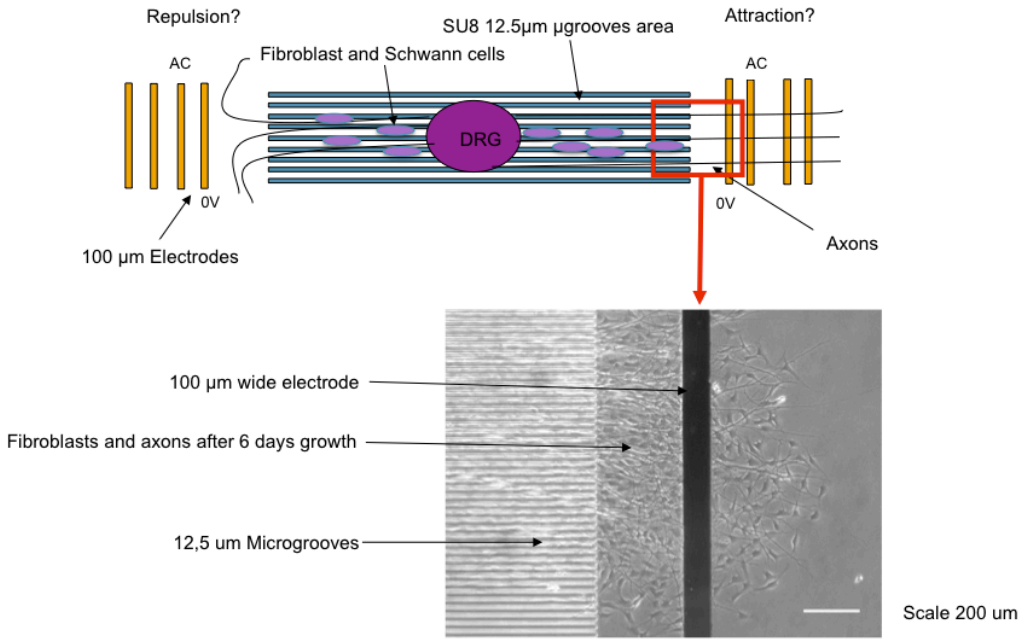

Figure 58: Schematic of the hybrid stimulation test module. The modules feature a microgrooved area providing topographical guidance to re-growing axons of a DRG towards two sets of four 100µm gold microelectrodes on either side. This device allows the observation of the effect of an electrical stimulation on regenerating axons in vitro. This figure is just an example showing cells and axons as they grow out, crossing the gold electrode unaffected.

These devices consist of two distinct parts: A central grooved region where the DRG is seeded, providing topographical guidance cues to the neurons under test; followed by patterned metal electrodes, providing electrical cues placed into a region where the neurons had exited the groove

region. Using a 5mm long grooved central area the axonal outgrowths from the DRGs reached the electrode area on either side of the microgrooved area after approximately 7-10 days. This design allowed for comparison between samples as the response of the DRG to the grooves during first days of regeneration lead to a standardised response, directional outgrowth and an uniform angle of interaction between the axons and the applied electrical field.

5.2.2 Fabrication of Hybrid Stimulation test modules

The optical transparency of SU-8 makes it a suitable choice for the microgrooves material. The fabrication process consists of two stages, the metal electrode patterning and the definition of the topographical groove section. This fabrication includes UV photolithography (Chapter 2 Figure 10, Chapter 3 Figure 29) in combination with other techniques such as metal deposition and a lift off process (Figure 59) to create electrodes and the SU8 grooves. This procedure has been developed by Christopher Martin.

S1818 photoresist was first spun onto a quartz microscope slide (Newcastle optical) at 4000 rpm for 30 s as a sacrificial layer (Figure 59A). After a soft bake of 95°C for 2 min, the resist was treated in MF319 developer for 1 min to harden the top surface of the resist film. This treatment allows the top surface of the S1818 photoresist layer to have a negative side wall after the development following the exposure to UV (Figure 59B) thus improving the resist lift-off process of the sacrificial S1818 layer (Figure 59C, D).

The resist was then exposed to UV light through a photo-mask using an MA6 mask aligner tool for 8 seconds. The resist was developed using MF319 developer for 75 s. Using a Plassys metal deposition tool, a 20 nm thick layer of Ti and a 200 nm thick layer of Au were coated onto the patterned resist (Figure 59C) prior to immersion in warm acetone to perform lift-off of the

sacrificial S1818 (Figure 59D) left after development. This yielded patterned metal electrodes on the quartz slide.

The second stage of fabrication is needed to pattern SU-8 microgrooves, which serve as physical guidance cues to the regenerating axons. After cleaning of the patterned electrodes on quartz, SU-8 3005 photoresist was spin-cast at 4000rpm for 30 seconds. Following a ramped soft-bake of 65 °C (1 min), 95 °C (3 min) and 65 °C (1 min) the sample was exposed to UV light through a photomask for 25 s (Figure 59E).

Once exposed, the SU-8 requires a post exposure bake (PEB) to further cross-link the exposed regions of the resist. The PEB uses the same baking cycle as the soft-bake with the exception that the 95 °C step lasts for 2 min. Using EC solvent, the unexposed areas of SU-8 are removed from the substrate, leaving behind patterned SU-8 microgrooves 12.5 µm wide with 12.5 µm spacing. The microgroove area is 1mm wide and 5 mm long. The final step is a hard-bake of the SU-8 at 180 °C for 20 min to harden the resist (Figure 59F)

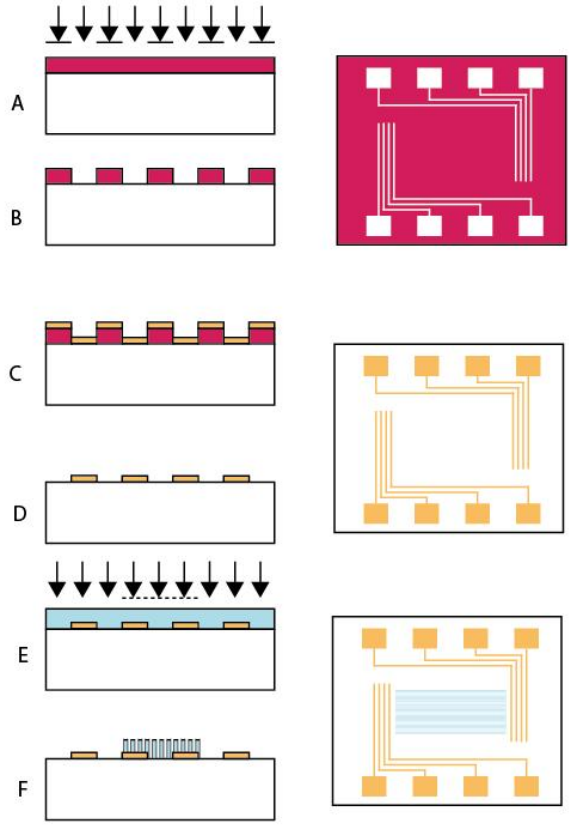

Figure 59: Microfabrication of the Hybrid Stimulation Test module. On the left a cross-section through a representative part of the device, right a view of the overall pattern: Exposure of S1818 photoresist (A) followed by pattern development (B). Evaporation and deposition of Au electrodes (C) and metal lift-off (D) created a specific electrode pattern. A Microgroove fabrication was done by UV exposure of a SU-8 layer (E) followed by pattern development in EC solvent (F). Courtesy of Christopher Martin

5.2.3 Electrode designs

The shape of the electrodes has been designed with the intention to investigate how the electrical guidance/inhibition potential influences axonal regeneration and the behaviour of other cells. The electrode designs used are:

1. Four electrodes perpendicular to the grooves: the “perpendicular” design (Figure 60A, Figure 61A): the perpendicular design allows to investigate the interaction of the regenerating axons with an electric field at approximately right angle to their direction of growth. The question to be addressed was, if the regenerating axons would cross- or be repelled by the field, or would they turn and align.

2. Electrodes aligned in parallel to the grooves, the “straight” design (Figure 60B, Figure 61B): here the interaction of the regenerating axons with an electric field in parallel to their direction of growth is assessed. The question to be addressed were, if the regenerating axons would be influenced by the field, repelled by the presence of a field in general, or would they be aligned and grow in parallel to the electrodes? In addition this design allows for a number of field patterns to be investigated (+-+-; ++--; +--+; -++-).

3. Two electrodes with wider squared areas: The “square” design (Figure 60C, Figure 61B): the square electrodes were designed to investigate if two distinct regions of electric field would influence the outgrowth and directionality of the regenerating axons. In the narrower sections the field would be three times more intense than that of the wider regions.

4. Four electrodes with turning areas: the “hairpin” design (Figure 60D, Figure 61D): the hairpin design is a modified straight design with added bends. This was designed to investigate if axonal turning would be induced, when the regenerating axons encountered these bends. Four electrodes are used to allow experimentation with different electric field patterns.

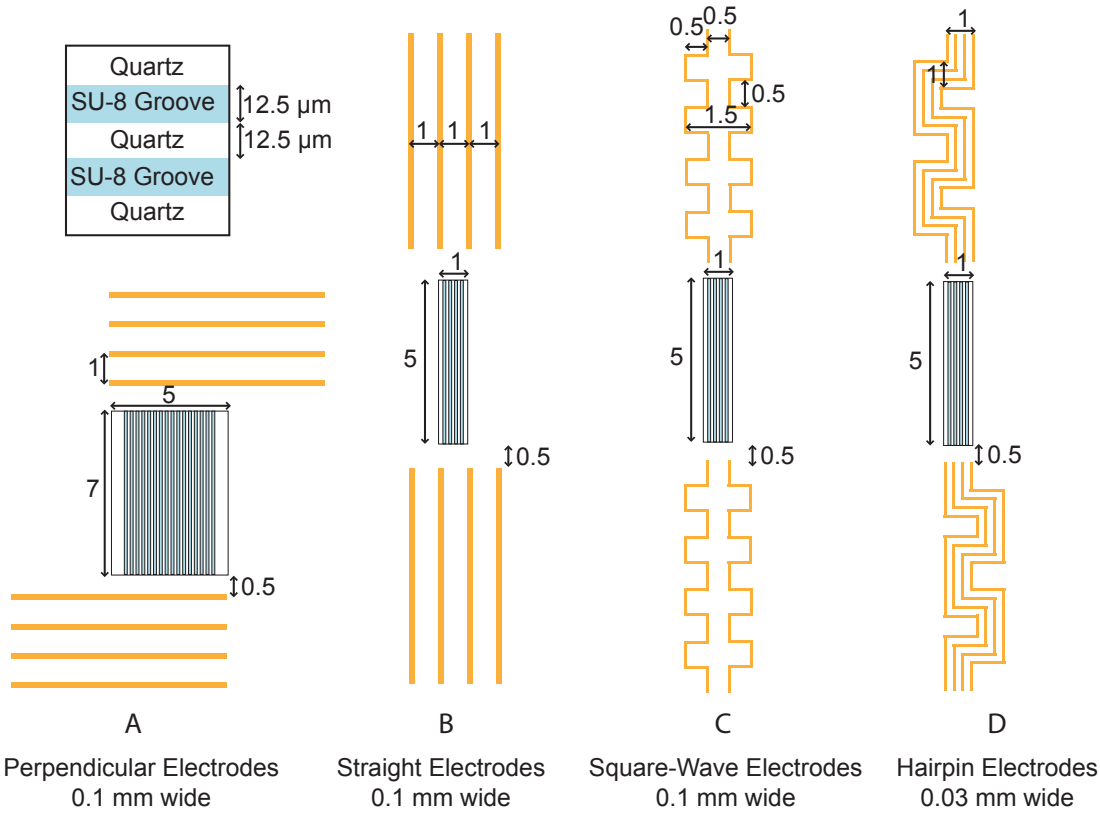

Figure 60: The Four electrode designs that have been designed and fabricated for the experiments. The perpendicular (A) design to investigate the ability of the regenerating axons to cross an electric field, the straight design (B) with four electrodes in parallel to the grooves to investigate their ability to interact with a field parallel to their initial direction of growth, the square wave design (C) with two electrodes with wider squared areas used to investigate the effect of having two distinct regions of electric field intensity: in the narrower sections the field would be three times more intense than in the wider regions. The "hairpin" design (D) with four electrodes with turning areas aimed to investigate if axonal turning would be induced upon the growth cone reaching a bend.

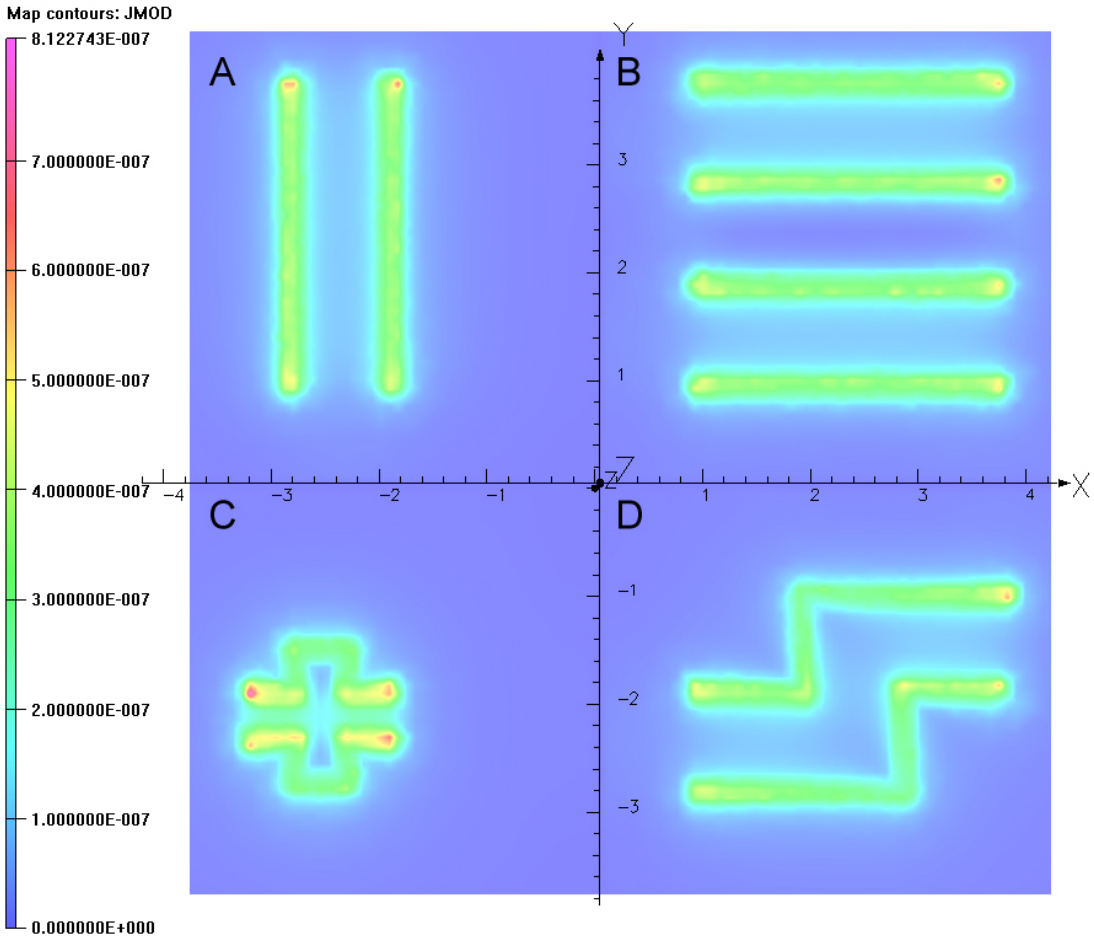

Figure 61: Electric field distribution of the four electrode designs used in this work. This simulation was done using Opera (Cobham, UK) software. The calculation was done 200 µm above the electrode in culture media: (A) perpendicular (Figure 60A), (B) straight (Figure 60B), (C) square (Figure 60C), (D) hairpin (Figure 60D) electrode designs. Conductivity of the culture medium was 3.3 S/m and the conductivity of gold was 4.1E+7 S/m. Scale in [A/mm^2]

5.2.4 Organotypic DRG culture on the hybrid stimulation test modules

DRG were isolated from 2-day old neonate Sprague Dawley rats as described in detail in Chapter 2 Figure 14 and placed at the centre of the hybrid stimulation test module microgrooved area (Figure 62B). The DRGs were then grown for 6 to 8 days at 37 °C, 5 % CO_2 with L15 media (Sigma) supplemented with 10 % FBS, NGF 2.5S (50 ng/mL) (Invitrogen), NAC (50 µg/mL) and 1 % antibiotics antimycotic (PAA p11-002) until they reach the electrode area. Half of the media (150 µL) was exchanged every day.

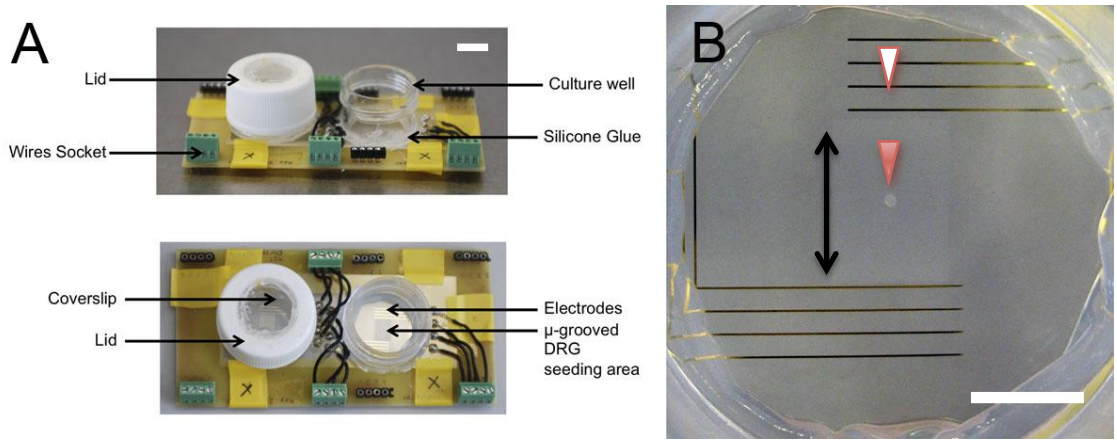

Figure 62: Hybrid Stimulation test module with perpendicular electrode design. Two stimulation devices were mounted on a PCB, connected, and the top of a plastic universal attached using aquarium glue to form a self-contained culture well. Each of the two wells (one shown with, the other without lid) contained connected electrodes (white arrowhead in B) and grooved surfaces to align DRG outgrowth. The DRGs are seeded in the middle of the micro grooved area on quartz/SU-8 (red arrowhead in B, direction of grooves indicated by double ended arrow). This device allowed the study of the effect of the electric field on directed axonal outgrowth from a DRG. Scale: (A) 1 cm and (B) 5 mm

5.2.5 Electrical stimulation system set up

After completion of the above fabrication steps, each quartz sample is attached to a PCB interface to connect the electrodes to terminal blocks. These allowed an easy way to establish connections to another interface PCB that in turn linked to the PC-interface hardware used.

The stimulation system connected to the electrodes was the same used, and described in the previous Chapter section 4.2.2. For each of these experiments, a rat DRG was used as a source of regenerating axons of sensory neurons.

The electrical signal protocol first includes high field strength (10 V/cm) with the idea to increase the chance of the observation of an effect, since no negative effects were observed on the MEA (Chapter 4 Table 6) when using these settings. We started with a frequency of 1Hz because some alignment was observed with this frequency in the MEA system (Chapter 4 Figure 53). The choice of the electrical protocol was then dependant on the following observations detailed in sequence in the results section.

Table 7: Summary of the electrical stimulation of DRGs with Hybrid Stimulation test module type "Perpendicular".

Test n°	Time	Voltage [V]	Ramp Voltage [1/h]	Frequency [Hz]	Ramp Frequency [1/h]	Pulse [Hz]	Max. Field [V/cm]	Live/zero electrode	Signal Type	Observations	Time of effect
1	24h30	1		1			10	2/3	Square	Repulsion (Figure 65)	5-6 h
2	26h	1		1			10	½	Square	Shrinking cells, tearing cell layer (Figure 66)	30 min-direct
3	24h20	1		1			10	½	Square	Shrinking cells, tearing cell layer	30 min-direct
4	17h	0.1	0.05	1			1	½	Square	Retraction	30 min-direct
5	21h30	13		1			130	½	Square	Electro-grilled	Direct
6	22h20	0.01	0.01	1			0.1	2/3	Square	Retraction	Direct-30min
7	1d22h	0	0.05	1			0.05	½	Sinusoidal	Retraction/ Growth	2h

Test n°	Time	Voltage [V]	Ramp Voltage [1/h]	Frequency [Hz]	Ramp Frequency [1/h]	Pulse [Hz]	Max. Field [V/cm]	Live/zero electrode	Signal Type	Observations	Time of effect
8	1d23h	0.01	0.01	1			0.1	2/3	Sinusoidal	Slow retraction	1h
12	2d21h	0.02	*0.5	2000	*0.5		0.2	2/3	Sinusoidal	Retraction	1h
14	1d21h40	0.02		100		20	0.2	¾	Sinusoidal	No effect	
15	18d1h20	0.02		100		20	0.2	2/3	Sinusoidal	Axons spread along the field area in both directions (Figure 68)	24h
21	11d01h	0.02		100		20	0.2	3/2	Sinusoidal	Axons spread along the field area in both directions	1d
23	3d	0.02		100		20	0.2	3/2	Sinusoidal	Axons spread along the field area in both directions (Figure 69B)	1d

Table 8: Summary of the electrical stimulation of DRGs Hybrid Stimulation test module type "Straight".

Test n°	Time	Voltage [V]	Frequency [Hz]	Pulse [Hz]	Field [V/cm]	Live/zero electrode	Signal Type	Observations	Time of effect
9	19h40	0.02	100		0.2	2/3	Sinusoidal	Retraction after touching electrode	When touching electrode
16	3d	0.02	100	20	0.2	1,4/2,3	Sinusoidal	Growth/ Retraction	1d
19	3d02h	0.02	100	20	0.2	1,4/2,3	Sinusoidal	MEDIA DRIED	35h
22	6d20h	0.02	100	20	0.2	1,4/2,3	Sinusoidal	Retraction / Growth (Figure 71B)	1d

Table 9: Summary of the electrical stimulation of DRGs with Hybrid Stimulation test module type "Hairpin".

Test nº	Time	Voltage [V]	Frequency [Hz]	Pulse [Hz]	Field [V/cm]	Live/zero electrode	Signal Type	Observations	Time of effect
10	1d19h10	0.02	100		0.2	¼	Sinusoidal	No effect	1h
11	2d21h	0.02	100		0.8	2/4	Sinusoidal	Retraction after touching electrode	When touching electrode
13	19h	0.02	100	20	0.2	¼	Sinusoidal	MEDIA DRIED	1h
17	6d23h	0.02	100	20	0.8	1,4/2,3	Sinusoidal	Growth/ Retraction (Figure 73	1d

Table 10: Summary of the electrical stimulation of DRGs with Hybrid Stimulation test module type "Square".

Test nº	Time	Voltage [V]	Frequency [Hz]	Pulse [Hz]	Field [V/cm]	Live/zero electrode	Signal Type	Observations	Time of effect
18	3d21h	0.02	100	20	0.2-0.13	½	Sinusoidal	Growth, Axon cluster (Figure 72)	1d
20	10d01h30	0.02	100	20	0.2-0.13	½	Sinusoidal	Growth, Axon cluster	1d

Table 11: Summary of the electrical stimulation of DRGs with Hybrid Stimulation test modules

Device	Tests n°	Voltage range [V]	Ramp	Frequency range	Max. Field [V/cm]	Signal Types	Main Effect Observed
Perpendicular	13	0.01-13	5 of Voltages 1 of Frequency	1-2000	130	Square Sinusoidal	Barrier Effect
Straight	4	0.02	No	100	0.2	Sinusoidal	Retraction Growth
Hairpin	4	0.02	No	100	0.8	Sinusoidal	Retraction Growth
Square	2	0.02	No	100	0.2	Sinusoidal	Growth Axon clusters

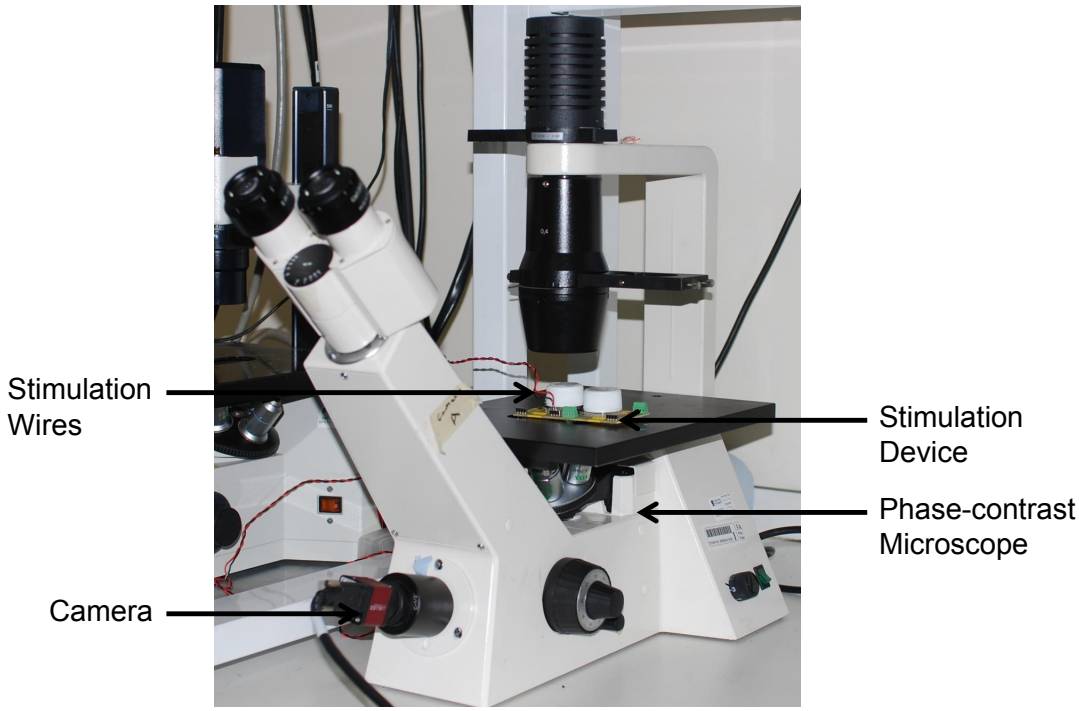

Figure 63: Picture of the experimental set up for the electrical stimulation. The electrical device was placed on the microscope for time-lapse recordings (1 frame/2 min) and connected to the stimulation system with wires. Timelapse recordings and stimulations were coordinated using a PC running Labview.

5.2.6 Immunostaining

Cells were fixed and immunostained for β3-tubulin (mouse anti-TU-20 Santa Cruz) as described in detail in section 2 2.2.8; in short: After the experiment was complete, DRG were fixed in 4 % formaldehyde/PBS solution for 15 minutes at 37 °C. They were then permeabilized in perm buffer (10.3 g sucrose, 0.292 g NaCl, 0.06 g $MgCl_2$, 0.476 g HEPES 0.5 mL Triton X-100 per 100 mL PBS Sigma, UK) at 4 °C for 15 min. A blocking solution of 1 % BSA/PBS was added at 37 °C for 5 min. The blocking solution was replaced by 1 % BSA/PBS solution containing anti-ß3-tubulin antibodies (1:100; mouse anti-TU-20 Santa Cruz, California). The samples were incubated at 37 °C for two hours then washed three times with a PBS/Tween20 (Sigma, UK) 0.5 % solution. They were then incubated for 1 h at 37 °C in 1 % BSA/PBS solution containing 1:100 biotinylated anti-mouse antibodies (Vector Laboratories)

and washed three times with Tween 20 0.5 %/PBS. Fluorescein Streptavidin 1:100 (Vector Laboratories) in 1 % BSA/PBS was then added to the sample for 30 minutes at 4 °C, before washing them again. The samples were viewed by fluorescence microscopy, and imaged using a Olympus BX51, with a QImaging camera, running on ImagePro+ (Media Cybernetics, UK) (Figure 64, Figure 69, Figure 71, and Figure 72).

5.3 Results

5.3.1 Hybrid stimulation test modules results

The control cultures, without any stimulation have quite a similar morphology independent of the electrode design. They grow aligned to the end of the microgrooved area and most of them, for an unknown reason, turn right at the end of micro patterned area, sometimes to the point that they form a U-turn shape (Figure 64 A-D).

The results of the tests using the Hybrid Stimulation test modules are summarised in Table 7, Table 8, Table 9, Table 10, and Table 11. The parameter space to be explored (device, shape of wave, frequency, timing, voltage, field strength) was huge and the time of stimulation varied depending on the real time observations. The culture systems were experimental and they changed over time to incorporate improvements or changes introduced to investigate a specific interaction, or to allow for better access. As these were hand-made in house, the organotypic DRG culture was not as easy to maintain as in the standard model used e.g. in Chapter 2. Therefore in each experiment a batch of DRGs where seeded and only those reaching the electrode area of the electrodes at the end of the microgrooves used for to investigate the effect of time variant electric fields. The main goal was here to define the main effects that a time variant, balanced electric field could have, to get an indication about the effectiveness of different frequencies, voltages and modulation of the applied field as well as the effect of different electrode designs had on regenerating neurons (Table 7, Table 8, Table 9, Table 10 and Table 11)

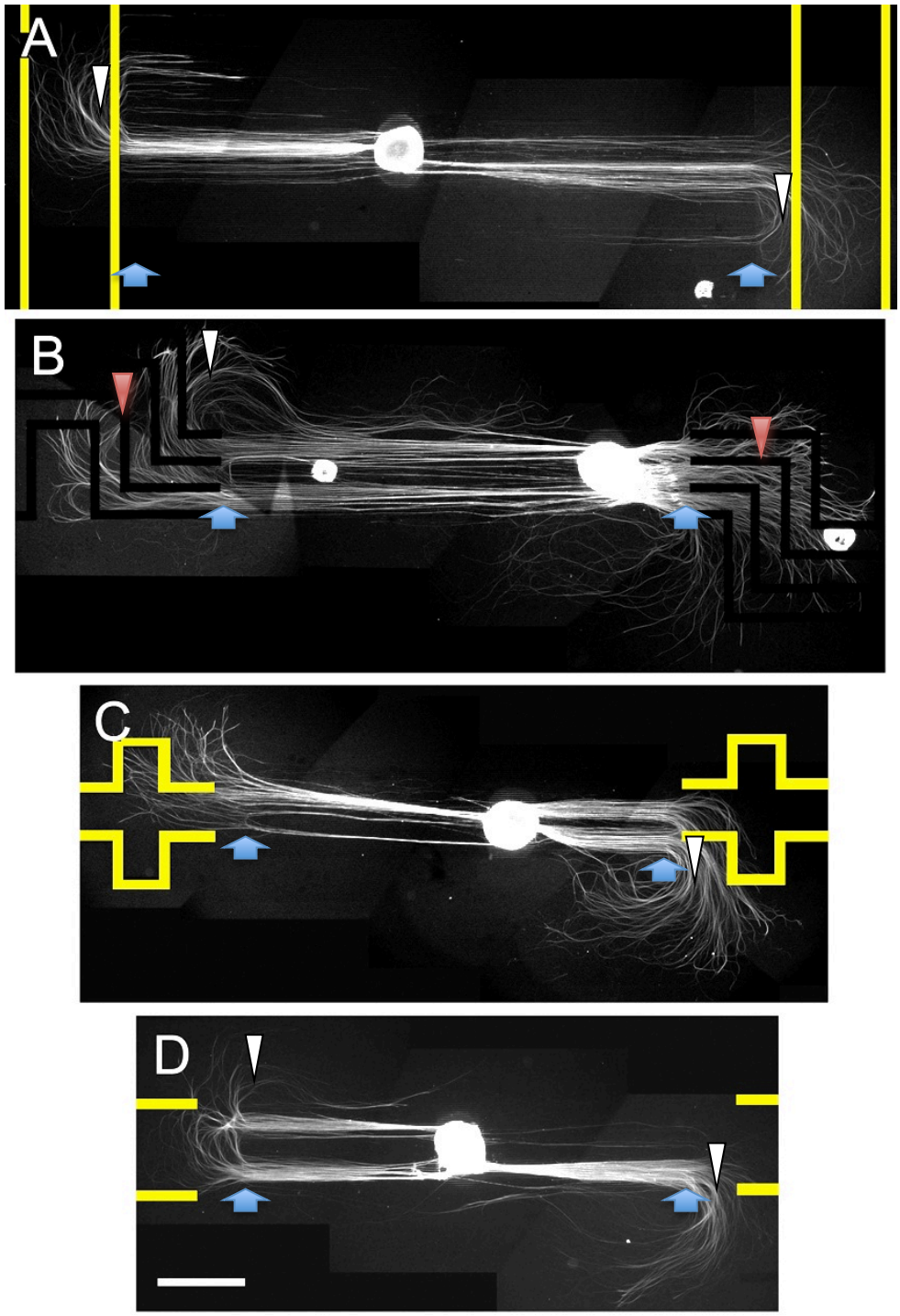

Figure 64: DRG control cultures after 15 days growths on the hybrid stimulation test module. The DRGs are fluorescently stained for axonal outgrowth using anti-β3-tubulin. The axons extend well beyond the microgrooved area (ends of microtopography indicated by bleu arrows) of non-connected/non-activated hybrid stimulation devices. Gold microelectrodes (red arrowheads/yellow highlight) of 100 µm on either sides were fabricated in four different designs: A) Four electrodes perpendicular to the grooves: the "perpendicular" design B) Four electrodes with turning areas: the "hairpin" design. C) Two electrodes with wider squared areas: The "square" design. D) Four electrodes parallel to the grooves: the "straight" design. (For dimensions details see Figure 59). The axon outgrowth is initially guided by the SU8 microstructure to the end of the microgrooved area. In absence of electrical field the regenerating axons are then turning right of the guided axonal network to form a U-turn shape (white arrowheads); Scale: 1 mm.

5.3.2 The barrier effect on the perpendicular electrode design

For the first experiment a 1 V 1 Hz (test 1 Table 7) square wave stimulation signal on the perpendicular design was used. The maximum fields strength between the microelectrodes was 10 V/cm (Figure 65).

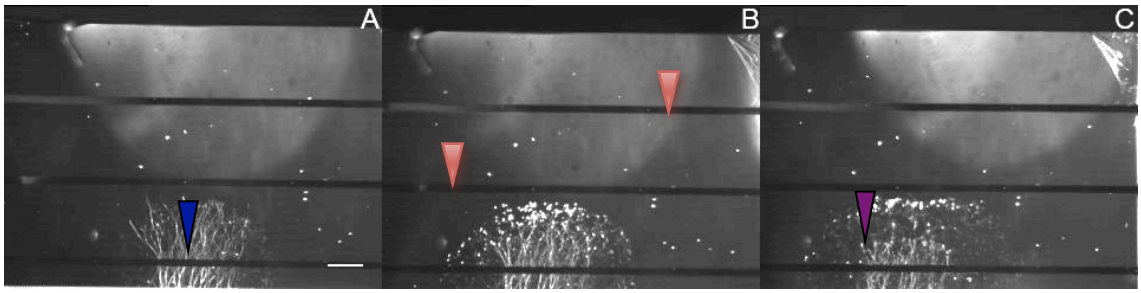

Figure 65: Axonal outgrowth (blue arrow) and fibroblast monolayer (purple arrow) from a DRG organotypic culture 0h (A) 6h (B) and 12h (C) after 1 Hz 1 V square wave AC electrical stimulation after 10 days growth on quartz featuring SU8 12.5 µm width 5 µm depth microgrooved area. The field generated between the microelectrodes (red arrows in (B)) was 10 V/cm. A retraction of the regenerating axonal network was observed within the first six hours suggesting that the field was not permissive to axonal outgrowth. The cell monolayers underneath, mainly fibroblasts, continued to grow and to expand horizontally alongside the electrode keeping a distance of 100 µm to it. However they could not cross the electrical field barrier. Scale: 500 µm.

A retraction of the regenerating axonal network was observed within the first six hours suggesting that the field was not permissive to axonal outgrowth. The cell monolayers underneath continued to grow and expand horizontally alongside the electrode at a distance of 100 µm. However they could not cross the electrical field barrier.

The effect was observed a second time on the same sample, with the fibroblast layer grown for ten more days (test 2, Table 7). During these ten days the axonal network didn't grow back, suggesting a mechanism inhibiting the regrowth after the regenerating axons had had contact with the electrical field. With the same parameters applied, cells detached and retracted again after only 30 minutes, clearing the area around the microelectrode (Figure 66).

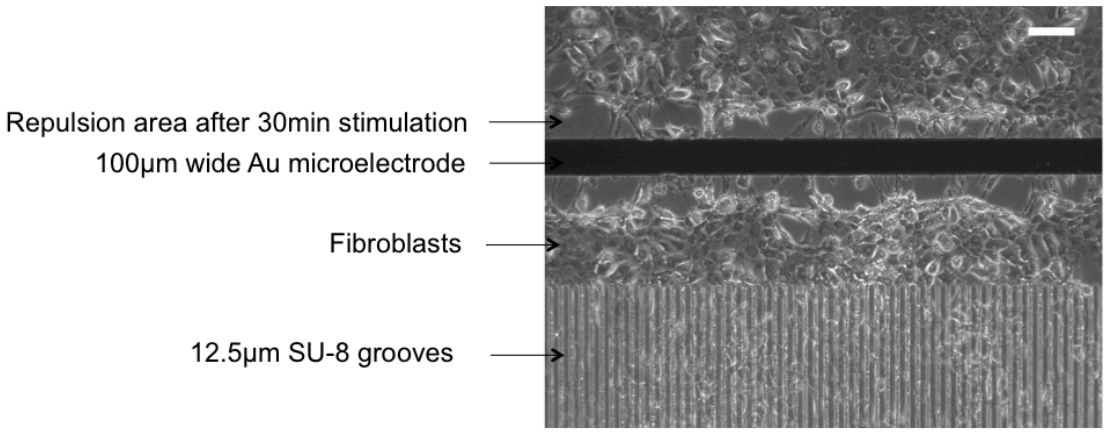

Figure 66: Fibroblast monolayer from a neonatal rat DRG culture repelled by an electrical field. After 20 days culture on quartz featuring SU8 12.5µm width 5µm depth microgrooved area, the fibroblast layer was ripped and repelled by a 1 V 1 Hz square wave electrical stimulation applied to two 100 µm wide gold microelectrodes, separated by 1 mm. Scale : 100 µm

After these initial experiments, a ramp in amplitude was used to identify at what field intensity the network would retract (test 4, and 6, Table 7). The first ramp test used a square wave of 100 mV amplitude with an increment of 50 mV per hour (test 4, Table 7) The second ramp test used a square wave of 10 mV amplitude with an increment of 10 mV per hour (test 6, Table 7). A quick retraction of the network was still observed despite using such a low electric field. Having used a square wave signal for these experiments, it was thought that the ramp test should be done again with sinusoidal pattern with a smaller rate of change of voltage, thus avoiding the fast transitions seen with square waves (test 7 and 8, Table 7). This resulted in a slower retraction of the network in addition to some growth near the field. In the next tests we decided to use a 20 mV 100 Hz electric signals as it was thought that the retraction started above this voltage. A slow retraction happening after only two hours suggested that using amplitude of 20mV still caused retractions, despite the switch to sinusoidal signals albeit at a slower rate of retraction. A ramp in frequency was tried in test 12 and the retraction was still observed.

5.3.3 Modulated stimulation

After the ramp tests, it was thought that some sort of relaxation phase should be introduced. Using the same 20 mV 100 Hz sinusoidal signal, but with an on/off ratio of 1:4, introduced a resting period for the network, in an attempt to alleviate the retractions (test 13 to 23, Figure 10).

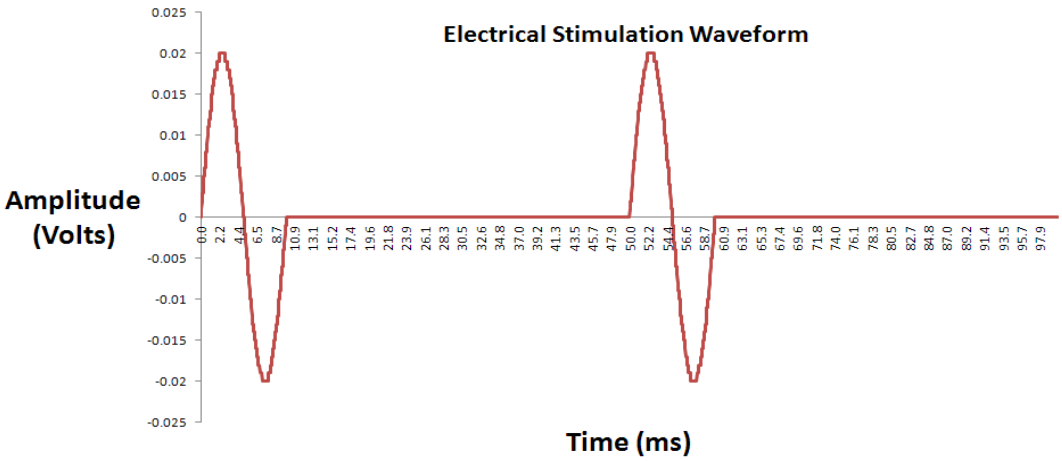

Figure 67: Modulation of sinusoidal signal used for electrical stimulation. The signal used isa 20 mV 100 Hz sinusoidal signal with an on/off ratio of 1:4 (20 Hz). Courtesy of Christopher Martin.

The observation mentioned as 'retraction/growth' in the observation column of the table mean that there was growth and retraction of the axons in the modulated electrical field area using this new protocol. It also allowed some growth of the regenerating axons in the electric field area (Figure 68) on the perpendicular straight and square electrode design. This represented a step forward to regenerating growth in the presence of electric fields (Figure 68, Figure 69B, Figure 70B).

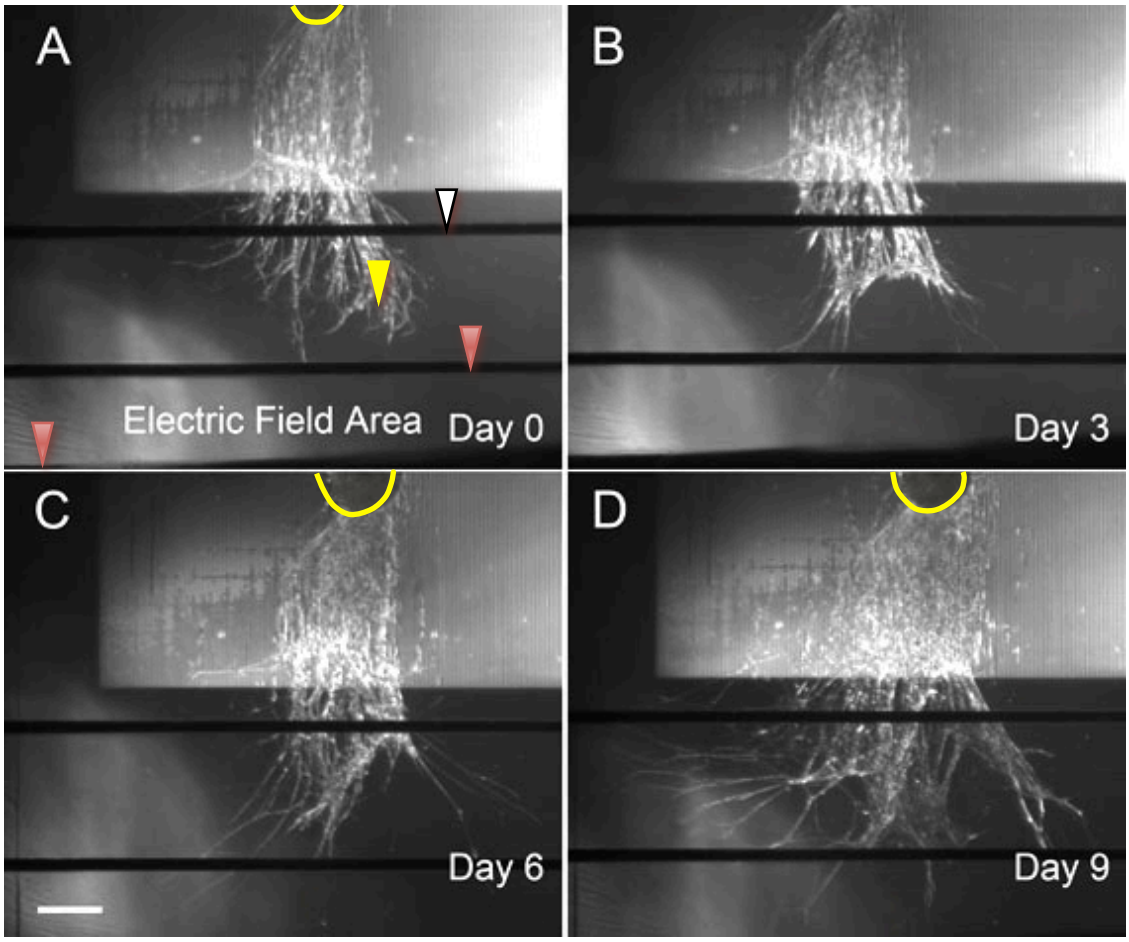

Figure 68: Axonal outgrowth from a DRG (outlined in yellow) organotypic culture on the hybrid stimulation test module with perpendicular electrodes after A) 0 B) 3 C) 6 D) 9 days growth under AC electrical stimulation with a 100 Hz 20 mV modulated sine wave, on quartz featuring microgrooved SU8 (12.5 µm wide 5 µm deep). The field generated between the microelectrodes (red arrowhead) allows the spreading of the regenerating network in either direction with the modulated stimulation instead of a unidirectional U-turn form network observed or the directional growth turning on the right of the axonal growth direction on the grooves observed on the control culture or before stimulation starts (yellow arrowhead in A, Figure 64). White arrowhead: electrode not connected. Scale: 500 µm. Bright field microscopy.

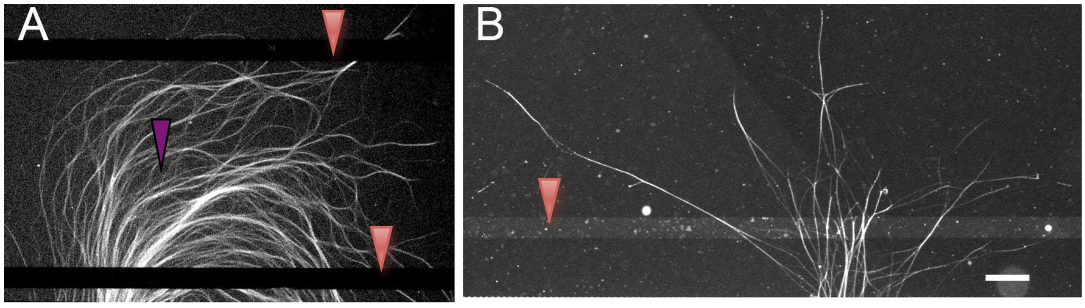

Figure 69: DRG axonal outgrowth culture on quartz featuring gold microelectrodes (red arrowheads) with and without electrical stimulation. Stain: β3-tubulin indicating axonal outgrowth. The axon outgrowth is guided by the SU8 microstructure to the end of the microgrooved area. In absence of an electrical field the regenerating axons turn right once off the guided axonal network to form a U-turn shape (A) (purple arrow) whereas in presence of a sine wave modulated electric AC field of 100 Hz 20mV (B) they tend to spread along the electrode following the both direction. Scale: 200 µm.

The pictures of the three most interesting and successful cultures under the modulated stimulation on the Hybrid Stimulation test module with perpendicular electrode design (test 15, 21, 23 Table 7) and control cultures of the DRG axon growth have been analysed by a Macro created by Frank Gesellchen for the OrientationJ plugin (Rezakhaniha *et al.*, 2012) for the ImageJ Software (Papadopulos *et al.*, 2007) and plotted as quiver plot using MATLAB and Statistics Toolbox (Release 2010b ,The MathWorks, Inc., Natick, Massachusetts, US).

In the analysis pictures have been divided in X region of interest in which the principal orientation of the axon specific marker ß3-tubulin within the images is measured. The regions of interest, which did not contain axons, have been removed from the analysis (Figure 70).

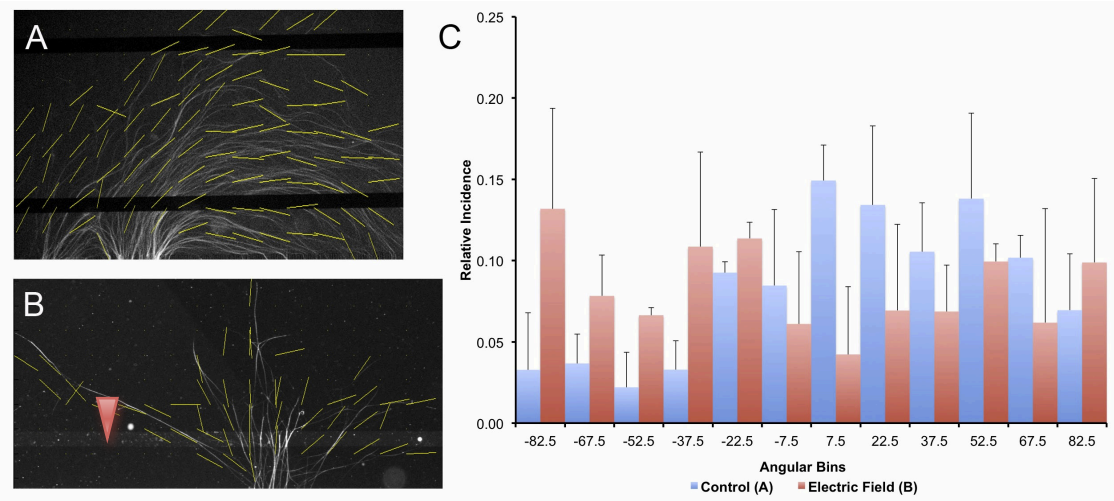

Figure 70: Image analysis of the control DRG culture (A) and the DRG culture in the presence of a 100 Hz 20 mV sine wave modulated AC electric field (B) on the hybrid stimulation test module with perpendicular electrode design. The images were divided in X region of interest in which the principal orientation of the pixel obtain by immunohistochemistry for the ß3tubulin axon specific marker was determined using OrientationJ plugin in ImageJ Software and then plotted as quiver plot (yellow lines) using MATLAB and Statistics © The data was then plotted as relative incidence for each angular bin for three controls culture and three cultures with electric field to determined a specific pattern and show the barrier effect of the electrical field. (red arrowhead : micro-electrode)

From the orientation data of Figure 70, we can make the assumption that the modulated AC electrical described above in Figure 67, might modulate the DRG outgrowth. The axon spread along the electrodes in presence of the

electric field instead of turning in a U-turn shape characteristic of the control culture.

5.3.4 The Channel Theory on the Straight Electrode Design

The straight electrode design allowed us to test if, when two parallel fields were used as barriers to spread axon growth along (as shown with the perpendicular design above), the neurons would grow in between the two fields, and progress through the gap between these. (test 16 and 22 Table 8, Figure 71)

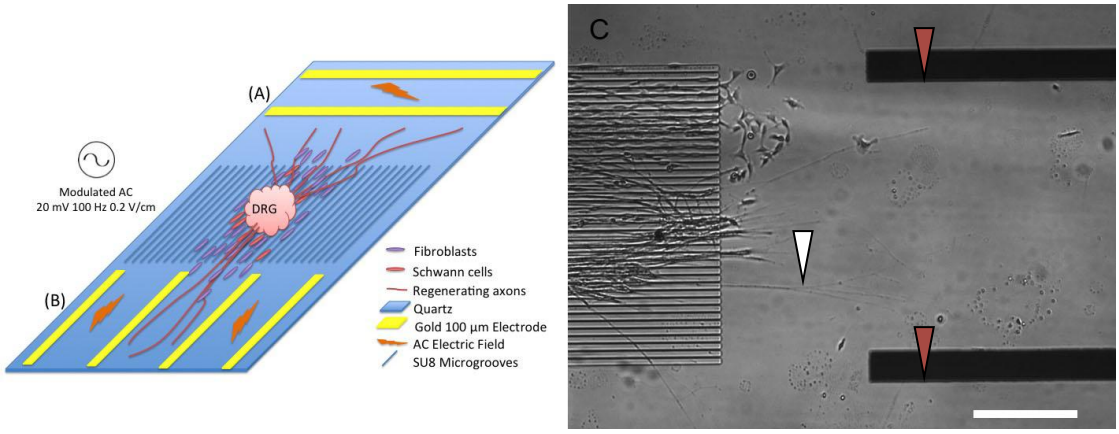

Figure 71: The barrier effect (A) and the channel hypothesis (B). We tried to create a permissive area for axonal regeneration guidance through two set of electrodes (red arrowhead in C) generating an electric field from a 100 Hz 20 mV sine wave modulated AC providing a barrier effect on each side of the regrowing axons (white arrowhead in C). C) DRG axonal outgrowth culture on quartz featuring SU8 12.5 µm width 5 µm depth microgrooved area on the hybrid stimulation test module with straight electrode design with two sets of 100 µm gold microelectrode on both sides generating an electrical field as shown in (B). Scale: 300 µm, Bright Field microscopy.

Theoretically, using four electrodes configured we could create a neutral channel where an axon can regrow enclosed by two barrier regions. Early results seem to indicate that this is the case (Figure 71) however more experiments and parameter refinement are required to further enhance the electrical waveform parameters needed to achieve this. This hypothesis will be tested further in Appendix 1 on PCL stimulation test modules.

5.3.5 Neuroma Like Formation and Growth on the Square Electrode design

On the square electrode design (Figure 72) during test number 18 and 20 Table 10 the regenerating network grew trough the electrodes and a axonal network, akin to that found in a neuroma could be observed on either side of the DRG. Strangely this time, the non-stimulated side growth was somehow inhibited.

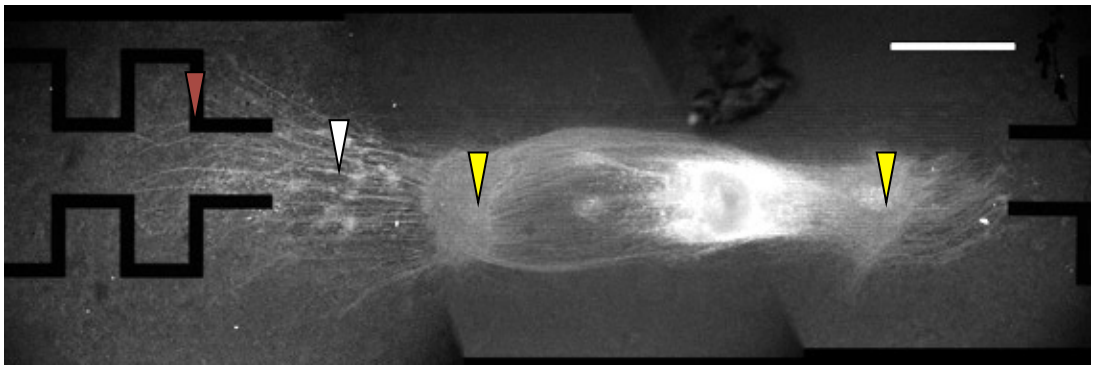

Figure 72: Axonal outgrowth (white arrowhead) from a DRG organotypic culture on the square electrode design of the hybrid stimulation test module with a 100 Hz 20 mV sine wave modulated AC electrical stimulation on quartz featuring SU8 12.5 µm width 5 µm depth microgrooved area. The field generated between the microelectrodes (red arrowhead) allow the growth of the network in the field area with the modulated stimulation instead of a directional U-turn form network observed on the control culture. Neuroma like formation (yellow arrowhead) are appearing on each side of the DRG. Stain:β3-tubulin. Scale: 500µm.

5.3.6 Retraction on the hairpin electrode design

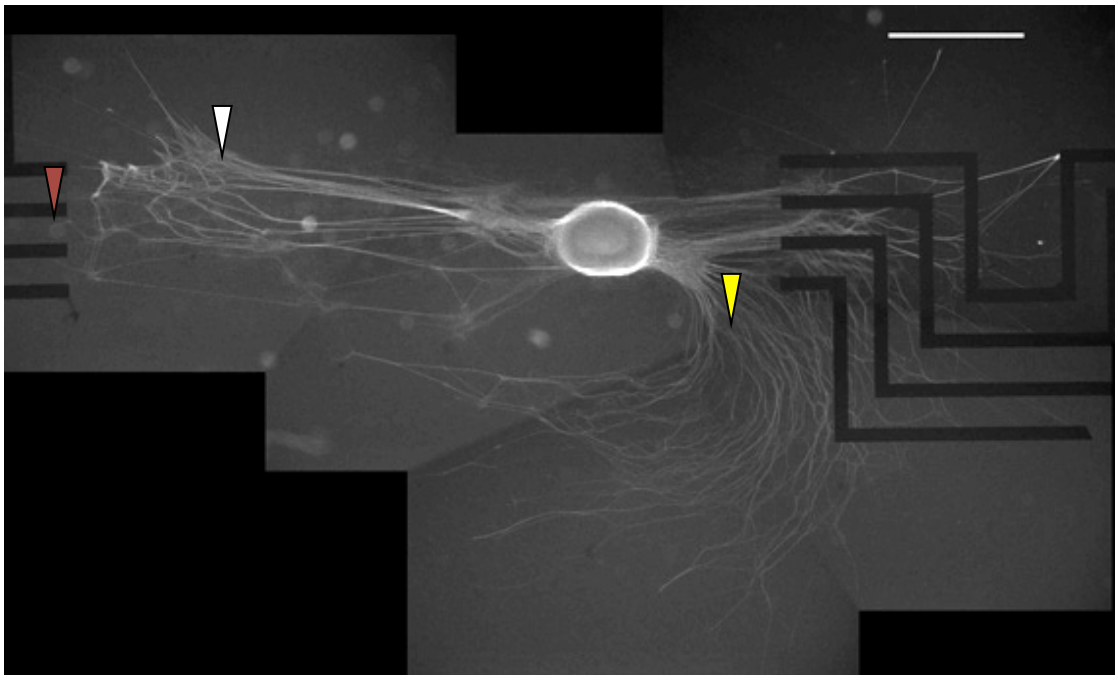

Figure 73: Axonal outgrowth from a DRG organotypic culture on the hairpin electrode design of the hybrid stimulation test module with a 100 Hz 20 mV sine wave modulated AC electrical stimulation on quartz featuring SU8 12.5 µm width 5 µm depth microgrooved area. The field generated between the microelectrodes (red arrows) with the modulated stimulation mainly inhibit the axonal growth (white arrow) instead of a directional U-turn form network observed on the control culture or here on the non stimulated axonal network end (yellow arrowhead). Scale: 500 µm. stain: B3-tubulin.

On the hairpin configuration (Figure 73, test 17 Table 9) an inhibition of the growth on the electrode resulted in a retracted axonal network, this could be interpreted in terms of field strength as due to the electrodes being

closer together, a higher electric field was generated which in turn could inhibit axonal outgrowth in that area.

5.4 Discussion

The possibility to direct axons and glial cell with electrical field *in vitro and in vivo* has been successfully demonstrated with DC fields (Patel and Poo, 1982, Schmidt *et al.*, 1997, Alexander *et al.*, 2006). Recent studies on the application of electrical fields to regenerative medicine focused on *in vivo* peripheral nerve regeneration with AC (Al-Majed *et al.*, 2000, Brushart *et al.*, 2002, Gordon *et al.*, 2008, Lu *et al.*, 2008). Our approach was to build a new system to define and observe the regeneration *in vitro* to further create an ideal stimulation system *in vivo* to aid peripheral nerve regeneration.

Preliminary results achieved using the pilot 2D model of the hybrid stimulation test module show that barriers to nerve outgrowth can be created using a modulated AC fields of 0.2 V/cm at a frequency of 100 Hz for the first time (Figure 68, Figure 69, Figure 70). These barriers can also be used to induce axonal turning in the face of such a field, demonstrating AC axonal turning, also for the first time.

Careful consideration of where these barriers are placed could result in alignment and manipulation of neurons in a useful manner as a channel permissive to axonal growth and barrier field to avoid axonal deviation (Figure 70).

Initial amplitudes tested of 10 V/cm were enough to cause a tear in the fibroblast layer under the outgrowth (Figure 65, Figure 66). The sharp rate of change associated with square waves causes a faster retraction than sinusoidal waveforms. This effect has potential for therapeutic applications in terms of inhibition of growth of cancerous cells (Veiga *et al.*, 2005), scar formation and axonal deviation.

Many studies show that the effect of AC fields on cells is mediated through calcium independent mechanisms (Cho *et al.*, 2002, Huang *et al.*, 2010). The use of calcium channel inhibitors and sodium channel inhibitors like tetrodoxin (Al-Majed *et al.*, 2000) could complete the study by investigating which mechanisms are involved in the axonal guidance. Taking to account this studies, we can make the assumption that the barrier effect observed could also be considered as an attractive feature for axonal growth due to the influence of the electric field on the extracellular and intracellular ion flux. This modified ions flux could attract and/or repulse axonal growth as shown with DC fields by Patel and Poo (1982).

With further work a catalogue of waveform values that can be used could be created. It is felt that a good starting point for a guiding waveform has been achieved here, and indeed, in making an effort to determine the effects of different parameters a good start has been made. In Appendix 1, an attempt was made to translate and apply these results and concepts on PCL to translate it to the nerve repair tube application.

6 Discussion-Conclusion

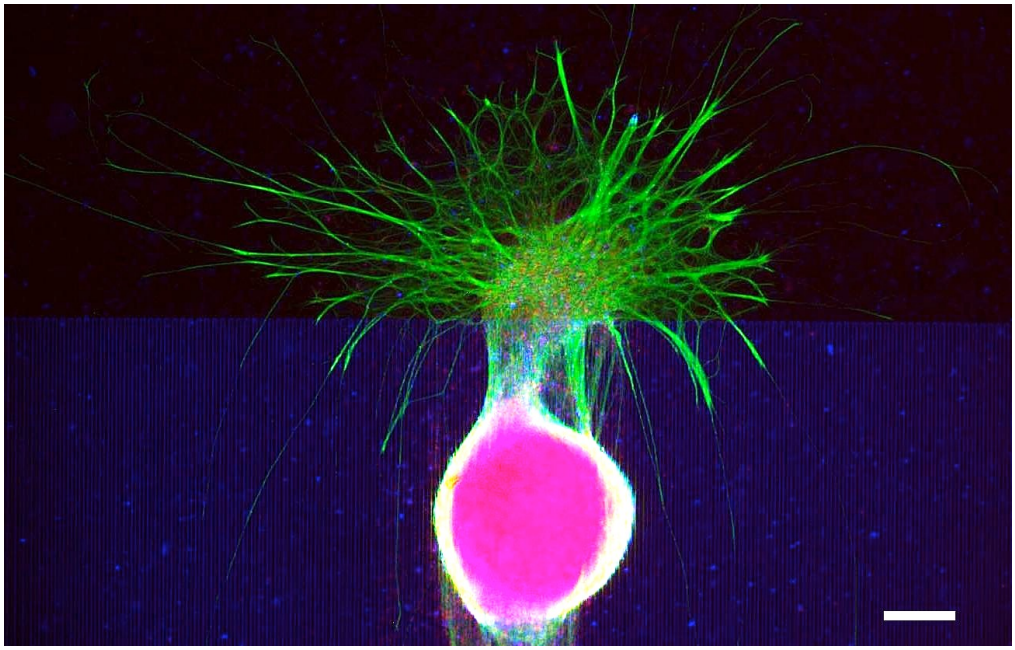

A DRG culture on the PDMS gap model. Scale : 200 µm

6.1 General discussion

Thus far, this thesis has presented chapters that report findings in isolation to the rest of the experimental work undertaken. This general discussion therefore seeks to integrate the findings presented in the preceding chapters.

6.1.1 Characterisation of a micropatterned polymer nerve repair conduit

Recent studies introduced the observation, that the stiffness of the substrate on which cells reside influences the differentiated cell phenotype, and stem cell fate (Discher *et al.*, 2005, Engler *et al.*, 2006, Guilak *et al.*, 2009). Stem cells can be differentiated into different cell types as a function of the stiffness of the tissue-engineered scaffold but also as a function of surface topography (Dalby *et al.*, 2007). In tissue engineering cells are generally pre-seeded in a biomaterial scaffold to enhance the regeneration of the injured tissue (Lietz *et al.*, 2006, Hart, 2011, Georgiou *et al.*, 2012, Georgiou *et al.*, 2013). This is why it is important to tune the biomaterial to the stiffness of the target tissue in a biomimetic approach e.g to use soft biomaterial for soft tissue like skin (KPa range) and hard ones for hard tissue like bones (MPa range).

As previously shown, e.g. by Balgude *et al.* (2001), Sundararaghavan *et al.* (2009) neuronal morphology in 3D collagen and agarose gels is affected by gel stiffness. The second chapter of this thesis therefore tested the postulate that the stiffness of the PDMS substrate would, independently of surface chemistry, influence the growth of regenerating DRG axons in presence of a guiding micro-grooved topography.

Since the use of growth factors and the effect of their concentration in neuro tissue engineering has been widely studied (Pfister *et al.*, 2007), the second parameter studied in Chapter 2 was the interaction between

substrate stiffness, micro-topography, and NGF concentration in the range previously shown to be effective in PC12 neural cell (Foley *et al.*, 2005). The results demonstrated a modulation of the DRG outgrowth response to the stiffness of the PDMS substrate. On a flat, hard, PDMS substrate, increasing NGF within the range 10 ng/mL to 100 ng/mL was associated with increased outgrowth from DRG explants. Interestingly the inverse effect was found when outgrowth followed micro-grooved topography. This demonstrated that the interaction between growth factor concentration, stiffness, and micro-topography is an important aspect determining the response of the growing axon to their regenerative micro-environment.

The optimal growth observed on the microstructure was found with hard PDMS using the lowest growth factor concentration tested (10 ng/mL). That echoes the demonstration by Koch *et al.* (2012) that the traction force interactions between the cytoskeleton network and the substrate which determines growth cone movements, migration, and guidance mechanisms occur by integrin-mediated mechanisms which sense substrate rigidity (Moore *et al.*, 2010). It was demonstrated that dissociated DRG neurons displayed maximal axonal outgrowth on stiff PAA (~1000 Pa), whereas extension from hippocampal neurons was independent of gel stiffness. In contrast to central nervous system neurons, which are uniformly exposed to the softest tissues of the body (Lu *et al.*, 2006), peripheral nervous system neurons develop and persist within different tissues that exhibit a wide range of stiffness and forces. That may explain the PNS neuron's greater differential response to substrate stiffness, shown here to be a critical parameter in peripheral nerve regeneration, and confirms the importance of the bio-mimetic approach to stiffness parameters in tissue engineering for peripheral nerve regeneration.

PDMS is unsuitable for *in vivo* use so another material was required. PCL has been widely used for neuro tissue engineering (Oliveira *et al.*, 2010, Sun *et al.*, 2010, Cirillo *et al.*, 2012, Donoghue *et al.*, 2013) and has a high Young's modulus that still allows flexibility. The material can mechanically protect the nerve repair site, and is fully bioresorbable (Sun *et al.*, 2006)

making it a suitable scaffolding material for nerve regeneration. The hard PDMS that was found to best support axonal outgrowth on patterned substrates in these experiments (Chapter 2) has a Young's modulus of 4.1 MPa, which approximates closely to that of PCL electrospun fibers (3.8 MPa)(Croisier *et al.*, 2012). These findings, and the materials other properties, led to the confirmation of PCL as a good candidate biomaterial for the nerve peripheral nerve regeneration conduit backbone described in Chapter 3, and in Appendix 1.

Chapter 3 reports the *in vitro* experimental development of a micropatterned PCL conduit for nerve repair. The necessary features of the tubular PCL Swiss roll scaffold design were tested, and included pores for nutrient, gas, and waste diffusion, pillars used as spacers between PCL layers, and micro-grooved wall surfaces to direct axonal growth. A previous design (Seunarine, 2008), was improved and fabrication steps were simplified to a spin coating and rolling step. PCL is opaque, precluding direct imaging, and its elasticity makes it difficult to section e.g. for histology or T.E.M. Hence evaluation required a "2D to 3D" approach to facilitate the observation of the DRG axonal network. The results of Chapter 3 show that the Swiss roll PCL conduit would provide a permissive environment for peripheral nerve regeneration.

Cells such as Schwann cells and fibroblasts that are part of the DRG model have also shown interesting growing behaviours in this work. In Chapter 4 Figure 48, the DRG *in vitro* model outgrowth developed spontaneously a directed outgrowth from its dorsal root stumps as observed on the microgrooved PDMS substrates (Chapter 2). This is probably due to the presence of activated and proliferative Schwann cells that are growing forming aligned colony, perhaps because of their inherent ability to form band of Büngner structures. The interaction of Schwann cells with the axons and their segregation from other cell types like fibroblast through Sox-2 dependent signalling has been demonstrated by Parrinello *et al.* (2010). This mechanism might be involved in the formation of Schwann colonies

developing on the fascicular like axon bundle observed. Interestingly, in Figure 18 and Figure 20, we can observe Schwann cells colonies interacting with axons around the DRG explant. It shows that axon regeneration can occur without the formation of band of Büngner formation *in vitro*.

6.1.2 Development of in situ electric stimulation within a polymer nerve conduit

This multidisciplinary work was undertaken in collaboration with the Microsystem Technology Team in the Department of the Electronic and Electrical Engineering of Glasgow University (Mr. Christopher Martin & Prof. David Cumming). Appendix 1 and Chapter 5 detail the development and experimental use of an *in vitro* microelectrode system used to observe the *in vitro* effect of the electric field on the DRG model. The hybrid electrode system designed on quartz enabled preliminary exploration of the necessarily huge stimulation parameter space (e.g. voltage, frequency, waveform shape), while the significant technical challenges in electrode printing were overcome.

As detailed in Chapter 4, the initial attempts at controlling axonal growth using AC electric field generation within the MEA system were unsuccessful.

The subsequent investigation of the effect of electric field of the DRG model outgrowth was more successful, particularly the perpendicular electrode design. The electric field was shown to have clear effects on DRG outgrowth. A low intensity field (0.2 V/cm) can create a spreading DRG axonal outgrowth alongside the field. Total and irreversible retraction of the growing axons, plus tearing of the cell monolayer growing underneath, was induced by higher field intensity (10 V/cm) (Figure 65 and Figure 66).

The design of four different gold microelectrodes added to the size of the parameter space by adding the choice of which ones to stimulate in respect to the other(s), but also suggested other effects of the electric field. From

the observation obtained from the DRG response to encountering the perpendicular electrodes it was thought, that four parallel electrodes generating two parallel electric field would constrain the growth of the axons in a central channel as shown in Figure 71.

Design-based fabrication of an electrode system that could be incorporated within a polymer nerve repair conduit was then taken forward. At this moment Christopher had the gold printing technique ready to test this envisaged constrained outgrowth in the electric channel with the straight electrode design on PCL (Appendix 1) using the DRG model. The first results suggested that this effect was observable as the aspect ratio and directionality of the electric field-constrained DRG increased while a healthy axonal outgrowth was observed on the gold microelectrode on the control culture without magnetic field. The fact that this technology has been translated to an implantable biomaterial such as PCL, allows the use of such electric devices to improve patient recovery is promising.

6.2 Future work

Chapter 2 demonstrated axonal outgrowth modulation by growth factor concentration and substrate microtopography and stiffness, using the organotypic DRG explant culture model. Explants include a large number of differentiated PNS neurons, along with support and structural fabrication cell lineages (e.g. Schwann cells, endothelial cells and fibroblasts). This culture system is an interesting *in vitro* model in which to study the biological mechanisms that control this topography/growth factor interaction.

Three additional lines of future work would include promoter/inhibitor mechanistic studies, 3Rs (replacement, reduction, refinement) of the model for the *in vitro* investigation of regeneration events that are previously only amenable to *in vivo* research, and interspecies research (e.g. replication using porcine or human neurons).

In addition there are obvious lines of translational research to further move towards an implantable bioelectric surface patterned conduit for peripheral nerve repair. These include optimisation of the 3D polymer construct, and refinement of the fabrication and stimulation parameters for electrical field generation at the site of repair

6.2.1 Promoter/Inhibitor studies

Firstly, interactions between topography and stiffness could be studied more accurately by using an inhibitor against the main source of tension force, which is at the interface between the substrate and the growth cone and of the cells. In the same view axon/axon interaction inhibitors, which affect the fasciculation and the shape of the network and subsequently the tension applied, could be a source of further investigation toward the understanding of the mechanisms involved in the change of architecture of the axonal network with the parameter studied in Chapter 2. Pathway relevant regulator genes / gene products could be manipulated (e.g. mTOR, PTEN, PI3K). Further investigation is required at the proteomic and molecular level to specify which mechanical, trophic and tropic pathways are responsible for this combinational modulation of the axonal outgrowth. Q-PCR analysis quantifying the expression of selected of genes involved in the process of nerve regeneration has been initiated (Miss Suzanne Thomson (MD)) with the aim of validating this model against *in vivo* gene expression changes induced by nerve injury and repair.

The interaction with growth factor concentration could initially be studied by the use of NGF pathway inhibitors that affect growth cone migration and morphology. Growth cone formation and migration determine the rate (Koch *et al.*, 2012) and shape of axonal regeneration. The main consideration for growth cone morphology, and its actin and myosin cytoskeletal network, is the role of the Rho family and small GTP binding proteins that are key regulators of actin cytoskeletal family (reviewed by Huber *et al.* (2003)). Kozma *et al.* (1997) have shown that RhoA and

lysophosphatidic acid microinjection induce a collapse of the growth cone in neuroblastoma cells. A similar experiment could be conducted with the DRG model to identify if the Rho family and its interaction with the NGF receptor are involved in the results shown in Chapter 2.

6.2.2 In vitro nerve injury gap model

The gap width is a critical parameter influencing the outcome of peripheral nerve regeneration (Daly *et al.*, 2012, Chang, 2009b). To develop an in vitro gap model, preliminary designs have been tried using the same microtopography described in chapter 2 including a gap on each side of the DRG seeding area (Figure 74). By modifying the photomask used in the microfabrication of the PDMS master, 100, 250, 500 µm and 1mm gap have been created in the resulting PDMS construct. These different gap sizes have been used in a first experiment under the same conditions as the culture system described in chapter 2 using 10 ng/mL NGF. The initial results are quite interesting (Figure 75), as we can see how gap size is a critical parameter for axon deviation, and that the outgrowth can turn at 90 degree in a 250 µm gap.

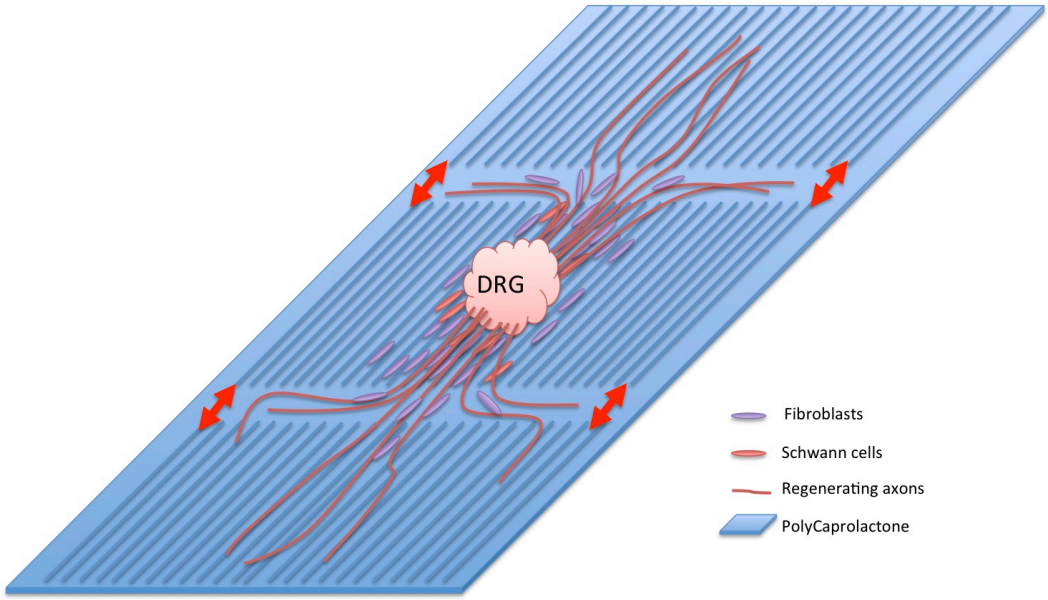

Figure 74: Scheme of the Nerve Injury Gap Model in vitro.A DRG is seeded on a guiding microgrooved substrate with two gaps in on each side. The width of the gaps (red arrows) will give information on how regrowing axon can be deviated when growing back in the case of an injury. In a preliminary test this width was set to a 100, 250, 500 µm and 1mm. This in vitro model would allow us to test different axonal guiding strategies through the gap in vitro and thus improve nerve guidance tube for clinical application.

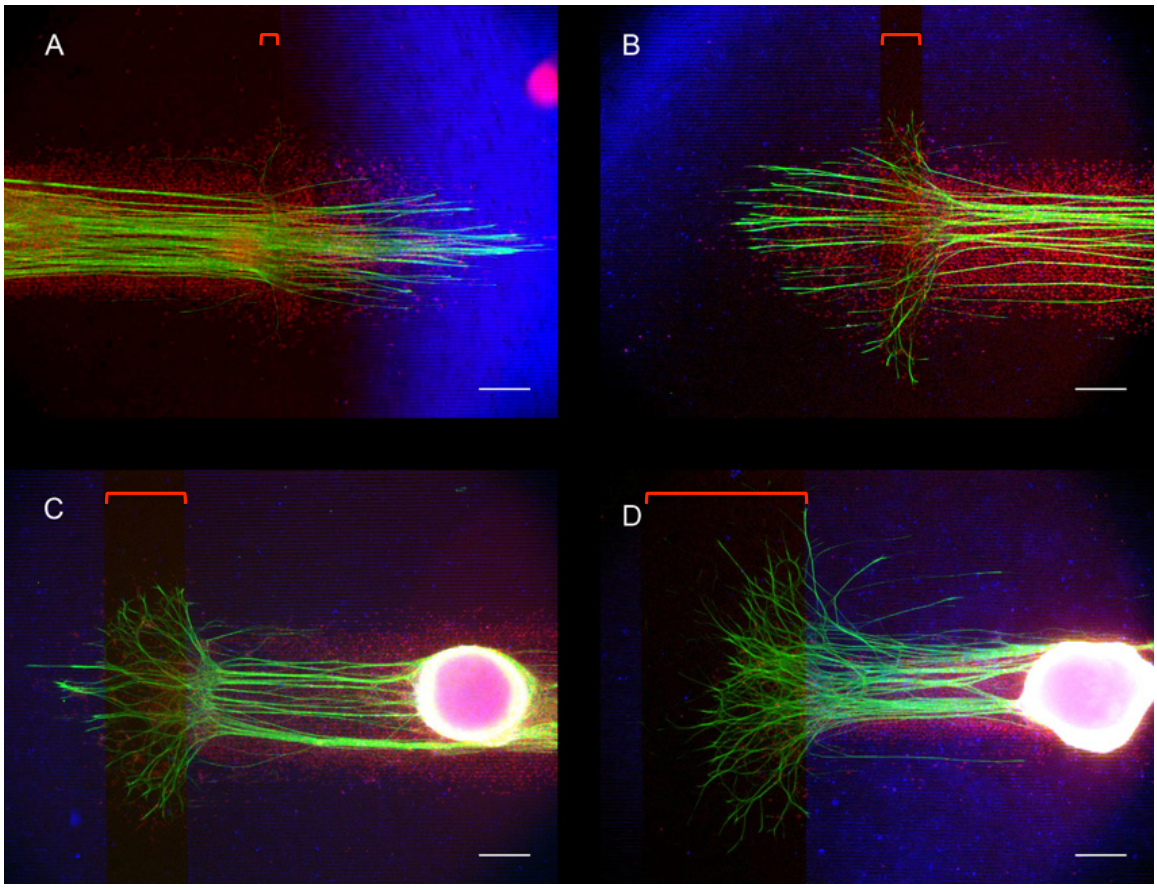

Figure 75: A DRG cultured on the gap injury modelwith a gap of (A) 100 ,(B) 250, (C) 500 µm, (D) 1mm in the micropatterned area in L15(NGF 10 ng/mL) for 15 days. A gap 250µm wide already deviates a third of the growing axons. The 500 µm wide gap deviates most of the growing axons in the gap (red brackets). Red: Dapi staining; Green: β3 tubulin; Blue: Bright field. Scale: 200 µm

An interesting progression of this *in vitro* model could be the addition of guiding features like aligned cells, patterning of guiding substances or devices to test their potential to guide the axons trough the gap. This would reduce the number of tests *in vivo* and the use of animal models.

6.2.3 Long term DRG culture: a good in vitro model?

Long-term cultures are usually considered costly and tedious because of the risk of contamination. We were curious to see which morphology the DRG organotypic culture would take after one-month culture. Surprisingly there was no contamination or death of the neurons and of the surrounding cells. The also axons quickly reached the side of the culture wall (Figure 76 and Figure 77).

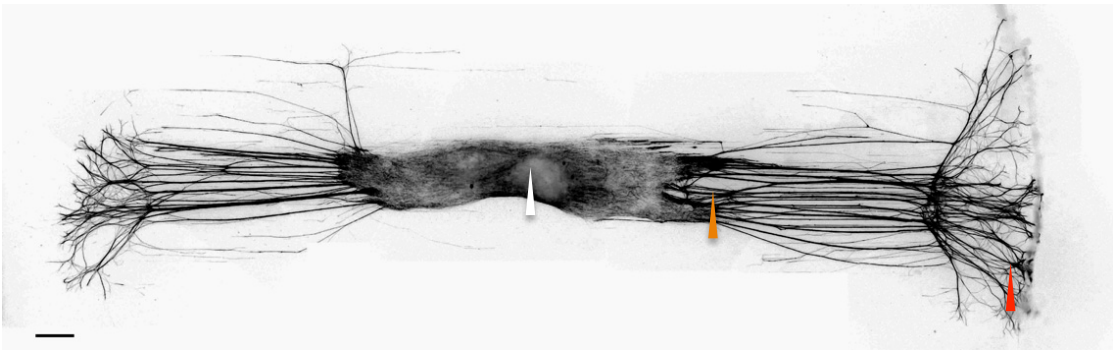

Figure 76: Fluorescence microscopy image of a one-month DRG culture on 12.5µm wide 5µm deep microgrooved PDMS substrate. Stain: β3 tubulin. We can see a complex axonal network in which Shwann cells and fibroblasts are present (orange arrowhead=Figure 77) on the side of the DRG seeded in the middle (white arrowhead). When the axonal growth has reach the end of the microtopography they spread radially on the unpatterned PDMS (red arrowhead). Scale: 500 µm.

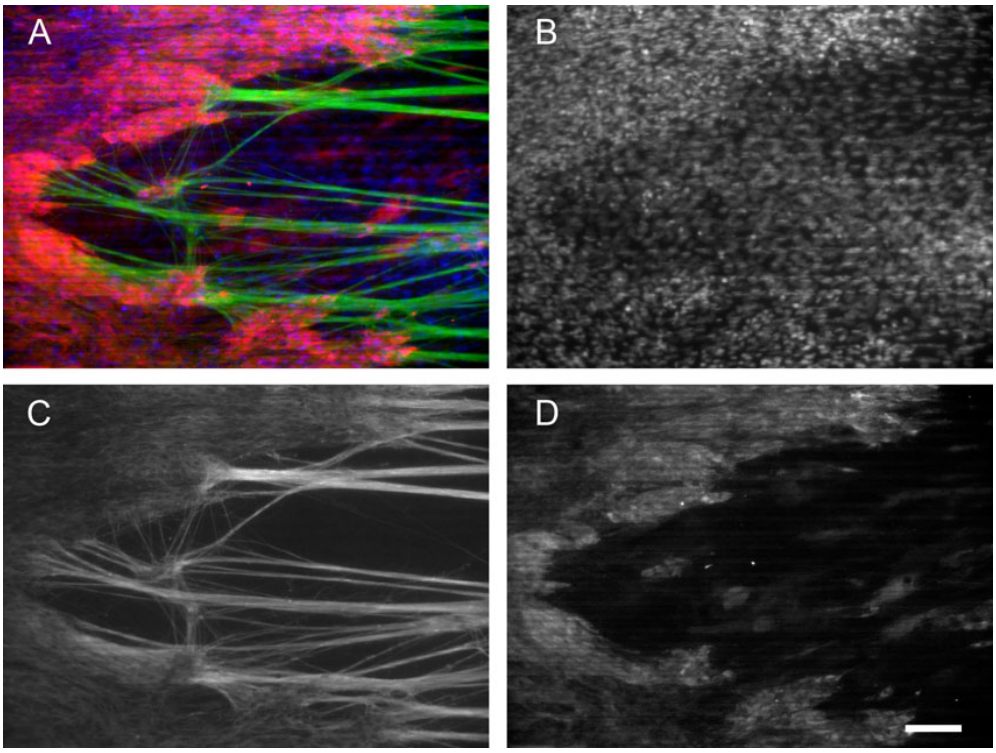

Figure 77: Fluorescence microscopy image of a one-month DRG culture on 12.5µm wide 5µm deep microgrooved PDMS substrate. Stain: β3tubulin. We can see a complex axonal network in which Schwann cells and fibroblast are present (orange arrowhead=figure) on the side of the DRG seeded in the middle (white arrowhead). Scale: 50 µm.

In this model it is interesting to see that Schwann cells and fibroblasts are accumulating as dense colonies around the axon bundle (also observed in 10 day cultures). These show that the interactions between the subfamililes of cell populations in the construct are somehow preserved and overcome the natural dissociation observed with most explant *in vitro* cultures. Again the development of such a model could help in refining and reducing animal use,

and investigate the interactions that took place in the axon cellular network reconstruction with the possibility of direct *in situ* observation.

6.2.4 In vitro stab injury model

The Stab model includes the same principle as the previous culture in chapter 2. The difference is that once the axons have grown long enough, a small vertical cut of the regrowing axons allows the observation of their regeneration. On Figure 78, the stab was done just before a time lapse recording was started, and we observed a retraction (red arrowhead Figure 78). After 16h the edge of the growing axonal network including supporting cells, had already reached the site of the stabbing. After 50 hours the stabbing site is crossed and axons and cells continued to grow further.

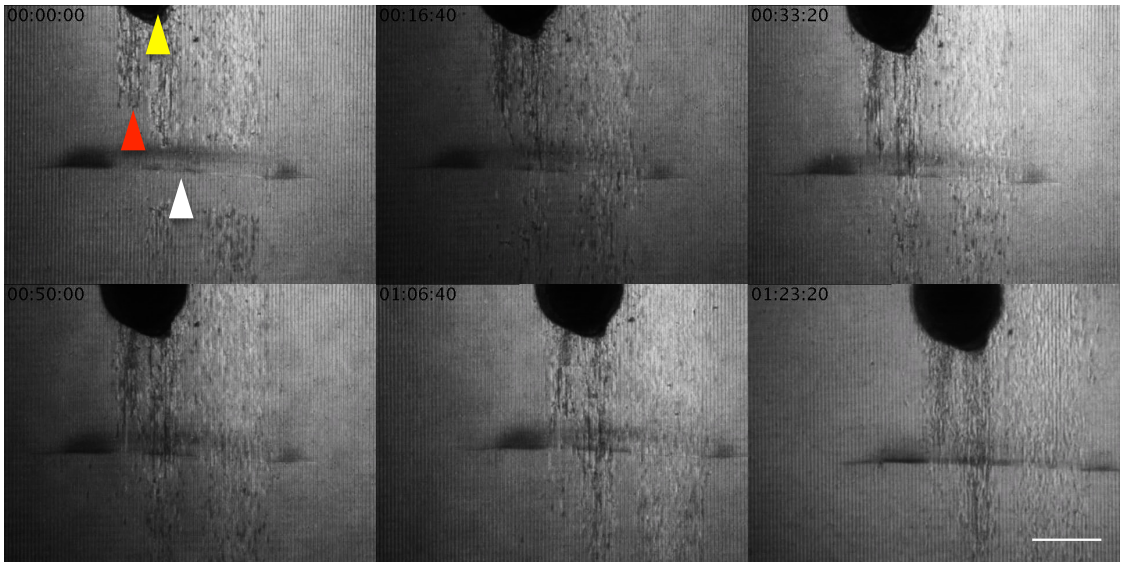

Figure 78: The stab injury in vitro model. Time-lapse recording of a DRG (yellow arrowhead) organotypic culture on PDMS substrate with 12.5 µm wide 5µm deep microgrooves, stabbed (white arrowhead) vertically after 5 days of culture. The axon network retracts immediately (red arrowhead) and starts re-growing to reach the stabbing site 16h hours afterwards. After 50 hours most of the axons crossed the stabbed site and continue growing beyond the stabbing site altogether with supporting cells. Phase contrast microscopy. Scale 500 µm

This model offers the possibility to observe *in vitro* what are the early events involved in axon reconstruction, to test different strategies to improve the regeneration speed and also the growing behaviours of cells beyond the injury site as their interaction with the regenerating axons is a key mechanism in peripheral nerve regeneration.

6.2.5 Interspecies validation

Finally, translational development (peripheral nerve repair) requires confirmation that human neurons respond optimally to the same topographical geometry and exact electrical stimulation parameters. That research requires access to human neurons of the peripheral nervous system, which is currently the focus of a separate research project in this group.

6.2.6 Upgrading the Swiss roll

As shown in Chapter 3, a new quicker technique has been developed to fabricate a robust PCL Swiss roll that allows axon growth and pre-seeding of supportive cells. This construct will be used as a nerve tube and will be tested at a later date by Miss Suzanne Thomson (MD) a surgeon doing research training. A new idea and potential future work would be to combine the PCL robustness with the advantages of a hydrogel system previously developed for neuro tissue engineering (McGrath *et al.*, 2010, Georgiou *et al.*, 2012, Lampe *et al.*, 2013). One of the main advantages of a hydrogel is that some are injectable and that they are softer than the PCL. Thus they could be used to fill the empty spaces of the Swiss roll, and increase the regenerative potential using a combinatorial approach.

Following this idea, a third part of this combinatorial approach would be to pre-seed the hydrogel as shown by Georgiou (2012), then roll it altogether with the PCL Swiss Roll. The second option would be to inject the hydrogel along with a supportive cell suspension. This approach would be ideal if we could control where the cell suspension could be injected in the Swiss roll. If so, we could then inject different cell types depending on the layer seeded. For example vascular and endothelial cells for the outer layer and Schwann cells in the central lumen. Such hydrogels could also be loaded with neuroprotective and neurotrophic factors.

These approaches would also allow us to test the potential of different supportive cells, and neurotrophic factors described in the introduction chapter using the upgraded Swiss roll for *in vitro* or *in vivo* investigations. In the same view, the Swiss roll wall and topography could be functionalized with different trophic factors. The choice of this trophic factor could be respectively adapted to the cell type Swiss roll layer the layer is supposed to provide a scaffold for in the regeneration process e.g GGF for Schwann cells and VEGF for endothelial cells.

6.2.7 Defining the optimal AC electric field

Chapter 5 demonstrated that axonal outgrowth can be directionally controlled by an electrical field created using a micro-engineered biocompatible stimulation apparatus. This new device built on quartz and on PCL could be used to define an optimal effect of oscillating electric field to improve nerve regeneration with an *in vitro* approach, to further create an ideal system to improve peripheral nerve regeneration *in vivo*.

For the first time, AC electrical stimulation (0.2 V/cm, 100 Hz) has clearly been demonstrated to direct axonal growth in vitro (Chapter 5, Figure 70 and Figure 71). Although further experimental work is required, certain concepts have emerged: the sharp rate of change associated with square waves causes a faster retraction than sinusoidal waveforms (Chapter 5, Table 7) and stronger electric fields (10 V/mm) are capable of tearing cell layers and repelling axons (Chapter 5, Figure 65 and Figure 66). These findings will direct further research, and engineering of great impact e.g. example in the treatment of cancer where the destruction of tissue is needed (Veiga *et al.*, 2005).

Future work could also confirm the hypothesis of the electric barrier by using inhibitors of biological electric field sensing mechanisms involving cells ions channel (Al-Majed *et al.*, 2000, Cho *et al.*, 2002, Huang *et al.*, 2010) and

try to determine if the barrier effect suggested attract or constrain axonal growth.

The huge parameter space makes this research a big challenge but the potential makes it worthy of further studies. It is felt that a start has been made and that the completion of this study would be of great importance to future applications in the field of tissue engineering, bioelectronics and medicine.

6.3 Collaborations outwith the main focus of this thesis

My experiences and skills in terms of DRG seeding and Schwann cell extraction have been used for collaborations on other projects closely related to my work.

The first was with Christopher Martin of the School of Engineering of Glasgow University. We used the DRG model for the preliminary testing of his PCL systems designed to improve peripheral nerve regeneration (Appendix 1).

The second collaboration was with Dr. Frank Gesellchen from the Centre for Cell Engineering. In this project we used sono-tweezer to control Schwann cell patterned seeding with the goal to guide neurites. We used the DRG model as a source of axonal outgrowth on the Schwann cells previously aligned with the sono-tweezer technology (Appendix 2).

6.3.1 Polycaprolactone systems design for improvement of peripheral nerve regeneration.

In this project we demonstrated how alternating electric fields have been successfully applied to growing sensory neurons by microelectrodes printed on PCL (a biodegradable FDA approved polymer) using a novel pattern transfer technique demonstrated and developed by Christopher Martin and used to grow and affect DRG axonal regeneration in vitro model.

The device features an electrical wireless inductive power supply from an external source. The flexible circuits designed in this work were used in planar form in order to optimise the control of cell culture and electrical parameters prior to the development 3D tubular implementation.

It is the first example of a wireless biodegradable electronic stimulation system demonstrating the possibility to restrain neuronal growth using an AC field. The detection of directional outgrowth from a DRG in vitro model in the presence of this field shows that even a 100 Hz signal is enough to produce a barrier effect, and of sufficient frequency to enable practical electronic implementation. Additional work is needed to study the rate of growth and percentage of aligned neurons using the huge parameter space for the electrical signal.

Wireless impedance measurements as a means of determining cell coverage through a conduit over time could be combined with the approaches above, as a means for assessing the repair procedure. Provisional data indicates a correlation between data measured at the transmitter and cell coverage at the receiver. A degradation study could be a good way to evaluate the time such a device could be active before it is bio-resorbed.

More advanced conduits could be designed with electrical functionalization in combination with the topographical guidance cues provided by the biomaterial substrate shown in Chapters 2 and 3, in addition to systems releasing optimal growth factors content, and to further improve clinical outcomes in the field of neuro-regenerative medicine.

6.3.2 Pre-aligned Schwann cells by sono-tweezer induce neurites alignment

In this project, a novel electronically controlled method was used to generate dynamic cell patterns by acoustic trapping of cells. The device built by Dr. Anne Bernassau of the School of Engineering (University of Glasgow) is

a heptagonal device with ultrasonic transducers called a sonotweezer device. The device creates complex patterns of cells using the device's ability to reposition acoustic traps by using a phase shift in the acoustic wave, and by switching the configuration of active piezoelectric transducers. Most of the cells migrated quite rapidly over night after patterned seeding except Schwann cells. We aligned them in a linear pattern to create Bands of Büngner-like structures on a non-patterned surface. These aligned cell colonies were able to guide axonal outgrowth from the DRGs. These techniques would be of great interest to improve existing protocols of tissue engineered scaffold pre-seeding for regenerative medicine and particularly in this case for peripheral nerve regeneration.

6.4 General conclusion

This thesis presents scientific research into key aspects of peripheral nerve injury and regeneration that remain significant barriers to the clinical care of many thousands of patients each year.

It has been clearly demonstrated that axonal outgrowth from DRG explants on polymer substrates such as PDMS can be morphologically enhanced, and rigidly directed by certain surface microtopographies. Control was maintained when using PCL substrates, facilitating the rapid translational 3D development of a nerve repair conduit. Of fundamental biological and therapeutic importance is the demonstration, for the first time, that there is a strong interaction between substrate topography and stiffness with NGF concentration.

Work with DRG explants and design-based, cell-scale electrical stimulation, has shown that AC electric field control can directionally control axonal growth. This has been carried out using stimulation parameters that can be delivered by a biocompatible microelectronic stimulation rig suitable for wireless powering (Appendix 1) and incorporation into the aforementioned surface patterned polymer nerve repair conduit.

In addition, the findings suggest that the DRG explant model can be refined by the use of surface microtopographical patterning to create elegant *in vitro* experimental models of nerve regeneration, injury and repair with significant benefits in terms of 3Rs, and scientific power.

Overall these findings lead, like most of the findings, to other questions and hopefully to more findings. This is how science and progress never stop but it is here that my thesis text ends.

Appendix 1

Directed Nerve Regeneration Enabled by Wirelessly Powered Electrodes Printed on a Biodegradable Polymer

Christopher Martin, Théophile Dejardin, Andrew Hart, Mathis O. Riehle and David R. S. Cumming

C. Martin, Prof. D. R. S. Cumming
Electronics Design Centre, School of Engineering, University of Glasgow, G12 8LT, UK.
E-mail: David.Cumming.2@research.glasgow.ac.uk
T. Dejardin, Prof. A. Hart, Dr. M. O. Riehle
Centre for Cell Engineering, Joseph Black Building, University of Glasgow, G12 8QQ, UK

Keywords: Peripheral Nerve Repair, Micro Transfer Printing, Biodegradable Electronics, Flexible Electronics, Electrical Stimulation of Neurons

1 Overview

Injuries to the peripheral nervous system (PNS) are extremely difficult to repair due to poor regeneration accuracy, scar formation, cell atrophy and axonal escape.[1, 2] Functionalised conduits are often used to improve repair outcomes using electrical,[3] biological,[4] chemical[5] or mechanical cues.[6, 7] We have designed and fabricated a novel inductively powered electrical stimulation circuit on sheets of a biodegradable polymer (polycaprolactone, PCL), and used these to apply alternating electric fields to sensory neurons in-vitro. Figure 1 shows both the target application and the experimental set-up. Gold micro-electrodes and an inductor were fabricated on thin PCL sheets by contact printing and used to apply balanced sinusoidal electric potentials to organotypic cultures of regenerating sensory neurons. The average aspect ratio of the stimulated cultures (4.105) was significantly higher than control cultures (2.328), indicating a higher degree of longitudinal alignment. This work illustrates progress towards the use of alternating electric fields in an electro-active biodegradable device as an alignment tool with potential applications in-vivo e.g. in nerve repair conduits.[8, 9] Functionalised biodegradable conduits using safe levels of balanced alternating electric fields could improve the outcomes of peripheral nerve repair surgery, particularly if combined with other technologies, such as mechanical, chemical and biological growth cues.

2 literature review

Traditional PNS repair procedures have centred around the use of end-to-end suture repair for short gaps,[10] and conduit tube repair [11, 12] often with an autologous donor nerve inside [13] or using acellular alternatives.[14, 15] These approaches suffer from poor functional recoveries, which have not improved much during the last few decades, due to poor alignment of axons to their targets, cell atrophy in the distal stump, axonal escape and the formation of painful neuroma or scar tissue.[16-18] The use of direct electric fields to orient neurons along a voltage gradient is well understood,[19, 20] but is impractical for use in vivo due to harmful levels of ion-flux associated with direct electric fields.[21] In the past decade, studies have sought to use alternating electric fields to augment conduit based repair, primarily using a 20 Hz, supra-threshold signal (sufficient to initiate an action potential) for 1 hour per day to increase type specificity,[22] to increase the number of sprouting axons[23] and to overcome the injury response delay.[24] Some authors have documented the effect of one electrical parameter, the stimulation frequency, [3, 25] which can be useful in optimising the stimulation waveform parameters. The electrical stimulation of Schwann cells can also play a vital role in the regeneration process, often through the release of nerve growth factor.[26, 27]

3. Novel Developments

Here we demonstrate the fabrication of wireless electronic systems on biodegradable polymers used to produce an alternating electric field protocol to align sensory neurons. The stimulation system has been designed to operate at sub-threshold so that it does not induce an action potential. 100 Hz sinusoidal signals with sub-threshold amplitudes were found experimentally to influence the growth of regenerating neurons. Microfabrication techniques often require photoresist baking temperatures in excess of 90°C, which greatly exceeds the melt-temperature of PCL (approximately 55°C). In addition the polymer used for repair is ideally thin, and flexible, rendering it mechanically weak and difficult to work with and therefore to carry out microfabrication. Finally, PCL, like many other biodegradable polymers used for nerve tubes, is incompatible with many of the chemicals required for traditional microfabrication techniques,[28] most notably acetone, propan-2-ol, and methanol, hence further complicating any fabrication procedure. Despite these difficulties, we have successfully developed a fabrication scheme and used it to build a wireless stimulator capable of being wrapped circumferentially round a nerve repair site which could align neurons through a conduit, avoiding the harmful effects associated with direct electric fields and non-degradable conduits.[29] In this article we demonstrate device performance using planar circuits with a view to using them in their rolled form once the appropriate parameters have been identified. Surface mount components, attached to the wireless stimulator with silver conducting paint, have been employed to demonstrate the utility of the device. The development of biocompatible components, attached via gold wire-bonding, could lead to an in-vivo implementation.[30] Building upon the broad application of alternating fields in a conduit repair, we also show the use of micro-electrodes to apply precise fields and thus further our understanding of how ac fields can affect regenerating neurons and support cells. This is believed to be the first instance of a wireless biodegradable electronic stimulation system demonstrating results at the cellular level, which could greatly improve functional outcomes and the rate of repair whilst, because it is degradable, eliminating the need for a follow-up surgical procedure. Advanced conduits could be designed with electrical functionalization and topographical guidance cues, in addition to the release of growth factors to further improve outcomes for patients.

4 Experimental Procedure

Inductive powering is a well understood technique which has been used to transfer data across a tissue barrier,[31, 32] or power indwelling devices in many biomedical applications, such as cochlear implants.[33] In general, a large alternating current in a transmitter inductor induces a small current in a

receiver inductor embedded within the patient. In this work, the receiver inductor and interconnect is transfer printed onto PCL using a novel fabrication procedure, described in the experimental section and shown in Figure 2. A class AB power amplifier designed on a printed circuit board (PCB) is used to power the transmitter inductor, shown in Figure 1. The receiver is placed above the transmitter inductor at a nominal distance of 5 mm. The receiver inductor geometry, of dimension 6 mm x 6 mm, is based on the requirement for a nerve conduit with a diameter of 5 mm. Experiments, investigating the effect of different stimulation frequencies on nerve regeneration, using wired devices showed that stimulation frequencies less than 200 Hz had a greater effect. However in order to achieve efficient power transfer it is necessary to operate the wireless system at a frequency of several hundred kilohertz.[34] We therefore modulate a 800 kHz carrier at 100 Hz and downconvert the received signal to produce a 100 Hz, 20 mV sinusoidal signal using detection electronics built into the implant. A stimulation test module is connected to the receiver circuit, consisting of Au electrodes on PCL and a glass ring that defines the cell culture area. The electrode configuration used in the modules, shown in Figure 3, is designed to confine neurons between two electrical barrier regions, preventing axonal escape. The expectation is that such an outcome will decrease the number of misguided axons, and thus increase the number of neurons that reach their target destination in a repair. These flexible circuits are used in planar form in order to optimise the control of cell culture and electrical parameters prior to the development of a flexible, 3D, implementation.

5 Results

Using the device described above, experiments and controls were conducted by applying a 20 mV, 100 Hz signal to the cells in culture. In the presence of the alternating electric fields the induced potential barriers, with a maximum electric field of 0.2 Vcm-1, confined the outgrowing support cells and the regenerating axons to the space between the electrodes. This phenomenon was not observed in the control cultures, where no stimulation was applied to the electrodes. Stimulated and control cultures were conducted in a 37 °C room. Control cultures were mounted on PCB without applied electrical stimulation. Six stimulated and seven control results were used across three independent experimental trials. The micrographs in Figure 4(A and B) demonstrate this behaviour. Note that in the activated example (Figure 3(A)) there is no cell growth on the electrodes, whereas in the control (Figure 4(B)), growth is prolific over the electrodes. The behaviour is repeated across the three independent trials. ImageJ software was used to measure the width and length of the axonal network for each sample, and its aspect ratio defined as the length of the network divided by the width, where the length was measured in the direction

of the neutral channel. The standard error was used to quantify any uncertainty in the aspect ratio. Measured aspect ratios for stimulated cultures were significantly higher than for the control cultures, indicating a higher degree of longitudinal alignment. The angular distribution of axonal orientation also helped to quantify the effect of the electrical stimulation, with a distinct alignment profile for stimulated cultures. Polar angular measurements were obtained by setting a 'dark threshold' for each image, and plotting an oval profile of the number of crossings that exceed the threshold. Experiments were conducted in three batches, with each module stimulated for seven days at 37ºC.

6 Discussion

We have shown here, for the first time, the use of alternating electric fields to influence neuronal growth at the cellular level by wireless stimulation of an electro-active device fabricated onto a biodegradable material. To do this we have designed and implemented a novel circuit on a biodegradable flexible membrane. Studies have shown the effectiveness of electrical stimulation applied during a PNS repair in a variety of ways. This study aims to provide the means to reliably fabricate a new type of device that will allow the use of electrical stimulation by applying sub-threshold inductively powered alternating electric fields, and that is suitable for implantation. The findings reported here indicate that neurons can be confined near an electrode using a region of alternating electric field. By growing the neurons between two electrodes, the neurons are faced with a barrier on either side. It has previously been established that neurons in culture will grow directionally in the presence of a direct electric field, with the growth cone being repelled by the anode and attracted to the cathode (cathode-preference).[19] This directed growth towards the cathode depends strongly with the electric field strength. Fields as low as 0.2-0.3 Vcm-1 caused 55-73 % of the neurons to turn,[35] and in some cases 0.07-0.09 Vcm-1 was applied to demonstrate a response of over 50%.[36] Because we wanted to build a wireless device we initially investigated the effect of applying a high frequency (> 1 kHz) alternating current stimulation, however there was no observable cellular response to the applied field. The majority of studies have shown the effects of electrical stimulation across the 1-200 Hz frequency band.[3, 25, 37] We describe the detection of a change in the outgrowth from a regenerating dorsal root ganglion (DRG) as a consequence of the application of a demodulated low frequency (100 Hz) signal. This 100 Hz signal is slow enough to produce a barrier effect,[38] whilst being of sufficient frequency to enable practical electronic implementation.

We have demonstrated the effects of electrical stimulation with a 0.2 Vcm-1 alternating electric field. This amplitude is within the range of direct electric field values that are known to cause a response in regenerating neurons. [35, 36]

Regenerating neurons can be confined between alternating electric fields with this type of signal. As a consequence of the opaque substrate, aspect ratio measurements were performed at the end of the experiment. This hinders our efforts in observing how the neurons react with the regions of electric field throughout each experiment.It is known that signalling between neurons, particularly when regenerating, is of vital importance. [39] Perhaps the small alternating electric field has a discernible influence over these internal signals, causing a change in the growth pattern. [40] It is perhaps the case that the neurons and support cells are attracted to the electric field for one half cycle, before being repelled for the opposite half cycle. This hypothesis was the inspiration for the electrode layout, which aimed to adopt the effects of direct stimulation, within a charge-balanced alternating electric field protocol.

Conclusion

Electrodes printed by using a novel technique on PCL, a biodegradable polymer that has FDA approval, have been used to apply alternating electric fields to sensory neurons. The device is envisaged to be implantable, and delivers the electrical fields using inductively powered electrical stimulation from an external, wireless, source. The system has been used to demonstrate increased alignment of sensory neurons in-vitro when compared with control cultures. This confinement has been shown to be possible using sub-threshold alternating electric fields by employing a novel four-electrode configuration, creating a channel with no electric field for neurons to propagate through. Further work is needed to study the rate of growth and percentage of aligned neurons by modifying the electrical parameters, and to show that an electro-activated neural conduit can be made. This system has the potential to be used in-vivo to improve existing repair rates and functional outcomes. It is hoped that there is good scope for a valuable nerve repair system to be developed.

Experimental Section

Despite the challenges associated with PCL, there are some advantages present that have been exploited in this work. Some chemicals are known to be compatible with PCL; in particular the use of AZ400k (Clariant, Germany) photoresist developer allows the use of AZ series photoresist.[41] The low melt-temperature of the polymer is of great assistance during transfer printing, preventing features on the stamp from deforming. The steps below outline how patterned thin-films of Au can be transferred to the thin-film polymer, and used in this work to create a 15 turn spiral inductor (6 mm x 6 mm area, 75 μm track width, 50 μm track spacing) in addition to the electrical interconnect and component footprints, shown in Figure 2.

The printing procedure is divided into two sections: stamp production and substrate preparation. The stamp is produced using photolithography and dry etch techniques in the following manner. A Si substrate is cleaned in acetone,

methanol, propan-2-ol, and deionized (DI) water, each for 5 minutes, followed by a blow dry in a pressurized stream of N2. A dehydration bake in a 180 °C oven for 5 minutes removes any residual moisture. A layer of AZ4562 (Clariant, Germany) photoresist is spin-cast onto the Si substrate using a spin speed of 1000 rpm with an acceleration ramp of 250 rpms-1 for 30 seconds. A soft-bake on a hot-plate for 15 minutes at 90 °C causes the solvent to evaporate from the photoresist. A second layer of AZ4562 is then applied in the same way; producing a 30 μm thick film of photoresist (2 x 15 μm). This resist height was found experimentally to be sufficient to prevent the PCL substrate coming into contact with the silicon substrate during printing. The resist film was left to rehydrate overnight before executing the exposure step. Exposure to UV light was performed through a photo-mask in 10 second bursts between 10 second relaxation periods to allow any N2 that is liberated to escape. The total exposure time was 110 seconds. The exposed regions of AZ4562 were removed by immersion in AZ400k developer in DI water (1:3) for 5 minutes. Residual photoresist was removed by an O2 plasma ash at 80 W for 2 minutes. Next the stamp is dry etched using the Bosch process for deep dry-etching of silicon in an STS-ICP machine (SPTS Technologies, USA). The Bosch process used here is modified to create a negative sidewall profile by increasing the flow rate of SF6. The modified process uses an SF6 flow rate of 40 sccm, platen power of 10 W, ICP power of 600 W, pressure of 10 mT for 5 minutes. This procedure leaves any undesired regions of metal deep within a silicon trench, with no connection to the resist sidewall, preventing their transfer to the PCL substrate. Prior to metal evaporation all photoresist is subjected to a flood-exposure of 120 seconds, allowing the use of AZ 400k for resist stripping. Evaporation of 400 nm of Au in a Plassys machine (Plassys Bestek, France) completes the stamp fabrication process. A SiO2 substrate is then cleaned in acetone, methanol, propan-2-ol, and deionized (DI) water, each for 5 minutes, followed by a blow dry in a pressurized stream of N2. PCL in chloroform (1:3) is spin-cast at 400 rpm with an acceleration ramp of 100 rpms-1 for 60 s. The chloroform is evaporated at room temperature leaving a 50 μm thick layer of PCL on the substrate.

To begin the transfer printing, both the stamp and the substrate are placed on a 65°C hot-plate. After reaching 65°C, the stamp is placed onto the PCL sample with enough pressure to push the stamp into the polymer. After 5 minutes the stamp/substrate is removed from the hot-plate and allowed to cool to room temperature. Removal of the stamp causes selective pattern transfer to the substrate. If the height of the photoresist is insufficient, the PCL will come into contact with the silicon substrate, adhering strongly to it, and thus the printing will fail as the stamp cannot be removed save for excessive force being applied (pattern deformation is certain). Printed samples were then electroplated in gold plating solution at 25 °C to a thickness of 30 μm. This plating step reduces the resistance of the inductor to a few Ohms, and allows wire bonding to be used to connect the lone via. Several wire bonds were added to connect the

inner contact of the spiral inductor to the rest of the circuit. By wire bonding in this way, only one printing step is required, with the wire bonds used as the second layer. Components were then attached to their respective footprints using silver conducting paint. The same process was used to fabricate electrodes on PCL used for cell culture and applying electric fields to the neurons. A 400 nm layer of Au was sufficient for the electrical stimulation modules.

Dorsal root ganglia (DRG) were isolated from 2-day old neonate Sprague-Dawley rats and placed between the electrodes on the PCL/electrode modules. The DRGs were then grown for 15 days at 37 °C, 5% CO2 with L15 media (Sigma) supplemented with 10% FBS, NGF 2.5S (50ng/ml) (Invitrogen), n-acetyl-cystein (50µg/ml) and 1% antibiotics antimycotic (PAA p11-002). Half of the media (150 µL) was exchanged every day. Cells were immunostained for ß3-tubulin (mouse anti-TU-20 Santa Cruz): After the experiment was complete, DRG were fixed in 4% formaldehyde/PBS solution for 15 minutes at 37°C. They were then permeabilised in perm. buffer (10.3g sucrose, 0.292g NaCl, 0.06 g MgCl2, 0.476 g HEPES 0.5ml Triton X-100 per 100ml PBS Sigma, UK) at 4 °C for 15 minutes. A blocking solution of 1% BSA/PBS was added at 37°C for 5 minutes. The blocking solution was replaced by 1% BSA/PBS solution containing anti-ß3-tubulin antibodies (1:100; mouse anti-TU-20 Santa Cruz, California). The samples were incubated at 37 °C for two hours then washed three times with a PBS/Tween20 (Sigma, UK) 0.5% solution. They were then incubated for 1 hour at 37 °C in 1% BSA/PBS solution containing 1:100 biotinylated anti-mouse antibodies (Vector Laboratories) and washed three times with Tween 20 0.5%/PBS. Fluorescein Streptavidin 1:100 (Vector Laboratories) in 1% BSA/PBS was then added to the sample for 30 minutes at 4 °C, before washing them again. The samples were viewed by fluorescence microscopy, and imaged using an Olympus BX51 microscope, with a QImaging camera, running on ImagePro+ (Media Cybernetics, UK). A total of 13 successful cultures were used for the experiments.

Acknowledgements

We would like to thank the Stephen Forrest Trust for supporting this work, as well as the EPRSC (UK). We are also grateful to the technical staff of the James Watt Nanofabrication Centre, and the Centre for Cell Engineering for their help in this work.

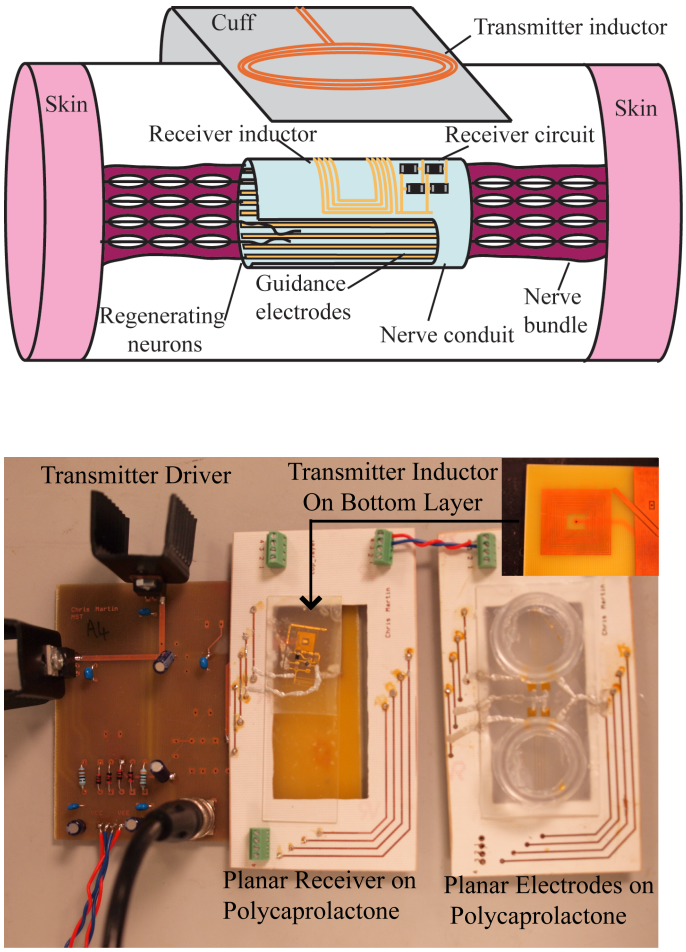

Figure 1. An illustration of the targeted application. An electro-active biodegradable conduit, powered via a transmitter driver worn as a cuff by the patient for the duration of a repair (top). The prototype used (below) throughout this work. The receiver and electrodes on polycaprolactone are held in planar form to demonstrate the utility of the system in guiding regenerating neurons. The driver is a class AB power amplifier connected to a 15 turn, 25 x 25 mm spiral inductor on printed circuit board. Work is on-going to progress from the prototype below to an implantable system capable of in-vivo nerve guidance.

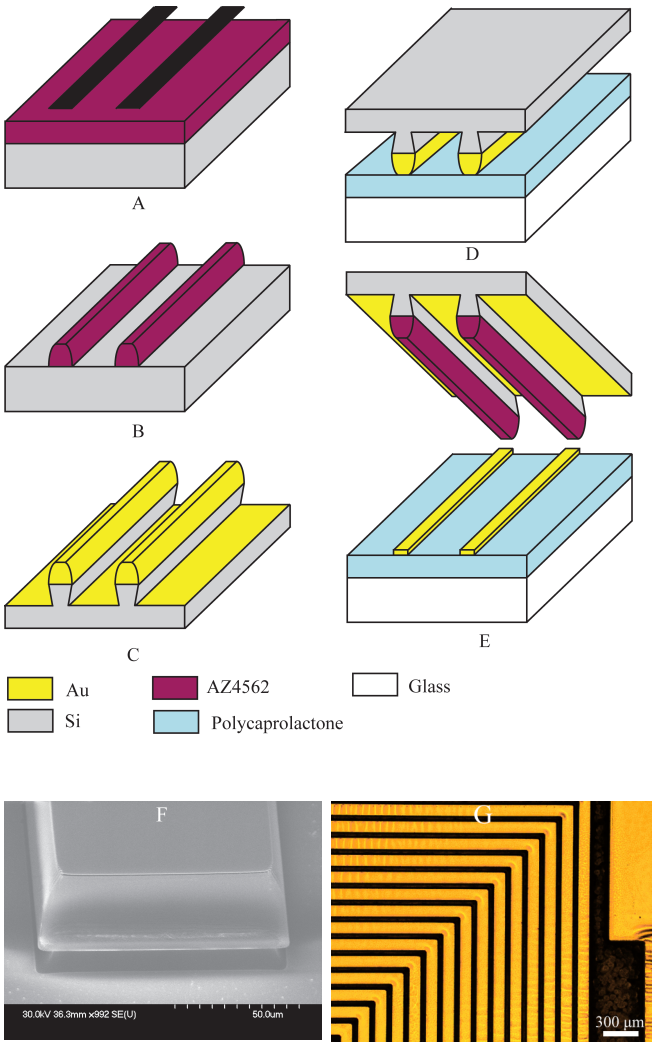

Figure 2. A schematic depicting the novel transfer-printing technique developed for polycaprolactone (top). A 30 µm layer of AZ4562 is exposed through a photo-mask (A) followed by development in AZ400k (B). The stamp is dry-etched in an STS-ICP machine using a modified Bosch process to produce a negative sidewall profile, prior to evaporation of 400 nm Au (C). Polycaprolactone is spun onto a glass substrate, followed by the imprinting of the stamp at 60 °C using moderate pressure (D). Upon cooling to room temperature, the stamp is removed, leaving metal transferred to the substrate (E). A scanning electron micrograph shows the thick-film of photoresist on Si, with the negative sidewall profile visible (F). A microscope image of 15 turns of an inductor (75 µm track width, 25 µm spacing) illustrates the print quality (G).

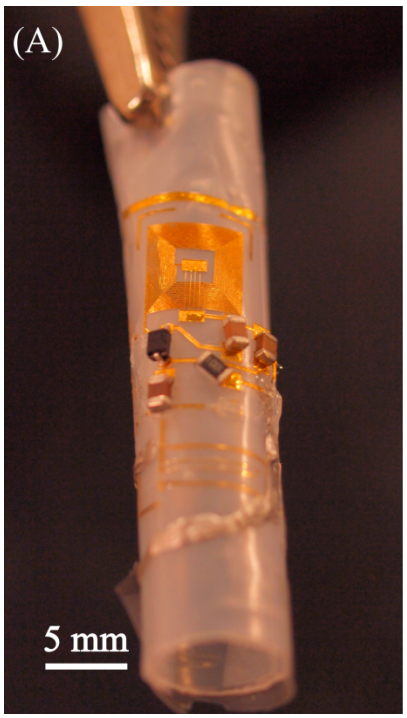
(A)
5 mm

(B)

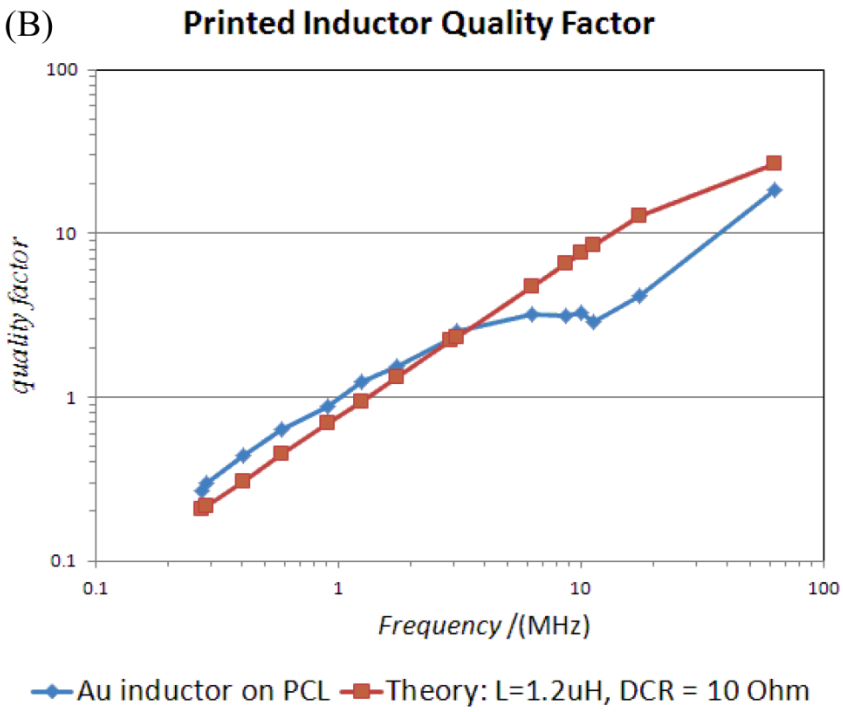
Printed Inductor Quality Factor
100
10
1
0.1
quality factor
0.1
1
10
100
Frequency /(MHz)
Au inductor on PCL
Theory: L=1.2uH, DCR = 10 Ohm

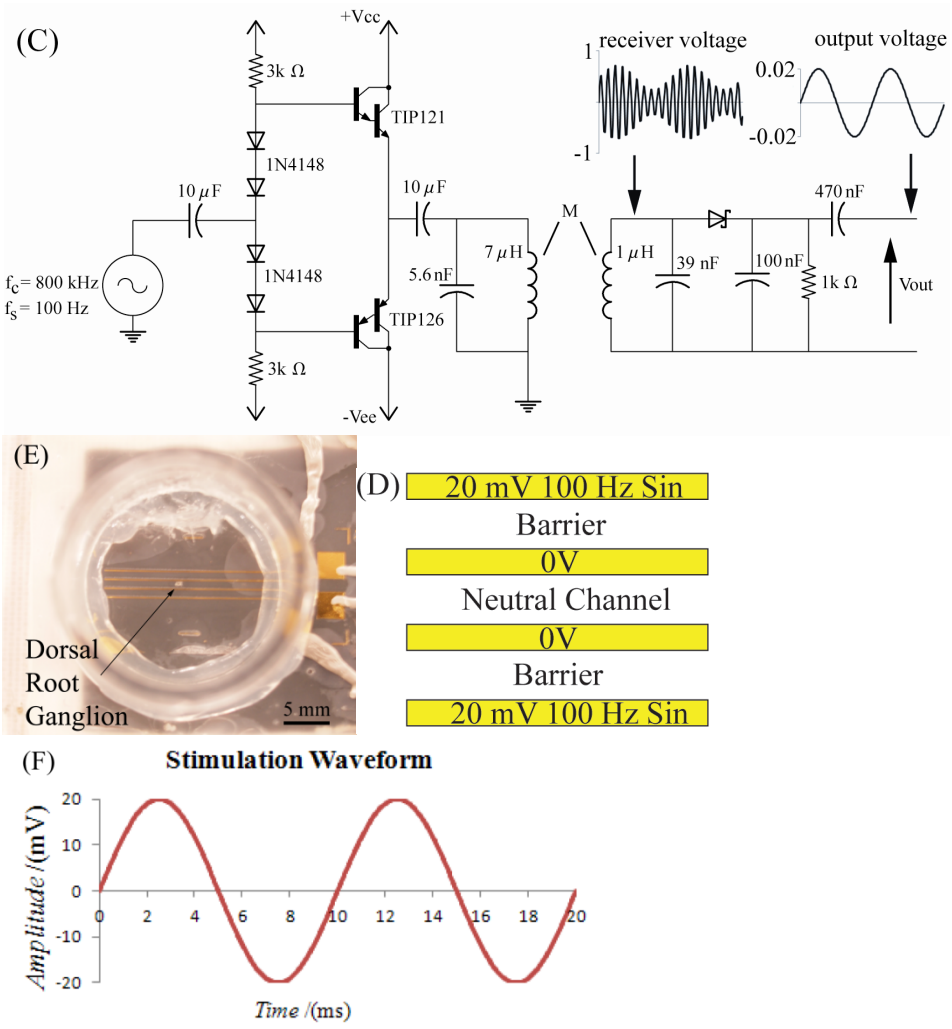

Figure 3. An assembled receiver system on polycaprolactone, rolled around a tube as in a nerve conduit repair (A). Components and wire-bonds have been orientated to improve reliability. The quality factor of the inductor is shown against theoretical values (B). A class AB push-pull driver is used to transmit amplitude modulated pulses to the envelope detector at the receiver (C). The output from the receiver is connected to a stimulation module containing the neurons under test. The electrode configuration (D) is designed to align neurons using electrical barrier regions, caused by controlled application of alternating electric fields. A Dorsal Root Ganglion (DRG) was seeded in the neutral channel (E) and stimulated using the waveform shown (F).

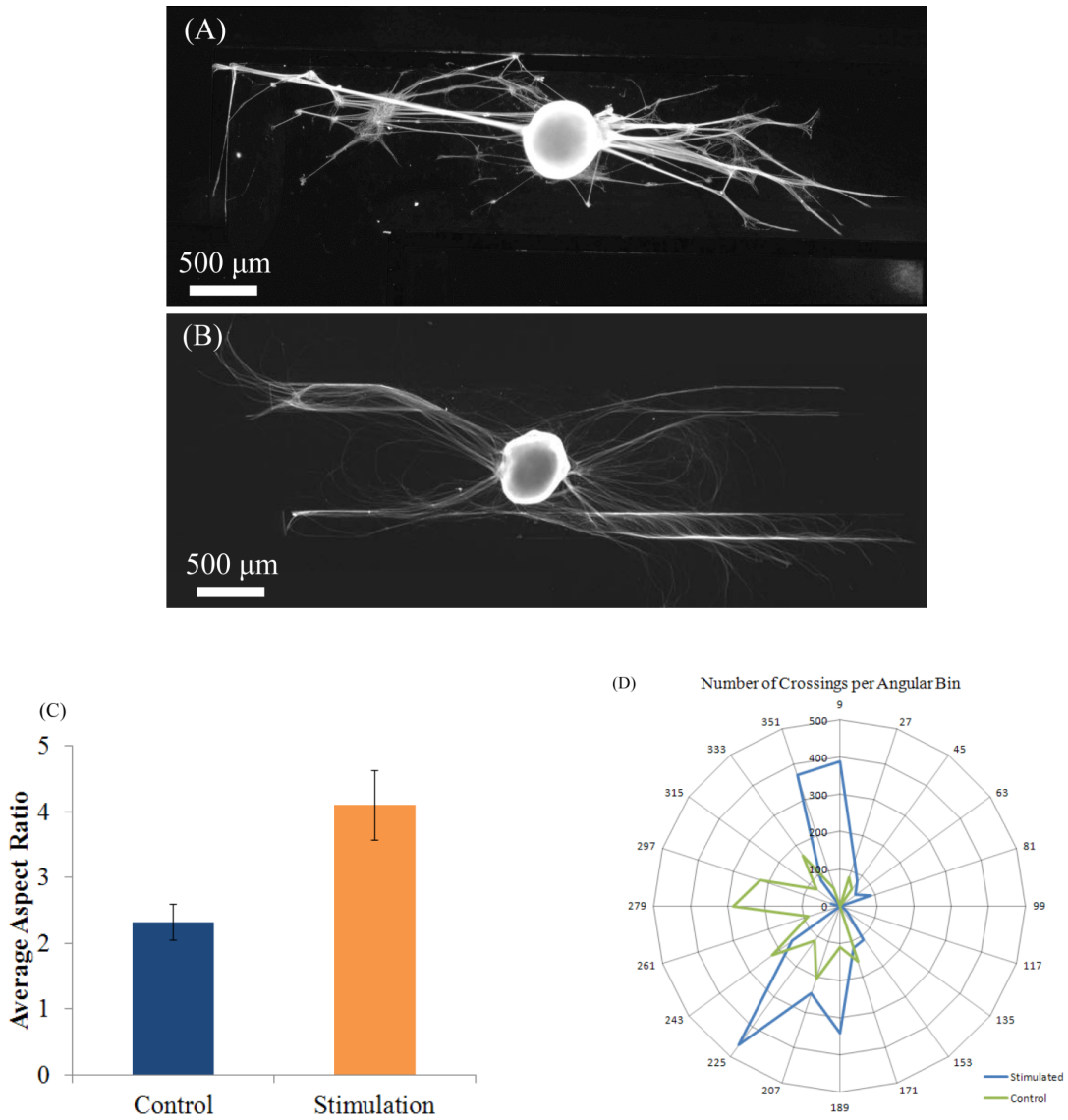

Figure 4. Stimulated sensory neurons growing from a dorsal root ganglion (A), versus a control culture (B) on planar polycaprolactone circuits powered wirelessly. Cells were stained using beta-III Tubulin. Stimulated cultures could not cross the electrical barriers on either side, resulting in an increase in the aspect ratio of the network (C). A measure of the number of neuronal crossings per angular bin provided an graphical representation of the orientation profile (D). Six stimulated and seven control cultures were used across three independent trials.

Reference List

[1] A. Hart, G. Terenghi, M. Wiberg, Tissue Engineering for Peripheral Nerve Regeneration 2010.

[2] J. IJkema-Paassen, K. Jansen, A. Gramsbergen, M. F. Meek, Biomaterials 2004, 25, 1583.

[3] W. L. Cheng, C. C. K. Lin, Journal of Trauma-Injury Infection and Critical Care 2004, 56, 1241.

[4] S. Madduri, K. Feldman, T. Tervoort, M. Papaloizos, B. Gander, Journal of Controlled Release 2010, 143, 168.

[5] A. Tsuruma, M. Tanaka, S. Yamamoto, N. Fukushima, H. Yabu, M. Shimomura, Colloids and Surfaces A-Physicochemical and Engineering Aspects 2006, 284, 470.

[6] J. M. Corey, D. Y. Lin, K. B. Mycek, Q. Chen, S. Samuel, E. L. Feldman, D. C. Martin, Journal of Biomedical Materials Research Part A 2007, 83A, 636.

[7] X. Jiang, S. H. Lim, H. Q. Mao, S. Y. Chew, Experimental Neurology 2010, 223, 86.

[8] G. C. W. de Ruiter, M. J. A. Malessy, M. J. Yaszemski, A. J. Windebank, R. J. Spinner, Neurosurgical Focus 2009, 26, E5.

[9] D. Angius, H. Wang, R. J. Spinner, Y. Gutierrez-Cotto, M. J. Yaszemski, A. J. Windebank, Biomaterials 2012, 33, 8034.

[10] L. Dvali, S. Mackinnon, Clin Plast Surg 2003, 30, 203.

[11] G. Lundborg, B. Rosén, L. Dahlin, J. Holmberg, I. Ros+®n, The Journal of Hand Surgery: British & European Volume 2004, 29, 100.

[12] G. +. Lundborg, L. B. Dahlin, N. Danielsen, R. H. Gelberman, F. M. Longo, H. C. Powell, S. Varon, Experimental Neurology 1982, 76, 361.

[13] H. Millesi, in How to Improve the Results of Peripheral Nerve Surgery (Eds: H. Millesi, R. Schmidhammer), Springer Vienna 2007, 37.

[14] T. W. Hudson, S. Y. Liu, C. E. Schmidt, Tissue Engineering 2004, 10, 1346.

[15] T. W. Hudson, S. Zawko, C. Deister, S. Lundy, C. Y. Hu, K. Lee, C. E. Schmidt, Tissue Engineering 2004, 10, 1641.

[16] R. Folt+ín, K. Kl+¡ma, J. +ápa-ìkov+í, J. +áed+¢, Medical Hypotheses 2008, 71, 572.

[17] S. Y. Fu, T. Gordon, Journal of Neuroscience 1995, 15, 3876.

[18] L. Stensaas, L. Monti Bloch, R. Garcia, J. Sotelo, Experimental Neurology 1989, 103, 135.

[19] C. D. McCaig, A. M. Rajnicek, Exp Physiol 1991, 76, 473.

[20] B. Pomeranz, J. J. Campbell, Brain Research 1993, 603, 271.

[21] E. W. Kellogg, M. G. Yost, E. J. Reed, A. P. Krueger, International Journal of Biometeorology 1985, 29, 253.

[22] A. A. Al-Majed, C. M. Neumann, T. M. Brushart, T. Gordon, Journal of Neuroscience 2000, 20, 2602.

[23] T. Gordon, O. A. R. Sulaiman, A. Ladak, in International Review of Neurobiology (Eds: Stefano Geuna, Pierluigi Tos and Bruno Battiston), Academic Press 2009, 433.

[24] T. Gordon, T. M. Brushart, K. M. Chan, Neurological Research 2008, 30, 1012.

[25] M. C. Lu, C. Y. Ho, S. F. Hsu, H. C. Lee, J. H. Lin, C. H. Yao, Y. S. Chen, Neurorehabilitation and Neural Repair 2008, 22, 367.

[26] L. Wan, S. Zhang, R. Xia, W. Ding, Journal of Neuroscience Research 2010, 88, 2578.

[27] J. Huang, Z. Ye, X. Hu, L. Lu, Z. Luo, Glia 2010, 58, 622.

[28] S.M.Sze, Semiconductor Devices: Physics and Technology 2002.

[29] M. Merle, A. L. Dellon, J. N. Campbell, P. S. Chang, Microsurgery 1989, 10, 130.

[30] C. J. Bettinger, Z. Bao, Advanced Materials 2010, 22, 651-+.

[31] Y. T. Li, C. W. Peng, L. T. Chen, W. S. Lin, C. H. Chu, J. J. J. Chen, Ieee Transactions on Neural Systems and Rehabilitation Engineering 2013, 21, 121.

[32] R. L. Hart, N. Bhadra, F. W. Montague, K. L. Kilgore, P. Peckham, Ieee Transactions on Neural Systems and Rehabilitation Engineering 2011, 19, 45.

[33] C. M. Zierhofer, I. J. Hochmair-Desoyer, E. S. Hochmair, Ieee Transactions on Rehabilitation Engineering 1995, 3, 112.

[34] K. Van Schuylenbergh, R. Puers, Inductive Powering Basic Theory and Application to Biomedical Systems, Springer 2009.

[35] C. D. McCaig, Journal of Embryology and Experimental Morphology 1986, 94, 245.

[36] L. Hinkle, C. D. McCaig, K. R. Robinson, Journal of Physiology-London 1981, 314, 121-&.

[37] A. Eberstein, S. Eberstein, Medicine and Science in Sports and Exercise 1996, 28, 1463.

[38] C. R. Keese, J. Wegener, S. R. Walker, L. Giaever, Proceedings of the National Academy of Sciences of the United States of America 2004, 101, 1554.

[39] M. Zhao, B. Song, J. Pu, T. Wada, B. Reid, G. Tai, F. Wang, A. Guo, P. Walczysko, Y. Gu, T. Sasaki, A. Suzuki, J. V. Forrester, H. R. Bourne, P. N. Devreotes, C. D. McCaig, J. M. Penninger, Nature 2006, 442, 457.

[40] C. D. McCaig, B. Song, A. M. Rajnicek, Journal of Cell Science 2009, 122, 4267.

[41] D. K. Armani, C. Liu, Journal of Micromechanics and Microengineering 2000, 10, 80.

Appendix 2

Cell Patterning with a Heptagon Acoustic Tweezer – Application in Neurite Guidance

Frank Gesellchen[a], Anne L. Bernassau[b], Théophile Déjardin[a], David R.S. Cumming[b] and Mathis O. Riehle[a]

[a] Centre for Cell Engineering, College of Medical, Veterinary & Life Sciences, University of Glasgow, Glasgow, United Kingdom
[b] School of Engineering, University of Glasgow, Glasgow, United Kingdom

Introduction

Accurate control over positioning of cells is a highly desirable feature in tissue engineering applications since it allows, for example, population of substrates in a controlled fashion, rather than relying on random seeding. Current methods to achieve a differential distribution of cells mostly use passive patterning methods to change chemical, mechanical or topographic properties of surfaces, making areas differentially permissive to the adhesion of cells. However, these methods have no *ad hoc* control over the actual deposition of cells. Direct patterning methods like bioprinting offer good control over cell position, but require sophisticated instrumentation and are often cost- and time-intensive. Here, we present a novel electronically controlled method of generating dynamic cell patterns by acoustic trapping of cells at a user-determined position, with a heptagonal acoustic tweezer device. We demonstrate the capability of the device to create complex patterns of cells using the device's ability to re-position acoustic traps by using a phase shift in the acoustic wave, and by switching the configuration of active piezoelectric transducers. Furthermore, we show that by arranging Schwann cells from neonatal rats in a linear pattern we are able to create Bands of Büngner-like structures on a non-structured surface and demonstrate that these features are able to guide neurite outgrowth from neonatal rat DRG.

Spatial control of cell positions is of particular importance in the field of tissue engineering. In complex tissues, cells rely on a variety of cues from their environment, such as cell-cell contacts (homo- or heterotypic), substrate adhesion and mechanical forces or extracellular stimuli such as signalling molecules (auto- or paracrine) (1). These factors are dependent on accurate positioning of cells in their microenvironment, which remains a

major challenge for replication of a functional histoarchitecture in tissue engineering.

A variety of microscale methods for patterning cells on a substrate with μm accuracy have been developed in recent years. They are based either on the direct patterning of cells, or indirect patterning via chemical (2), topographic (3), or mechanical (4, 5) modification of surfaces to direct differential cell adhesion. Direct cell patterning has been demonstrated with inkjet or laser assisted cell printing (6, 7), as well as electrical force (dielectrophoresis (8, 9)), optical force (laser guided direct writing (10) and laser guided micropatterning (11)) and magnetic forces using iron oxide-labelled cells (12). Indirect patterning by selective surface modification is mostly done by microcontact printing (μCP) using poly-di-methyl-siloxane (PDMS) stamps fabricated from a master made using photolithography (1, 13). The PDMS stamp is then used to print self -assembling monolayers of derivatized alkanethiols, on to a solid substrate, that promote matrix protein and thus cell adhesion. Alternatively, extracellular matrix proteins can also be printed directly on a substrate to permit cell adhesion (14, 15). PDMS stamps have also been used to create microfluidic devices for cell and protein patterning (2, 16). Other approaches use dynamic substrates, i.e. "switchable surfaces", whose cell adhesiveness can be modified by light (3, 17), temperature (4, 5, 18) or voltage (6, 7, 19).

While these methods have been successfully employed to create cell patterns and co-cultures of varying complexity, they often require specialized equipment, and can be cost- and time intensive. Furthermore, many of these methods are inflexible and do not offer dynamic *ad hoc* geometric control over the pattern; in the case of PDMS stamps, for example, the pattern is limited to that of the lithographic mask used to create the stamp. To address some of these shortcomings we have recently developed a portable device based on acoustic force for spatial manipulation of cells and particles (20) (Fig. 1*A*). The use of acoustic force for immobilization of cells is well established, employing either bulk or surface acoustic waves in a resonant structure that produces a fixed standing wave pattern (10, 21-23). Cells or dense particles agglomerate at nodes with lowest acoustic pressure. The position of these pressure nodes is determined by the geometry of the device and the frequency at which piezoelectric transducers generating the standing acoustic wave are operated. Control over the position of the pressure nodes in conventional transducer-reflector devices is therefore limited. Our device overcomes this limitation by using a heptagonal geometry with transducers that generate travelling waves. The interference pattern produced at the intersection of two or more forward travelling waves creates a nodal pattern that is capable of trapping cells (11, 24) (Fig. 1*B*). Waves are

either absorbed at the vertex opposing the transducer, or scattered away from the central region of the device. Because the device operation relies on the use of travelling waves, the precise interference pattern, hence the acoustic pressure nodes, may be electronically controlled by adjusting the phase of the excitation to each transducer (12, 20). The distance between two adjacent pressure nodes is given by $d=\theta/2\sin(\lambda/2)$, where θ is the angle formed between the normals to the planes of the active transducers. In a regular heptagonal device with sides numbered 1-7, when transducers placed on two adjacent odd, or equivalently even-numbered, sides and activated at a frequency of 4 MHz (λ=375 µm in water), θ=103˚. The separation distance between nodes is therefore d = 240 µm. Using the phase shifting capabilities of the device, linear acoustic pressure nodes can then be moved linearly to any desired position in the range d (20).

Our aim in this study was to investigate patterning of multiple cell types using acoustic tweezers for application in tissue engineering. We have previously shown that acoustic tweezers are capable of trapping micron-scale particles, and cells at nodes of minimal acoustic pressure (24). Here, we demonstrate complex multistep cell patterning using phase shifting and varying transducer configurations to arrange cells in six different successive patterns. Furthermore, we show the usefulness of the device for tissue engineering, by patterning Schwann cells into linear arrangements resembling Bands of Büngner, that guide neurite outgrowth from rat DRG (DRG), as an *in vitro* model for nerve regeneration.

Results

Initial experiments to demonstrate the feasibility of the approach were conducted using fluorescently labelled C2C12 cells (ATCC CRL 1772). Three sets of C2C12 stained with different fluorescent dyes (MitoTracker Green, MitoTracker Red and Hoechst 33342) were used in order to visualize successive patterning events. Once we had demonstrated to our satisfaction that acoustic tweezing could be used to manipulate multiple batches of cells in successive cycles of patterning, we then went to demonstrate that manipulated cells could be used to in turn align neurite outgrowth in a peripheral nerve injury model.

Acoustic trapping. It was first necessary to show that lines of cells could be formed using the acoustic tweezer, and that they would adhere and begin to culture on a planar surface as determined by the user. The surface was a 13 mm PLL-coated glass coverslip inserted into the centre of the acoustic tweezer device. The cell alignment is illustrated in Fig. 1C where C2C12 that

were stained with MitoTracker (MT) red were patterned using transducer pair 2-4.

Patterning with transducer switching only. Complex cell patterns can be generated by operating different sets of transducers in succession. C2C12 cells stained with CellTracker (CT) Orange dye were initially patterned on a PLL-coated coverslip in parallel lines using transducers 2 and 4 as in the previous experiment (Fig. 1*C*). After cells had adhered to the substrate for 30 min, the active transducers were switched from a 2-4 to a 4-6 configuration. The pattern of acoustic pressure nodes was rotated by $2 \times 360^\circ/7 = 102.9^\circ$ by this action. Fig. 1*D* shows the result of a patterning experiment after addition of a second aliquot of CT Orange stained C2C12 cells to the initially patterned lines and left for at least a further 30 mins, up to 60 mins. Consequently, the combination of the two successive additions of cells formed a lattice pattern at the centre of the device. Measurement of the obtuse angle formed by the patterned cells with ImageJ confirmed that the lines intersected at $102\pm4^\circ$ (n=10). We conclude that switching the transducer configuration could be used to create lattice patterns at angles defined in accordance with the geometry of the heptagon.

Patterning with phase shift only. Next, we explored the capability of the device to dynamically create complex cell patterns using phase shifts to re-position acoustic pressure nodes. As before, C2C12 cells stained with MT Red were patterned in lines on a PLL-coated coverslip using a 2-4 transducer configuration. After a period of 45 mins the cells had adhered to the substrate and the phase of the acoustic wave emanating from transducer 2 was shifted by 120° (for a schematic depiction see Fig. 2*A*). This change in phase resulted in a shift of acoustic pressure nodes by 80 µm at the centre of the device (60 µm per 90° shift, i.e. 80 µm for 120° shift). Adherent cells were not moved by this shift of the position of the pressure nodes of the acoustic pattern. A fresh batch of cells, this time labelled with MitoTracker Green dye, was added to the device and left to adhere for 45 min, as before. Finally, another phase shift of transducer 2, again by 120° (for a total of 240°) was performed and C2C12 cells labelled with Hoechst 33342 (blue) were added to the device. Fig. 2*C* shows the final result of this patterning experiment. Cells had adhered in a pattern of parallel lines with a spacing of ~80 µm between neighbouring ones. Detailed evaluation showed the separations to be 86±6 µm between red and green, 76±10 µm between green and blue, 82±7 µm between blue and red for $n \geq 21$, The separation between cells of the same colour should ideally be 240 µm was experimentally found to be 239±8 µm, 237±8 µm and 241±7 µm for red, green and blue labelled cells, respectively, for $n \geq 15$. The error between the experimentally

obtained values and expectation is attributed to slight deviations in the geometry of the device from that of a perfectly regular heptagon.

Although 90% of cells remained attached at the point where they had initially settled some (~10%) were moved to the new position of the pressure node when the phase was shifted, as evident by the presence of green (11.4%) and red cells (9.1%) mixed with the blue cells, which had been patterned last (Fig. 2*C*).

Patterning with transducer switching and phase shift. To complete our initial patterning study, we investigated whether or not a combination of phase-shifts and transducer switching could be employed to create an even more elaborate cellular pattern. We started out by creating a striped cell pattern using MT Red, MT Green and Hoechst 33342 stained C2C12 cells and used two successive 120˚ phase shifts (+120º, +240˚) of the acoustic wave at a 2-4 transducer configuration. After patterning the three sets of labelled cells in this direction, we switched to a 4-6 active transducer setup to pattern cells in a second direction (at an ~103˚ angle to the first). This was followed again by two successive 120˚ phase shifts of the acoustic wave, in order to pattern all three labelled cell types in a parallel fashion at the new angle (see Fig. 2*B* for a schematic). In this manner, we were able to dynamically build up the complex pattern of cell tissue seen in Fig. 2*D* - a "tartan-like" arrangement of the cells, essentially a superposition of two successively derived striped patterns at an angle of 103˚ to one another.

From these experiments we concluded that a high degree of control over cell position and orientation could be achieved when culturing successive additions of cells in a culture controlled by an acoustic tweezer.

Schwann cell patterning for neurite guidance. After establishing the capability of the acoustic tweezer in cell patterning, we aimed to test its usefulness in a model system for tissue engineering, specifically in peripheral nerve regeneration. To this end we deposited Schwann cells isolated from neonatal rat sciatic nerves in a linear pattern on PLL-coated cover slips in the heptagon acoustic tweezer device, using a 1-3 transducer configuration. After overnight incubation the cells had largely retained the linear pattern and had partially arranged in a columnar fashion reminiscent of bands of Büngner (Fig. 3A + inset), formed by denervated Schwann cells during peripheral nerve regeneration. In contrast, randomly seeded Schwann cells displayed no preferential orientation after overnight incubation (Fig. 3D). Neonatal rat DRGs seeded on the patterned and randomly seeded Schwann

cells (Fig. 3B and E, respectively) both showed substantial outgrowth of neurites after 4 days in culture (Fig. 3C and F).

In order to visualize the direction of outgrowing neurites, cells were stained for bIII-tubulin, which revealed an extensive network of neurites on patterned as well as non-patterned Schwann cells (Fig. 4). Neurites growing on a patterned Schwann cell layer exhibited an orientation along a preferred axis, while those on randomly seeded Schwann cells projected networks in several directions at once (Fig. 4A and D). We used the ImageJ plug-in OrientationJ (27) to obtain a quantitative measure of neurite orientations on patterned versus randomly orientated Schwann cell layers. OrientationJ derives the local orientation and isotropic values (coherency and energy) of every pixel in an image and outputs a color-coded representation of local angles and isotropy of features. Fig. 4B and E show the output generated for the images in Fig. 4A and D respectively. For those neurites outgrowing on patterned Schwann cells (Fig. 4B) it shows a clear preference for directions around +90 and -90 degrees, which is in good accordance with the original Schwann cell pattern (Fig. 3B). The neurites on randomly seeded Schwann cells appear to show a preferential orientation as well (around 45°), which is probably due to a self-organization of the underlying Schwann cell layer. However, compared to the axon network on patterned Schwann cells, other local angles are strongly represented as well, indicating a more random pathfinding of the axon network. This becomes even more evident when comparing the local angle histograms from three separate experiments (Fig. 3C and F). The local angles of neurites growing on patterned Schwann cells display a preferred direction around the initial angle of the respective Schwann cell pattern (defined as zero degrees) compared to the random controls (where zero denotes the horizontal axis of the image), indicating that the initially patterned Schwann cells provide an efficient guidance cue for neurites outgrowing from the DRGs.

A second analysis using OrientationJ's Measure function, which determines the dominant orientation (as well as coherency and energy) of features within a user defined ROI, allowed us to include faintly stained areas, that were excluded from the measurement of pixel orientation due to the threshold being set for the whole image. Using a custom-written macro each image was divided into adjoining 250x250 pixel ROIs that were individually analyzed, if their integrated density value exceeded a user-defined threshold. In this way we were able to include even faintly stained neurites in our analysis (Fig. S1). The relative frequency distributions of local directions, obtained with this analysis are shown in Fig. 5, using 20 degree bins centered on zero degrees (Fig. 5A). Despite experimental variability, neurites growing on patterned Schwann cells show a clustering around the

zero degree orientation, with ~60% of the analyzed areas oriented within +/- 30 degrees of the initial Schwann cell pattern, and angles >50 degrees relative to the pattern clearly underrepresented. In contrast the neurite outgrowth on randomly seeded Schwann cells shows no preferred direction (Fig. 5B). A Chi-square test showed a highly significant difference between the two frequency distributions ($p<<0.001$), indicating that the initial patterning of Schwann cells by acoustic force had a significant influence on the subsequent outgrowth of neurites from explanted DRGs.

Discussion

In the present study we have shown that the acoustic tweezer is capable of trapping cells at predetermined positions and, by using the ability to switch and operate different sets of transducers, we can generate complex cellular patterns.

Compared to other methods such as laser guided direct writing (LGDW), the new device has the advantage of being small, electronically controlled, flexible in the patterning and can be easily be integrated with standard microscopy equipment. The device can handle high cell densities and consequently has a relatively good throughput, which is very beneficial for applications in tissue engineering. Additionally it allows handling of different cell types sequentially; if an initially patterned cell type is left to adhere for a sufficient amount of time (usually 30 min) these cells stay in position when the position of the acoustic traps is shifted. Another cell type can then be seeded at the newly positioned pressure nodes, as exemplified by the patterning experiments with fluorescently labelled cells. The technique is made possible because cells, once adhered to a surface, are sufficiently firmly bound that the acoustic forces exerted by the tweezing device cannot move them. Therefore, successive additions of cells can be moved and manipulated substantially independently from previous aliquots of cells. The forces exerted onto individual cells by the acoustic tweezer is in the range 2-10 pN, or 71 kPa. However, the forces needed to detach individual cells are of the order of tens, to several hundreds of nNs (28-30). Even individual integrin/fibronectin binding events have been shown to have rupture strength of around 90 pN (31), which exceeds the maximal forces applied by the acoustic tweezer by a factor of about 10-20.

While the topologies of the patterns that can be generated with the acoustic tweezer are set by the device geometry, it is possible to actively control the position of any further cell types by adjusting the position of the acoustic pressure nodes by phase shifts, or transducer switching with an

accuracy of less than 10 μm, which is smaller than a tissue cell diameter. No specific treatment of cells or surfaces is necessary as long as they are generally cell adhesive. The number of different cell types that can be patterned in this fashion is only limited by space available between the pressure nodes. Our standard 1-3 or 2-4 transducer configuration, operated at a frequency of 4 MHz, results in a spacing of ~240 μm between the nodes, taking the size of cells into account (10-30 μm diameter) this would at best, limit side-by-side patterning with successive 90° phase shifts (~60 μm spacing) to four different cell types. Space permitting, cells can then be patterned at an angle to the initial pattern as evidenced by the "cell tartan" (Fig. 2*D*). Available space being the main limitation in this case, for C2C12 cells, some cells are inevitably stacked on top of previously patterned cells. This prevented them from adhering to the substrate and they were moved out of position with the next phase shift. Nevertheless, this type of patterning illustrates the versatility of the acoustic tweezer device for complex cell patterning.

After demonstrating the versatility of the acoustic tweezer for manipulating multiple cells groups, we tested its usefulness in a model system for tissue engineering, specifically in peripheral nerve regeneration. Although peripheral nerves have good regenerative properties, the outcome is often less than optimal, highlighting the importance of supporting strategies in nerve repair (35). Schwann cells are instrumental in supporting the repair process, first by initiating clearance of axonal and myelin debris at the injury site and subsequently supporting regrowth of axons sprouting from the proximal stump (36). However, functional outcomes are often suboptimal, limited by misdirection of outgrowing neurites and a slow regeneration rate, leading to chronic denervation of Schwann cells distal to the injury site (37). This in turn causes those Schwann cells to lose their growth supporting phenotype, ultimately leading to a failure to re-innervate the target organ (38).

While autologous nerve grafts still represent the gold standards in peripheral nerve repair, tissue engineering approaches to improve the functional outcome have received increasing attention in recent years (39). Several studies utilized Schwann cells to generate a repair-permissive environment in *in vitro* or animal models of nerve repair (40-45). While these approaches used micropatterned or microstructured surfaces or polymer scaffolds our goal was to investigate whether it is possible to align Schwann cells for nerve repair without underlying guidance cues in a self-organizing, scaffold-free approach.

A simple, linear pattern of Schwann cells was chosen to assess if we can influence the direction of neurite outgrowth from explanted DRGs in this manner. Interestingly, once patterned, the Schwann cells maintained their linear orientation and formed columnar structure similar to Bands of Büngner in regenerating peripheral nerves (Fig. 3*A*), a phenomena that has also been observed previously in scaffold based Schwann cell alignment (44). Outgrowth of neurites on the layer of Schwann cells was obvious after 4 days when observed through brightfield microscopy, but directional information could not be extracted due to the background of cells and high density of neurites growing on top of them. We utilized βIII-tubulin staining to visualize the neurites and analyzed a scan of the relevant area taken with a motorized stage. Due to the high density of neurites a tracing of single neurites was not feasible. We therefore used the *ImageJ* plug-in *OrientationJ* to obtain quantitative data on directionality. Analyses on a single pixel level (Fig. 4) using the *Distribution* function of *OritentationJ* showed that the outgrowth of neurites largely followed the orientation of the initial Schwann cell pattern. While the analysis of pixel orientations provided useful information on the direction of neurite outgrowth, it also had some limitations. In order to restrict the analysis to actual features (i.e. neurites) and omit isotropic areas, the threshold for analysis parameters – coherency and energy – had to be chosen accordingly. Invariably, in some of the images this caused some of the more faintly stained neurites to be omitted from analysis as well (compare Fig.4 A+B and D+E). In addition, the fact that the distribution histogram is weighted by the coherency parameter makes it difficult to compare the results from different experiments. An additional analysis on 250x250 pixel areas (Fig.5 and Fig. S1) with OrientationJ's Measure function confirmed the majority of neurites growing on patterned Schwann cells were orientated within +/- 30˚ of the pre-patterned direction. This is in good agreement with other studies, which aligned Schwann cells using micropatterned laminin (43) or a stretched collagen matrix (46). The fact that in our experimental setup, the Schwann cells had no external guidance cues after the initial patterning by acoustic force suggests that there was a significant degree of self-organization involved. A study by Parrinello *et al.* found that after peripheral nerve injury, fibroblast are instrumental in organizing Schwann cells into cords, in a cell-sorting process mediated by Sox-2 (47). It appears that the acoustic force-mediated "sorting" was sufficient to promote a similar process of self-organization. Further studies using the phase-shift capabilities of our acoustic tweezer device could explore if including fibroblasts in the patterning process would improve the neurite guiding properties of the patterned cell layer.

Materials and Methods

Sample preparation including cell culture and staining, magnetic labelling and separation, immunofluorescence and image analysis of DRG are described in *SI Appendix*.

Acoustic tweezer operation. The design and construction of the heptagon acoustic tweezer is described in detail elsewhere (20). The transducers were driven by a 4 MHz sine wave (corresponding to a wavelength of 375 µm in water) at an amplitude of 8 Vpp, generated from an arbitrary waveform generator (TGA12104, Thurlby Thandar Instruments Ltd,). The waveform generator enabled synchronisation between channels and independent control of frequency, phase and amplitude to each transducer. Signals were amplified and electronically matched using high-speed buffers (BUF634T, Texas Instruments).

Prior to the patterning experiments, a layer of 1.5% agar in PBS was deposited inside the heptagon cell, filling the cavity up to approximately halfway (~1.2 mL) in order to reduce acoustic streaming that can occur in liquid medium (25).

Cell patterning. A 13 mm glass cover slip coated with Poly-L-Lysine (Sigma-Aldrich), to facilitate cell adhesion, was placed at the centre of the cavity and covered with 0.5 mL of DMEM. The differently labelled cells were introduced to the cavity in successive stages, with different patterns of acoustic excitation for each. For each round of patterning, 50-100 µl of cells (25 – 50,000 cells) were carefully added to the centre of the device (See *SI text* for more details).

Microscopy & Image analysis. For microscopic observation the device was placed on the stage of an upright epifluorescence microscope (Olympus BX51, Olympus; Fig 1A) equipped with a tri-pass filter cube (U-M61002, DAPI/FITC/TexasRed) and a motorized stage (H1P1BX, Prior Scientific). Micrographs were taken at 40 or 50X magnification using the *ImagePro Plus* 7.0 software package (Media Cybernetics) with a cooled CCD camera (QImaging). Tiled images of neurite outgrowth from DRGs were taken with the *StagePro* module of the *ImagePro Plus* software; the scan area was manually defined to encompass the entire area of interest and image stitching was performed automatically. Image analysis for measuring distances and angles was performed using the corresponding tools in *ImageJ* (version 1.44p; http://imagej.nih.gov/ij) (26). Qualitative and quantitative analysis of the directionality of neurite outgrowth was performed using the *ImageJ* plug-in *OrientationJ* (27) (see *SI Text* for more details). A Chi-square

test was performed to compare the frequency distributions obtained for neurite outgrowth on patterned and randomly seeded Schwann cells.

Acknowledgements

The authors would like to acknowledge support by the Engineering and Physical Sciences Research Council in the UK under the Sonotweezers program grant (grant ref.: EP/G011494/1), AB also thanks the University of Glasgow for support through a Lord Kelvin Adam Smith Fellowship in Sensor Systems, and we thank the Stephen Forrest Charitable Trust for funding TD. We also thank the staff of the James Watt Nanofabrication Centre for support in the cleanroom (http://www.jwnc.gla.ac.uk).

References

1. Lanza R, Langer R, Vacanti JP eds. (2007) *Principles of Tissue Engineering* (Academic Press, Burlington)Third Edition. Available at: http://www.sciencedirect.com/science/book/9780123706157#ancPA2.
2. Chen CS, Mrksich M, Huang S, Whitesides GM, Ingber DE (1997) Geometric control of cell life and death. *Science* 276:1425–1428.
3. Csaderova L *et al*. (2010) A biodegradable and biocompatible regular nanopattern for large-scale selective cell growth. *Small* 6:2755–2761.
4. Lo CM, Wang HB, Dembo M, Wang YL (2000) Cell movement is guided by the rigidity of the substrate. *Biophys J* 79:144–152.
5. Cortese B, Gigli G, Riehle M (2009) Mechanical Gradient Cues for Guided Cell Motility and Control of Cell Behavior on Uniform Substrates. *Adv Funct Mater* 19:2961–2968.
6. Xu T, Jin J, Gregory C, Hickman JJ, Boland T (2005) Inkjet printing of viable mammalian cells. *Biomaterials* 26:93–99.
7. Barron JA, Wu P, Ladouceur HD, Ringeisen BR (2004) Biological laser printing: a novel technique for creating heterogeneous 3-dimensional cell patterns. *Biomedical Microdevices* 6:139–147.
8. Voldman J (2006) Electrical forces for microscale cell manipulation. *Annu Rev Biomed Eng* 8:425–454.
9. Suzuki M, Yasukawa T, Shiku H, Matsue T (2008) Negative dielectrophoretic patterning with different cell types. *Biosens Bioelectron* 24:1043–1047.
10. Nahmias Y, Schwartz RE, Verfaillie CM, Odde DJ (2005) Laser-guided direct writing for three-dimensional tissue engineering. *Biotechnol Bioeng* 92:129–136.
11. Pirlo RK *et al*. (2011) Laser-guided cell micropatterning system. *Rev Sci Instrum* 82:013708.
12. Grogan SP *et al*. (2012) In situ tissue engineering using magnetically guided 3D cell patterning. *Tissue Eng Part C Methods*.
13. Singhvi R *et al*. (1994) Engineering cell shape and function. *Science* 264:696–698.

14. Guillotin B, Guillemot F (2011) Cell patterning technologies for organotypic tissue fabrication. *Trends Biotechnol* 29:183–190. Available at: http://www.sciencedirect.com/science/article/pii/S0167779910002209.
15. Tan JL, Liu W, Nelson CM, Raghavan S, Chen CS (2004) Simple approach to micropattern cells on common culture substrates by tuning substrate wettability. *Tissue Eng* 10:865–872.
16. Chiu DT *et al.* (2000) Patterned deposition of cells and proteins onto surfaces by using three-dimensional microfluidic systems. *Proc Natl Acad Sci USA* 97:2408–2413. Available at: http://www.pnas.org/cgi/doi/10.1073/pnas.040562297.
17. Nakayama Y, Furumoto A, Kidoaki S, Matsuda T (2003) Photocontrol of cell adhesion and proliferation by a photoinduced cationic polymer surface. *Photochem Photobiol* 77:480–486.
18. Yamato M, Kwon OH, Hirose M, Kikuchi A, Okano T (2001) Novel patterned cell coculture utilizing thermally responsive grafted polymer surfaces. *J Biomed Mater Res* 55:137–140.
19. Yousaf MN, Houseman BT, Mrksich M (2001) Using electroactive substrates to pattern the attachment of two different cell populations. *Proc Natl Acad Sci USA* 98:5992–5996.
20. Bernassau A *et al.* (2011) Two-dimensional manipulation of micro particles by acoustic radiation pressure in a heptagon cell. *IEEE Trans Ultrason, Ferroelect, Freq Contr* 58:2132–2138.
21. Gherardini L *et al.* (2001) A study of the spatial organisation of microbial cells in a gel matrix subjected to treatment with ultrasound standing waves. *Bioseparation* 10:153–162.
22. Garvin KA, Hocking DC, Dalecki D (2010) Controlling the spatial organization of cells and extracellular matrix proteins in engineered tissues using ultrasound standing wave fields. *Ultrasound in Medicine & Biology* 36:1919–1932.
23. Shi J *et al.* (2009) Acoustic tweezers: patterning cells and microparticles using standing surface acoustic waves (SSAW). *Lab Chip* 9:2890–2895.
24. Bernassau AL, Gesellchen F, MacPherson PGA, Riehle M, Cumming DRS (2012) Direct patterning of mammalian cells in an ultrasonic heptagon stencil. *Biomedical Microdevices* 14:559–564.
25. Bernassau AL *et al.* (2013) Controlling acoustic streaming in an ultrasonic heptagonal tweezers with application to cell manipulation. *Ultrasonics*.
26. Schneider CA, Rasband WS, Eliceiri KW (2012) NIH Image to ImageJ: 25 years of image analysis. *Nat Meth* 9:671–675.
27. Rezakhaniha R *et al.* (2012) Experimental investigation of collagen waviness and orientation in the arterial adventitia using confocal laser scanning microscopy. *Biomech Model Mechanobiol* 11:461–473.
28. Potthoff E *et al.* (2012) Rapid and serial quantification of adhesion forces of yeast and Mammalian cells. *PLoS ONE* 7:e52712.
29. Weder G *et al.* (2010) Use of force spectroscopy to investigate the adhesion of living adherent cells. *Langmuir* 26:8180–8186.
30. Lamers E *et al.* (2012) Dynamic cell adhesion and migration on nanoscale grooved substrates. *Eur Cell Mater* 23:182–93– discussion 193–4.

31. Litvinov RI, Shuman H, Bennett JS, Weisel JW (2002) Binding strength and activation state of single fibrinogen-integrin pairs on living cells. *Proc Natl Acad Sci USA* 99:7426–7431.
32. Kane RS, Takayama S, Ostuni E, Ingber DE, Whitesides GM (1999) Patterning proteins and cells using soft lithography. *Biomaterials* 20:2363–2376.
33. Bhatia S, Yarmush M, Toner M (1997) Controlling cell interactions by micropatterning in co-cultures: Hepatocytes and 3T3 fibroblasts. *J Biomed Mater Res* 34:189–199.
34. Tien J, Nelson CM, Chen CS (2002) Fabrication of aligned microstructures with a single elastomeric stamp. *Proc Natl Acad Sci USA* 99:1758–1762.
35. Khuong HT, Midha R (2013) Advances in nerve repair. *Curr Neurol Neurosci Rep* 13:322.
36. Son YJ, Thompson WJ (1995) Schwann-Cell Processes Guide Regeneration of Peripheral Axons. *Neuron* 14:125–132.
37. Hall SM (1999) The biology of chronically denervated Schwann cells. *Ann N Y Acad Sci* 883:215–233.
38. Fu SY, Gordon T (1995) Contributing factors to poor functional recovery after delayed nerve repair: prolonged denervation. *J Neurosci* 15:3886–3895.
39. Deumens R *et al*. (2010) Repairing injured peripheral nerves: Bridging the gap. *Prog Neurobiol* 92:245–276.
40. Schmalenberg KE, Uhrich KE (2005) Micropatterned polymer substrates control alignment of proliferating Schwann cells to direct neuronal regeneration. *Biomaterials* 26:1423–1430.
41. Phillips JB, Bunting SCJ, Hall SM, Brown RA (2005) Neural tissue engineering: a self-organizing collagen guidance conduit. *Tissue Eng* 11:1611–1617.
42. Miller C, Jeftinija S, Mallapragada S (2001) Micropatterned Schwann cell-seeded biodegradable polymer substrates significantly enhance neurite alignment and outgrowth. *Tissue Eng* 7:705–715.
43. Thompson DM, Buettner HM (2004) Oriented Schwann cell monolayers for directed neurite outgrowth. *Ann Biomed Eng* 32:1120–1130.
44. Bozkurt A *et al*. (2009) In vitro cell alignment obtained with a Schwann cell enriched microstructured nerve guide with longitudinal guidance channels. *Biomaterials* 30:169–179.
45. Zhang Y-G *et al*. (2013) Schwann cell-seeded scaffold with longitudinally oriented micro-channels for reconstruction of sciatic nerve in rats. *J Mater Sci Mater Med*.
46. Georgiou M *et al*. (2013) Engineered neural tissue for peripheral nerve repair. *Biomaterials* 34:7335–7343.
47. Parrinello S *et al*. (2010) EphB signaling directs peripheral nerve regeneration through Sox2-dependent Schwann cell sorting. *Cell* 143:145–155.

Figures

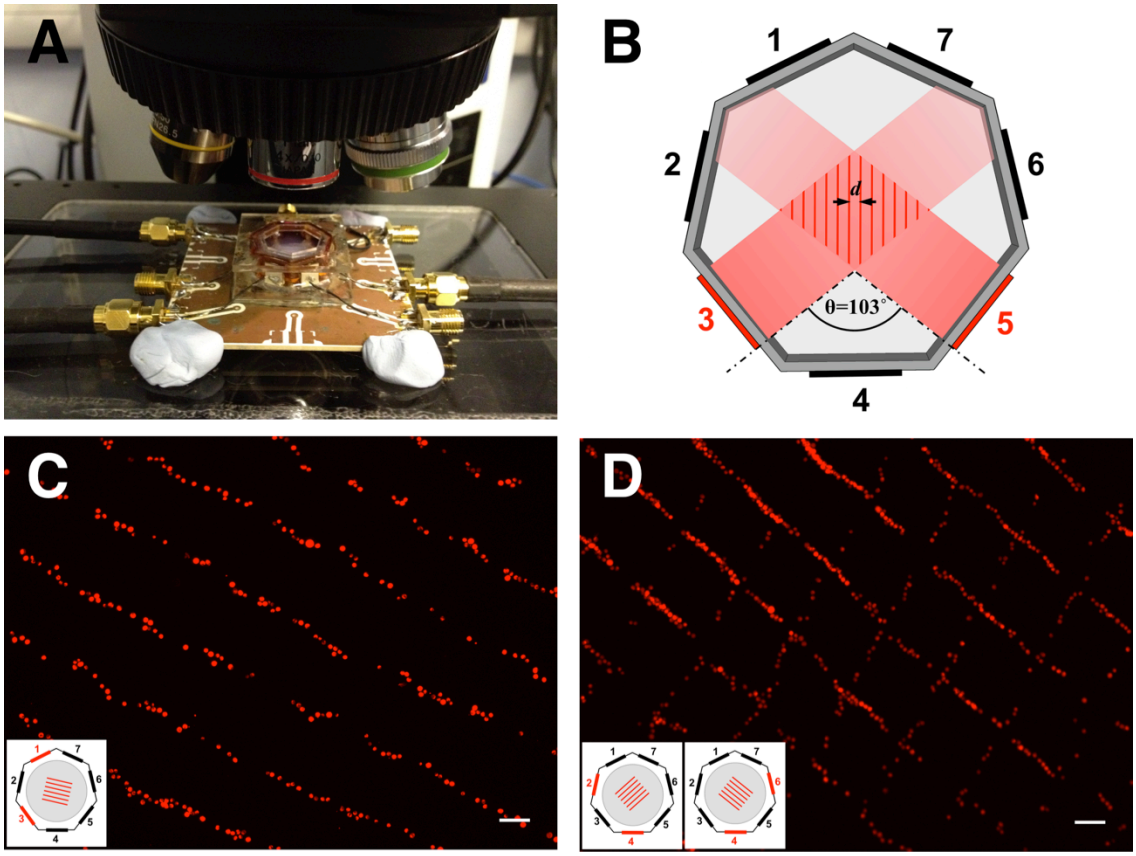

Figure 1: Device setup and simple cell patterning

Setup of the heptagon acoustic tweezer on a microscope stage (Olympus BX51). The device is connected to a wave generator on three connectors, allowing each of the connected transducers (1, 3 and 5) to be addressed individually. A 4X objective is used to observe the experiment. (B) Principle of device operation. Acoustic waves emanating from two activated non-adjacent transducers (3 and 5, highlighted in red) interfere at the center of the device, combining to form a standing wave pattern where nodes of minimal acoustic energy act as acoustic traps (schematically depicted as vertical red lines). 1-7, piezoelectric transducers, black-inactive, red – active; dashed lines, normals to the plane of active transducers; d, distance between two neighbouring acoustic traps determined by the angle θ. (C) Pattern of MitoTracker Red labelled C2C12 cells aligned in parallel using a 1-3 transducer configuration (see inset). (D) “Lattice” pattern of C2C12 cells generated by two successive patterning steps (see inset). Scale bars – 100 µm.

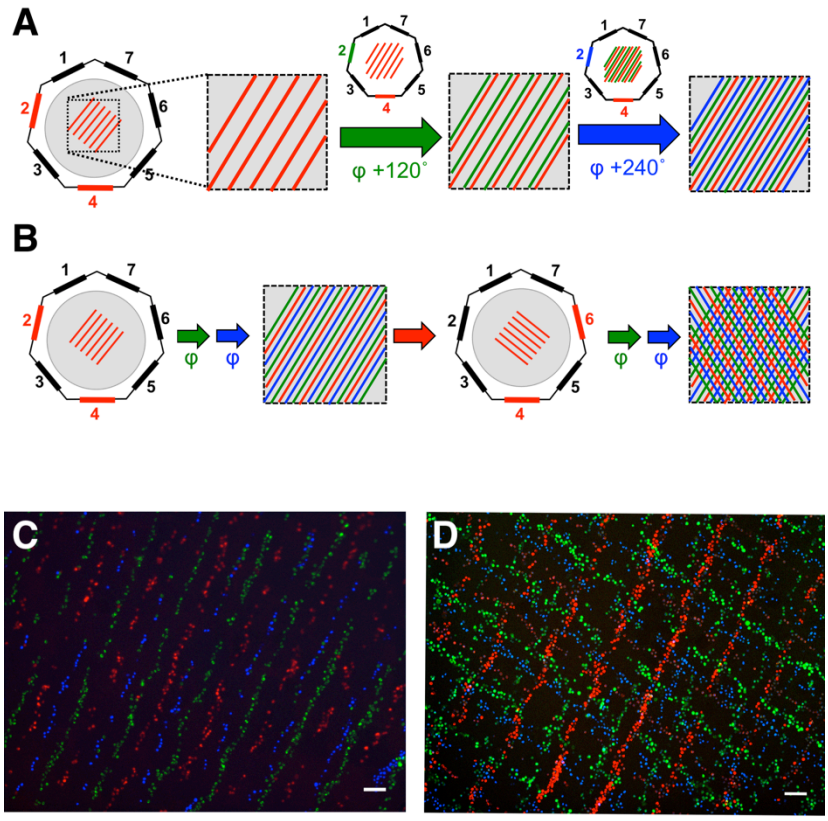

Figure 2: Complex cell patterning by phase shift and transducer switching

(A) Cartoon depicting the generation of a complex striped pattern by applying successive phase shifts of an acoustic wave at one transducer. Differently colored lines (red, green and blue) represent successive patterning events. Active transducers are highlighted, with the colour indicating the phase φ of the acoustic wave emanating from the transducer: red - 0˚, blue - 120˚, green - 240˚. (B) Schematic representation of phase shifts and transducer switches used to pattern cells in a “tartan”-like pattern. Active transducers are highlighted in red, coloured arrows indicate successive phase shifts (blue 120˚, green 240˚), red arrow indicates a transducer switch. Shown are schematic representations of the pattern obtained before the transducer switch and the final pattern. (C) Composite of fluorescent micrographs taken after patterning fluorescently labelled C2C12 cells as depicted in (A). (D) Composite of fluorescent micrographs taken after patterning fluorescently labelled C2C12 cells as depicted in (B). Cells in (C) and (D) stained with MitoTracker Red, MitoTracker Green and Hoechst 33342, Scale bar 100 µm.

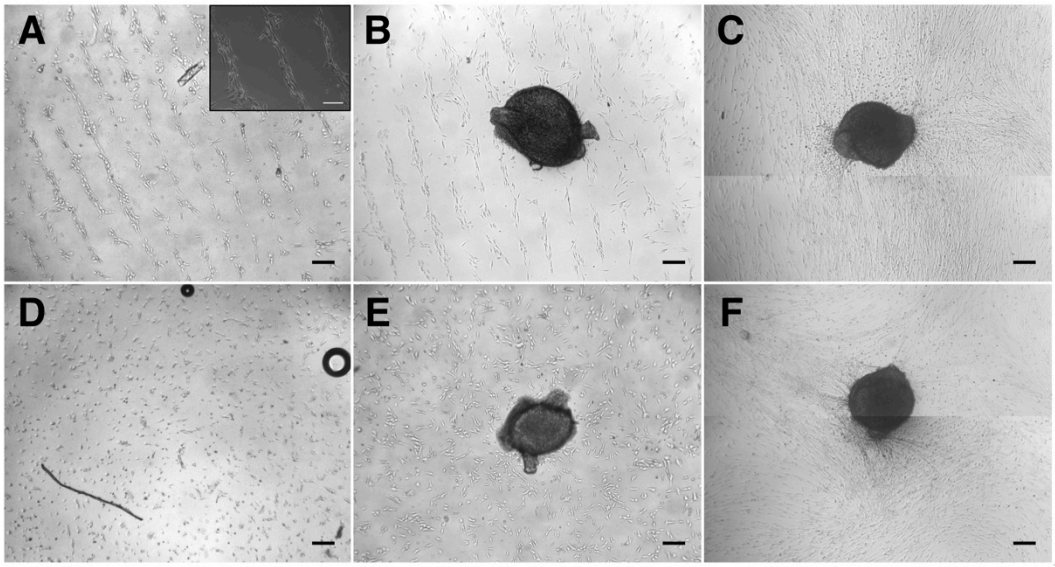

Figure 3: Seeding of DRGs on acoustically patterned Schwann cells

Schwann cells patterned in lines have formed columnar structures 18 h after seeding (A), while randomly seeded cells have not (D). Explanted neonatal rat DRGs are positioned at the center of the coverslip (D, E) and neurite outgrowth from DRGs is assessed after 4 d (C, F). Top panels – patterned Schwann cells, lower panels – randomly seeded Schwann cells. Scale bars 200 µm. Inset shows Bands of Büngner-like structures at higher magnification using a phase contrast objective, Scale bar 100 µm.

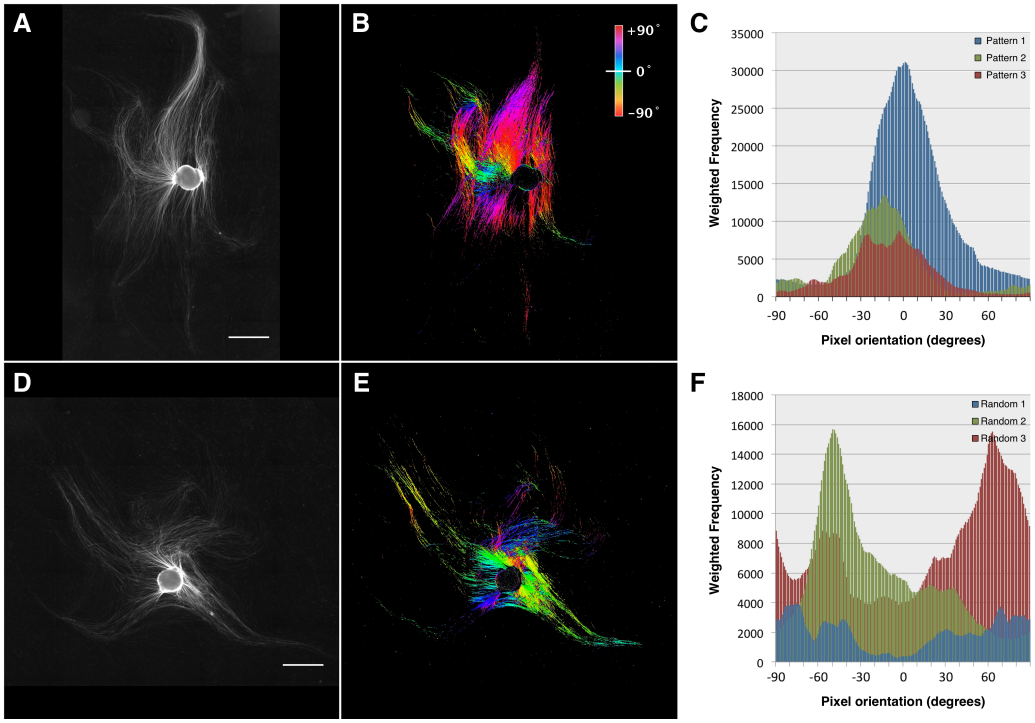

Figure 4: Analysis of neurite outgrowth on patterned and non-patterned Schwann cells

β3-tubulin stain of neurites outgrowing from DRGs on patterned (A) and randomly seeded Schwann cells (D) after 4d and false-color representation of pixel orientations computed using the ImageJ plug-in OrientationJ (B, E). Scale bars 1 mm.(C) and (F): Weighted frequencies of pixel orientations obtained with OrientationJ for three different patterned (C) and randomly seeded cover slips (F). Pixel orientation in (C) normalized to the initial angle of patterned Schwann cells.

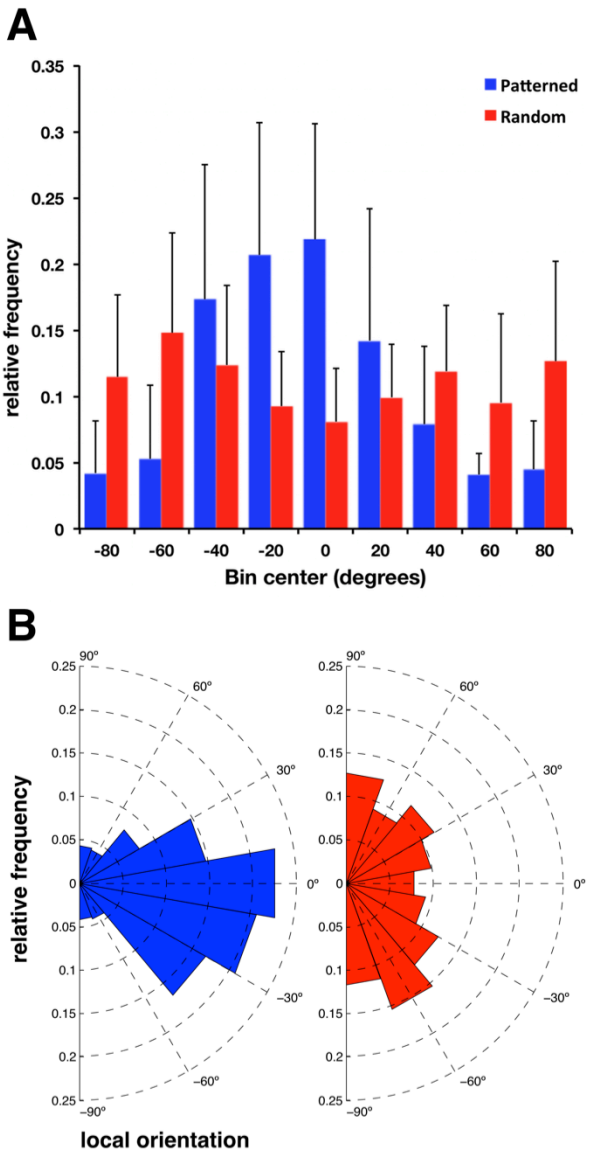

Figure 5: direction of neurite outgrowth on patterned and non-patterned Schwann cells

(A) Histogram of neurite orientations on patterned and randomly seeded Schwann cells as determined with OrientationJ's *Measure* function. Zero degrees is defined as either the initial angle of Schwann cell patterning (Patterned) or the horizontal axis (Random). Bin size is 20 degrees centred on zero, error bars represent standard deviation from n=6 different patterning events. (B) Wind rose plot of the data in (A) illustrating bias introduced to neurite outgrowth by patterning Schwann cells.

Cell culture. C2C12 cells (ATCC CRL 1772) were cultured in 75 cm^2 tissue culture vessels (Corning Life Sciences) at 37˚C, 5% CO_2 in Dulbecco's Modified Eagle Medium supplemented with 10% FBS, 2 mM Glutamine, Penicillin (10 U/mL^{-1}), Streptomycin (100 $\mu g/mL^{-1}$) and Sodium Pyruvate (all from Sigma-Aldrich).

Schwann cells were isolated from neonatal rat sciatic nerves by positive selection with an anti-p75 antibody captured on MACS microbeads (Miltenyi Biotec) according to the manufacturer's instructions. Briefly, sciatic nerve tissue was cut into ~1 mm pieces and digested overnight at 37˚C using 250 U/mL Hyaluronidase Type I-S and 160 U/mL Collagenase Type I in culture medium (DMEM/F12 with 10%FBS), followed by trituration. Cells were plated on two poly-L-ornithine/laminin coated 25 cm^2 culture flasks and cultivated for 24h at 37˚C, 5% CO_2.

Live cell staining. Cells were fluorescently labelled in three colors to aid subsequent imaging to verify the experimental results. For fluorescent labelling, cells were plated at ~40% confluency in 10 mm tissue culture dishes. The following day, prior to the patterning experiment, the medium was replaced with 10 mL of DMEM containing Mitotracker Red FM (500 ng μl^{-1}), MitoTracker Green FM (200 ng μl^{-1}, both Life Technologies) or Hoechst 33342 (5 $\mu g\ \mu l^{-1}$) for blue fluorescence. After 45 min incubation at 37˚C, 5% CO_2, medium was removed, cells washed twice with HEPES saline solution (140 mM NaCl, 5 mM KCl, 5 mM D-Glucose, 0.001% Phenol Red Na-salt, 10 mM HEPES pH 7.2; all from Sigma-Aldrich), and detached from the culture dish using a 0.25% Trypsin solution in HEPES saline containing 0.5 mM EDTA. After harvesting, cells were resuspended in 10 mL DMEM without Phenol Red to an approximate cell density of $5x10^5\ mL^{-1}$.

For some experiments, CellTracker Orange Dye (Life Technologies) was used instead of MitoTracker Red FM. In these cases cells were incubated in working solution (10 $\mu mol\ l^{-1}$ CellTracker Orange in serum-free DMEM) for 45 min before removing the dye-containing medium and replacing it with serum-containing DMEM for an additional 30 min. Cell harvest was conducted as described above.

Magnetic Labelling and Separation of Schwann cells. For magnetic labeling, cells were detached with Trypsin/EDTA, harvested by centrifugation and washed in 10 mL wash buffer (PBS + 2mM EDTA). Cells were resuspended

in 100 µl separation buffer containing 5 µl mouse anti-NGFR (p75) antibody (clone 192-IgG, Millipore) and incubated for 10 min at room temperature. After washing with 10 mL wash buffer and centrifugation, cells were resuspended in 80 ul separation buffer and 20 ul Rat anti-Mouse IgG1 MicroBeads, followed by 15 min incubation at 4˚C. Cells were washed with 10 mL wash buffer, centrifuged and resuspended in 500 µl separation buffer for magnetic separation.

For magnetic separation the cell suspension was applied to a MACS column (Miltenyi Biotec) equilibrated with 500 µl separation buffer on a magnetic separator. Unlabelled cells were washed off by three consecutive washes with 500 µl separation buffer. Bound cells were eluted by flushing 1 mL separation buffer through the column. Eluted cells were collected by centrifugation and resuspended in 1 mL Schwann cell growth medium (SCGM – DMEM/F-12 with 10% FCS, 2mM L-glutamine, 1.4 mM forskolin and 10 ng/mL GGF/neuregulin) before plating on poly-L-ornithine/laminin coated culture flasks.

Immunodepletion of fibroblasts was performed, if required, by labelling cells with anti-rat CD90 antibody (AbD Serotec) for 10 min at 37˚C before addition of rabbit complement followed by a 30 min incubation at 37˚C. Immunodepleted cultures contained < 1% fibroblasts even after several weeks of culture.

Immunofluorescence. Cells were fixed in 4% formaldehyde, permeabilized (10.3 g sucrose, 0.292 g NaCl, 0.06 g $MgCl_2$, 0.476 g HEPES 0.5 ml Triton X-100 in 100ml PBS) and blocked using 1% BSA in PBS. Neurons were immunostained with a βIII-tubulin antibody (mouse anti-TU-20, Santa Cruz Biotechnologies), followed by biotinylated anti-mouse IgG and Fluorescein-labelled streptavidin. All antibodies were diluted 1:100 in PBS/1%BSA.

Patterning of Schwann cells for DRG neurite outgrowth. Schwann cells at P0 or P1 were detached from tissue culture flasks with Trypsin/EDTA and resuspended at a concentration of $5x10^5$ cells/mL in DMEM/F12. $5x10^4$ cells were patterned in the heptagon acoustic tweezer using two active transducers as described above. After 1 h, the 13 mm coverslips with patterned cells were carefully removed from the device, transferred to a 24 well plate and 500 µl of culture medium carefully added. After 24 h incubation (37˚C, 5% CO_2, 100% humidity) freshly isolated DRGs were placed onto the patterned area at the center of the coverslip and incubation continued for 4 days in SCGM.

Schwann cells seeded randomly at the same concentration and treated identically throughout served as controls.

Image Analysis of DRG. For the color representation of neurite outgrowth tiled images of βIII-tubulin labeled neurons were analyzed with the *OrientationJ* Distribution plug-in with the following parameters: Structure tensor - Gaussian window σ 1 pixel, Cubic Spline Gradient; Min Coherency 30%, Min Energy 1%. Higher threshold settings, especially for *Min Energy* resulted in a substantial reduction of pixels included in the output. Further reduction of this parameter on the other hand caused isotropic regions of the image to be included, distorting the analysis.

For quantitative analysis we used the *OrientationJ* Measure plug-in to determine the dominant direction in 250x250 pixel Regions of Interest (ROI). An *ImageJ* macro (available upon request) was programmed to divide the image into 250x250 pixel ROIs and, using a user-defined Integrated Density value, select those ROIs for analysis that contained βIII-tubulin labeled neurites (Figure S1). Areas that contained background fluorescence only, the DRG itself and areas that were out of focus were manually excluded from the analysis, as they provided no directional information. The calculated orientations (in degrees) were statistically analyzed using Microsoft *Excel* after correcting the values for rotation during handling of the cover slips. This correction was based on the position of the DRG after immunostaining relative to the initial position at the time of DRG seeding. The angle of rotation was determined by superimposing the two corresponding images and rotating one until the DRGs in both images were aligned. The corrected values were then normalized to the original angle of the Schwann cell pattern as determined at the time of DRG seeding with the angle tool of *ImageJ*. For DRGs on randomly seeded Schwann cells the horizontal axis of the image was defined as zero degrees.

Supporting Figure1:

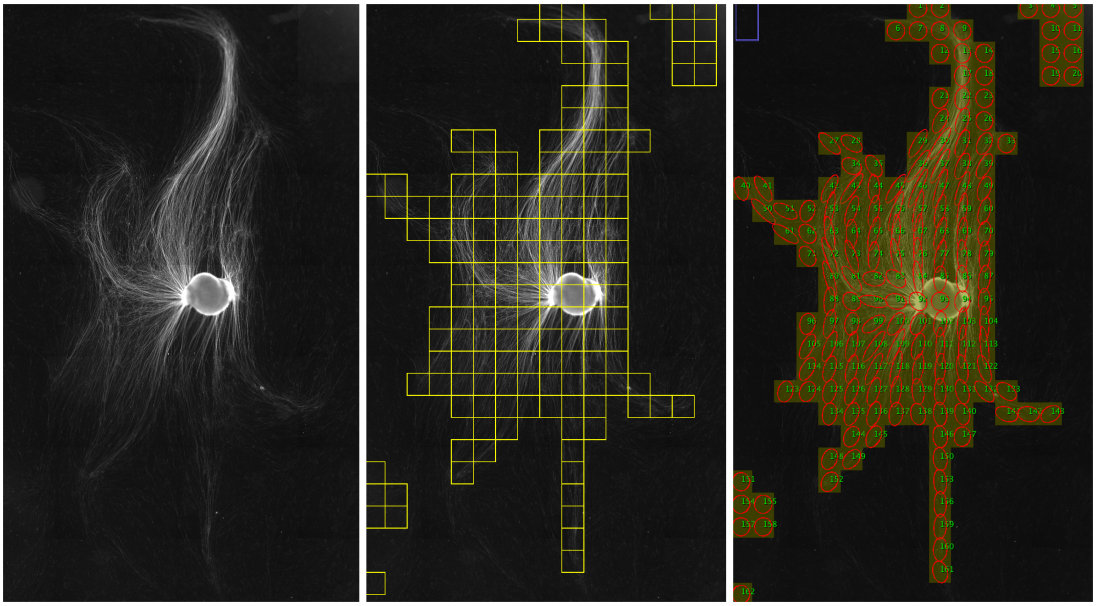

Fig S1: Quantitative analysis using OrientationJ's Measure function

The original image of the βIII-tubulin stained neurite network (left panel) was subdivided into 250x250 pixel ROIs using a custom-written macro and those ROIs that exceeded a user-defined intensity threshold were passed on for analysis using OrientationJ's *Measure* function (middle panel). The graphical output (right panel) displays the dominant direction within an ROI as an ellipse, with more slender ellipses indicating greater directional coherency.Note that ROIs which were created due to high background (lower left and upper right corner in middle and right panel) as well as those that contained mainly the DRG (at the center) were omitted from subsequent analysis.

References

ABE, N., BORSON, S. H., GAMBELLO, M. J., WANG, F. & CAVALLI, V. (2010) Mammalian target of rapamycin (mTOR) activation increases axonal growth capacity of injured peripheral nerves. *J Biol Chem,* 285**,** 28034-43.

ABIDIAN, M. R., DANESHVAR, E. D., EGELAND, B. M., KIPKE, D. R., CEDERNA, P. S. & URBANCHEK, M. G. (2012) Hybrid Conducting Polymer-Hydrogel Conduits for Axonal Growth and Neural Tissue Engineering. *Advanced Healthcare Materials,* 1**,** 762-767.

AGTHONG, S., KAEWSEMA, A., TANOMSRIDEJCHAI, N. & CHENTANEZ, V. (2006) Activation of MAPK ERK in peripheral nerve after injury. *Bmc Neuroscience,* 7.

AGTHONG, S., KOONAM, J., KAEWSEMA, A. & CHENTANEZ, V. (2009) Inhibition of MAPK ERK impairs axonal regeneration without an effect on neuronal loss after nerve injury. *Neurological Research,* 31**,** 1068-1074.

AHMED, Z., BROWN, R. A., LJUNGBERG, C., WIBERG, M. & TERENGHI, G. (1999) Nerve growth factor enhances peripheral nerve regeneration in non-human primates. *Scand J Plast Reconstr Surg Hand Surg,* 33**,** 393-401.

AHVAZ, H. H., MOBASHERI, H., BAKHSHANDEH, B., SHAKHSSALIM, N., NAJI, M., DODEL, M. & SOLEIMANI, M. (2013) Mechanical characteristics of electrospun aligned PCL/PLLA nanofibrous scaffolds conduct cell differentiation in human bladder tissue engineering. *J Nanosci Nanotechnol,* 13**,** 4736-43.

AL-MAJED, A. A., NEUMANN, C. M., BRUSHART, T. M. & GORDON, T. (2000) Brief electrical stimulation promotes the speed and accuracy of motor axonal regeneration. *J Neurosci,* 20**,** 2602-8.

ALDSKOGIUS, H. & ARVIDSSON, J. (1978) Nerve cell degeneration and death in the trigeminal ganglion of the adult rat following peripheral nerve transection. *J Neurocytol,* 7**,** 229-50.

ALEXANDER, J. K., FUSS, B. & COLELLO, R. J. (2006) Electric field-induced astrocyte alignment directs neurite outgrowth. *Neuron Glia Biol,* 2**,** 93-103.

ALLODI, I., UDINA, E. & NAVARRO, X. (2012) Specificity of peripheral nerve regeneration: Interactions at the axon level. *Progress in Neurobiology,* 98**,** 16-37.

ARTHUR-FARRAJ, P. J., LATOUCHE, M., WILTON, D. K., QUINTES, S., CHABROL, E., BANERJEE, A., WOODHOO, A., JENKINS, B., RAHMAN, M., TURMAINE, M., WICHER, G. K., MITTER, R., GREENSMITH, L., BEHRENS, A., RAIVICH, G., MIRSKY, R. & JESSEN, K. R. (2012) c-Jun Reprograms Schwann Cells of Injured Nerves to Generate a Repair Cell Essential for Regeneration. *Neuron,* 75**,** 633-647.

ATZET, S., CURTIN, S., TRINH, P., BRYANT, S. & RATNER, B. (2008) Degradable Poly(2-hydroxyethyl methacrylate)-co-polycaprolactone Hydrogels for Tissue Engineering Scaffolds. *Biomacromolecules,* 9**,** 3370-3377.

BALABAN, N. Q., SCHWARZ, U. S., RIVELINE, D., GOICHBERG, P., TZUR, G., SABANAY, I., MAHALU, D., SAFRAN, S., BERSHADSKY, A., ADDADI, L. & GEIGER, B. (2001) Force and focal adhesion assembly: a close relationship studied using elastic micropatterned substrates. *Nat Cell Biol,* 3**,** 466-72.

BALGUDE, A. P., YU, X., SZYMANSKI, A. & BELLAMKONDA, R. V. (2001) Agarose gel stiffness determines rate of DRG neurite extension in 3D cultures. *Biomaterials,* 22**,** 1077-84.

BETTINGER, C. J., BRUGGEMAN, J. P., MISRA, A., BORENSTEIN, J. T. & LANGER, R. (2009) Biocompatibility of biodegradable semiconducting melanin films for nerve tissue engineering. *Biomaterials,* 30**,** 3050-7.

BETZ, T., KOCH, D., LU, Y. B., FRANZE, K. & KAS, J. A. (2011) Growth cones as soft and weak force generators. *Proceedings of the National Academy of Sciences of the United States of America,* 108**,** 13420-13425.

BORGENS, R. B. (1988a) Stimulation of neuronal regeneration and development by steady electrical fields. *Adv Neurol,* 47**,** 547-64.

BORGENS, R. B. (1988b) Voltage gradients and ionic currents in injured and regenerating axons. *Adv Neurol,* 47**,** 51-66.

BORGENS, R. B. (2003) Restoring function to the injured human spinal cord. *Adv Anat Embryol Cell Biol,* 171**,** III-IV, 1-155.

BORGENS, R. B., BLIGHT, A. R. & MCGINNIS, M. E. (1990) Functional recovery after spinal cord hemisection in guinea pigs: the effects of applied electric fields. *J Comp Neurol,* 296**,** 634-53.

BORGENS, R. B., JAFFE, L. F. & COHEN, M. J. (1980) Large and persistent electrical currents enter the transected lamprey spinal cord. *Proc Natl Acad Sci U S A,* 77**,** 1209-13.

BORGENS, R. B., TOOMBS, J. P., BREUR, G., WIDMER, W. R., WATERS, D., HARBATH, A. M., MARCH, P. & ADAMS, L. G. (1999) An imposed oscillating electrical field improves the recovery of function in neurologically complete paraplegic dogs. *J Neurotrauma,* 16**,** 639-57.

BORSCHEL, G. H., KIA, K. F., KUZON, W. M., JR. & DENNIS, R. G. (2003) Mechanical properties of acellular peripheral nerve. *J Surg Res,* 114**,** 133-9.

BOZKURT, A., BROOK, G. A., MOELLERS, S., LASSNER, F., SELLHAUS, B., WEIS, J., WOELTJE, M., TANK, J., BECKMANN, C., FUCHS, P., DAMINK, L. O., SCHUGNER, F., HESCHEL, I. & PALLUA, N. (2007) In vitro assessment of axonal growth using dorsal root ganglia explants in a novel three-dimensional collagen matrix. *Tissue Engineering,* 13**,** 2971-2979.

BROHLIN, M., MAHAY, D., NOVIKOV, L. N., TERENGHI, G., WIBERG, M., SHAWCROSS, S. G. & NOVIKOVA, L. N. (2009) Characterisation of human mesenchymal stem cells following differentiation into Schwann cell-like cells. *Neurosci Res,* 64**,** 41-9.

BROWN, A., RICCI, M. J. & WEAVER, L. C. (2007) NGF mRNA is expressed in the dorsal root ganglia after spinal cord injury in the rat. *Experimental Neurology,* 205**,** 283-286.

BRUDER, J. M., LEE, A. P. & HOFFMAN-KIM, D. (2007) Biomimetic materials replicating Schwann cell topography enhance neuronal adhesion and neurite alignment in vitro. *J Biomater Sci Polym Ed,* 18**,** 967-82.

BRUSHART, T. M., HOFFMAN, P. N., ROYALL, R. M., MURINSON, B. B., WITZEL, C. & GORDON, T. (2002) Electrical stimulation promotes motoneuron regeneration without increasing its speed or conditioning the neuron. *J Neurosci,* 22**,** 6631-8.

BRUSHART, T. M., JARI, R., VERGE, V., ROHDE, C. & GORDON, T. (2005) Electrical stimulation restores the specificity of sensory axon regeneration. *Exp Neurol,* 194**,** 221-9.

BRYAN, D. J., HOLWAY, A. H., WANG, K. K., SILVA, A. E., TRANTOLO, D. J., WISE, D. & SUMMERHAYES, I. C. (2000) Influence of glial growth factor and

Schwann cells in a bioresorbable guidance channel on peripheral nerve regeneration. *Tissue Eng,* 6**,** 129-38.

BUNTING, S., DI SILVIO, L., DEB, S. & HALL, S. (2005) Bioresorbable glass fibres facilitate peripheral nerve regeneration. *Journal of Hand Surgery-British and European Volume,* 30B**,** 242-247.

BURGESS, P. R., ENGLISH, K. B., HORCH, K. W. & STENSAAS, L. J. (1974) Patterning in the regeneration of type I cutaneous receptors. *J Physiol,* 236**,** 57-82.

CADDICK, J., KINGHAM, P. J., GARDINER, N. J., WIBERG, M. & TERENGHI, G. (2006) Phenotypic and functional characteristics of mesenchymal stem cells differentiated along a Schwann cell lineage. *Glia,* 54**,** 840-9.

CAMPBELL, W. W. (2008) Evaluation and management of peripheral nerve injury. *Clinical Neurophysiology,* 119**,** 1951-1965.

CAO, H. Q., LIU, T. & CHEW, S. Y. (2009) The application of nanofibrous scaffolds in neural tissue engineering. *Advanced Drug Delivery Reviews,* 61**,** 1055-1064.

CAREY, D. J., ELDRIDGE, C. F., CORNBROOKS, C. J., TIMPL, R. & BUNGE, R. P. (1983) Biosynthesis of Type-Iv Collagen by Cultured Rat Schwann-Cells. *Journal of Cell Biology,* 97**,** 473-479.

CHANG, C. J. (2009a) Effects of nerve growth factor from genipin-crosslinked gelatin in polycaprolactone conduit on peripheral nerve regeneration--in vitro and in vivo. *J Biomed Mater Res A,* 91**,** 586-96.

CHANG, C. J. (2009b) The Effect of Pulse-Released Nerve Growth Factor from Genipin-Crosslinked Gelatin in Schwann Cell-Seeded Polycaprolactone Conduits on Large-Gap Peripheral Nerve Regeneration. *Tissue Engineering Part A,* 15**,** 547-557.

CHAO, P. L., FAN, S. F., CHOU, Y. H. & LIN, A. M. (2007) N-acetylcysteine attenuates arsenite-induced oxidative injury in dorsal root ganglion explants. *Ann N Y Acad Sci,* 1122**,** 276-88.

CHENG, W. L. & LIN, C. C. (2004) The effects of different electrical stimulation protocols on nerve regeneration through silicone conduits. *J Trauma,* 56**,** 1241-6.

CHIONO, V., VOZZI, G., VOZZI, F., SALVADORI, C., DINI, F., CARLUCCI, F., ARISPICI, M., BURCHIELLI, S., DI SCIPIO, F., GEUNA, S., FORNARO, M., TOS, P., NICOLINO, S., AUDISIO, C., PERROTEAU, I., CHIARAVALLOTI, A., DOMENICI, C., GIUSTI, P. & CIARDELLI, G. (2009) Melt-extruded guides for peripheral nerve regeneration. Part I: Poly(epsilon-caprolactone). *Biomed Microdevices*.

CHO, M. R., MARLER, J. P., THATTE, H. S. & GOLAN, D. E. (2002) Control of calcium entry in human fibroblasts by frequency-dependent electrical stimulation. *Front Biosci,* 7**,** a1-8.

CHRISTIE, K. J., WEBBER, C. A., MARTINEZ, J. A. & ZOCHODNE, D. W. (2009) Manipulation of the Pi3-K Pathway in Peripheral Neurons through Pten Inhibition Enhances Axon Outgrowth. *Journal of the Peripheral Nervous System,* 14**,** 33-33.

CIRILLO, V., CLEMENTS, B. A., GUARINO, V., KOHN, J. & AMBROSIO, L. (2012) Design of PCL and PCL/gelatin electrospun conduits for in vivo evaluation in rat sciatic nerve model. *Journal of Tissue Engineering and Regenerative Medicine,* 6**,** 81-81.

COHEN, S., LEVI-MONTALCINI, R. & HAMBURGER, V. (1954) A Nerve Growth-Stimulating Factor Isolated from Sarcom as 37 and 180. *Proc Natl Acad Sci U S A,* 40**,** 1014-8.

COREY, J. M., LIN, D. Y., MYCEK, K. B., CHEN, Q., SAMUEL, S., FELDMAN, E. L. & MARTIN, D. C. (2007) Aligned electrospun nanofibers specify the direction of dorsal root ganglia neurite growth. *J Biomed Mater Res A,* 83**,** 636-45.

COSTIGAN, M., BEFORT, K., KARCHEWSKI, L., GRIFFIN, R. S., D'URSO, D., ALLCHORNE, A., SITARSKI, J., MANNION, J. W., PRATT, R. E. & WOOLF, C. J. (2002) Replicate high-density rat genome oligonucleotide microarrays reveal hundreds of regulated genes in the dorsal root ganglion after peripheral nerve injury. *BMC Neurosci,* 3**,** 16.

CROISIER, F., DUWEZ, A. S., JEROME, C., LEONARD, A. F., VAN DER WERF, K. O., DIJKSTRA, P. J. & BENNINK, M. L. (2012) Mechanical testing of electrospun PCL fibers. *Acta Biomater,* 8**,** 218-24.

CURTIS, R. (1993) Growth-Associated Protein-43 (Gap-43) Is Expressed by Glial-Cells of the Central and Peripheral Nervous-System. *Annals of the New York Academy of Sciences,* 679**,** 407-411.

DALBY, M. J., GADEGAARD, N., TARE, R., ANDAR, A., RIEHLE, M. O., HERZYK, P., WILKINSON, C. D. & OREFFO, R. O. (2007) The control of human mesenchymal cell differentiation using nanoscale symmetry and disorder. *Nat Mater,* 6**,** 997-1003.

DALBY, M. J., RIEHLE, M. O., JOHNSTONE, H., AFFROSSMAN, S. & CURTIS, A. S. G. (2004) Investigating the limits of filopodial sensing: a brief report using SEM to image the interaction between 10 nm high nano-topography and fibroblast filopodia. *Cell Biol Internat,* 28**,** 229-236.

DALY, W., YAO, L., ZEUGOLIS, D., WINDEBANK, A. & PANDIT, A. (2012) A biomaterials approach to peripheral nerve regeneration: bridging the peripheral nerve gap and enhancing functional recovery. *Journal of the Royal Society Interface,* 9**,** 202-221.

DAS, D., ZHANG, Z., WINKLER, T., MOUR, M., GUNTER, C. I., MORLOCK, M. M., MACHENS, H. G. & SCHILLING, A. F. (2011) Bioresorption and Degradation of Biomaterials. *Adv Biochem Eng Biotechnol*.

DE RUITER, G. C., MALESSY, M. J., YASZEMSKI, M. J., WINDEBANK, A. J. & SPINNER, R. J. (2009) Designing ideal conduits for peripheral nerve repair. *Neurosurg Focus,* 26**,** E5.

DE RUITER, G. C. W., MALESSY, M. J. A., ALAID, A. O., SPINNER, R. J., ENGELSTAD, J. K., SORENSON, E. J., KAUFMAN, K. R., DYCK, P. J. & WINDEBANK, A. J. (2008) Misdirection of regenerating motor axons after nerve injury and repair in the rat sciatic nerve model. *Experimental Neurology,* 211**,** 339-350.

DELCROIX, J. D., VALLETTA, J. S., WU, C. B., HUNT, S. J., KOWAL, A. S. & MOBLEY, W. C. (2003) NGF signaling in sensory neurons: Evidence that early endosomes carry NGF retrograde signals. *Neuron,* 39**,** 69-84.

DENDUNNEN, W. F. A., SCHAKENRAAD, J. M., ZONDERVAN, G. J., PENNINGS, A. J., VANDERLEI, B. & ROBINSON, P. H. (1993) A New Plla Pcl Copolymer for Nerve Regeneration. *Journal of Materials Science-Materials in Medicine,* 4**,** 521-525.

DEUMENS, R., KOOPMANS, G. C., HONIG, W. M. M., HAMERS, F. P. T., MAQUET, V., JEROME, R., STEINBUSCH, H. W. M. & JOOSTEN, E. A. J. (2006)

Olfactory ensheathing cells, olfactory nerve fibroblasts and biomatrices to promote long-distance axon regrowth and functional recovery in the dorsally hemisected adult rat spinal cord. *Experimental Neurology,* 200**,** 89-103.

DI SUMMA, P. G., KINGHAM, P. J., RAFFOUL, W., WIBERG, M., TERENGHI, G. & KALBERMATTEN, D. F. (2009) Adipose-derived stem cells enhance peripheral nerve regeneration. *J Plast Reconstr Aesthet Surg.*

DIBIRDIK, I., KRISTUPAITIS, D., KUROSAKI, T., TUEL-AHLGREN, L., CHU, A., POND, D., TUONG, D., LUBEN, R. & UCKUN, F. M. (1998) Stimulation of Src family protein-tyrosine kinases as a proximal and mandatory step for SYK kinase-dependent phospholipase Cgamma2 activation in lymphoma B cells exposed to low energy electromagnetic fields. *J Biol Chem,* 273**,** 4035-9.

DISCHER, D. E., JANMEY, P. & WANG, Y. L. (2005) Tissue cells feel and respond to the stiffness of their substrate. *Science,* 310**,** 1139-43.

DODLA, M. C. & BELLAMKONDA, R. V. (2008) Differences between the effect of anisotropic and isotropic laminin and nerve growth factor presenting scaffolds on nerve regeneration across long peripheral nerve gaps. *Biomaterials,* 29**,** 33-46.

DONNERER, J., LIEBMANN, I. & SCHICHO, R. (2005) ERK and STAT3 phosphorylation in sensory neurons during capsaicin-induced impairment and nerve growth factor treatment. *Pharmacology,* 75**,** 116-121.

DONOGHUE, P. S., LAMOND, R., BOOMKAMP, S. D., SUN, T., GADEGAARD, N., RIEHLE, M. O. & BARNETT, S. C. (2013) The development of a epsilon-polycaprolactone scaffold for central nervous system repair. *Tissue Eng Part A,* 19**,** 497-507.

EBEL, H., BALOGH, A., VOLZ, M. & KLUG, N. (2000) Augmentative treatment of chronic deafferentation pain syndromes after peripheral nerve lesions. *Minimally Invasive Neurosurgery,* 43**,** 44-50.

EKSTROM, P. A., MAYER, U., PANJWANI, A., POUNTNEY, D., PIZZEY, J. & TONGE, D. A. (2003) Involvement of alpha7beta1 integrin in the conditioning-lesion effect on sensory axon regeneration. *Mol Cell Neurosci,* 22**,** 383-95.

ENGLER, A. J., SEN, S., SWEENEY, H. L. & DISCHER, D. E. (2006) Matrix elasticity directs stem cell lineage specification. *Cell,* 126**,** 677-89.

ERIKSSON, N. P., ALDSKOGIUS, H., GRANT, G., LINDSAY, R. M. & RIVEROMELIAN, C. (1997) Effects of nerve growth factor, brain-derived neurotrophic factor and neurotrophin-3 on the laminar distribution of transganglionically transported choleragenoid in the spinal cord dorsal horn following transection of the sciatic nerve in the adult rat. *Neuroscience,* 78**,** 863-872.

FANSA, H., SCHNEIDER, W., WOLF, G. & KEILHOFF, G. (2002) Influence of insulin-like growth factor-I (IGF-I) on nerve autografts and tissue-engineered nerve grafts. *Muscle & Nerve,* 26**,** 87-93.

FAWCETT, J. R., CHEN, X., RAHMAN, Y. E. & FREY, W. H. (1999) Previously reported nerve growth factor levels are underestimated due to an incomplete release from receptors and interaction with standard curve media. *Brain Res,* 842**,** 206-10.

FAWCETT, J. W. & KEYNES, R. J. (1990) Peripheral-Nerve Regeneration. *Annual Review of Neuroscience,* 13**,** 43-60.

FENG, S. Q., KONG, X. H., GUO, S. F., WANG, P., LI, L., ZHONG, J. H. & ZHOU, X. F. (2005) Treatment of spinal cord injury with co-grafts of genetically modified Schwann cells and fetal spinal cord cell suspension in the rat. *Neurotoxicity Research,* 7**,** 169-177.

FIELDS, R. D., ESHETE, F., STEVENS, B. & ITOH, K. (1997) Action potential-dependent regulation of gene expression: temporal specificity in ca2+, cAMP-responsive element binding proteins, and mitogen-activated protein kinase signaling. *J Neurosci,* 17**,** 7252-66.

FODOR, W., RADTKE, C., BROKAW, J., YUKINORI, A., LANKFORD, K., VELARDO, J., REIER, P., ANDERSON, D. & KOCSIS, J. (2002) Xenotransplantation of transgenic pig olfactory ensheathing cells promotes remyelination and axonal regeneration in lesioned rodent and primate spinal cords. *Experimental Neurology,* 175**,** 426-426.

FOLEY, J. D., GRUNWALD, E. W., NEALEY, P. F. & MURPHY, C. J. (2005) Cooperative modulation of neuritogenesis by PC12 cells by topography and nerve growth factor. *Biomaterials,* 26**,** 3639-44.

FRANKLIN, R. J. M. & BARNETT, S. C. (2000) Olfactory ensheathing cells and CNS regeneration: The sweet smell of success? *Neuron,* 28**,** 15-18.

FU, K. Y., DAI, L. G., CHIU, I. M., CHEN, J. R. & HSU, S. H. (2011) Sciatic nerve regeneration by microporous nerve conduits seeded with glial cell line-derived neurotrophic factor or brain-derived neurotrophic factor gene transfected neural stem cells. *Artif Organs,* 35**,** 363-72.

FU, S. Y. & GORDON, T. (1995) Contributing Factors to Poor Functional Recovery after Delayed Nerve Repair - Prolonged Denervation. *Journal of Neuroscience,* 15**,** 3886-3895.

FU, S. Y. & GORDON, T. (1997) The cellular and molecular basis of peripheral nerve regeneration. *Mol Neurobiol,* 14**,** 67-116.

FUJITANI, M., KAWAI, H., PROIA, R. L., KASHIWAGI, A., YASUDA, H. & YAMASHITA, T. (2005) Binding of soluble myelin-associated glycoprotein to specific gangliosides induces the association of p75(NTR) to lipid rafts and signal transduction. *Journal of Neurochemistry,* 94**,** 15-21.

GAMEZ, E., GOTO, Y., NAGATA, K., IWAKI, T., SASAKI, T. & MATSUDA, T. (2004) Photofabricated gelatin-based nerve conduits: Nerve tissue regeneration potentials. *Cell Transplantation,* 13**,** 549-564.

GARCIA, J. L., ASADINEZHAD, A., PACHERNIK, J., LEHOCKY, M., JUNKAR, I., HUMPOLICEK, P., SAHA, P. & VALASEK, P. (2010) Cell Proliferation of HaCaT Keratinocytes on Collagen Films Modified by Argon Plasma Treatment. *Molecules,* 15**,** 2845-2856.

GARDINER, N. J., FERNYHOUGH, P., TOMLINSON, D. R., MAYER, U., VON DER MARK, H. & STREULI, C. H. (2005) Alpha7 integrin mediates neurite outgrowth of distinct populations of adult sensory neurons. *Mol Cell Neurosci,* 28**,** 229-40.

GARDINER, N. J., MOFFATT, S., FERNYHOUGH, P., HUMPHRIES, M. J., STREULI, C. H. & TOMLINSON, D. R. (2007) Preconditioning injury-induced neurite outgrowth of adult rat sensory neurons on fibronectin is mediated by mobilisation of axonal alpha5 integrin. *Mol Cell Neurosci,* 35**,** 249-60.

GARTNER, A., PEREIRA, T., ARMADA-DA-SILVA, P. A. S., AMORIM, I., GOMES, R., RIBEIRO, J., FRANCA, M. L., LOPES, C., PORTO, B., SOUSA, R., BOMBACI, A., RONCHI, G., FREGNAN, F., VAREJAO, A. S. P., LUIS, A. L., GEUNA, S. &

MAURICO, A. C. (2012) Use of poly(DL-lactide-epsilon-caprolactone) membranes and mesenchymal stem cells from the Wharton's jelly of the umbilical cord for promoting nerve regeneration in axonotmesis: In vitro and in vivo analysis. *Differentiation,* 84**,** 355-365.

GARTNER, A. G. & STAIGER, V. (2002) Neurotrophin secretion from hippocampal neurons evoked by long-term-potentiation-inducing electrical stimulation patterns. *Proceedings of the National Academy of Sciences of the United States of America,* 99**,** 6386-6391.

GEORGE, P. M., SAIGAL, R., LAWLOR, M. W., MOORE, M. J., LAVAN, D. A., MARINI, R. P., SELIG, M., MAKHNI, M., BURDICK, J. A., LANGER, R. & KOHANE, D. S. (2009) Three-dimensional conductive constructs for nerve regeneration. *J Biomed Mater Res A,* 91**,** 519-27.

GEORGIOU, M., BUNTING, S. C. J., DAVIES, H. A., LOUGHLIN, A. J., GOLDING, J. P. & PHILLIPS, J. B. (2013) Engineered neural tissue for peripheral nerve repair. *Biomaterials,* 34**,** 7335-7343.

GEORGIOU, M., KINGHAM, P. J., BUNTING, S. C., GOLDING, J. P., LOUGHLIN, A. J. & PHILLIPS, J. B. (2012) A nerve repair conduit containing differentiated adipose-derived stem cells within engineered neural tissue can support and guide neuronal growth in vitro and in vivo. *Journal of Tissue Engineering and Regenerative Medicine,* 6**,** 259-259.

GHISLAIN, J., DESMARQUET-TRIN-DINH, C., JAEGLE, M., MEIJER, D., CHARNAY, P. & FRAIN, M. (2002) Characterisation of cis-acting sequences reveals a biphasic, axon-dependent regulation of Krox20 during Schwann cell development. *Development,* 129**,** 155-166.

GIBBONS, A., WREFORD, N., PANKHURST, J. & BAILEY, K. (2005) Continuous supply of the neurotrophins BDNF and NT-3 improve chick motor neuron survival in vivo. *International Journal of Developmental Neuroscience,* 23**,** 389-396.

GILLEN, C., KORFHAGE, C. & MULLER, H. W. (1997) Gene expression in nerve regeneration. *Neuroscientist,* 3**,** 112-122.

GOLD, B. G. (1997) Axonal regeneration of sensory nerves is delayed by continuous intrathecal infusion of nerve growth factor. *Neuroscience,* 76**,** 1153-1158.

GORDON, T., BRUSHART, T. M. & CHAN, K. M. (2008) Augmenting nerve regeneration with electrical stimulation. *Neurol Res,* 30**,** 1012-22.

GORDON, T., SULAIMAN, O. A. & LADAK, A. (2009) Chapter 24: Electrical stimulation for improving nerve regeneration: where do we stand? *Int Rev Neurobiol,* 87**,** 433-44.

GORDONWEEKS, P. R. & MANSFIELD, S. G. (1991) Assembly of Microtubules in Growth Cones - the Role of Microtubule-Associated Proteins. *Nerve Growth Cone*, 55-64.

GRAVVANIS, A. I., TSOUTSOS, D. A., TAGARIS, G. A., PAPALOIS, A. E., PATRALEXIS, C. G., ICONOMOU, T. G., PANAYOTOU, P. N. & IOANNOVICH, J. D. (2004) Beneficial effect of nerve growth factor-7S on peripheral nerve regeneration through inside-out vein grafts: an experimental study. *Microsurgery,* 24**,** 408-15.

GREEN, R. A., LOVELL, N. H., WALLACE, G. G. & POOLE-WARREN, L. A. (2008) Conducting polymers for neural interfaces: Challenges in developing an effective long-term implant. *Biomaterials,* 29**,** 3393-3399.

GRINNELL, F. & HO, C. H. (2013) The effect of growth factor environment on fibroblast morphological response to substrate stiffness. *Biomaterials,* 34**,** 965-74.

GROTHE, C. & NIKKHAH, G. (2001) The role of basic fibroblast growth factor in peripheral nerve regeneration. *Anat Embryol (Berl),* 204**,** 171-7.

GROVES, M. J., AN, S. F., GIOMETTO, B. & SCARAVILLI, F. (1999) Inhibition of sensory neuron apoptosis and prevention of loss by NT-3 administration following axotomy. *Experimental Neurology,* 155**,** 284-294.

GU, H. Y., Z (2012) Controlled Release Strategy Based on Biodegradable Microspheres for Neurodegenerative Disease Therapy, Basic Principles of Peripheral Nerve Disorders. *InTech,* Chapter 4.

GUEROUT, N., DUCLOS, C., DROUOT, L., ABRAMOVICI, O., BON-MARDION, N., LACOUME, Y., JEAN, L., BOYER, O. & MARIE, J. P. (2011) Transplantation of Olfactory Ensheathing Cells Promotes Axonal Regeneration and Functional Recovery of Peripheral Nerve Lesion in Rats. *Muscle & Nerve,* 43**,** 543-551.

GUILAK, F., COHEN, D. M., ESTES, B. T., GIMBLE, J. M., LIEDTKE, W. & CHEN, C. S. (2009) Control of stem cell fate by physical interactions with the extracellular matrix. *Cell Stem Cell,* 5**,** 17-26.

GUIRLAND, C., SUZUKI, S., KOJIMA, M., LU, B. & ZHENG, J. Q. (2004) Lipid rafts mediate chemotropic guidance of nerve growth cones. *Neuron,* 42**,** 51-62.

HADLOCK, T., SUNDBACK, C., HUNTER, D., CHENEY, M. & VACANTI, J. P. (2000) A polymer foam conduit seeded with Schwann cells promotes guided peripheral nerve regeneration. *Tissue Eng,* 6**,** 119-27.

HAKIM, A. M. (1999) The neuron: Cell and molecular biology, 2nd edition. *Journal of Psychiatry & Neuroscience,* 24**,** 355-356.

HALL, S. (2001) Nerve repair: a neurobiologist's view. *J Hand Surg Br,* 26**,** 129-36.

HAMBURGER, V., BRUNSOBECHTOLD, J. K. & YIP, J. W. (1981) Neuronal Death in the Spinal Ganglia of the Chick-Embryo and Its Reduction by Nerve Growth-Factor. *Journal of Neuroscience,* 1**,** 60-71.

HAMMARBERG, H., PIEHL, F., CULLHEIM, S., FJELL, J., HOKFELT, T. & FRIED, K. (1996) GDNF mRNA in Schwann cells and DRG satellite cells after chronic sciatic nerve injury. *Neuroreport,* 7**,** 857-860.

HAMMARBERG, H., WALLQUIST, W., PIEHL, F., RISLING, M. & CULLHEIM, S. (2000) Regulation of laminin-associated integrin subunit mRNAs in rat spinal motoneurons during postnatal development and after axonal injury. *J Comp Neurol,* 428**,** 294-304.

HANLEY, M. R. (1992) The Neuron - Cell and Molecular-Biology - Levitan,Ib, Kaczmarek,Lk. *Nature,* 359**,** 686-686.

HANZ, S., PERLSON, E., WILLIS, D., ZHENG, J. Q., MASSARWA, R., HUERTA, J. J., KOLTZENBURG, M., KOHLER, M., VAN-MINNEN, J., TWISS, J. L. & FAINZILBER, M. (2003) Axoplasmic importins enable retrograde injury signaling in lesioned nerve. *Neuron,* 40**,** 1095-1104.

HART, A. M., TERENGHI, G., KELLERTH, J. O. & WIBERG, M. (2004) Sensory neuroprotection, mitochondrial preservation, and therapeutic potential of N-acetyl-cysteine after nerve injury. *Neuroscience,* 125**,** 91-101.

HART, A. M., TERENGHI, G. & WIBERG, M. (2008) Neuronal death after peripheral nerve injury and experimental strategies for neuroprotection. *Neurol Res,* 30**,** 999-1011.

HART, A. M., WIBERG, M. & TERENGHI, G. (2002) Pharmacological enhancement of peripheral nerve regeneration in the rat by systemic acetyl-L-carnitine treatment. *Neuroscience Letters,* 334**,** 181-185.

HART, A. M., WIBERG, M. & TERENGHI, G. (2003) Exogenous leukaemia inhibitory factor enhances nerve regeneration after late secondary repair using a bioartificial nerve conduit. *British Journal of Plastic Surgery,* 56**,** 444-450.

HART, A. T., G.; WIBERG, M (2011) Tissue Engineering: From Lab to Clinic ; Tissue Engineering for Peripheral Nerve Regeneration. *Tissue Engineering: From Lab to Clinic,* Part 2, Chapter 13 247.

HEIDEMANN, S. R., LAMOUREUX, P. & BUXBAUM, R. E. (1990) Growth Cone Behavior and Production of Traction Force. *Journal of Cell Biology,* 111**,** 1949-1957.

HEINE, W., CONANT, K., GRIFFIN, J. W. & HOKE, A. (2004) Transplanted neural stem cells promote axonal regeneration through chronically denervated peripheral nerves. *Exp Neurol,* 189**,** 231-40.

HERDEGEN, T., BASTMEYER, M., BAHR, M., STUERMER, C., BRAVO, R. & ZIMMERMANN, M. (1993) Expression of Jun, Krox, and Creb Transcription Factors in Goldfish and Rat Retinal Ganglion-Cells Following Optic-Nerve Lesion Is Related to Axonal Sprouting. *Journal of Neurobiology,* 24**,** 528-543.

HERDEGEN, T., SKENE, P. & BAHR, M. (1997) The c-Jun transcription factor - Bipotential mediator of neuronal death, survival and regeneration. *Trends in Neurosciences,* 20**,** 227-231.

HEUSCHKEL, M. O., FEJTL, M., RAGGENBASS, M., BERTRAND, D. & RENAUD, P. (2002) A three-dimensional multi-electrode array for multi-site stimulation and recording in acute brain slices. *J Neurosci Methods,* 114**,** 135-48.

HIGGINSON, J. R. & BARNETT, S. C. (2011) The culture of olfactory ensheathing cells (OECs)-a distinct glial cell type. *Experimental Neurology,* 229**,** 2-9.

HIRATA, A., MASAKI, T., MOTOYOSHI, K. & KAMAKURA, K. (2002) Intrathecal administration of nerve growth factor delays GAP 43 expression and early phase regeneration of adult rat peripheral nerve. *Brain Res,* 944**,** 146-56.

HO, P. R., COAN, G. M., CHENG, E. T., NIELL, C., TARN, D. M., ZHOU, H., SIERRA, D. & TERRIS, D. J. (1998) Repair with collagen tubules linked with brain-derived neurotrophic factor and ciliary neurotrophic factor in a rat sciatic nerve injury model. *Archives of Otolaryngology-Head & Neck Surgery,* 124**,** 761-766.

HODGKIN, A. L. & HUXLEY, A. F. (1939) Action potentials recorded from inside a nerve fibre. *Nature,* 144**,** 710-711.

HOFFMAN, P. N. & CLEVELAND, D. W. (1988) Neurofilament and Tubulin Expression Recapitulates the Developmental Program during Axonal Regeneration - Induction of a Specific Beta-Tubulin Isotype. *Proceedings of the National Academy of Sciences of the United States of America,* 85**,** 4530-4533.

HOKE, A., REDETT, R., HAMEED, H., JARI, R., ZHOU, C., LI, Z. B., GRIFFIN, J. W. & BRUSHART, T. M. (2006) Schwann cells express motor and sensory

phenotypes that regulate axon regeneration. *Journal of Neuroscience,* 26**,** 9646-9655.

HORSTKORTE, R. & FUSS, B. (2012) Chapter 9 – Cell Adhesion Molecules. *Basic Neurochemistry (Eighth Edition)*

Principles of Molecular, Cellular, and Medical Neurobiology.

HU, X., HUANG, J., YE, Z., XIA, L., LI, M., LV, B., SHEN, X. & LUO, Z. (2009) A novel scaffold with longitudinally oriented microchannels promotes peripheral nerve regeneration. *Tissue Eng Part A,* 15**,** 3297-308.

HUANG, J. H., YE, Z. X., HU, X. Y., LU, L. & LUO, Z. J. (2010) Electrical Stimulation Induces Calcium-Dependent Release of NGF From Cultured Schwann Cells. *Glia,* 58**,** 622-631.

HURTADO, A., CREGG, J. M., WANG, H. B., WENDELL, D. F., OUDEGA, M., GILBERT, R. J. & MCDONALD, J. W. (2011) Robust CNS regeneration after complete spinal cord transection using aligned poly-L-lactic acid microfibers. *Biomaterials,* 32**,** 6068-6079.

HUXLEY, A. F. & STAMPFLI, R. (1949) Evidence for Saltatory Conduction in Peripheral Myelinated Nerve Fibres. *Journal of Physiology-London,* 108**,** 315-339.

INAISHI, Y., KASHIHARA, Y., SAKAGUCHI, M., NAWA, H. & KUNO, M. (1992) Cooperative Regulation of Calcitonin Gene Related Peptide Levels in Rat Sensory Neurons Via Their Central and Peripheral Processes. *Journal of Neuroscience,* 12**,** 518-524.

ISAACSON, L. G. & CRUTCHER, K. A. (1998) Uninjured aged sympathetic neurons sprout in response to exogenous NGF in vivo. *Neurobiol Aging,* 19**,** 333-9.

ITO, T., NAKAMURA, T., SUZUKI, K., TAKAGI, T., TOBA, T., HAGIWARA, A., KIHARA, K., MIKI, T., YAMAGISHI, H. & SHIMIZU, Y. (2003) Regeneration of hypogastric nerve using a polyglycolic acid (PGA)-collagen nerve conduit filled with collagen sponge proved electrophysiologically in a canine model. *Int J Artif Organs,* 26**,** 245-51.

JANKOWSKI, M. P., MCILWRATH, S. L., JING, X. T., CORNUET, P. K., SALERNO, K. M., KOERBER, H. R. & ALBERS, K. M. (2009) Sox11 transcription factor modulates peripheral nerve regeneration in adult mice. *Brain Research,* 1256**,** 43-54.

JOHNSON, E. O., ZOUBOS, A. B. & SOUCACOS, P. N. (2005) Regeneration and repair of peripheral nerves. *Injury,* 36 Suppl 4**,** S24-9.

KALBERMATTEN, D. F., ERBA, P., MAHAY, D., WIBERG, M., PIERER, G. & TERENGHI, G. (2008) Schwann cell strip for peripheral nerve repair. *J Hand Surg Eur Vol,* 33**,** 587-94.

KALOUS, A. & KEAST, J. R. (2010) Conditioning Lesions Enhance Growth State Only in Sensory Neurons Lacking Calcitonin Gene-Related Peptide and Isolectin B4-Binding. *Neuroscience,* 166**,** 107-121.

KANJE, M., RUSOVAN, A., SISKEN, B. & LUNDBORG, G. (1993) Pretreatment of rats with pulsed electromagnetic fields enhances regeneration of the sciatic nerve. *Bioelectromagnetics,* 14**,** 353-9.

KASHIBA, H. & SENBA, E. (1999) Up- and down-regulation of BDNF mRNA in distinct subgroups of rat sensory neurons after axotomy. *Neuroreport,* 10**,** 3561-3565.

KELLEHER, M. O., AL-ABRI, R. K., LENIHAN, D. V. & GLASBY, M. A. (2006) Use of a static magnetic field to promote recovery after peripheral nerve injury. *J Neurosurg,* 105**,** 610-5.

KEMP, S. W., WALSH, S. K. & MIDHA, R. (2008) Growth factor and stem cell enhanced conduits in peripheral nerve regeneration and repair. *Neurol Res,* 30**,** 1030-8.

KEOHAN, F., WEI, X. F., WONGSARNPIGOON, A., LAZARO, E., DARGA, J. E. & GRILL, W. M. (2007) Fabrication and evaluation of conductive elastomer electrodes for neural stimulation. *J Biomater Sci Polym Ed,* 18**,** 1057-73.

KERNS, J. M., PAVKOVIC, I. M., FAKHOURI, A. J., WICKERSHAM, K. L. & FREEMAN, J. A. (1987) An experimental implant for applying a DC electrical field to peripheral nerve. *J Neurosci Methods,* 19**,** 217-23.

KIM, S. M., LEE, S. K. & LEE, J. H. (2007) Peripheral nerve regeneration using a three dimensionally cultured schwann cell conduit. *J Craniofac Surg,* 18**,** 475-88.

KINGHAM, P. J., KALBERMATTEN, D. F., MAHAY, D., ARMSTRONG, S. J., WIBERG, M. & TERENGHI, G. (2007) Adipose-derived stem cells differentiate into a Schwann cell phenotype and promote neurite outgrowth in vitro. *Exp Neurol,* 207**,** 267-74.

KINGHAM, P. J. & TERENGHI, G. (2006) Bioengineered nerve regeneration and muscle reinnervation. *J Anat,* 209**,** 511-26.

KIRSCH, M., TERHEGGEN, U. & HOFMANN, H. D. (2003) Ciliary neurotrophic factor is an early lesion-induced retrograde signal for axotomized facial motoneurons. *Molecular and Cellular Neuroscience,* 24**,** 130-138.

KITZMAN, P. H., PERRONE, T. N., LEMASTER, A. M., DAVIS, B. M. & ALBERS, K. M. (1998) Level of p75 receptor expression in sensory ganglia is modulated by NGF level in the target tissue. *J Neurobiol,* 35**,** 258-70.

KLIMASCHEWSKI, L., MEISINGER, C. & GROTHE, C. (1999) Localization and regulation of basic fibroblast growth factor (FGF-2) and FGF receptor-1 in rat superior cervical ganglion after axotomy. *Journal of Neurobiology,* 38**,** 499-506.

KOBAYASHI, N. R., BEDARD, A. M., HINCKE, M. T. & TETZLAFF, W. (1996) Increased expression of BDNF and trkB mRNA in rat facial motoneurons after axotomy. *European Journal of Neuroscience,* 8**,** 1018-1029.

KOCH, D., ROSOFF, W. J., JIANG, J., GELLER, H. M. & URBACH, J. S. (2012) Strength in the periphery: growth cone biomechanics and substrate rigidity response in peripheral and central nervous system neurons. *Biophys J,* 102**,** 452-60.

KOLIATSOS, V. E., PRICE, W. L., PARDO, C. A. & PRICE, D. L. (1994) Ventral Root Avulsion - an Experimental-Model of Death of Adult Motor-Neurons. *Journal of Comparative Neurology,* 342**,** 35-44.

KORSCHING, S. & THOENEN, H. (1983) Quantitative Demonstration of the Retrograde Axonal-Transport of Endogenous Nerve Growth-Factor. *Neurosci Lett,* 39**,** 1-4.

KOZMA, R., SARNER, S., AHMED, S. & LIM, L. (1997) Rho family GTPases and neuronal growth cone remodelling: Relationship between increased complexity induced by Cdc42Hs, Rac1, and acetylcholine and collapse induced by RhoA and lysophosphatidic acid. *Molecular and Cellular Biology,* 17**,** 1201-1211.

KRISTUPAITIS, D., DIBIRDIK, I., VASSILEV, A., MAHAJAN, S., KUROSAKI, T., CHU, A., TUEL-AHLGREN, L., TUONG, D., POND, D., LUBEN, R. & UCKUN, F. M. (1998) Electromagnetic field-induced stimulation of Bruton's tyrosine kinase. *J Biol Chem,* 273**,** 12397-401.

KUPPAN, P., SETHURAMAN, S. & KRISHNAN, U. M. (2013) PCL and PCL-gelatin nanofibers as esophageal tissue scaffolds: optimization, characterization and cell-matrix interactions. *J Biomed Nanotechnol,* 9**,** 1540-55.

LAMPE, K. J., ANTARIS, A. L. & HEILSHORN, S. C. (2013) Design of three-dimensional engineered protein hydrogels for tailored control of neurite growth. *Acta Biomater,* 9**,** 5590-9.

LANGONE, F., LORA, S., VERONESE, F. M., CALICETI, P., PARNIGOTTO, P. P., VALENTI, F. & PALMA, G. (1995) Peripheral-Nerve Repair Using a Poly(Organo)Phosphazene Tubular Prosthesis. *Biomaterials,* 16**,** 347-353.

LEAH, J. D., HERDEGEN, T. & BRAVO, R. (1991) Selective Expression of Jun Proteins Following Axotomy and Axonal-Transport Block in Peripheral-Nerves in the Rat - Evidence for a Role in the Regeneration Process. *Brain Research,* 566**,** 198-207.

LEE, S. E., SHEN, H., TAGLIALATELA, G., CHUNG, J. M. & CHUNG, K. (1998) Expression of nerve growth factor in the dorsal root ganglion after peripheral nerve injury. *Brain Res,* 796**,** 99-106.

LEE, Y. S., COLLINS, G. & ARINZEH, T. L. (2011) Neurite extension of primary neurons on electrospun piezoelectric scaffolds. *Acta Biomaterialia,* 7**,** 3877-3886.

LI, H., TERENGHI, G. & HALL, S. M. (1997) Effects of delayed re-innervation on the expression of c-erbB receptors by chronically denervated rat Schwann cells in vivo. *Glia,* 20**,** 333-47.

LI, J., CONNELL, S.;SHI, R. (2010) Biomimetic Architectures for Tissue Engineering, Biomimetics Learning From Nature. *InTech,* Chapter 24.

LI, Y., SAUVE, Y., LI, D. Q., LUND, R. D. & RAISMAN, G. (2003) Transplanted olfactory ensheathing cells promote regeneration of cut adult rat optic nerve axons. *Journal of Neuroscience,* 23**,** 7783-7788.

LI, Z., PENG, J., WANG, G., YANG, Q., YU, H., GUO, Q., WANG, A., ZHAO, B. & LU, S. (2008) Effects of local release of hepatocyte growth factor on peripheral nerve regeneration in acellular nerve grafts. *Exp Neurol.*

LIETZ, M., DREESMANN, L., HOSS, M., OBERHOFFNER, S. & SCHLOSSHAUER, B. (2006) Neuro tissue engineering of glial nerve guides and the impact of different cell types. *Biomaterials,* 27**,** 1425-1436.

LIN, Y. L., JEN, J. C., HSU, S. H. & CHIU, I. M. (2008) Sciatic nerve repair by microgrooved nerve conduits made of chitosan-gold nanocomposites. *Surgical Neurology,* 70**,** 9-18.

LINDWALL, C. & KANJE, M. (2005) Retrograde axonal transport of JNK signaling molecules influence injury induced nuclear changes in p-c-Jun and ATF3 in adult rat sensory neurons. *Molecular and Cellular Neuroscience,* 29**,** 269-282.

LIU, J. J., WANG, C. Y., WANG, J. G., RUAN, H. J. & FAN, C. Y. (2010) Peripheral nerve regeneration using composite poly(lactic acid-caprolactone)/nerve growth factor conduits prepared by coaxial electrospinning. *J Biomed Mater Res A,* 96**,** 13-20.

LOEB, G. E., MARKS, W. B. & HOFFER, J. A. (1987) Cat Hindlimb Motoneurons during Locomotion .4. Participation in Cutaneous Reflexes. *Journal of Neurophysiology,* 57**,** 563-573.

LOWERY, L. A. & VAN VACTOR, D. (2009) The trip of the tip: understanding the growth cone machinery. *Nature Reviews Molecular Cell Biology,* 10**,** 332-343.

LU, M. C., HO, C. Y., HSU, S. F., LEE, H. C., LIN, J. H., YAO, C. H. & CHEN, Y. S. (2008) Effects of electrical stimulation at different frequencies on regeneration of transected peripheral nerve. *Neurorehabil Neural Repair,* 22**,** 367-73.

LU, Y. B., FRANZE, K., SEIFERT, G., STEINHAUSER, C., KIRCHHOFF, F., WOLBURG, H., GUCK, J., JANMEY, P., WEI, E. Q., KAS, J. & REICHENBACH, A. (2006) Viscoelastic properties of individual glial cells and neurons in the CNS. *Proc Natl Acad Sci U S A,* 103**,** 17759-64.

LUIS, A. L., RODRIGUES, J. M., GEUNA, S., AMADO, S., SIMOES, M. I., FREGNAN, F., FERREIRA, A. J., VELOSO, A. P., ARMADA-DA-SILVA, P. A. S., VAREJAO, A. S. P. & MAURICIO, A. C. (2008) Neural cell transplantation effects on sciatic nerve regeneration after a standardized crush injury in the rat. *Microsurgery,* 28**,** 458-470.

LUO, L. Q. (2002) Actin cytoskeleton regulation in neuronal morphogenesis and structural plasticity. *Annual Review of Cell and Developmental Biology,* 18**,** 601-635.

MACKINNON, S. E. (1989) New Directions in Peripheral-Nerve Surgery. *Annals of Plastic Surgery,* 22**,** 257-273.

MACKINNON, S. E. & DELLON, A. L. (1990) Clinical Nerve Reconstruction with a Bioabsorbable Polyglycolic Acid Tube. *Plastic and Reconstructive Surgery,* 85**,** 419-424.

MADDURI, S., PAPALOIZOS, M. & GANDER, B. (2010) Trophically and topographically functionalized silk fibroin nerve conduits for guided peripheral nerve regeneration. *Biomaterials,* 31**,** 2323-34.

MAHAY, D., TERENGHI, G. & SHAWCROSS, S. G. (2008) Schwann cell mediated trophic effects by differentiated mesenchymal stem cells. *Exp Cell Res,* 314**,** 2692-701.

MANDOLESI, G., MADEDDU, F., BOZZI, Y., MAFFEI, L. & RATTO, G. M. (2004) Acute physiological response of mammalian central neurons to axotomy: ionic regulation and electrical activity. *Faseb Journal,* 18**,** 1934-+.

MARMIGERE, F. & ERNFORS, P. (2007) Specification and connectivity of neuronal subtypes in the sensory lineage. *Nat Rev Neurosci,* 8**,** 114-27.

MARTIN, L. J., KAISER, A. & PRICE, A. C. (1999) Motor neuron degeneration after sciatic nerve avulsion in adult rat evolves with oxidative stress and is apoptosis. *Journal of Neurobiology,* 40**,** 185-201.

MARTOCCHIA, A., SIGALA, S., PROIETTI, A., D'URSO, R., SPANO, P. F., MISSALE, C. & FALASCHI, P. (2002) Sex-related variations in serum nerve growth factor concentration in humans. *Neuropeptides,* 36**,** 391-5.

MARUDA, T. (2012) Pathophysiology of Peripheral Nerve Injury, Basic Principles of Nerves Disorders. *InTech,* Chapter 1.

MCGRATH, A. M., NOVIKOVA, L. N., NOVIKOV, L. N. & WIBERG, M. (2010) BD PuraMatrix peptide hydrogel seeded with Schwann cells for peripheral nerve regeneration. *Brain Res Bull,* 83**,** 207-13.

MEAROW, K. M. & KRIL, Y. (1995) Anti-NGF treatment blocks the upregulation of NGF receptor mRNA expression associated with collateral sprouting of rat dorsal root ganglion neurons. *Neurosci Lett,* 184**,** 55-8.

MEEK, M. F. & COERT, J. H. (2013) Recovery of two-point discrimination function after digital nerve repair in the hand using resorbable FDA- and CE-approved nerve conduits. *J Plast Reconstr Aesthet Surg,* 66**,** 1307-15.

MIDHA, R., MUNRO, C. A., DALTON, P. D., TATOR, C. H. & SHOICHET, M. S. (2003) Growth factor enhancement of peripheral nerve regeneration through a novel synthetic hydrogel tube. *J Neurosurg,* 99**,** 555-65.

MILORO, M. & MACY, J. M. (2000) Expanded polytetrafluoroethylene entubulation of the rabbit inferior alveolar nerve. *Oral Surgery Oral Medicine Oral Pathology Oral Radiology and Endodontics,* 89**,** 292-298.

MIRSKY, R., JESSEN, K. R., BRENNAN, A., PARKINSON, D., DONG, Z. P., MEIER, C., PARMANTIER, E. & LAWSON, D. (2002) Schwann cells as regulators of nerve development. *Journal of Physiology-Paris,* 96**,** 17-24.

MLIGILICHE, N. L., TABATA, Y. & IDE, C. (1999) Nerve regeneration through biodegradable gelatin conduits in mice. *East African Medical Journal,* 76**,** 400-406.

MOORE, S. W., ROCA-CUSACHS, P. & SHEETZ, M. P. (2010) Stretchy proteins on stretchy substrates: the important elements of integrin-mediated rigidity sensing. *Dev Cell,* 19**,** 194-206.

MORADZADEH, A., BORSCHEL, G. H., LUCIANO, J. P., WHITLOCK, E. L., HAYASHI, A., HUNTER, D. A. & MACKINNON, S. E. (2008) The impact of motor and sensory nerve architecture on nerve regeneration. *Exp Neurol,* 212**,** 370-6.

MUKHATYAR, V. J., SALMERON-SANCHEZ, M., RUDRA, S., MUKHOPADAYA, S., BARKER, T. H., GARCIA, A. J. & BELLAMKONDA, R. V. (2011) Role of fibronectin in topographical guidance of neurite extension on electrospun fibers. *Biomaterials,* 32**,** 3958-68.

MURASE, K., TAKEUCHI, R., FURUKAWA, S., FURUKAWA, Y. & HAYASHI, K. (1990) Highly sensitive enzyme immunoassay for beta-nerve growth factor (NGF): a tool for measurement of NGF level in rat serum. *Biochem Int,* 22**,** 807-13.

NASCIMENTO, R. S., SANTIAGO, M. F., MARQUES, S. A., ALLODI, S. & MARTINEZ, A. M. (2008) Diversity among satellite glial cells in dorsal root ganglia of the rat. *Braz J Med Biol Res,* 41**,** 1011-7.

NICOLINI, G., NOBBIO, L., MAGGIONI, D., SCHENONE, A., TREDICI, G. & CAVALETTI, G. (2011) Embryonic Rat Dorsal Root Ganglia Organotypic Culture: A Reliable Model to Test Neurotoxicology. *Journal of the Peripheral Nervous System,* 16**,** S98-S99.

NIX, W. A. & HOPF, H. C. (1983) Electrical-Stimulation of Regenerating Nerve and Its Effect on Motor Recovery. *Brain Research,* 272**,** 21-25.

OBATA, K., YAMANAKA, H., DAI, Y., TACHIBANA, T., FUKUOKA, T., TOKUNAGA, A., YOSHIKAWA, H. & NOGUCHI, K. (2003) Differential activation of extracellular signal-regulated protein kinase in primary afferent neurons regulates brain-derived neurotrophic factor expression after peripheral inflammation and nerve injury. *Journal of Neuroscience,* 23**,** 4117-4126.

OHTA, M., SUZUKI, Y., CHOU, H., ISHIKAWA, N., SUZUKI, S., TANIHARA, M., SUZUKI, Y., MIZUSHIMA, Y., DEZAWA, M. & IDE, C. (2004) Novel heparin/alginate gel combined with basic fibroblast growth factor

promotes nerve regeneration in rat sciatic nerve. *Journal of Biomedical Materials Research Part A,* 71A**,** 661-668.

OLIVEIRA, J. T., ALMEIDA, F. M., BIANCALANA, A., BAPTISTA, A. F., TOMAZ, M. A., MELO, P. A. & MARTINEZ, A. M. (2010) Mesenchymal stem cells in a polycaprolactone conduit enhance median-nerve regeneration, prevent decrease of creatine phosphokinase levels in muscle, and improve functional recovery in mice. *Neuroscience,* 170**,** 1295-303.

PANG, Q. J., LUO, Y. X., WU, Y. G., LI, Z. F., FANG, H., YUAN, T. Z., ZHANG, W. R. & CHEN, Q. W. (1993) Experimental studies on peripheral nerve regeneration enhanced by nerve growth factor. *J Tongji Med Univ,* 13**,** 34-9.

PAPADOPULOS, F., SPINELLI, M., VALENTE, S., FORONI, L., ORRICO, C., ALVIANO, F. & PASQUINELLI, G. (2007) Common tasks in microscopic and ultrastructural image analysis using ImageJ. *Ultrastruct Pathol,* 31**,** 401-7.

PARK, K. K., LIU, K., HU, Y., SMITH, P. D., WANG, C., CAI, B., XU, B. G., CONNOLLY, L., KRAMVIS, I., SAHIN, M. & HE, Z. G. (2008) Promoting Axon Regeneration in the Adult CNS by Modulation of the PTEN/mTOR Pathway. *Science,* 322**,** 963-966.

PARKER, M. A., ANDERSON, J. K., CORLISS, D. A., ABRARIA, V. E., SIDMAN, R. L., PARK, K. I., TENG, Y. D., COTANCHE, D. A. & SNYDER, E. Y. (2005) Expression profile of an operationally-defined neural stem cell clone. *Exp Neurol,* 194**,** 320-32.

PARKINSON, D. B., BHASKARAN, A., DROGGITI, A., DICKINSON, S., D'ANTONIO, M., MIRSKY, R. & JESSEN, K. R. (2004) Krox-20 inhibits Jun-NH(2)-terminal kinase/c-Jun to control Schwann cell proliferation and death. *Journal of Cell Biology,* 164**,** 385-394.

PARRINELLO, S., NAPOLI, I., RIBEIRO, S., DIGBY, P. W., FEDOROVA, M., PARKINSON, D. B., DODDRELL, R. D. S., NAKAYAMA, M., ADAMS, R. H. & LLOYD, A. C. (2010) EphB Signaling Directs Peripheral Nerve Regeneration through Sox2-Dependent Schwann Cell Sorting. *Cell,* 143**,** 145-155.

PASCUAL, J. I., GUDINO-CABRERA, G., INSAUSTI, R. & NIETO-SAMPEDRO, M. (2002) Spinal implants of olfactory ensheathing cells promote axon regeneration and bladder activity after bilateral lumbosacral dorsal rhizotomy in the adult rat. *Journal of Urology,* 167**,** 1522-1526.

PATEL, N. & POO, M. M. (1982) Orientation of Neurite Growth by Extracellular Electric-Fields. *Journal of Neuroscience,* 2**,** 483-496.

PEAN, J. M., BOURY, F., VENIER-JULIENNE, M. C., MENEI, P., PROUST, J. E. & BENOIT, J. P. (1999) Why does PEG 400 co-encapsulation improve NGF stability and release from PLGA biodegradable microspheres? *Pharmaceutical Research,* 16**,** 1294-1299.

PETERSON, S. L. & GORDON, M. J. (2004) Recurrent neuroma formation after lateral arm free flap coverage with neurorraphy to the posteroantebrachial nerve. *British Journal of Plastic Surgery,* 57**,** 585-587.

PFISTER, L. A., PAPALOIZOS, M., MERKLE, H. P. & GANDER, B. (2007) Nerve conduits and growth factor delivery in peripheral nerve repair. *Journal of the Peripheral Nervous System,* 12**,** 65-82.

PIANTINO, J., GOLDBERG, D., BURDICK, J. A., FISCHER, D., LANGER, R. & BENOWITZ, L. I. (2005) Combinatorial treatment after spinal cord injury:

Nt-3 delivery via hydrogel and inactivation of RhoA enhance spinal cord reinnervation and improve functional outcome. *Journal of Neurotrauma,* 22, 1243-1243.

PINKSTAFF, J. K., LYNCH, G. & GALL, C. M. (1998) Localization and seizure-regulation of integrin beta 1 mRNA in adult rat brain. *Brain Res Mol Brain Res,* 55, 265-76.

PLANTMAN, S., PATARROYO, M., FRIED, K., DOMOGATSKAYA, A., TRYGGVASON, K., HAMMARBERG, H. & CULLHEIM, S. (2008) Integrin-laminin interactions controlling neurite outgrowth from adult DRG neurons in vitro. *Mol Cell Neurosci,* 39, 50-62.

POCKETT, S. & GAVIN, R. M. (1985) Acceleration of Peripheral-Nerve Regeneration after Crush Injury in Rat. *Neuroscience Letters,* 59, 221-224.

RADTKE, C., AIZER, A. A., AGULIAN, S. K., LANKFORD, K. L., VOGT, P. M. & KOCSIS, J. D. (2009) Transplantation of olfactory ensheathing cells enhances peripheral nerve regeneration after microsurgical nerve repair. *Brain Research,* 1254, 10-17.

RAIVICH, G., HELLWEG, R. & KREUTZBERG, G. W. (1991) Ngf Receptor Mediated Reduction in Axonal Ngf Uptake and Retrograde Transport Following Sciatic-Nerve Injury and during Regeneration. *Neuron,* 7, 151-164.

RAJNICEK, A., BRITLAND, S. & MCCAIG, C. (1997) Contact guidance of CNS neurites on grooved quartz: influence of groove dimensions, neuronal age and cell type. *J Cell Sci,* 110 (Pt 23), 2905-13.

RAMER, L. M., AU, E., RICHTER, M. W., LIU, J., TETZLAFF, W. & ROSKAMS, A. J. (2004) Peripheral olfactory ensheathing cells reduce scar and cavity formation and promote regeneration after spinal cord injury. *Journal of Comparative Neurology,* 473, 1-15.

REYNOLDS, B. A. & WEISS, S. (1992) Generation of neurons and astrocytes from isolated cells of the adult mammalian central nervous system. *Science,* 255, 1707-10.

REZAKHANIHA, R., AGIANNIOTIS, A., SCHRAUWEN, J. T., GRIFFA, A., SAGE, D., BOUTEN, C. V., VAN DE VOSSE, F. N., UNSER, M. & STERGIOPULOS, N. (2012) Experimental investigation of collagen waviness and orientation in the arterial adventitia using confocal laser scanning microscopy. *Biomech Model Mechanobiol,* 11, 461-73.

RIBEIRO-RESENDE, V. T., KOENIG, B., NICHTERWITZ, S., OBERHOFFNER, S. & SCHLOSSHAUER, B. (2009) Strategies for inducing the formation of bands of Bungner in peripheral nerve regeneration. *Biomaterials,* 30, 5251-9.

RICH, K. M., LUSZCZYNSKI, J. R., OSBORNE, P. A. & JOHNSON, E. M. (1987) Nerve Growth-Factor Protects Adult Sensory Neurons from Cell-Death and Atrophy Caused by Nerve Injury. *Journal of Neurocytology,* 16, 261-268.

ROMAN, G. C., STRAHLENDORF, H. K., COATES, P. W. & ROWLEY, B. A. (1987) Stimulation of Sciatic-Nerve Regeneration in the Adult-Rat by Low-Intensity Electric-Current. *Experimental Neurology,* 98, 222-232.

ROSSI, F., GIANOLA, S. & CORVETTI, L. (2007) Regulation of intrinsic neuronal properties for axon growth and regeneration. *Progress in Neurobiology,* 81, 1-28.

ROSSON, G. D., WILLIAMS, E. H. & DELLON, A. L. (2009) Motor nerve regeneration across a conduit. *Microsurgery,* 29, 107-14.

RUNGE, M. B., DADSETAN, M., BALTRUSAITIS, J., KNIGHT, A. M., RUESINK, T., LAZCANO, E. A., LU, L. C., WINDEBANK, A. J. & YASZEMSKI, M. J. (2010) The development of electrically conductive polycaprolactone fumarate-polypyrrole composite materials for nerve regeneration. *Biomaterials,* 31**,** 5916-5926.

SANTOS, X., RODRIGO, J., HONTANILLA, B. & BILBAO, G. (1998) Evaluation of peripheral nerve regeneration by nerve growth factor locally administered with a novel system. *J Neurosci Methods,* 85**,** 119-27.

SCHMIDT, C. E., SHASTRI, V. R., VACANTI, J. P. & LANGER, R. (1997) Stimulation of neurite outgrowth using an electrically conducting polymer. *Proceedings of the National Academy of Sciences of the United States of America,* 94**,** 8948-8953.

SCHNELL, E., KLINKHAMMER, K., BALZER, S., BROOK, G., KLEE, D., DALTON, P. & MEY, J. (2007) Guidance of glial cell migration and axonal growth on electrospun nanofibers of poly-epsilon-caprolactone and a collagen/poly-epsilon-caprolactone blend. *Biomaterials,* 28**,** 3012-25.

SCHONAUER, F. M., S.; AVVEDIMENTO, S.; MOLEA, G (2012) Peripheral Nerve Reconstruction with Autologous Grafts, Basic Principles of Peripheral Nerve Disorders. *InTech,* Chapter 6.

SCHWAIGER, F. W., HAGER, G., SCHMITT, A. B., HORVAT, A., HAGER, G., STREIF, R., SPITZER, C., GAMAL, S., BREUER, S., BROOK, G. A., NACIMIENTO, W. & KREUTZBERG, G. W. (2000) Peripheral but not central axotomy induces changes in Janus kinases (JAK) and signal transducers and activators of transcription (STAT). *European Journal of Neuroscience,* 12**,** 1165-1176.

SEDDON, H. J. (1943) Three types of nerve injury. *Brain,* 66**,** 237-288.

SEIJFFERS, R., MILLS, C. D. & WOOLF, C. J. (2007) ATF3 increases the intrinsic growth state of DRG neurons to enhance peripheral nerve regeneration. *Journal of Neuroscience,* 27**,** 7911-7920.

SEUNARINE, K. G., N (2008) Biodegradable polymer tubes with lithographically controlled 3D micro- and nanotopography. *Microelectronic Engineering*.

SHADIACK, A. M., SUN, Y. & ZIGMOND, R. E. (2001) Nerve growth factor antiserum induces axotomy-like changes in neuropeptide expression in intact sympathetic and sensory neurons. *Journal of Neuroscience,* 21**,** 363-371.

SHADIACK, A. M. & ZIGMOND, R. E. (1998) Galanin induced in sympathetic neurons after axotomy is anterogradely transported toward regenerating nerve endings. *Neuropeptides,* 32**,** 257-264.

SHAKHBAZAU, A., SHCHARBIN, D., BRYSZEWSKA, M., KUMAR, R., WOBMA, H. M., KALLOS, M. S., GONCHAROVA, N., SEVIARYN, I., KOSMACHEVA, S., POTAPNEV, M. & MIDHA, R. (2012) Non-viral engineering of skin precursor-derived Schwann cells for enhanced NT-3 production in adherent and microcarrier culture. *Curr Med Chem,* 19**,** 5572-9.

SHAPIRO, S., BORGENS, R., PASCUZZI, R., ROOS, K., GROFF, M., PURVINES, S., RODGERS, R. B., HAGY, S. & NELSON, P. (2005) Oscillating field stimulation for complete spinal cord injury in humans: a phase 1 trial. *J Neurosurg Spine,* 2**,** 3-10.

SHEU, J. Y., KULHANEK, D. J. & ECKENSTEIN, F. P. (2000) Differential patterns of ERK and STAT3 phosphorylation after sciatic nerve transection in the rat. *Experimental Neurology,* 166**,** 392-402.

SHI, G., ROUABHIA, M., WANG, Z., DAO, L. H. & ZHANG, Z. (2004) A novel electrically conductive and biodegradable composite made of polypyrrole nanoparticles and polylactide. *Biomaterials,* 25**,** 2477-88.

SHI, G. X., ZHANG, Z. & ROUABHIA, M. (2008) The regulation of cell functions electrically using biodegradable polypyrrole-polylactide conductors. *Biomaterials,* 29**,** 3792-3798.

SIEMIONOW, M. & BRZEZICKI, G. (2009) Chapter 8: Current techniques and concepts in peripheral nerve repair. *Int Rev Neurobiol,* 87**,** 141-72.

SINGH, S., WU, B. M. & DUNN, J. C. (2011) The enhancement of VEGF-mediated angiogenesis by polycaprolactone scaffolds with surface cross-linked heparin. *Biomaterials,* 32**,** 2059-69.

SINIS, N., HAERLE, M., BECKER, S. T., SCHULTE-EVERSUM, C., VONTHEIN, R., ROSNER, H. & SCHALLER, H. E. (2007) Neuroma formation in a rat median nerve model: Influence of distal stump and muscular coating. *Plastic and Reconstructive Surgery,* 119**,** 960-966.

SISKEN, B. F., KANJE, M., LUNDBORG, G., HERBST, E. & KURTZ, W. (1989) Stimulation of rat sciatic nerve regeneration with pulsed electromagnetic fields. *Brain Res,* 485**,** 309-16.

SKENE, J. H. P. (1989) Axonal Growth-Associated Proteins. *Annual Review of Neuroscience,* 12**,** 127-156.

SMITH, M. S. & BROWNE, J. D. (1998) The effect of endothelial cell growth factor on peripheral nerve regeneration. *Otolaryngol Head Neck Surg,* 118**,** 178-82.

SOFRONIEW, M. V., HOWE, C. L. & MOBLEY, W. C. (2001) Nerve growth factor signaling, neuroprotection, and neural repair. *Annu Rev Neurosci,* 24**,** 1217-81.

SONG, B., ZHAO, M., FORRESTER, J. & MCCAIG, C. (2004) Nerve regeneration and wound healing are stimulated and directed by an endogenous electrical field in vivo. *J Cell Sci,* 117**,** 4681-90.

SORENSEN, A., ALEKSEEVA, T., KATECHIA, K., ROBERTSON, M., RIEHLE, M. O. & BARNETT, S. C. (2007) Long-term neurite orientation on astrocyte monolayers aligned by microtopography. *Biomaterials,* 28**,** 5498-508.

STANEC, S. & STANEC, Z. (1998) Ulnar nerve reconstruction with an expanded polytetrafluoroethylene conduit. *British Journal of Plastic Surgery,* 51**,** 637-639.

STETT, A., EGERT, U., GUENTHER, E., HOFMANN, F., MEYER, T., NISCH, W. & HAEMMERLE, H. (2003) Biological application of microelectrode arrays in drug discovery and basic research. *Anal Bioanal Chem,* 377**,** 486-95.

STOECKEL, K., SCHWAB, M. & THOENEN, H. (1975) Specificity of Retrograde Transport of Nerve Growth-Factor (Ngf) in Sensory Neurons - Biochemical and Morphological Study. *Brain Research,* 89**,** 1-14.

SULAIMAN, O. A. & GORDON, T. (2000) Effects of short- and long-term Schwann cell denervation on peripheral nerve regeneration, myelination, and size. *Glia,* 32**,** 234-46.

SULAIMAN, O. A. & GORDON, T. (2002) Transforming growth factor-beta and forskolin attenuate the adverse effects of long-term Schwann cell denervation on peripheral nerve regeneration in vivo. *Glia,* 37**,** 206-18.

SUN, H., MEI, L., SONG, C., CUI, X. & WANG, P. (2006) The in vivo degradation, absorption and excretion of PCL-based implant. *Biomaterials,* 27**,** 1735-40.

SUN, M. Z., MCGOWAN, M., KINGHAM, P. J., TERENGHI, G. & DOWNES, S. (2010) Novel thin-walled nerve conduit with microgrooved surface patterns for enhanced peripheral nerve repair. *Journal of Materials Science-Materials in Medicine,* 21**,** 2765-2774.

SUN, T., DONOGHUE, P. S., HIGGINSON, J. R., GADEGAARD, N., BARNETT, S. C. & RIEHLE, M. O. (2011) The interactions of astrocytes and fibroblasts with defined pore structures in static and perfusion cultures. *Biomaterials,* 32**,** 2021-31.

SUNDARARAGHAVAN, H. G., MONTEIRO, G. A., FIRESTEIN, B. L. & SHREIBER, D. I. (2009) Neurite growth in 3D collagen gels with gradients of mechanical properties. *Biotechnol Bioeng,* 102**,** 632-43.

SUNDERLAND, S. (1951) The function of nerve fibers whose structure has been disorganized. *Anat Rec,* 109**,** 503-13.

SUNDERLAND, S. (1990) The anatomy and physiology of nerve injury. *Muscle Nerve,* 13**,** 771-84.

TERENGHI, G. (1999) Peripheral nerve regeneration and neurotrophic factors. *J Anat,* 194 (Pt 1)**,** 1-14.

TERENGHI, G., CALDER, J. S., BIRCH, R. & HALL, S. M. (1998) A morphological study of Schwann cells and axonal regeneration in chronically transected human peripheral nerves. *J Hand Surg Br,* 23**,** 583-7.

TERENGHI, G., WIBERG, M. & KINGHAM, P. J. (2009) Chapter 21: Use of stem cells for improving nerve regeneration. *Int Rev Neurobiol,* 87**,** 393-403.

THOLPADY, S. S., KATZ, A. J. & OGLE, R. C. (2003) Mesenchymal stem cells from rat visceral fat exhibit multipotential differentiation in vitro. *Anatomical Record Part a-Discoveries in Molecular Cellular and Evolutionary Biology,* 272A**,** 398-402.

TOHILL, M., MANTOVANI, C., WIBERG, M. & TERENGHI, G. (2004) Rat bone marrow mesenchymal stem cells express glial markers and stimulate nerve regeneration. *Neurosci Lett,* 362**,** 200-3.

TOMASELLI, K. J. (1991) Beta 1-integrin-mediated neuronal responses to extracellular matrix proteins. *Ann N Y Acad Sci,* 633**,** 100-4.

TORVIK, A. (1976) Central Chromatolysis and Axon Reaction - Reappraisal. *Neuropathology and Applied Neurobiology,* 2**,** 423-432.

TRIGG, D. J., O'GRADY, K. M., BHATTACHARYYA, T., REINKE, M. & TORIUMI, D. M. (1998) Peripheral nerve regeneration: comparison of laminin and acidic fibroblast growth factor. *Am J Otolaryngol,* 19**,** 29-32.

VALMIKINATHAN, C. M., DEFRODA, S. & YU, X. (2009) Polycaprolactone and bovine serum albumin based nanofibers for controlled release of nerve growth factor. *Biomacromolecules,* 10**,** 1084-9.

VASCONCELOS, B. C. E. & GAY-ESCODA, C. (2000) Facial nerve repair with expanded polytetrafluoroethylene and collagen conduits: An experimental study in the rabbit. *Journal of Oral and Maxillofacial Surgery,* 58**,** 1257-1262.

VEIGA, V. F., NIMRICHTER, L., TEIXEIRA, C. A., MORALES, M. M., ALVIANO, C. S., RODRIGUES, M. L. & HOLANDINO, C. (2005) Exposure of human leukemic

cells to direct electric current: generation of toxic compounds inducing cell death by different mechanisms. *Cell Biochem Biophys,* 42**,** 61-74.

VERDU, E., NAVARRO, X., GUDINO-CABRERA, G., RODRIGUEZ, F. J., CEBALLOS, D., VALERO, A. & NIETO-SAMPEDRO, M. (1999) Olfactory bulb ensheathing cells enhance peripheral nerve regeneration. *Neuroreport,* 10**,** 1097-1101.

VILLAR, M. J., CORTES, R., THEODORSSON, E., WIESENFELDHALLIN, Z., SCHALLING, M., FAHRENKRUG, J., EMSON, P. C. & HOKFELT, T. (1989) Neuropeptide Expression in Rat Dorsal-Root Ganglion-Cells and Spinal-Cord after Peripheral-Nerve Injury with Special Reference to Galanin. *Neuroscience,* 33**,** 587-604.

VILLAR, M. J., WIESENFELDHALLIN, Z., XU, X. J., THEODORSSON, E., EMSON, P. C. & HOKFELT, T. (1991) Further-Studies on Galanin-Like, Substance-P-Like, and Cgrp-Like Immunoreactivities in Primary Sensory Neurons and Spinal-Cord - Effects of Dorsal Rhizotomies and Sciatic-Nerve Lesions. *Experimental Neurology,* 112**,** 29-39.

VOGELEZANG, M. G., LIU, Z., RELVAS, J. B., RAIVICH, G., SCHERER, S. S. & FFRENCH-CONSTANT, C. (2001) Alpha4 integrin is expressed during peripheral nerve regeneration and enhances neurite outgrowth. *J Neurosci,* 21**,** 6732-44.

VOGELIN, E., BAKER, J. M., GATES, J., DIXIT, V., CONSTANTINESCU, M. A. & JONES, N. F. (2006) Effects of local continuous release of brain derived neurotrophic factor (BDNF) on peripheral nerve regeneration in a rat model. *Experimental Neurology,* 199**,** 348-353.

WAGENAAR, D. A., PINE, J. & POTTER, S. M. (2006) Searching for plasticity in dissociated cortical cultures on multi-electrode arrays. *J Negat Results Biomed,* 5**,** 16.

WALSH, S. & MIDHA, R. (2009) Practical considerations concerning the use of stem cells for peripheral nerve repair. *Neurosurg Focus,* 26**,** E2.

WALTER, M. A., KUROUGLU, R., CAULFIELD, J. B., VASCONEZ, L. O. & THOMPSON, J. A. (1993) Enhanced peripheral nerve regeneration by acidic fibroblast growth factor. *Lymphokine Cytokine Res,* 12**,** 135-41.

WANG, J. T., MEDRESS, Z. A. & BARRES, B. A. (2012) Axon degeneration: molecular mechanisms of a self-destruction pathway. *J Cell Biol,* 196**,** 7-18.

WANG, S., CAI, Q., HOU, J., BEI, J., ZHANG, T., YANG, J. & WAN, Y. (2003) Acceleration effect of basic fibroblast growth factor on the regeneration of peripheral nerve through a 15-mm gap. *J Biomed Mater Res A,* 66**,** 522-31.

WANG, Z., ROBERGE, C., DAO, L. H., WAN, Y., SHI, G., ROUABHIA, M., GUIDOIN, R. & ZHANG, Z. (2004) In vivo evaluation of a novel electrically conductive polypyrrole/poly(D,L-lactide) composite and polypyrrole-coated poly(D,L-lactide-co-glycolide) membranes. *J Biomed Mater Res A,* 70**,** 28-38.

WERNER, A., WILLEM, M., JONES, L. L., KREUTZBERG, G. W., MAYER, U. & RAIVICH, G. (2000) Impaired axonal regeneration in alpha7 integrin-deficient mice. *J Neurosci,* 20**,** 1822-30.

WHITWAM, J. G. (1976) Classification of Peripheral-Nerve Fibers - Historical-Perspective. *Anaesthesia,* 31**,** 494-503.

WIBERG, M. & TERENGHI, G. (2003) Will it be possible to produce peripheral nerves? *Surg Technol Int,* 11**,** 303-10.

WIDMER, M. S., GUPTA, P. K., LU, L., MESZLENYI, R. K., EVANS, G. R., BRANDT, K., SAVEL, T., GURLEK, A., PATRICK, C. W., JR. & MIKOS, A. G. (1998) Manufacture of porous biodegradable polymer conduits by an extrusion process for guided tissue regeneration. *Biomaterials,* 19**,** 1945-55.

WILSON, A. D. H., HART, A., BRANNSTROM, T., WIBERG, M. & TERENGHI, G. (2003) Primary sensory neuronal rescue with systemic acetyl-L-carnitine following peripheral axotomy. A dose-response analysis. *British Journal of Plastic Surgery,* 56**,** 732-739.

WILSON, A. D. H., HART, A., BRANNSTROM, T., WIBERG, M. & TERENGHI, G. (2007) Delayed acetyl-L-carnitine administration and its effect on sensory neuronal rescue after peripheral nerve injury. *Journal of Plastic Reconstructive and Aesthetic Surgery,* 60**,** 114-118.

XU, X., YEE, W. C., HWANG, P. Y., YU, H., WAN, A. C., GAO, S., BOON, K. L., MAO, H. Q., LEONG, K. W. & WANG, S. (2003) Peripheral nerve regeneration with sustained release of poly(phosphoester) microencapsulated nerve growth factor within nerve guide conduits. *Biomaterials,* 24**,** 2405-12.

YANG, Y. C., SHEN, C. C., CHENG, H. C. & LIU, B. S. (2011) Sciatic nerve repair by reinforced nerve conduits made of gelatin-tricalcium phosphate composites. *Journal of Biomedical Materials Research Part A,* 96A**,** 288-300.

YANG, Y. M., WU, J., WANG, X. D., LIU, J., DING, F. & GU, X. S. (2009) Fabrication and Evaluation of Chitin-Based Nerve Guidance Conduits Used to Promote Peripheral Nerve Regeneration. *Advanced Engineering Materials,* 11**,** B209-B218.

YGGE, J. (1989) Neuronal Loss in Lumbar Dorsal-Root Ganglia after Proximal Compared to Distal Sciatic-Nerve Resection - a Quantitative Study in the Rat. *Brain Research,* 478**,** 193-195.

YOSHII, S., YAMAMURO, T., ITO, S. & HAYASHI, M. (1987) In vivo guidance of regenerating nerve by laminin-coated filaments. *Exp Neurol,* 96**,** 469-73.

YOSHITANI, M., FUKUDA, S., ITOI, S., MORINO, S., TAO, H., NAKADA, A., INADA, Y., ENDO, K. & NAKAMURA, T. (2007) Experimental repair of phrenic nerve using a polyglycolic acid and collagen tube. *Journal of Thoracic and Cardiovascular Surgery,* 133**,** 726-U82.

YOUNG, R. C., WIBERG, M. & TERENGHI, G. (2002) Poly-3-hydroxybutyrate (PHB): a resorbable conduit for long-gap repair in peripheral nerves. *Br J Plast Surg,* 55**,** 235-40.

ZAREEN, N. & GREENE, L. A. (2009) Protocol for culturing sympathetic neurons from rat superior cervical ganglia (SCG). *J Vis Exp*.

ZELENA, J. (1982) Survival of Pacinian corpuscles after denervation in adult rats. *Cell Tissue Res,* 224**,** 673-83.

ZHANG, H., WEI, Y. T., TSANG, K. S., SUN, C. R., LI, J., HUANG, H., CUI, F. Z. & AN, Y. H. (2008) Implantation of neural stem cells embedded in hyaluronic acid and collagen composite conduit promotes regeneration in a rabbit facial nerve injury model. *J Transl Med,* 6**,** 67.

ZHANG, P. X., HE, X. J., ZHAO, F. Q., ZHANG, D. Y., FU, Z. G. & JIANG, B. G. (2005) Bridging small-gap peripheral nerve defects using biodegradable

chitin conduits with cultured Schwann and bone marrow stromal cells in rats. *Journal of Reconstructive Microsurgery,* 21**,** 565-571.

ZHANG, Q. S., YAN, Y. H., LI, S. P. & FENG, T. (2010) The synthesis and characterization of a novel biodegradable and electroactive polyphosphazene for nerve regeneration. *Materials Science & Engineering C-Materials for Biological Applications,* 30**,** 160-166.

ZHANG, X., JU, G., ELDE, R. & HOKFELT, T. (1993) Effect of Peripheral-Nerve Cut on Neuropeptides in Dorsal-Root Ganglia and the Spinal-Cord of Monkey with Special Reference to Galanin. *Journal of Neurocytology,* 22**,** 342-381.

ZHANG, Z., ROUABHIA, M., WANG, Z. X., ROBERGE, C., SHI, G. X., ROCHE, P., LI, J. M. & DAO, L. H. (2007) Electrically conductive biodegradable polymer composite for nerve regeneration: Electricity-stimulated neurite outgrowth and axon regeneration. *Artificial Organs,* 31**,** 13-22.

ZHAO, M., SONG, B., PU, J., WADA, T., REID, B., TAI, G., WANG, F., GUO, A., WALCZYSKO, P., GU, Y., SASAKI, T., SUZUKI, A., FORRESTER, J. V., BOURNE, H. R., DEVREOTES, P. N., MCCAIG, C. D. & PENNINGER, J. M. (2006) Electrical signals control wound healing through phosphatidylinositol-3-OH kinase-gamma and PTEN. *Nature,* 442**,** 457-60.

ZHOU, F. Q., ZHOU, J., DEDHAR, S., WU, Y. H. & SNIDER, W. D. (2004) NGF-induced axon growth is mediated by localized inactivation of GSK-3beta and functions of the microtubule plus end binding protein APC. *Neuron,* 42**,** 897-912.

ZHOU, Y., LU, T. J. & XIONG, Z. Q. (2009) NGF-dependent retrograde signaling: survival versus death. *Cell Res,* 19**,** 525-6.